

Aus der/dem Institute for Lung Biology and Disease (ILBD)
Klinikum/Institut der Ludwig-Maximilians-Universität München



Dissertation
zum Erwerb des Doctor of Philosophy (Ph.D.)
an der Medizinischen Fakultät der
Ludwig-Maximilians-Universität zu München

***Latent MHV-68 reactivation – The link between acute pulmonary
inflammation and chronic lung diseases***

vorgelegt von:
Verena Häfner

aus:
Waiblingen

Jahr:
2023

Mit Genehmigung der Medizinischen Fakultät der
Ludwig-Maximilians-Universität zu München

Erster Gutachter: Frau Prof. Dr. Erika von Mutius
Zweiter Gutachter: Herr Prof. Dr. Heiko Adler
Dritter Gutachter: Frau Priv. Doz. Dr. Teresa Kauke
Vierter Gutachter: Herr Prof. Dr. Dr. Nikolaus Kneidinger

Dekan: **Prof. Dr. med. Thomas Gudermann**

Datum der Verteidigung:

07.06.2023

Table of content

Inhalt

Abstract.....	1
Zusammenfassung.....	3
List of figures.....	5
List of tables.....	6
List of abbreviations.....	7
1. Introduction.....	12
1.1 Ambient particles.....	12
1.1.1 Nanoparticle cause acute and chronic pulmonary inflammation.....	14
1.2 Nanoparticles and their role in chronic lung diseases.....	18
1.2.1 Chronic obstructive pulmonary disease (COPD).....	19
1.2.2 Asthma.....	21
1.2.3 Idiopathic Pulmonary Fibrosis (IPF).....	23
1.2.4 Lung cancer.....	25
1.3 Virus Infection, Air pollution and Chronic Lung Diseases.....	27
1.4 Herpesviruses.....	27
1.4.1 Herpesvirus life cycle and pathogenesis.....	27
1.4.2 Murine gammaherpesvirus-68 (MHV-68) as a mouse model.....	31
1.5 Aim of the study.....	32
2. Materials and Methods.....	33
2.1 Materials.....	33
2.1.1 Nanoparticles.....	33
2.1.2 Mice.....	33
2.1.3 Chemicals and Reagents.....	33
2.1.4 Buffers and Stock Solutions.....	36
2.1.5 Cell culture solutions.....	38
2.1.6 recombinant proteins.....	39
2.1.7 Antibodies.....	39
2.1.8 Kits.....	41
2.1.9 Primer sequences.....	42
2.1.10 Equipment and General Consumables.....	43
2.1.11 Softwares.....	46
2.2 Methods.....	47
2.2.1 <i>in vivo</i> mice experiments.....	47
2.2.2 Harvesting mice lungs for histology.....	48
2.2.3 Harvesting serum from mice.....	48

2.2.4	Bronchoalveolar Lavage (BAL).....	49
2.2.5	BAL cytopsin	49
2.2.6	BAL cell staining – May-Gruenwald-Giemsa staining	50
2.2.7	BAL cell differentiation.....	50
2.2.8	Harvesting mice lungs for protein and RNA isolation	50
2.2.9	Lung homogenate preparation	50
2.2.10	Preparation of carbon nanoparticle (CNP) and double walled carbon nanotube (DWCNT) dispersions.....	51
2.2.11	Characterization of particle dispersion.....	51
2.2.12	Cell culture	52
2.2.13	Freezing of cells	52
2.2.14	Thawing of cells	53
2.2.15	Counting cells.....	53
2.2.16	Alveolar macrophage cell line – ANA-1	54
2.2.17	Bone Marrow derived macrophage cell line – latently infected MHV-68/ANA-1 54	
2.2.18	Alveolar macrophage cell line – MHS	54
2.2.19	Alveolar epithelial cell line – MLE-12	55
2.2.20	Alveolar epithelial cell line – LA4	55
2.2.21	Cultivation of non-infected and MHV-68 latently infected ANA-1 cells on transwell insert	55
2.2.22	Transwell co-culture of alveolar epithelial cells and bone marrow derived macrophages	55
2.2.23	ALICE-Cloud treatment of non-infected cells with carbon nanoparticle dispersion.....	56
2.2.24	ALICE-Cloud prototype treatment of ANA-1/MHV-68 latently infected cells with carbon nanoparticle dispersion.....	57
2.2.25	Sterilization of cut 5-well plates for ALICE-Cloud prototype	57
2.2.26	Immunofluorescence (IF) staining of fixed cell culture cells	58
2.2.27	Water soluble tetrazolium (WST-1) cell viability assay.....	58
2.2.28	Lactate Dehydrogenase (LDH) assay – assessment of cytotoxicity in BALF and <i>in vitro</i> 59	
2.2.29	Plaque assay.....	60
2.2.30	Enzyme-linked Immunosorbent assay (ELISA).....	60
2.2.31	Luminex analysis.....	61
2.2.32	Measurement of dsDNA in BALF.....	62
2.2.33	Protein extraction	62
2.2.34	Protein quantification with BCA assay	63
2.2.35	RNA purification from tissue homogenates.....	64
2.2.36	cDNA synthesis.....	64

Table of content

2.2.37	quantified PCR (qPCR) – Transcriptome analysis	65
2.2.38	Sodium dodecyl sulfate polyacrylamide gel electrophoresis (SDS-PAGE).....	65
2.2.39	Western blotting transfer	66
2.2.40	Microtome cutting	68
2.2.41	Immunohistochemistry (IHC) staining of lung tissue sections – Vulcan fast red 68	
2.2.42	Immunohistochemistry (IHC) staining of lung tissue sections – DAB	69
2.2.43	Immunofluorescence (IF) staining of lung tissue sections.....	71
2.2.44	Detecting DNA fragmentation with TUNEL assay	73
2.2.45	Hematoxylin and Eosin (H&E) staining	74
2.2.46	Masson’s Goldner Trichrome staining	75
2.2.47	Imaging of histological stainings	76
2.2.48	Quantitative morphometry of mean linear chord length (MCL), IHC stains and tissue inflammation.....	76
2.2.49	Statistical analysis	77
3.	Results	79
3.1	Characterization of CNP and DWCNT for <i>in vitro</i> and <i>in vivo</i> application.....	79
3.2	Repeated CNP and DWCNT instillation trigger MHV-68 reactivation in the lungs...80	
3.2.1	Repeated CNP and DWCNT instillation approaches environmental NP exposure	80
3.2.2	CNP and DWCNT trigger virus reactivation in the lung in first and repeated exposure	81
3.2.3	CD11b and IBA1 positive recruited macrophages are the main cell type for nanoparticle-triggered virus reactivation	83
3.3	BAL cell differentiation – Airspace accumulation of lymphocytes and neutrophils in repeated CNP exposure of latently infected mice.....	86
3.4	Increased lung tissue inflammation in 2 nd hit model	88
3.5	Increased Leakage of Proteins and IgM into bronchoalveolar space	90
3.6	Elevated levels of neutrophil chemoattractants after repeated CNP exposure in 2 nd hit model.....	92
3.7	Investigation of lymphocytes in the 2 nd hit model	93
3.7.1	No change in CD45R+ B-lymphocyte numbers after viral infection and NP treatment.....	93
3.7.2	Increased infiltration of CD8+ T-lymphocytes in lungs after viral infection	95
3.7.3	Increased CD8+ T-lymphocytes in BAL cells.....	98
3.7.4	Elevated cytotoxic potential of BAL T-lymphocytes in CNP induced 2 nd hit model	100
3.8	Inflammatory response of virus infection and nanoparticle exposure	101
3.8.1	The effect of virus infection and CNP or DWCNT exposure on IL-6.....	101
3.8.2	Elevated interferon- γ (<i>Ifnγ</i>) expression in BAL cells in the CNP induced second hit model	103

3.8.3	The effect of virus infection and CNP or DWCNT exposure on Lipocalin-2....	104
3.8.4	The effect of virus infection and CNP or DWCNT exposure on TNF-a.....	106
3.8.5	The effect of virus infection and CNP or DWCNT exposure on CCL17.....	107
3.8.6	The effect of virus infection and NP exposure on cell migrating and priming chemokines.....	109
3.8.7	Elevated macrophage activation in 2 nd hit model.....	110
3.8.8	The effect of virus infection and NP exposure macrophage inflammatory proteins CCL3 and CCL4.....	110
3.8.9	The effect of virus reactivation on the expression of osteopontin in lung.....	112
3.8.10	Increased GM-CSF release in CNP exposure.....	115
3.9	Effect of MHV-68 infection and NP exposure on pulmonary morphology.....	117
3.9.1	Reduction of alveolar epithelial type II (AT2) cell numbers in second hit model	117
3.9.2	Increased alveolar air space in chronic time points of virus reactivation.....	118
3.9.3	No changes in pulmonary collagen deposition.....	120
3.9.4	No changes in goblet cell morphology and mucus production.....	123
3.9.5	DNA damage and dsDNA release increased after nanoparticle exposure.....	124
4.	Discussion.....	128
4.1	NP-triggered MHV-68 reactivation detected in lung recruited inflammatory monocyte-derived macrophages.....	128
4.2	Elevated cytotoxic T-lymphocyte infiltration into the air space with higher cytotoxic potential in the repeated second hit model.....	130
4.3	Elevated inflammatory response in repeated NP exposure in latently infected vs. adaptive response in non-infected mice.....	133
4.4	Elevated injury of pulmonary barrier integrity in NP induced second hit model.....	134
4.5	CNP and DWCNT exposure differentially activate pulmonary inflammatory response	135
4.6	Effect of MHV-68 infection and nanoparticle exposure on macrophage activation	136
4.7	Inflammatory response to NP exposure and virus infection and the development of chronic lung diseases.....	141
5.	Conclusion and Outlook.....	146
5.1	Conclusion.....	146
5.2	Outlook.....	148
	References.....	149
6.	Appendix A:.....	176
6.1	Background – Inhaled particles influence systemic inflammation.....	176
6.2	Results – Indication for elevated systemic inflammation after repeated particle instillation.....	177
6.3	Discussion – Systemic inflammation and extrapulmonary effects of pulmonary nanoparticle exposure and respiratory virus infection.....	180
7.	Appendix B:.....	183

Table of content

7.1	Background - <i>In vitro</i> models to test environmental particles	183
7.2	Results – Establishing of an air liquid exposure system - CNP nebulization trigger MHV-68 reactivation in ANA-1 cell line cultured on air liquid interface	183
7.2.1	CNP exposure effect cell viability in dose dependent manner on non-infected ANA-1, MHS and LA4	184
7.2.2	CNP exposure on ANA-1/MHV-68 affect the virus reactivation on gene in dose dependent manner	186
7.2.3	CNP nebulization on epithelial-macrophage co-culture system in the ALICE- Cloud system doesn't influence MHV-68 reactivation from ANA-1 cells and cell viability 190	
7.3	Discussion – MHV-68 reactivation induced by CNP in ALICE-Cloud system	193
	Acknowledgements	196
	Affidavit	198
	Confirmation of congruency.....	199
	Curriculum vitae	Fehler! Textmarke nicht definiert.
	List of publications.....	Fehler! Textmarke nicht definiert.

Abstract

Inhalation of airborne particles such as particulate matter and lifelong persistent infection with herpes viruses are ubiquitous and unavoidable to our lives and in our current environment. Both factors are associated with chronic lung disease. Herpesviruses are of particular interest because of their biphasic cycles of infection consisting of the lytic and latent phases of infection. Latent infection means that the herpesvirus remains in the host body throughout its life in a dormant state and undetected by the immune system, but from which it can be reactivated by various stimuli into its lytic phase generating infectious virus particles. Previous studies in our group have shown that inhalation of nanoparticles such as soot-like carbonaceous nanoparticles (CNP) and fibrous engineered double-walled carbon nanotubes (DWCNT) reactivates latent murine gammaherpesvirus 68 (MHV-68) in the lung, thereby restoring gene expression and metabolome patterns in the lung similar to that of acute infection (Sattler et al., 2017).

Given several studies independently linking gammaherpesvirus infections or air pollution to the development and exacerbation of chronic lung disease, I would like to investigate the interaction of these two environmental factors in my animal-based study. The hypothesis of my study is that, at least in mice, the combination of latent gammaherpesvirus infection and repeated exposure, as a model of persistent air pollution, will lead to the development of symptoms known to be associated with chronic lung disease and its exacerbation.

For my studies, mice were intranasally infected with MHV-68 and pulmonary exposed to either CNP or DWCNT, with one or two particle doses, and examined the lungs either 24 hours or 6 days afterwards. This model is referred to in this study as the virus reactivation model (virus infection only), second-hit model (virus infection and one dose of nanoparticles) or repeated second-hit model (virus infection and two doses of nanoparticles), depending on the number of nanoparticle exposures. As expected, MHV-68 reactivation, detected by immunohistochemical staining of lytic viral proteins was evident after one-time and two-time particle exposures. The cell type in which virus reactivation was detected I identified as CD11b+, IBA1+, inflammatory, and thus apparently monocyte-derived macrophages.

Further, the second-hit model showed that although latent infection attenuated acute particle-induced alveolar neutrophilia, CNP-induced alveolitis was significantly more pronounced in the repeated second-hit model than in the second-hit model. This difference was associated with increased interstitial inflammation as well as an increase in lymphocyte counts, particularly cytotoxic T-cells, 6 days after the second CNP dose.

Of note, exclusively the repeated second-hit model caused marked injury to lung tissue, characterized by epithelial and endothelial barrier damage, increased cellular DNA fragmentation, a reduction in alveolar epithelial type II cell numbers, and ultimately an increase in alveolar airspace, as a sign of emphysema formation, which further worsened by day 6 after the second CNP exposure.

In conclusion, the animal study shows that repeated reactivation of gamma-herpesviruses triggered by nanoparticle inhalation can lead to the development or even exacerbation of chronic lung disease, such as emphysema.

Zusammenfassung

Das Einatmen von luftgetragener Partikel wie Feinstaub und die lebenslange persistente Infektion mit Herpesviren sind für unser Leben und in unserer gegenwärtigen Umwelt allgegenwärtig und unvermeidlich. Beide Faktoren werden mit chronischen Lungenkrankheiten in Verbindung gebracht. Herpesviren zeichnen sich durch ihren zweiphasigen Infektionsverlauf aus einer lytischen und einer latenten Phase. Die latente Infektion bedeutet, dass das Herpesvirus ein ganzes Leben lang im Wirtskörper in einer Art vom Immunsystem versteckten Schlafzustand verbleibt, aus dem es jedoch durch verschiedene Reize in seine lytische Phase reaktiviert werden kann, um sich durch die Produktion infektiöser Viruspartikel zu vermehren und zu verbreiten. Frühere Untersuchungen in unserer Gruppe haben gezeigt, dass die Inhalation von Stäuben wie zum Beispiel rußartige Kohlenstoff-Nanopartikeln (CNP) und faserförmigen doppelwandige Kohlenstoffnanoröhren (DWCNT) das latente murine Gammaherpesvirus 68 (MHV-68) in der Lunge reaktiviert und dabei in der Lunge Genexpressions- und Metabolom-Muster erzeugt, die der einer akuten Infektion ähneln (Sattler et al., 2017).

In Anbetracht der Studien, welche Gammaherpesvirusinfektionen oder Luftverschmutzung unabhängig voneinander mit der Entwicklung und Exazerbation chronischer Lungenerkrankungen in Zusammenhang bringen, möchte ich in meiner tierexperimentellen Studie das Zusammenwirken dieser beiden Umweltfaktoren untersuchen. Die Hypothese meiner Studie ist, dass zumindest in der Maus, die die Kombination aus latenter Gammaherpesvirusinfektion und wiederholter Nanopartikel-Exposition, als Modell der anhaltenden Luftverschmutzung, zur Entwicklung von Symptomen führt, wie sie für chronische Lungenerkrankungen und deren Exazerbation bekannt sind.

Für meine Studien wurden Mäuse intranasal mit MHV-68 infiziert und deren Lunge entweder mit CNP oder DWCNT, mit einer oder zwei Partikeldosen exponiert und entweder 24 Stunden oder 6 Tage danach untersucht. Dieses Modell wird in dieser Studie als Virusreaktivierungsmodell (nur Virusinfektion), Second-Hit-Modell (Virusinfektion und eine Dosis Nanopartikel) oder wiederholtes Second-Hit-Modell (Virusinfektion und zwei Dosen Nanopartikel) bezeichnet, je nach der Anzahl der Partikelexpositionen. Wie erwartet zeigte sich die MHV-68 Reaktivierung,

nachgewiesen durch immunhistochemische Färbung der lytischen Virusproteine, nach einmaliger und zweimaliger Partikelexpositionen. Der Zelltyp, in dem eine Virusreaktivierung beobachtet wurde, identifizierte ich als CD11b+, IBA1+, entzündliche und damit offensichtlich von Monozyten differenzierten Makrophagen. Weiter zeigte sich im Second-Hit-Modell, dass die latente Infektion zwar eine Abschwächung der akuten Partikel-induzierten alveolären Neutrophilie bewirkte, die durch CNP bedingte Alveolitis jedoch im wiederholten Second-Hit-Modell deutlich stärker ausgeprägt war als im Second-Hit-Modell. Dieser Unterschied ging mit verstärkter interstitieller Entzündung sowie einem Anstieg der Lymphozytenzahlen, insbesondere zytotoxischer T Zellen, 6 Tage nach der zweiten CNP-Dosis einher. Bemerkenswert war, dass ausschließlich das wiederholte Second-Hit-Modell eine deutliche Verletzung des Lungengewebes verursachte, charakterisiert durch die Schädigung der Epithel- und Endothelbarriere, eine verstärkte zelluläre DNA-Fragmentierung, eine Verringerung der Alveolarepithel Typ II Zellzahl und letztendlich eine Vergrößerung des alveolären Luftraums, als ein Zeichen für die Bildung eines Emphysems, welches sich bis zum Tag 6 nach der zweiten CNP-Exposition weiter verschlimmerte. Zusammenfassend zeigt die Tierstudie, dass eine wiederholte, durch Nanopartikel Inhalation ausgelöste Reaktivierung von Gammaherpesviren zur Entwicklung oder auch Exazerbation von chronischen Lungenerkrankung, wie dem Emphysem führen kann.

List of figures

Figure 1.1 Transmission electron microscopic images of the nanoparticles used in this study. Fehler! Textmarke nicht definiert.	
Figure 1.2 Cigarette smoke exposure contributes to COPD progression.	21
Figure 1.3 Environmental factors trigger mechanism of non-Th2 asthma exacerbation	23
Figure 1.4 Carbon nanotube-induced pulmonary fibrosis.....	24
Figure 1.5 Carbon black and diesel exhaust trigger lung cancer.	26
Figure 1.6 Latent and lytic infection course of MHV-68 in mice.....	29
Figure 1.7 Classical and novel triggers can reactivate latent herpesvirus.....	30
Figure 3.1 Schematic illustration of repeated CNP and DWCNT instillation into MHV-68 infected mice.	80
Figure 3.2 Nanoparticles trigger virus reactivation in first and repeated exposure in lung tissue.	82
Figure 3.3 NP-triggered MHV-68 reactivation occurs in CD11b+/IBA1+ cells.	85
Figure 3.4 Differentiation of BAL cells show significant increase of lymphocytes and neutrophils in 2 nd hit model.	87
Figure 3.5 Increased tissue inflammation level in 2 nd hit model.	89
Figure 3.6 Increased BAL protein and BAL IgM levels in 2 nd hit model indicate elevated epithelial endothelial barrier damage.....	91
Figure 3.7 Increased neutrophil chemoattractants in BAL fluid after CNP exposure....	92
Figure 3.8 B-lymphocytes are not recruited to the lungs after NP exposure into latent virus infection.....	94
Figure 3.9 CD8 IHC staining, and quantification show elevated T-lymphocyte recruitment to the lungs during MHV-68 infection.....	97
Figure 3.10 CD8+ T-lymphocytes proliferate in 2 nd hit model.....	98
Figure 3.11. High expression of cytotoxic T-lymphocyte markers in BAL cells of CNP induced 2 nd hit model.....	99
Figure 3.12 Elevated markers for cytotoxic T-lymphocyte potential.	100
Figure 3.13 Increase of IL-6 release after repeated CNP exposure in virus latency and early NP exposure without virus infection.	102
Figure 3.14. Expression of <i>Inf-γ</i> in BAL cells.	103
Figure 3.15 Elevated Lipocalin-2 release and gene expression after NP treatment. ...	105
Figure 3.16 Increased lung gene expression of <i>Tnf</i> in the 2 nd hit model and particle treatment.....	107
Figure 3.17 Increased CCL17 release and gene expression after CNP exposure in virus infected and not infected lungs.....	108
Figure 3.18. Bio-Plex analysis of eosinophil migrating chemokines in bronchoalveolar lavage.....	109
Figure 3.19. Increased CCL3 and CCL4 release to the airspace after nanoparticle exposure.	111
Figure 3.20. Increased lung and BAL cell gene expression of <i>Spp1</i> in the 2 nd hit model and particle treatment.....	113

Figure 3.21 Increased Osteopontin in alveolar macrophages and release into airspace after particle treatment.....	114
Figure 3.22. Increased GM-CSF release into bronchoalveolar lavage after CNP exposure and CNP induced 2 nd hit model with repeated exposure.	116
Figure 3.23 Repeated CNP exposure to MHV-68 latency decrease AT2 cell numbers in lung tissue.	118
Figure 3.24 Repeated CNP exposure of MHV-68 infected mice increase alveolar air space and lung tissue inflammation.	120
Figure 3.25 Masson's-Goldner-Trichrome staining shows no change in collagen deposition during virus infection or NP treatment.....	121
Figure 3.26 Effect of virus and NP treatment to the expression of pro-fibrotic markers.	122
Figure 3.27 PAS staining shows no goblet cell hyperplasia.	123
Figure 3.28 No changes of airway mucus gene <i>Muc5ac</i>	124
Figure 3.29. Increased DNA fragmentation in repeated CNP exposure in 2 nd hit model.	126
Figure 3.30 dsDNA release into airspace.....	126
Figure 3.31. Increased lung and BAL cell gene expression of Saa3 in CNP exposure.	177
Figure 5.1 Graphical presentation of the proposed response to NP-triggered virus reactivation and the contribution to chronic lung disease and cardiovascular disease.	147
Figure 6.32. Increasing SAA3 protein in lung after repeated CNP instillation in MHV-68 latency and decreasing SAA3 protein in non-infected lungs.	179
Figure 6.33. Elevated serum SAA3 in 2 nd hit model of repeated CNP exposure.	180
Figure 7.34. ANA-1, MHS, LA4 cell viability alteration induced by CNP exposure at air liquid interface.....	185
Figure 7.35. No alteration of LDH release depending on CNP deposition.....	186
Figure 7.36. Schematic illustration of experimental setting of <i>in vitro</i> reactivation testing in ALICE-Cloud exposure.....	188
Figure 7.37. CNP-triggers MHV-68 reactivation in dose dependent manner.....	189
Figure 7.38. Schematic illustration of the similarities of the <i>in vitro</i> approach of co-culture reactivation model and <i>in vivo</i> situation.....	191
Figure 7.39. Schematic illustration of the ALICE-Cloud exposure of CNP to the co-culture system of LA4 or MLE-12 and ANA-1/MHV68.	191
Figure 7.40. CNP does not trigger MHV-68 reactivation co-culture model.....	192

List of tables

Table 3.1 Characterization of nanoparticles used in the study	79
Table 3.2 Marker co-localization with lytic MHV-68 proteins	83

List of abbreviations

List of abbreviations

ACE-2	Angiotensin-converting enzyme 2
ALI	Air-Liquid interface
ALI	Acute Lung injury
AFC	Alveolar fluid clearance
AHR	Airway hyperresponsiveness
ALICE	Air-Liquid interface cell exposure
ANA-1	Murine bone marrow derived macrophage cell line
ANA-1/MHV-68	Murine gammaherpesvirus-68 latently infected ANA-1 cells
AP	Alkaline Phosphatase
APC	Antigen presenting cell
APS	Ammonium persulfate
ATI	Alveolar epithelial type 1 cell
ATII	Alveolar epithelial type 2 cell
BAL	Bronchoalveolar lavage
BALF	Bronchoalveolar lavage fluid
BCA	Bicinchoninic acid
BHK-21	Baby hamster kidney cell line
BMDM	Bone Marrow Derived Macrophages
β -ME	beta-Mercaptoethanol
BSA	Bovine serum albumin
CAST	Computer-assisted stereological toolbox
CB	Carbon black
CCL	C-C motif chemokine ligand
CCR	C-C motif chemokine receptor
CD	Cluster of differentiation
cDNA	Complementary DNA
CLD	Chronic lung disease
CMV	Cytomegalovirus
CNP	Carbonaceous nanoparticle/Printex 90/Carbon black
COPD	Chronic obstructive pulmonary disease
Ct	Threshold cycle
CXCL	Chemokine (C-X-C motif) ligand

CXCR	C-X-C chemokine receptor
DAPI	4',6-Diamidin-2-phenylindol
d	Day
DC	Dendritic cell
DLCO	Diffusion capacity for carbon monoxide
DLS	Dynamic laser scatter
DNA	Deoxyribonucleic acid
DMEM	Dulbecco's modified Eagle's medium
DMSO	Dimethyl sulfoxide
DPBS	Dulbecco's Phosphate Buffered Saline
d.p.	Days post
dsDNA	Double stranded DNA
DTT	Dithiothreitol, C ₄ H ₁₀ O ₂ S ₂
DWCNT	Double walled carbon nanotubes
EBV	Epstein-Barr Virus
ECL	Enhanced chemoluminescence
EDTA	Ethylenediaminetetraacetic acid
ELISA	Enzyme-linked immunosorbent assay
ENM	Engineered nanomaterial
EPA	United States Environmental Protection Agency
et al.	et alii (latin) – and others
EtOH	Ethanol
EV	Extracellular vesicle
FBS	Fetal bovine serum
FEV ₁	Forced expiratory volume in 1 second
g (weight)	Gram
g (centrifugation)	acceleration of gravity
GFP	Green fluorescent protein
GSEA	Gene Set Enrichment Analysis
h	Hour
HCl	Hydrogen chloride
H&E	Hematoxylin & Eosin
HHV-4	Human Herpesvirus 4
HHV-6	Human Herpesvirus 6
HHV-8	Human Herpesvirus 8
HIER	Heat-Induced Epitope Retrieval

List of abbreviations

HPRT	Hypoxanthine-guanine phosphoribosyl transferase
HRP	Horseradish peroxidase
H ₂ O	Dihydrogen monoxide
iBAL	Inducible bronchus-associated lymphoid tissue
ICC	Immunocytochemistry
IAV	Influenza A virus
IF	Immunofluorescence
IFN	Interferon
IHC	Immunohistochemistry
IL	Interleukin
i.p.	Intraperitoneal
IPF	Idiopathic pulmonary fibrosis
i.n.	Intranasal
IVC	Individual ventilated cage
k	kilo
KCl	Potassium chloride
kDa	kilo Dalton
KH ₂ PO ₄	Potassium dihydrogen phosphate
KSHV	Kaposi's sarcoma-associated herpesvirus
L	Liter
LA4	Murine AT2 cell line
LDH	Lactate dehydrogenase
LDL	Low-density-lipoprotein
Lm	Mean linear intercept
LPS	Bacterial lipopolysaccharide
m	milli
MCL	Mean chord length
MHS	Murine alveolar macrophage cell line
MHV-68	murine gamma herpesvirus 68
min.	Minute
MLE-12	Murine AT2 cell line
MMF	Medetomidin- Midazolam-Fentanyl mixture
MPO	Myeloperoxidase
mRNA	Messenger RNA
mtDNA	Mitochondrial DNA
MWCNT	Multi walled carbon nanotubes

μ	micro
N	Normal
n	nano
NP	Nanoparticle
NaCl	Sodium chloride
Na ₂ HPO ₄	Disodium hydrogen phosphate
NEAA	non-essential amino acids
neg.	negative
NET	Neutrophil extracellular traps
NK cells	Natural killer cells
NO _x	Nitrogen oxide compound
NPs	Nanoparticles
OPN	Osetopontin
ORF	open reading frame
PBS	Phosphate buffered saline
PCR	Polymerase chain reaction
PFA	Paraformaldehyde
PFU	Plaque-forming unit
pH	the negative of the logarithm to base 10 of the activity of the hydrogen ion
PM	Particulate matter
pos.	positive
PVDF	Polyvinylidenfluorid
QCM	quartz crystal microbalance
qPCR	Quantitative polymerase chain reaction
RG	Research Group
RNA	Ribonucleic acid
rpm	rounds per minute
ROS	Reactive oxygen species
RSV	Respiratory syncytial virus
RT	Room temperature
s	Second
SAA3	Serum amyloid A-3 protein
SARS-CoV-2	Severe acute respiratory coronavirus type 2
SD	Standard deviation
SDS-PAGE	Sodium dodecyl sulfate polyacrylamide gel electrophoresis

List of abbreviations

SWCNT	Single walled carbon nanotube
Taq polymerase	<i>Thermophilus aquaticus</i> DNA polymerase
TEMED	Tetramethylethylenediamine
THP-1	Human leukemia monocytic cell line
TLR	Toll-like receptor
TNF	Tumor necrosis factor
Tris	Tris-(hydroxymethyl)-aminomethan
TUNEL	TdT-mediated dUTP-biotin nick end labeling
UFP	Ultra-fine particle
V	Voltage
WHO	World Health Organization
WST-1	Water Soluble Tetrazolium-1
z.B.	zum Beispiel
%	Percent
&	And

1. Introduction

1.1 Ambient particles

The debate on air pollution and its consequences has become increasingly important in recent years. Air pollution is a main contributor to acute and chronic lung and cardiovascular diseases. In recent decades, the number of fatalities caused by air pollution and toxic chemicals has increased by 66% due to population growth, population aging, uncontrolled urbanization, industrialization, and fossil fuel burning (Fuller et al., 2022). At the same time, there is a lack of adequate national and international chemical policies. The World Health Organization (WHO) has reported that about 7 million people die each year as a result of polluted air. Similar numbers are published by Fuller et al. (2022), who report 6.67 million people died worldwide in 2019 due to air pollution, of which 2.31 are due to household air pollution and 4.14 are due to ambient particulate matter.

Air quality can fluctuate from day to day and is affected by emissions, as well as natural events such as dust storms, wildfires, and weather fluctuations. The U.S. Environmental Protection Agency (EPA) has established "criteria" air pollutants for six pollutants. These six pollutants are lead, carbon monoxide, nitrogen oxide, ground-level ozone, sulfur oxide, and particulate pollution. As one of the solid components of air pollution, particle pollution is also known as particulate matter (PM). PM is a globally occurring atmospheric aerosol that has both of natural and anthropogenic sources and has been associated with a range of health effects (Kelly and Fussell, 2012). Even though fine PM levels have decreased in the U.S., the severity, duration, and frequency of wildfires are increasing, affecting air quality in fire-prone areas (Aguilera et al., 2022). Yang et al., 2022 found main contributions to particulate matter were soil dust, coal combustion and biomass burning/petrochemical. Particulate matter is categorized based on its aerodynamic diameter. This also implies the typical localization of pulmonary deposition when inhaled. Coarse particulate matter with an aerodynamic diameter of 2.5 to 10 μm is deposited primarily in the large airways. Fine particulate matter or PM_{2.5}, which is 2.5 μm or smaller, deposits throughout the respiratory tract, especially in the small airways and alveoli, and ultrafine particulate matter (UFP), which

Introduction

is less than 100 nm in size, deposits effectively in the alveoli (Guarnieri and Balmes, 2014).

Due to the ultrafine structure of nanoparticles with a small diameter, they can remain suspended in the air for a long time.

Carbonaceous nanoparticles (CNP) or carbon black (CB), is a particulate form of pure elemental carbon consisting of aggregated and agglomerated 10 – 20 nm primary particles. It is produced by partial combustion or pyrolysis of gaseous or liquid hydrocarbons under controlled conditions (Valberg et al., 2006), as well as produced for various industrial purposes (Baan, 2007). CNP can also be released during the use of toner and printing inks (Morimoto et al. 2010; Yang et al., 2007). Characterizations of urban and highway air quality revealed that levels of CB, particulate matter ($PM \leq 2.5 \mu m$), and ultrafine particles ($PM \leq 0.1 \mu m$) are mainly affected by vehicle emissions and traffic events in urban areas (Frey et al., 2022; Shah et al., 2023; Habre et al., 2023; Canagaratna et al., 2010; Reche et al., 2015; Kelly et al., 2011).

Most notably, CB is widely used as a surrogate for the carbonaceous core of combustion nanoparticles or as a representative of PM (Zhen et al., 2017; Hakkarainen et al., 2022; Kheradmand et al., 2017; Medalia et al., 1983) to test its nanotoxicology under various conditions. CB is also known by the trade names such as Printex-90, Printex-140, Printex-G, and Lampblack-101 (Long et al., 2013; Jeong et al., 2013), which vary in primary particle size and the level of hydrocarbons.

The production rate of engineered nanomaterials increases each year. One of the most dynamic classes of this engineered materials are carbon nanotubes (CNTs), which are increasing in demand in developing countries (Carbon Nanotube Market, 2021). They have unique optical, physical, and conductive properties to make them attractive to change the functionality of polymers, sensors, batteries, panel displays, chemical storage and new applications are under development for example for microwave antennas, aerospace, medical implants, drug delivery, coatings and car body panels (Cha et al., 2013; Carbon Nanotubes Market, 2021). There are different types of CNTs, the single-walled CNTs (SWCNTs), the double-walled CNTs (DWCNTs), and the multi-walled CNTs (MWCNTs). SWCNTs are a rolled graphene sheet with a diameter of 1 - 4 nm. DWCNTs and MWCNTs consist of two or more concentric graphene layers with a diameter between 10 and 100 nm. CNTs have a length in the μm range. As the production of CNTs increases, the risk of occupational exposure and the risk of

developing CNT-induced lung diseases increases (Cha et al., 2013; Duke and Bonner, 2017).

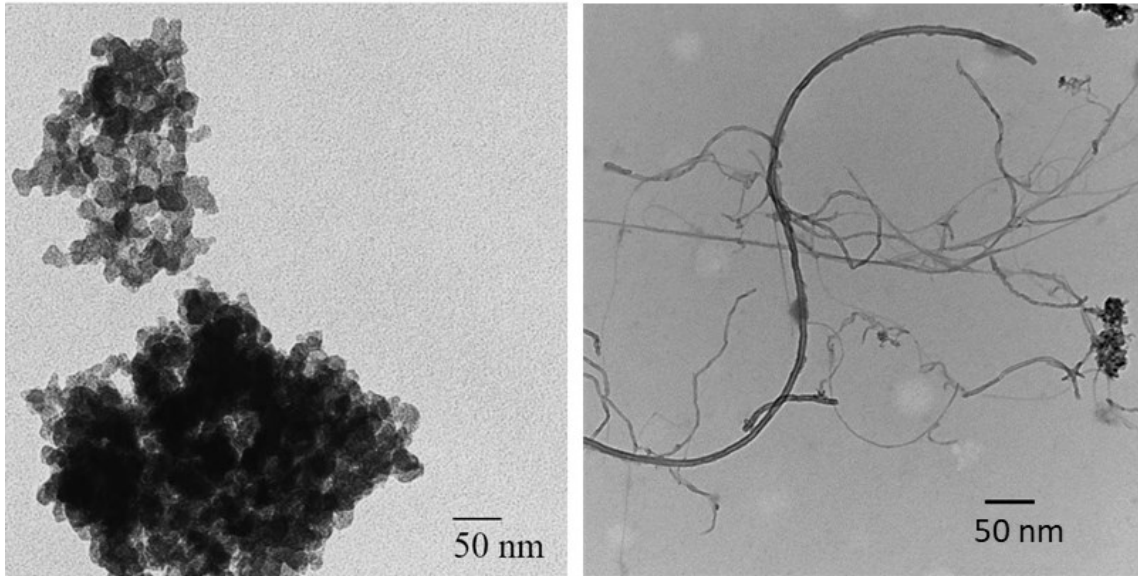


Figure 1.1 Transmission electron microscopic images of the nanoparticles used in this study.

Left image shows CNP, right image shows DWCNT (provided by Shinji Takenaka, 2010).

1.1.1 Nanoparticle cause acute and chronic pulmonary inflammation

Airborne particles have been described to activate several mechanisms of cellular effects, such as oxidative stress with cytotoxicity, mutagenicity, and proinflammatory stimulation (Valavanidis et al., 2008). In the pathway activations, the particle size is described to be an important role. The smaller the particle size, the higher the inflammation and pulmonary toxicity of oxidative stress, mostly because of their large surface area (Valavanidis et al., 2008; Mazzoli-Rocha et al., 2010). The particle size and surface are described to linearly correlates with inflammatory response (Stoeger et al., 2009). The extractable organic compounds are also described to highly contribute to cytotoxicity and DNA damage and membrane lipid peroxidation (Valavanidis et al., 2008).

Several pathways are observed to be activated by PM exposure. Activation of aryl hydrocarbon receptor, Toll-like receptor and IL-1 receptor are described, which lead to NF-kB, MAPK and AP-1 signaling (Wu et al., 2018).

Introduction

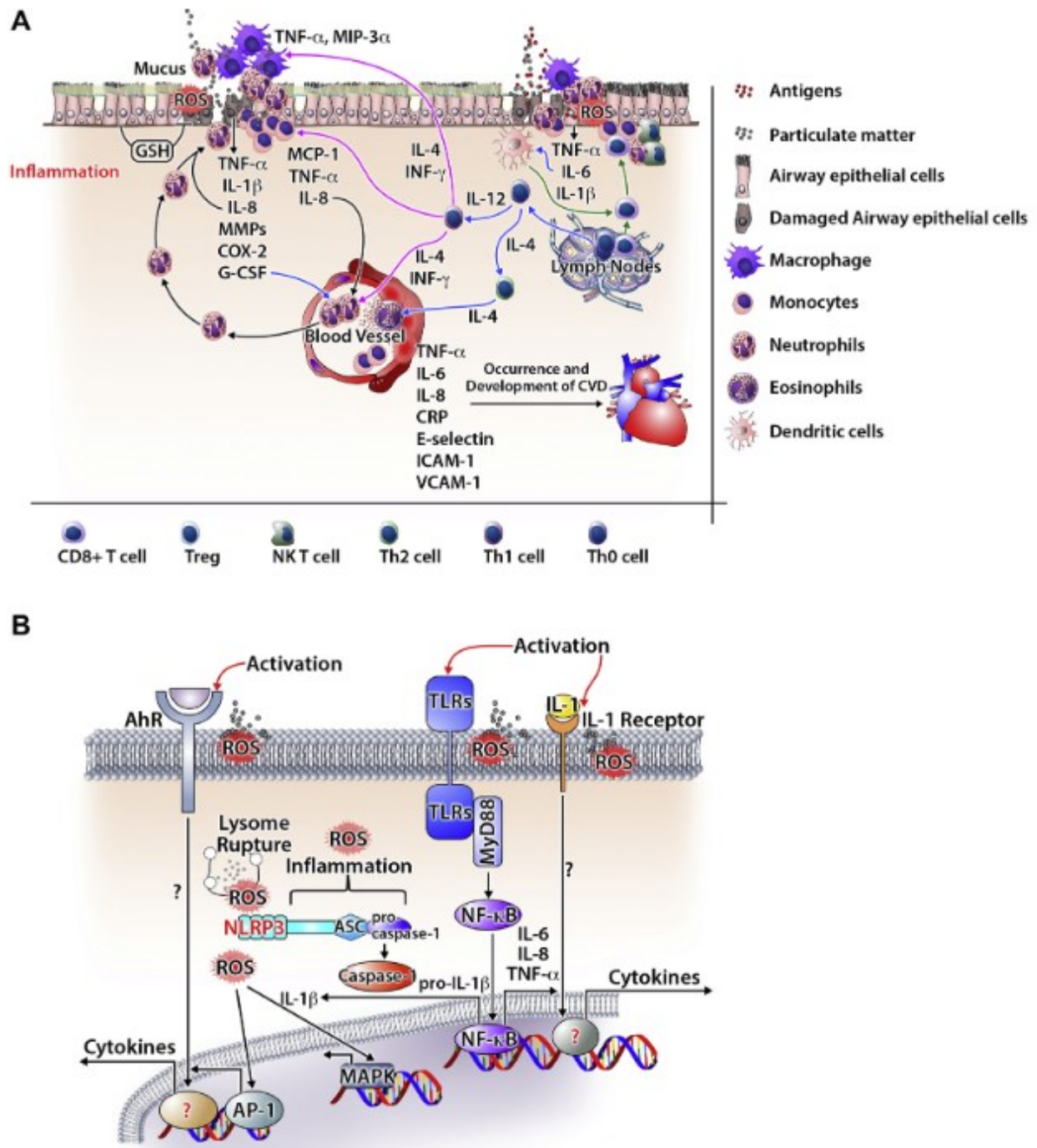


Figure 1.2 Nanoparticle activated innate immune response and pathway activations

PM cause injury in alveolar and airway epithelial cells, monocyte and macrophages as first defense release chemokines to recruit neutrophils and macrophages. Toll-like receptor (TLR), aryl hydrocarbon receptor (AhR) and IL-1 receptor get activated, which lead to activation of NF- κ B, MAPK and AP-1 signaling. (adapted from Wu et al., 2018).

Air pollution, indoor and ambient PM as well as engineered nanomaterials are described to induce acute and chronic inflammatory responses in the lungs. Due to the high deposited fraction, distal of the mucociliary clearance protected bronchiolar region, and thus slow clearance, nanoparticle inhalation results in persistent particle retention in the alveolar region of the lung. Deposition on the fragile alveolar epithelium in turn is known to cause pulmonary inflammation (Elder et al., 2005; Halappanavar et al., 2011; Chen et al., 2016). CNPs are frequently reported to cause acute, fast resolving lung inflammation (Bourdon et al., 2012; Renwick et al., 2004; Ganguly et al., 2017). Moreover, results of our research group have previously shown, that CNP inhalation in mice even at low doses causing only 3 μg CNP deposition per lung, triggers an increase of neutrophil numbers in the airspace (André et al., 2006). Gene expression analysis revealed a pro-inflammatory response in alveolar epithelial cells and alveolar macrophages induced by CNP exposure within 24h. Osteopontin (Spp1), Serum amyloid A-3 (Saa3), Lipocalin 2 (Lcn2) and Interleukin-1 β (Il1b) gene expression were highly elevated as well as the expression and release of CXCL1 was increased into the bronchoalveolar space 24h after CNP exposure. Altogether, indicating pulmonary inflammation. Similar findings were observed in lungs exposed to engineered nanomaterials like CNTs. Neutrophil and macrophage numbers markedly increased in the lung tissue, which indicates their important role in the frontline response to acute particle inflammation (Tian et al., 2013; Shvedova et al., 2005; Rydmann et al., 2015; Nikota et al., 2017). This accumulation of inflammatory cells is not only induced by release of chemoattractant but also leads to elevated expression and secretion of proinflammatory cytokines and chemokines like TNF- α , IL-1 α , IL-1 β , IL-6, CCL2, CCL5 and CXCL2 (Tian et al., 2013; Borthwick et al., 2013; Sahin and Wasmuth, 2013). Incomplete combustion of tobacco such as during cigarette smoking also generates nano-sized carbon particles, which has been described to accumulate in lung myeloid dendritic cells and macrophages, and causes airway inflammation, DNA double strand breaks and emphysema development in man and mouse models (Kheradmand et al., 2017; You et al., 2015; John et al., 2014). Yuan et al. (2020) demonstrated the CB induced necrosis and alveolar macrophages play critical roles in CB-induced lung inflammation, where they could induce the release of mitochondrial DNA (mtDNA) and inflammatory cytokines.

Introduction

O'Shaughnessy and colleagues (2014) showed that exposure to DWCNT induce acute inflammation and injury in the lungs. Similar results show rodents after DWCNT exposure, with increased cytotoxicity by elevated lactate dehydrogenase (LDH) activity in fluid obtained from bronchoalveolar lavage (BAL) as well as decreased integrity of blood-gas barrier in the lung. Also in more chronic endpoints, DWCNT exposure showed significant alveolitis and fibrosis (Sager et al., 2013). Tian et al. (2013) also detected high neutrophil numbers as well as elevated neutrophil recruiting cytokines during acute inflammation phase due to DWCNT exposure and a chronification of the inflammation with greater contribution of macrophages and lymphocytes. DWCNT induce acute pulmonary inflammation at an equal surface dose compared to CNPs. However, unlike CNP, CNTs remain in the lung for longer time and subsequently induce persistent inflammation that last for weeks (Ganguly et al., 2017).

MWCNT have been found to be biopersistent in the lungs, eliciting a neutrophil and T-cell response, inflammation in mesothelial cells, as well as ROS production in macrophages and neutrophils and fibrotic pathological alterations similar to asbestos (Snyder-Talkington et al., 2016; Murphy et al., 2012).

A two-year *in vivo* study rated the effects of DWCNTs in the lung and pleura of rats. DWCNTs were found to be biopersistent in the lungs of rats, inducing chronic inflammation where they developed lung tumors and pleural fibrosis (Saleh et al., 2022). Sing et al. (2022) reported pro-inflammatory, pro-fibrotic and pro-angiogenic biomarkers upregulated in epithelial cells interacting with unaged lifecycle particulate matter which is released under occupational conditions. Multiwalled carbon nanoparticle exposure induces matrix proteases and induce complex peptidomic responses across the lung compartments (Mostovenko et al., 2019). CNTs are also described in chronic inflammations with granulomas and fibrosis with increased macrophage and T-lymphocyte numbers in the lungs (Rydman et al., 2015; Huizar et al., 2011; Dong and Ma, 2017).

In addition, the development of lung edema was described after CB exposure, indicating damage to the epithelial endothelial barrier (Inoue et al., 2006). Cell membrane permeability also decreased significantly after the exposure to CB, even at low doses (Wang et al., 2021). The exposure to PM₁₀₋₂ significantly decreased mitochondrial activity and increased inflammatory response and oxidative stress. Impaired cell membrane integrity and DNA damage were mostly detected with PM exposure, below 100 nm (Yang et al., 2022).

Airport emission particles exposed to mice resulted in increasing numbers of neutrophil and eosinophil cells in bronchoalveolar lavage (BAL) in the early exposure time after one day. Increased lymphocyte numbers were found in the later time points after 28 days. Serum amyloid A 3 (SAA3) is an acute phase protein. Increased Saa3 expression and SAA3 protein levels were found in the plasma, as well as DNA fragmentation in BAL cells were detected (Bendtsen et al., 2019). Bourdon and colleagues (2012) have been described carbon black inducing lung inflammation and genotoxic effects in mouse lung and BAL cells, as well as in the liver. Furthermore, there is a correlation of robust influx of neutrophils and particle exposure into the lung (Christophersen et al., 2016). This particle-induced neutrophilia in the lung is reported several times,

Thus, there is a lot of evidence that exposure to various carbon nanoparticles can induce acute and chronic pulmonary inflammation.

1.2 Nanoparticles and their role in chronic lung diseases

Various studies and publications claim and describe, that ambient and indoor air pollution can play an essential role in exacerbation and development of chronic lung diseases.

Soriano and colleagues (2020) made a study for the global burden of diseases, injuries and risk factors to estimate the prevalence and health burden of chronic respiratory diseases. They found 454 million people suffering from chronic respiratory disease with the highest prevalence for chronic obstructive pulmonary disease (COPD). COPD and asthma were the top leading cause of death in the high-income countries, Caribbean, Latin America, and central and eastern Europe and central Asia, while the regions of South Asia and Sub-Saharan Africa have the lowest prevalence (GBD, 2017a; Labaki et al., 2020). The absolute prevalence of chronic respiratory disease increased between 1990 and 2017. Smoking and household air pollution from solid fuel, exposure to ambient particulate matter accounted for disability attributed to chronic respiratory disease.

About 21.4 million deaths from chronic respiratory diseases between 2010 and 2017 in Asian countries (Baptista, Dey and Pal, 2021) and 150,000 deaths in the United States in 2020 are counted from chronic lung diseases (Labaki and Han, 2020). Lou and colleagues (2022) found short-term increase of PM_{2.5} with 10 µg/m³ was

significantly associated with increases of respiratory and cardiovascular mortality and morbidity. Furthermore, a long-term increase of PM_{2.5} with 10 µg/m³ was significantly associated increase in cardiovascular, stroke and lung cancer mortality in the period of 2016 to 2020 in China.

Taken together, nanoparticles and air pollution are shown to be associated with many different cardiovascular and chronic lung diseases. In the following subsections, individual chronic lung diseases related to air pollution will be discussed in more detail.

1.2.1 Chronic obstructive pulmonary disease (COPD)

Chronic obstructive pulmonary disease (COPD) is a chronic pulmonary inflammatory disease with high mortality, usually caused by cigarette smoking. Currently it is worldwide the third common cause of death (Disease et al., 2018). As the global population is increasing in age, the morbidity and mortality of COPD is increasing proportional (Feenstra et al., 2001). COPD is characterized by lung tissue disruption and airflow limitations (Brusselle et al., 2009). The most common respiratory symptoms associated with COPD are cough, dyspnea, and production of sputum (Global initiative for Chronic Obstructive Lung Disease, 2020). The main reason for mucus excess affecting chronic bronchitis is impaired mucus elimination originated of poor ciliary clearance as well as mucus overproduction by goblet cells (Kim and Criner, 2013).

A pathological characteristic of COPD is destruction of parenchyma (emphysema formation), which is described and observed at the anatomical level by the destruction of alveolar walls in the alveolar sacs/ducts, with an abnormal increase in size of distal airways (Snider, 1985). This damage not only lead to a loss of lung elasticity with collapsed airways (Rennard et al, 2006), but the emphysema mainly causes a detrimental reduction of respiratory surface area required for gas exchange (Saetta, 1999).

Another hallmark is the chronic obstruction of the airways with progressive reductions in spirometry measures such as forced expiratory volume in 1 second (FEV₁) over time (Lange et al., 2015). Chronic bronchitis, with an obstructive ventilation pattern is described by the ratio of FEV₁ to forced vital capacity (FVC) lower than 70% (Snider, 1985). COPD has four severity stages defined on airflow limitation calculated by the ratio of FEV₁/FVC (Mannino et al., 2006). Additionally different methods can be used to diagnose the disease. One method is the diffusion capacity for carbon monoxide

(DLCO) (Viegi et al., 1990). In COPD, the diffusion capacity declines with the severity of the emphysema (Weinreich et al., 2015; Balasubramanian et al., 2019). Another method to diagnose changes in the lung morphology are computer-assisted tomography (CT) as well as X-ray based scans of the patient's chest (Kolodziej et al., 2017).

Chronic exposure of cigarette smoke induces inflammatory cells recruitment to the lungs, like innate immune cells (neutrophils, monocytes and macrophages) and adaptive immune cells (B- and T-lymphocytes) (Barnes et al., 2003; Hogg, 2004). Inducible bronchus-associated lymphoid tissue (iBALT) formations have been described in lungs of COPD *in vivo* models (D'hulst et al., 2005; van der Strate et al., 2006, John-Schuster and Hager et al., 2014; Conlon and John-Schuster et al., 2020; Günes Günsel, Conlon and Jeridi et al., 2022). These formations are highly organized ectopic lymphoid follicles and referred as tertiary lymphoid organs. They have structural similarities to secondary lymphoid organs with distinct B-cells and T-cell areas, germinal centers and high endothelial venules (Aloisi and Pujol-Borrell, 2006; Carragher et al., 2008; Motallebzadeh et al., 2012). It has been described that cigarette smoke induces macrophage activation in iBALT, which contribute to emphysema development (John-Schuster and Hager et al., 2014).

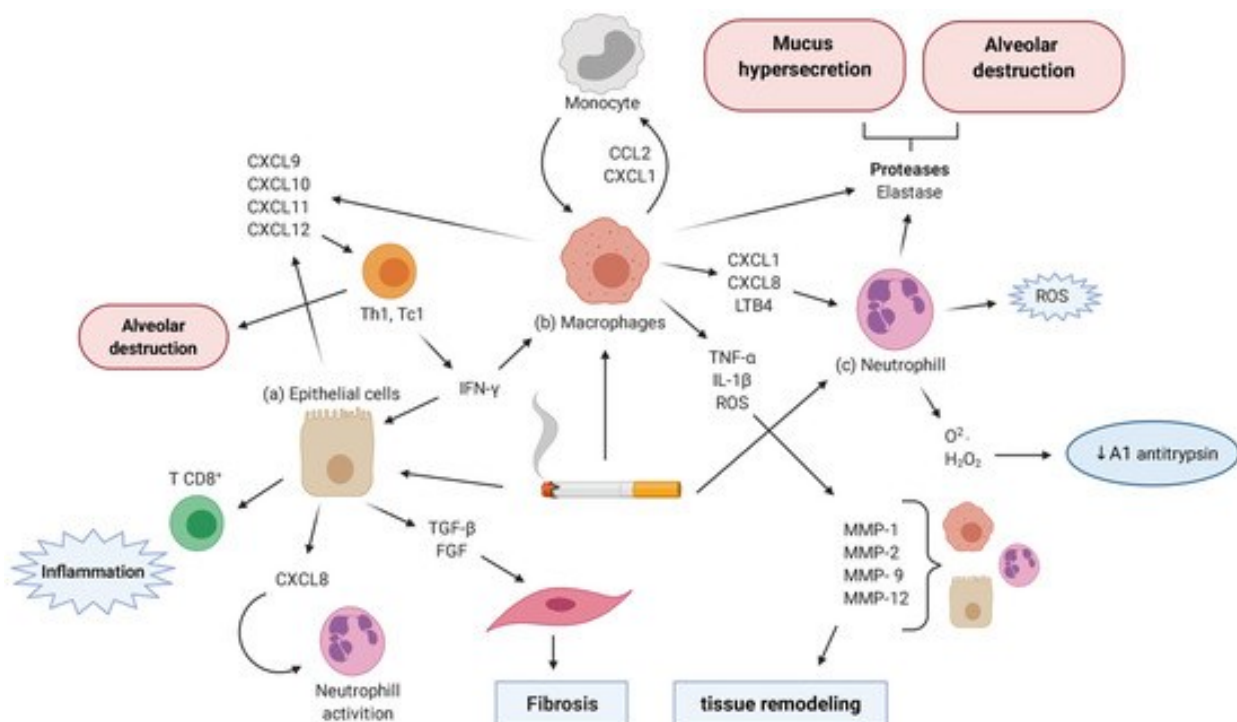


Figure 1.3 Cigarette smoke exposure contributes to COPD progression.

Cigarette smoke exposure leads to the recruitment of inflammatory cells and release of inflammatory mediators, which can induce exacerbation in COPD (adapted from Rodrigues et al., 2021).

Respiratory tract infections, both viral and bacterial, are major causes of acute exacerbation of COPD. Mohan et al. (2010) found 34% of acute exacerbations of COPD were induced by respiratory viral infections, with geographical variations in viral prevalence. With influenza virus mostly common in Asia, while picornavirus was more common in Europe, Australia and North America (Mohan et al., 2010). Compared to non-infected acute exacerbations, those with virus infection showed more severe clinical outcome, with longer hospitalization, deterioration of lung function and worse hypoxemia (Mohan et al., 2010).

COPD is a progressive disease caused among others by inhalation of air pollutant emissions, toxic gases and tobacco smoking (Mathers and Loncar, 2006; GOLD, 2021; Senior et al., 1998; Labaki and Rosenberg, 2020; Halpin et al., 2019). Cigarette smoke is the major known cause of emphysema development (Cosio Piqueras and Cosio, 2001). The molecular mechanism underlying emphysema and its persistence despite cigarette smoking is getting revealed over the years. Inoue and colleagues (2010b, 2011) found carbon black can exacerbate pulmonary inflammation and emphysema in mice, depending on particle size and dose. Furthermore, nano-sized CB was found to accumulate in dendritic cells (DCs) of lungs from emphysema patients and in mouse CD11c positive antigen presenting cells (APCs) exposed to smoke (You et al., 2015). Experimentally, carbon black caused sterile lung inflammation, DNA double strand breaks and emphysema in mice, implicating the danger of carbon black in non-smokers (You et al., 2015).

In summary, nanoparticle exposure is a risk factor for emphysema development and playing a role in worsening and disease progression. In addition, COPD patients may have higher susceptibility to environmental factors such as air pollutants.

1.2.2 Asthma

Asthma is a heterogeneous disease with chronic airway inflammation and variable remodeling, depending on the clinical presentation and treatment response (GINA - Global Strategy for Asthma Management and Prevention, 2015). More than 300 million

people are suffering from asthma worldwide (WHO, 2017). Asthma symptoms can change over time as well as in intensity. Common symptoms are wheezing, cough, shortness of breath and chest tightness. Expiratory airflow limitation and airway hyper-responsiveness to stimuli also vary in intensity, and airflow obstructions can get prominent in late-onset asthma (Lange et al., 1998; Porsbjerg et al., 2005). Asthma exacerbations can be stimulated by viral infections and exposure to allergens, air pollution and various drugs (Custovic et al., 2013). Different asthma phenotypes have been defined (Wenzel et al., 1999; Wenzel, 2012). A Th2-associated asthma, which consists early- and later-onset disease but usually its development is described in early childhood and has an atopic and allergic component. The modulation of Th2 cytokines and Th2 associated inflammation (Umetsu and DeKruyff, 2006; Maneechotesuwan et al., 2009) is accompanied with eosinophil infiltration. Most people with asthma have this Th2-associated asthma phenotype. Another phenotype is called non-Th2 asthma and it is an asthma subset with no Th2 immunity (Flood-Page et al., 2007; Kim et al., 2010). This non-Th2 asthma encompasses for example the neutrophilic categories, where neutrophilic asthma is defined as more than 50% neutrophils in the sputum (Hastie et al., 2020). The paucigranulocytic asthma has been defined by the absence of increased neutrophils or eosinophils, coupled with stereotypical features of asthma. And the classification of mixed granulocytic asthma when sputum eosinophils and neutrophils are increased (Simpson et al., 2006). Non-Th2 asthma is non-uniform and reflects the combination of paucigranulocytic and neutrophilic categories, and its more abundant in those with adult-onset disease (Ray and Kolls, 2017). Known triggers for neutrophilic airway infiltration include air pollution and smoking.

Furthermore, it has been reported that carbon-rich PM is able to enhance allergic sensitization (Singh, Madden and Gilmour, 2004). In addition, ultrafine carbon particle exposure before and after an allergen challenge, induces increased allergen-induced lung inflammation (Alessandrini et al., 2006, 2009, 2010). Liu et al., 2009 found air pollution like SO₂, NO₂, and PM_{2.5}, increase oxidative stress and decrease function of small airway of asthmatic children. Furthermore, it has been described that nanoparticle exposure can exacerbate allergic asthma (Inoue et al., 2005, 2007, 2009, 2010a; de Haar et al., 2006; Nygaard et al., 2009; Ryman-Rasmussen et al., 2009; Hussain et al., 2010). Co-exposure of MWCNT with house dust mite increases airway fibrosis and perivascular and peribronchial lung inflammation (Ihrie et al., 2021). Cigarette smoking is also found to be as risk factor in poor asthma control and airway

pathology and reduces the sensitivity to corticosteroid treatment (Thomson and Chaudhuri, 2009; Thomson et al., 2004).

Overall, it is already known that air pollution plays a crucial role in asthma exacerbation and that allergic individuals may be more susceptible to particle exposure, so air pollution must be considered as an important factor in disease progression.

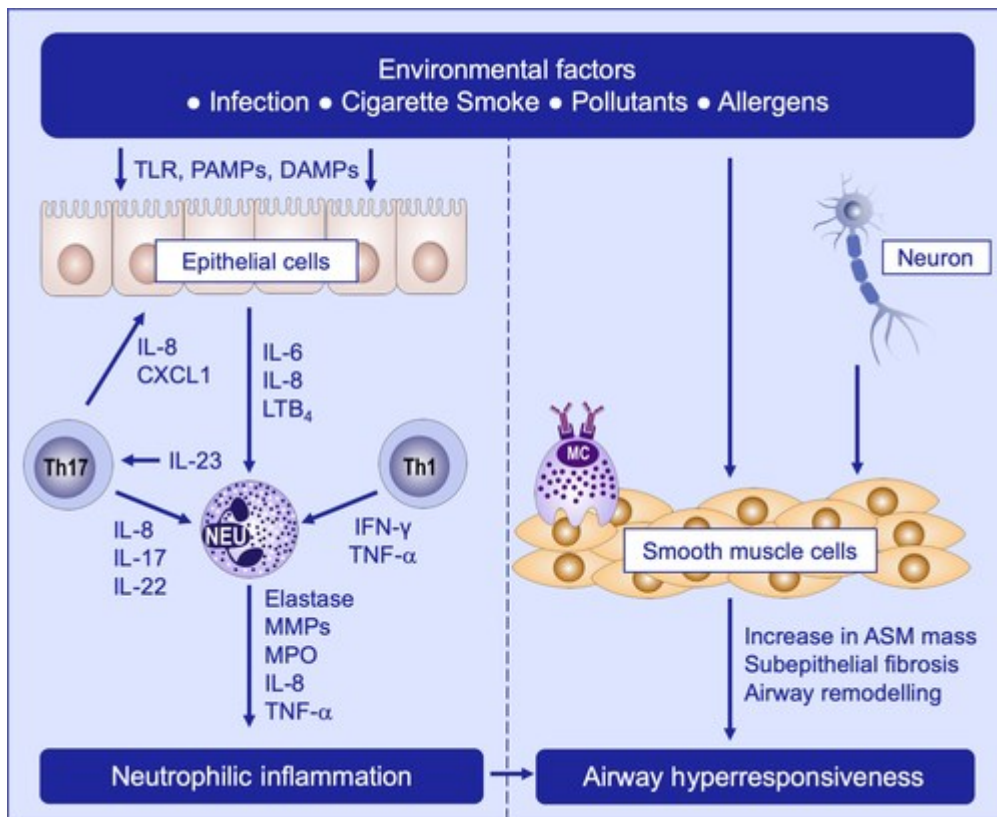


Figure 1.4 Environmental factors trigger mechanism of non-Th2 asthma exacerbation

Neutrophilic inflammation and airway hyperresponsiveness. Airway epithelium induced by virus infection or air pollutants (adapted from Sze et al., 2019).

1.2.3 Idiopathic Pulmonary Fibrosis (IPF)

Idiopathic pulmonary fibrosis (IPF) is a chronic, progressive interstitial lung disease which is characterized by an excessive deposition of extracellular matrix proteins in the lung intersitium, leading to the destruction of the lung structure and function. IPF occurs primarily in patients over 50 years with an estimated prevalence of 10 to 20 per 100,000 people in Europe and in the United States (Coultas et al., 1994; Raghu et al., 2016; Ley et al., 2013; Nalysnyk et al., 2012) and more in current or former cigarette

smokers (Baumgartner et al., 1997). IPF is a fatal disorder with a median survival of 3-5 years (Sauleda et al, 2018; Lederer and Martinez, 2018).

IPF is based on the dysregulated wound healing response in the lung (Betensley et al., 2016). Fibroblasts are mesenchymal cells and essential in facilitating and maintaining a structured extracellular matrix (ECM). After wound healing, epithelial cells get activated and the epithelial-mesenchymal signaling induce the activation of fibroblasts as well as their migration and differentiation into myofibroblasts and remodeling of ECM (Tager et al, 2008). One main paradigm of the disease pathophysiology is the aberrant interaction between fibroblasts and epithelial cells or abnormal epithelial-mesenchymal transition, which lead to uncontrolled activation of myofibroblast and deposition of ECM (Selman et al., 2001; Noble, 2008; Chang et al., 2012).

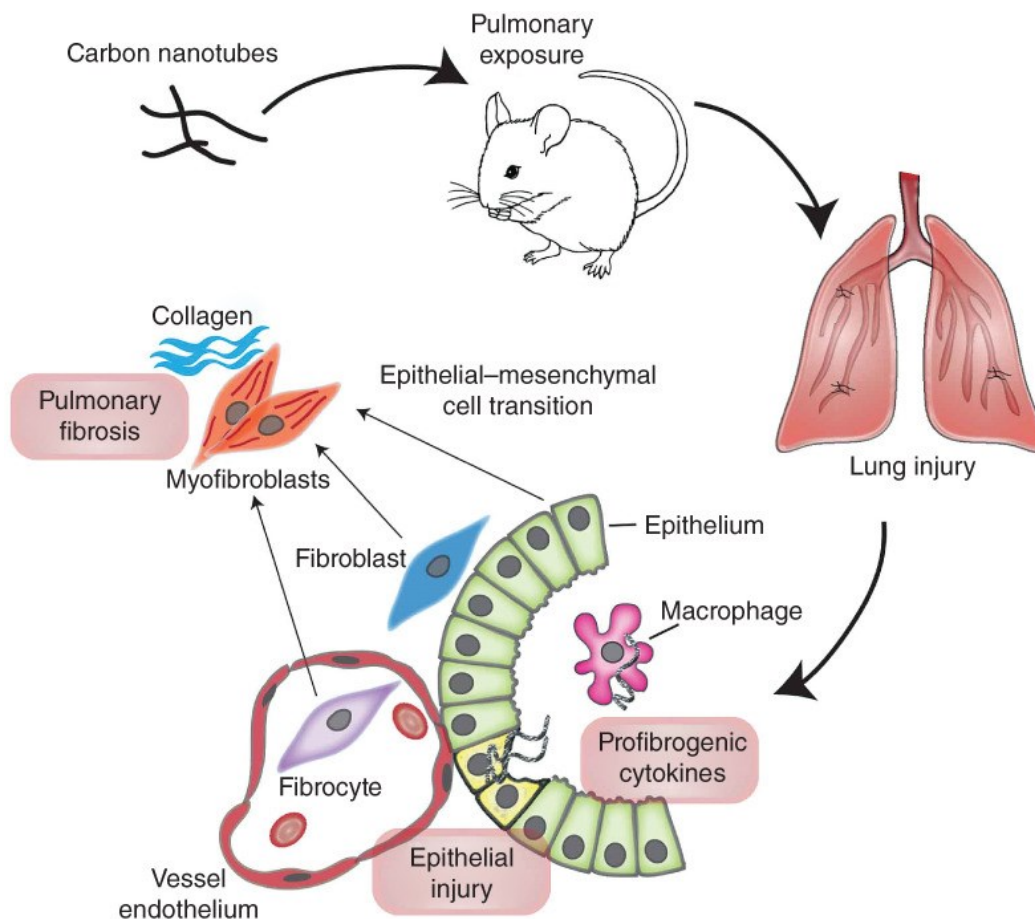


Figure 1.5 Carbon nanotube-induced pulmonary fibrosis

Engineered nanomaterials like carbon nanotubes exposure to the lungs, drives the development of pulmonary fibrosis in rodents (adapted from Duke and Bonner, 2017).

Proinflammatory cytokines have been increased such as TNF- α and IL-8 in IPF patients lungs (Carre et al., 1991; Parra et al., 2007). But also the dysregulation of M2

macrophages, Th17 and CD8+ T-lymphocytes were found to promote fibrosis (Shenderov et al., 2021).

However the fundamental disease processes involved in IPF progression is not fully understand, but the chronic or repetitive damage to the alveolar epithelium is clearly important (Sauleda et al., 2018; Raghu et al., 2011).

Air pollution is associated with telomere shortening which is a known factor to be related with aging and the susceptibility to IPF (Zhao et al., 2018; Alder et al., 2008; Armanios, 2011; Tomos et al., 2020) and long-term exposure to increased air pollutants is associated with increased risk of acute exacerbation in IPF patients (Tomos et al., 2021).

PM_{2.5} were found to increase the risk of IPF in human and has also shown to induce lung injury and IPF in mice (Yang et al, 2020). Additionally, CB was found to increase inflammatory response of bleomycin-induced lung inflammation in the numbers of inflammatory cells in BAL fluid and cytokine release as well as expression of an indicator of oxidant injury (Kamata et al., 2011).

Furthermore, engineered nanomaterials and particular carbon nanotubes were found to be a driver in the development of IPF, due to their length, rigidity, aggregation status and surface charge (Duke and Bonner, 2017), and one pathway might be their ability of activating TGF- β 1 signaling and myofibroblast differentiation (Dong and Ma, 2017).

1.2.4 Lung cancer

Air pollution and other environmental factors are known to cause pulmonary cancer (Christiani, 2021). Also, Pope and colleagues (2011) already described ambient air pollution and cigarette smoke is associated with lung cancer. Cigarette smoke is predominantly associated with lung cancer. However, a minority of patients have never smoked. Several factors found to be associated with lung cancer in never smokers including genetic susceptibility, secondhand smoke, indoor air pollution, occupationally exposure and PM_{2.5} level changes among others (Rivera and Wakelee, 2016). Also, Tseng and colleagues (2019) assume PM_{2.5} air levels affect adenocarcinoma lung cancer in around 50% of patients never smoked.

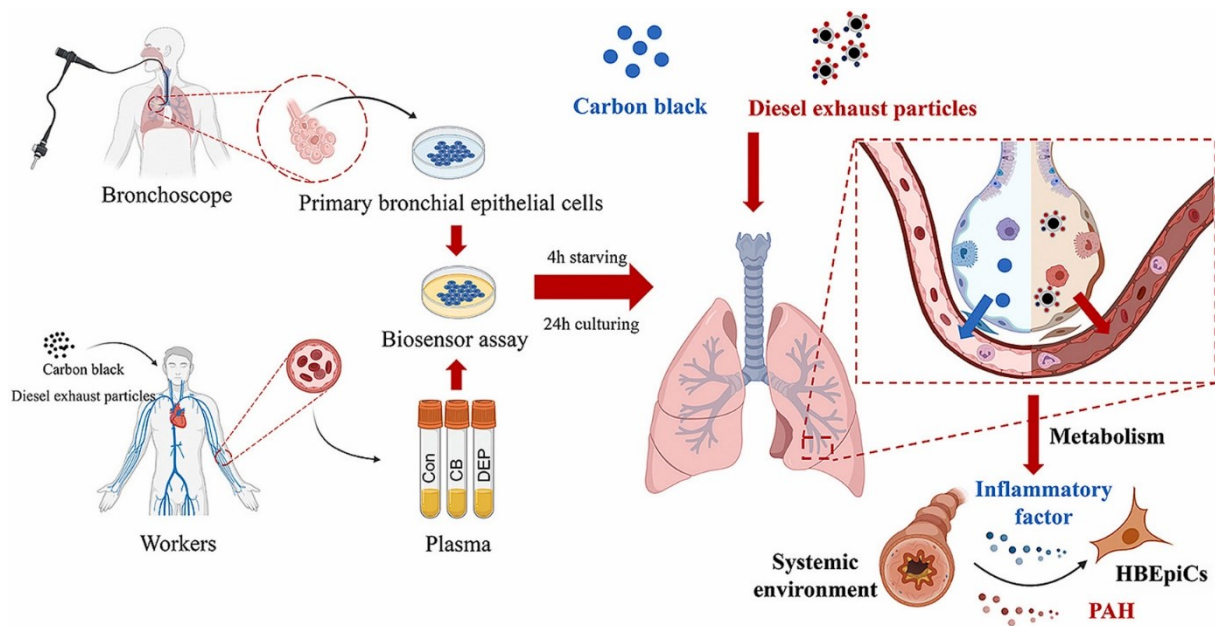


Figure 1.6 Carbon black and diesel exhaust trigger lung cancer.

(adapted from Zhang et al., 2022a).

The synthetic carbon material multi-walled carbon nanotube (MWCNT) is described for similarities to asbestos and asbestos-like pathogenicity (Poland et al., 2008; Murphy et al., 2012) indeed including mesothelial carcinogenesis in mice and rats (Takagi et al., 2008; Sakamoto et al., 2009; Nagai et al., 2011; Toyokuni et al., 2013). Diameter and particle rigidity are critical for mesothelial cell inflammation and injury and cancer development (Nagai et al., 2010, 2011, 2012; Toyokuni et al., 2013; Jiang et al., 2012). CNT exposure and inflammation were associated with tumorigenesis during chronic stage of exposure, for instance the exposure of long MWCNT over 15 μm resulted in chronic pulmonary inflammation and mesotheliomas in the pleura (Chernova et al., 2017; Dong and Ma, 2019).

In Denmark, increased respiratory and lung cancer mortality were robustly associated with elemental carbon and mineral dust concentration estimated and assessed with air pollution model (Raashou-Nielsen et al., 2022). Tseng and colleagues (2019) assume $\text{PM}_{2.5}$ air levels affect adenocarcinoma lung cancer in around 50% of patients which have never smoked.

In summary, air pollution and engineered nanomaterial exposure are known to induce or exacerbate lung cancer.

1.3 Virus Infection, Air pollution and Chronic Lung Diseases

Not only air pollution has been described to play an essential and critical role in the development and exacerbation of chronic lung diseases, also, respiratory virus infections are well known key factors in disease progression. Additionally, the co-stimulation of air pollutants and virus infections can worsen pulmonary diseases.

Ma et al., 2022 found increased higher risk susceptibility of flu infection with Influenza A and B when coexisting with main pollutants including NO₂, Ozone and particulate matters in Shenzhen, China. Epidemiological studies suggested recently that air pollution exposure is associated with increased severe acute respiratory coronavirus-2 (SARS-CoV-2) infection cases and COVID-19-associated mortality. But not only SARS-CoV-2 was described to be associated in hospitalizations, clinical visits and disease severity with air pollution. Also, measles, mumps, rhinovirus and respiratory syncytial virus (RSV) have been found to be in association (Karr et al., 2006; Karr et al., 2019; Fukuda et al., 2011; Silva et al., 2014; Pan et al., 2014; Chen et al., 2017a; Feng et al., 2016; Hwang et al., 2002; Lin et al., 2005; Peel et al., 2005; Liang et al., 2014; Martins et al., Le et al., 2012; Wong et al., 2009; Croft et al., 2019; Vempilly et al., 2013; Pan et al., 2016; Horne et al., 2018; Greenburg et al., 1967; Su et al., 2019; Liu et al., 2019; Carugno et al., 2018; Chen et al., 2017b; Hao et al., 2019).

Respiratory viruses are described to exacerbate asthma, COPD, IPF and cancer (Simoes et al., 2010; Jartti et al., 2009; Turunen et al., 2016; Ko et al., 2016; George et al., 2020; Fu et al., 2022b).

1.4 Herpesviruses

1.4.1 Herpesvirus life cycle and pathogenesis

The viruses in the family of herpesviruses (*herpesviridae*) are enveloped viruses with large double-stranded DNA genome, which vary from size 125 to 240 kilobase pairs. Packed in the virions, the genome is in a linear form, which becomes circulated once it enters the nucleus (Warden et al., 2011). The virus members of the *herpesviridae* family are defined into three categories are based on their genetic organization, host range and replication strategies (Whitley, 1996). The categories are alpha (α), beta (β), and gamma (γ) herpesviruses. Examples for α -herpesviruses are varicella zoster virus

(VZV) and herpes simplex virus (HSV) 1, 2, examples for β -herpesviruses are cytomegalovirus (CMV), human herpesvirus (HHV)-6 and 7, while examples for γ -herpesviruses are Human herpesvirus 8 (HHV8 – also called KS-associated herpesvirus (KSHV)) and Epstein-Barr virus (EBV). Every human become infected with at least one herpesvirus during the time of their life (Boshoff and Weiss, 2001; Virgin et al., 2009; Sehrawat et al., 2018). EBV infects at least 90% of population worldwide before the age of 30 (Venkitaraman et al., 1985; de-The et al., 1975; Levin et al., 2010) and typically causes infectious mononucleosis. But EBV infection also can cause malignancies, including Hodgkin's or Burkitt's lymphoma or other lymphoproliferative diseases (Balfour et al., 2013; Dunmire et al., 2015; Heslop, 2020; Murray and Young, 2019). KSHV is known to play a role in the development of B-cell primary effusion lymphoma, multicentric Castleman's disease and body cavity-based B-cell lymphoma (Chang et al., 1994; Ganem, 2005).

Herpesviruses are particular interesting for the interplay between virus and its host, because of their long-term persistence or lifelong latency, following after primary infection (Taylor et al., 2015). In the latent phase, the expression of most viral peptides is usually at very low levels. However, latency can be interrupted by stress responses during clinically asymptomatic episodes (Stevens, 1989; Kelly et al., 2006; Upal et al., 2014). γ -Herpesviruses like EBV are known to establish latency in macrophages, dendritic cells and B cells (Klein et al., 1989; Slobedman and Mocarski, 1999; Kelly et al., 2006; Khirallah et al., 2017).

The acute gammaherpesvirus infection has been described to be controlled by T-lymphocyte immunity. CD8⁺ T-lymphocyte response is important to control the acute herpesvirus infection (Ehtisham et al., 1993), whereas the control of latent infection is maintained by a collaborative endeavor of CD4⁺ and CD8⁺ T-lymphocytes B-lymphocytes and IFN- γ signaling (Stevenson et al., 1999).

Infection with gamma herpesvirus EBV is suggested to cause chronic epithelial injury which may contribute to the progression of IPF, as herpesvirus DNA has been found in the lungs of IPF patients more frequently compared to healthy controls (Stewart et al., 1999).

Previous work in our research group showed that the murine gamma herpesvirus-68 can be reactivated in the lungs after pulmonary exposure to CNP, DEP and DWCNT

Introduction

and thereby restore molecular pattern similar to that investigated during acute virus infection (Sattler et al., 2017).

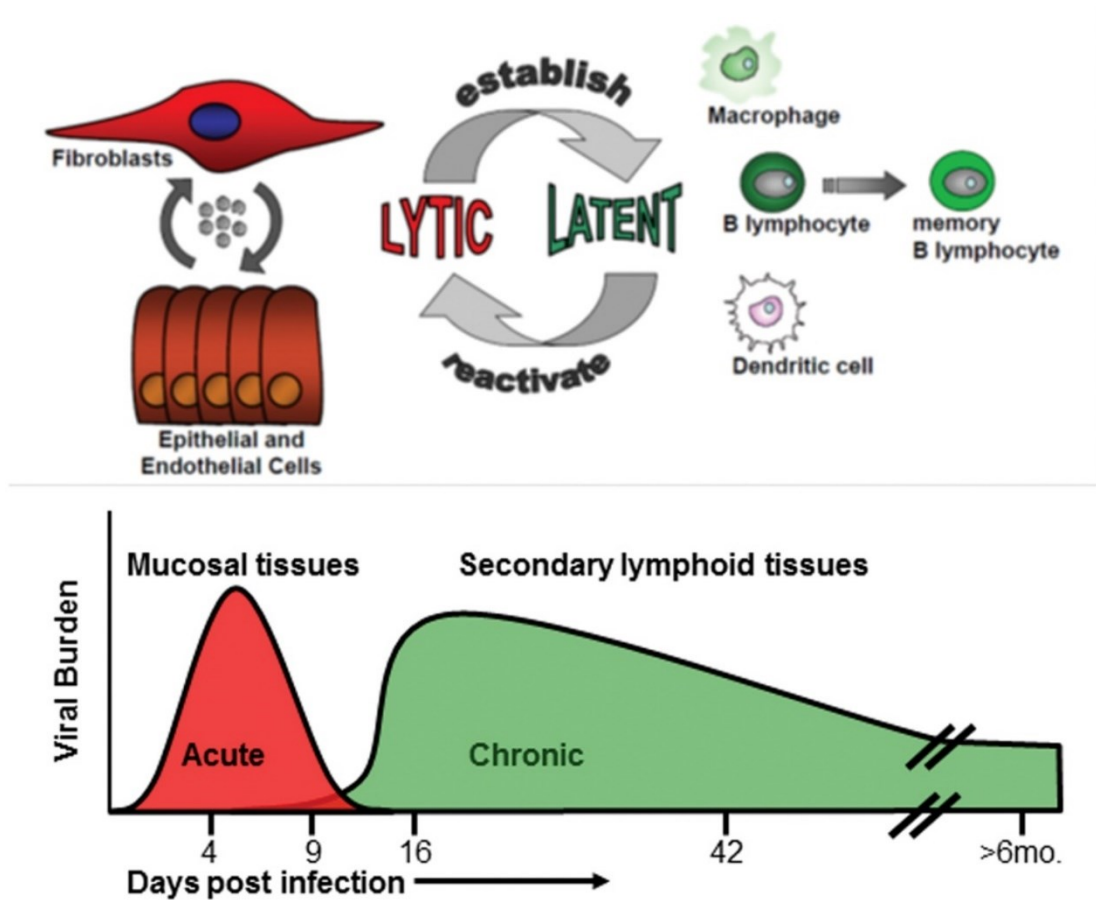


Figure 1.7 Latent and lytic infection course of MHV-68 in mice.

Acute virus infection happens mainly in epithelial cells with high viral burden in mucosal tissue. This acute infection peaks after 6 days and latency establishment start after 12 days mainly in macrophages, B-lymphocytes and dendritic cells. (adapted from Cieniewicz et al., 2016)

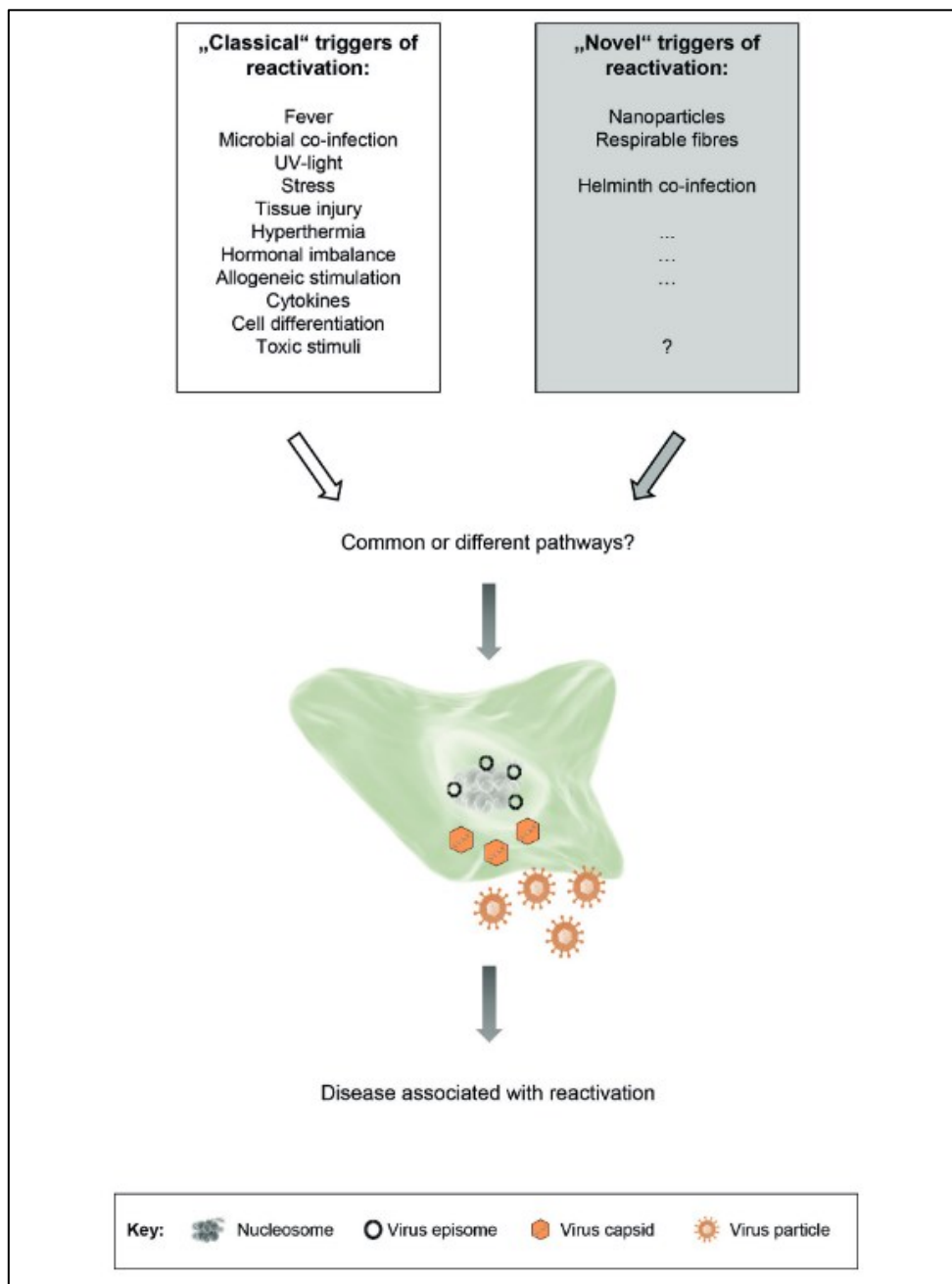


Figure 1.8 Classical and novel triggers can reactivate latent herpesvirus.
(adapted from (Stoeger and Adler, 2018))

However, several different stimuli have been described to reactivate latent herpesvirus infection to its lytic infection phase as for example by activation of the immune system (Hwang et al., 2008; Sunil-Chandra et al., 1994; Yarilin et al., 2004), Stoeger and Adler (2018) described “classical” and “novel” triggers for herpesvirus reactivation (**Fig. 1.6**). For instance, classical triggers are local tissue injuries, systemic, physical or emotional

stress, fever, microbial co-infections as well as UV light, hormonal imbalance, in condition of immunosuppression or cell differentiations (B-lymphocyte differentiation into plasma cells or monocyte differentiation into macrophages or dendritic cells). (Roizman and Whitley, 2013; Liu et al., 2013; Dupont and Reeves, 2016; Liebermann, 2016; Murata, 2014). Novel triggers described for herpesvirus reactivation are helminth co-infections, carbon nanoparticle exposures and engineered fiber shaped carbon nanotube exposures to the lungs (Reese et al., 2014; Reese, 2016; Sattler et al., 2017).

1.4.2 Murine gammaherpesvirus-68 (MHV-68) as a mouse model

To study human gammaherpesvirus infection and its pathogenesis and reactivation, murine gammaherpesvirus 68 (MHV-68) can be used as a robust mouse model.

MHV-68 is genetically highly related to EBV or KSHV and accordingly shares a lot of features with these viruses (Aligo et al., 2014).

Like all gammaherpesviruses, also MHV-68 express the replication and transcriptional activator gene (RTA) or open reading frame 50 (ORF50) (Staudt and Dittmer, 2007). This is required for lytic virus replication as well as for reactivation through DNA binding or protein-protein interactions (Speck and Ganem, 2010; Wu et al., 2000). Leading ORF50 to the marker for lytic viral gene expression.

In the same time, γ -herpesviruses also continuously express few genes during latent infection, which generally help the virus to persist in the infected host. One of those genes is latency-associated nuclear antigen (LANA) for KSHV and open reading frame 73 (ORF73) for MHV-68. These genes are necessary to establish and maintain the latent infection phase (Barton et al., 2011; Wen and Damania, 2010). The ratio between ORF50 and ORF 73 can thus be used to define different phases of MHV-68 infection with increasing ration in virus reactivation and lytic viral gene expression.

Acute infections in the lungs with gammaherpesvirus can cause bronchiolitis (Nash et al., 2001; Sunil-Chandra et al., 1992). Later the virus spreads from the lungs to the lymph node and persists in B-lymphocytes, dendritic cells and macrophages (Barton et al., 2011; Sunil-Chandra et al., 1992; Weck et al., 1996, 1999).

Overall, MHV-68 can be used as a mouse model to study the effects of gammaherpesvirus infection on the lung, which resembles human gammaherpesvirus infection in humans. Epstein-Barr virus (EBV), a human gammaherpesvirus infecting

up to 95% of adults worldwide (Jha et al., 2015), thus omnipresent in human population.

1.5 Aim of the study

In a previous study, colleagues in our group discovered nanoparticle-triggered latent virus reactivation in the lungs of latent MHV-68 infected mice, thereby restoring the acute virus expression pattern after CNP and DWCNT exposure (Sattler et al., 2017). However, we don't know how and whether this reactivation is able to contribute to development or exacerbation of chronic lung disease in a mouse model of repeated nanoparticle dosing, a situation similar to ambient exposure scenarios.

Little is known about latent virus infection and particle exposure as a co-challenge in the lung potentially leading to worsening of chronic lung diseases and other comorbidities like cardiovascular diseases. To address this knowledge gap, this study is focused on latent gamma herpesvirus 68 (MHV-68) reactivation in mice lungs following at least two times repeated CNP exposure. In addition, the role of viral reactivation and subsequent activation of the immune system to the exacerbation of chronic lung disease and systemic inflammatory responses which might lead to extra-pulmonary comorbidities will be investigated.

Thus, in this study, I aim to better understand their differences between the known particle triggered inflammatory response in the lungs, and that under conditions of gammaherpesvirus latency, as to which type of cells get recruited to the lungs and which cytokines and chemokines are altered in expression and release. Additionally, I investigate whether and how lung epithelial cells get affected by the infection and the particle treatment, also on a structural level by stereological investigation of the alveolar air space as indicator of emphysema, and tissue remodeling for fibrosis.

Additionally, I aim to establish an *in vitro* inhalation system, in collaboration with aerosol specialist to test environmental relevant particles emission on their potential to trigger the reactivation of latent virus in lung cells, growing on air liquid interface.

2. Materials and Methods

2.1 Materials

2.1.1 Nanoparticles

Nanoparticles used for this study:

For *in vitro* and *in vivo* testing, carbon black was used. These particles are spherical shaped and used in research as a surrogate for combustion derived carbon nanoparticles. Carbon black is also called carbon nanoparticles (CNP) and the product name is Printex90. It is purchased from Degussa, Frankfurt, Germany.

In *in vivo* testing, double walled carbon nanotubes (DWCNT) were used. They are fiber shaped and are engineered particles. The abbreviation is DWCNT and are purchased from Nanocyl, Auvelais, Belgium.

2.1.2 Mice

Wildtype C57BL/6N mice were purchased from Charles River Laboratories (Sulzfeld, Germany). 10 weeks old female mice were used in all experiments. The mice were bred under specific pathogen free conditions in individually ventilated cages (IVC) with a constant temperature and humidity with 12-hours light cycle in accordance with Helmholtz Zentrum Muenchen institutional, state and federal guidelines.

2.1.3 Chemicals and Reagents

Substance	Company
Absolute ethanol	Sigma Aldrich
Acetic Acid	Merck Millipore
Acrylamide/Bis Solution 30%	Bio-Rad
Ammonium persulfate (APS)	Sigma Aldrich
β -Mercaptoethanol	Sigma Aldrich
Blot Stripping Buffer	Thermo Fisher Scientific

Bovine Serum Albumin (BSA)	Sigma Aldrich
Dakopen for histology	Dako
4',6-Diamidin-2-phenylindol (DAPI)	Sigma Aldrich
Dimethyl sulfoxide (DMSO)	Sigma Aldrich
20 x 4dNTP mix 10 mM each NTP	Carl Roth
10 x DTT	Carl Roth
ECL™ Western Blotting Detection Reagents	GE Healthcare Life Science
EDTA buffer, pH 9.0	Roche Diagnostics
Ethanol	Carl Roth
Entellan	Merck Millipore
Eosin	Sigma Aldrich
Fluorescence Mounting Medium	Dako
Formaldehyde	Thermo Fisher Scientific
Giemsa stain	Sigma Aldrich
Glycin	Carl Roth
Halt Protease & Phosphatase Inhibitor-Cocktails	Thermo Fisher
HCl 32%	Thermo Fisher
Hematoxilin Solution Gill No.2	Sigma Aldrich
H ₂ O ₂ (30%)	Sigma Aldrich
H ₂ SO ₄ (2N) Stop solution ELISA	Fulka Biochemika
KCl	Merck Millipore
KH ₂ PO ₄	Merck Millipore
4 X Laemmli buffer	Bio-Rad
LDH standard	Roche
May-Grünwald stain	Sigma Aldrich
Methanol	Merck Millipore
Sodium chloride powder (NaCl)	Carl Roth
NaCl 0,9% (liquid)	Braun
Na ₂ HPO ₄	Sigma Aldrich

Materials and Methods

Normal goat serum	Thermo Fisher
Normal mouse serum	Thermo Fisher
Normal rabbit serum	Thermo Fisher
PageRuler Prestained Protein Ladder	Bio-Rad
Paraformaldehyde (PFA)	Alfa Aesar
Phalloidin-555	Invitrogen
Pluronic 10% (F-127)	Sigma Aldrich
Proteinase K 200 µg/mL	Sigma Aldrich
PureSeptA	Schülke
Random Nonamers	Metabion
RNase free	Bela-pharm
RNase Out Inhibitor 40 U/µL	Invitrogen
Rodent block M	Biocare Medical
Roti-Quick	Carl Roth
Sodium dodecyl sulfate (SDS) – solution 10 %	PanReac AppliChem
Sodium Deoxycholate	Sigma Aldrich
Superscript II RT 200 U/µL	Invitrogen
SuperSignal™ West Femto Maximum Sensitive Substrate	Thermo Fisher Scientific
SYBR Green Master Mix	Thermo Fisher Scientific
TEMED	Bio-Rad
Tetramethylbenzidine (TMB) for ELISA	Sigma Aldrich
Trichostatin A	Sigma Aldrich
Tris	Carl Roth
Triton-X-100	Sigma-Aldrich
TRIzol™	Thermo Fisher Scientific
Trypan Blue Stain	Sigma-Aldrich
Tween-20	Sigma-Aldrich

2.1.4 Buffers and Stock Solutions

Buffers and Solutions	Company/Ingredients
Antibody Diluent (cell staining)	5 % BSA 0.01 % Triton X-100 In PBS
Antibody Diluent (histology)	1 % BSA 0.3 % Triton X-100 In PBS
5 x First Strand Buffer (cDNA)	Invitrogen
1.8% of H ₂ O ₂ solution	6 mL of 30% H ₂ O ₂ , 14 mL of dH ₂ O, 80 mL of 100% methanol
HIER Citrate Buffer pH 6,0 (10 x)	Zytomed Systems
HIER EDTA Buffer pH 8,0 (10 x)	Zytomed Systems
H ₂ O ₂ -Methanol solution (ICH)	6 mL 30% H ₂ O ₂ 14 mL distilled water 80 mL Methanol
IF Blocking solution (histology)	5 % normal goat serum 0.3% Triton X-100 In PBS
IF Blocking solution (cell staining)	5 % BSA 0.1% Triton X-100 In PBS
1 x Laemmli Sample Buffer	10 µL of β-mercaptoethanol and 90 µL of 4 X Laemmli buffer
10 x PBS	Biochrom
10 x PBS	80 g NaCl 2 g KCl 14.4 g Na ₂ HPO ₄ 2.4 g KH ₂ PO ₄

Materials and Methods

	Dissolve in distilled water Adjust to pH 7.4 Make up to 1 L with distilled water
1x PBS	100 mL 10 x PBS 900 mL distilled water
PBS-T Buffer (wash buffer)	1 % Tween-20 In PBS
Rabbit serum blocking solution	5 % normal rabbit serum 0.1 % Triton-X-100 In PBS
Reagent Diluent (ELISA)	1 % BSA in PBS 0.2 µm filtered
Restore PLUS Western Blot Stripping Buffer	Thermo Scientific
Rodent Block M (for IHC)	Biocare Medical
Roti®-Block (Western Blot)	Roth
5x Running Buffer (SDS PAGE)	15.1 g Tris 94 g Glycin 50 mL SDS 10% Make up to 1 L with distilled water
RIPA Lysis Buffer	0.877 g NaCl 1 g Sodium Deoxycholate 0.66 mL Tris pH 7.2 5 mL EDTA (from stock 100 mM) 1 mL Triton X-100 1 mL SDS 10% Make up to 100 mL with distilled water
Tris-EDTA Buffer (100 x)	Fulka Biochemika
10 x Transfer Buffer (Western Transfer)	24.2 g Tris 112 g Glycin Make up to 1 L with distilled water
1 x Transfer Buffer (Western Transfer)	100 mL 10 x Transfer Buffer 200 mL Methanol

	700 mL distilled water
TRIS Wash Buffer (20 x)	Zytomed Systems
Tris 1.5M (pH 8.8)	181.71 g Tris Dissolve in distilled water Adjust pH value to pH 8.8 Make up to 1 L with distilled water
Tris 0.5M (pH 6.8)	60.57 g Tris Dissolve in distilled water Adjust pH value to pH 6.8 Make up to 1 L with distilled water
Wash Buffer (ELISA)	0.05% Tween-20 In PBS

2.1.5 Cell culture solutions

solution	Ingredients/Company
ANA-1 growth medium	Invitrogen, GibcoTM
BAL cell medium	Invitrogen, GibcoTM
Cell proliferating reagent WST-1	Roche Diagnostics
Dispase	Invitrogen, GibcoTM
DMEM F12	Invitrogen, GibcoTM
DPBS	Invitrogen, GibcoTM
FBS Superior	Sigma Aldrich
Freezing medium for mammal cell lines	Invitrogen, GibcoTM
Entellan mounting medium	Merck
Glasgow-MEM Medium	Invitrogen, GibcoTM
16HBE growth medium	Invitrogen, GibcoTM
Ham's F-12K Medium	Invitrogen, GibcoTM
Hygromycin B	Invitrogen
LA4 growth medium	Invitrogen, GibcoTM
L-Glutamine 200mM (100X)	Invitrogen, GibcoTM
Matrigel® Matrix, growth factor reduced	Corning

Materials and Methods

Methylcellulose	Merck
MHS growth medium	Invitrogen, Gibco™
MLE-12 growth medium	Invitrogen, Gibco™
Non-essential amino acids (NEAAs)	Invitrogen, Gibco™
Penicillin Streptomycin (10,000 U/mL Penicillin, 10,000 µg/mL Streptomycin)	Invitrogen, Gibco™
RPMI 1460	Invitrogen, Gibco™
Ultra-pure water	Invitrogen, Gibco™
0.25 % Trypsin-EDTA (1X)	Invitrogen, Gibco™
0.05 % Trypsin-EDTA (1X)	Invitrogen, Gibco™
Tryptose Phosphate Broth	Thermo Fisher Scientific

2.1.6 Recombinant proteins

Recombinant protein	Company
Lipopolysaccharide (LPS)	Sigma-Aldrich
Recombinant mouse interferon gamma (rm IFN γ)	ImmunoTools
Recombinant mouse interleukin 4 (rm IL-4)	ImmunoTools

2.1.7 Antibodies

Antibodies used for immunofluorescence or immunohistological staining and western blot. Polyclonal Rabbit serum, containing antibodies against lytic proteins of MHV-68 was used to label lytic virus proteins, which was described before (Steer et al., 2010).

Antibody	Host	Dilution	Company
Primary:			
Anti-Arginase 1	Rabbit	1:600	Cell Signaling Technology
Anti-OPN	Rabbit	1:500	Assay designs
Anti-CCR2	Rabbit	1:200	Abcam

Anti-Cleaved caspase 3	Rabbit	1:200	Cell Signaling Technology
Anti-b-Actin HRP-linked		1:5,000 WB	Sigma Aldrich
Anti-GPNMB	Rabbit	1:800	Abcam
Anti-SAA3	Rat	1:1,000 WB	Abcam
Anti-IBA1	Rabbit	1:600	WAKO
Anti-MHV-68 serum	Rabbit	1:2,000	Sattler et al., 2017
Anti-MPO	Rabbit		Abcam
Anti-CD11b	Rabbit	1:3,000	Abcam
Anti-CD11c	Rabbit	1:200	Cell Signaling Technology
Anti-CD3	Rabbit	1:3,000	Sigma Aldrich
Anti-CD45R/B220	Rat	1:100	BD Biosciences
Anti-CD8a	Rabbit	1:4,000	Abcam
Anti-CXCL2	Goat		Santa Cruz Biotechnology
Anti-pro SPC	rabbit	1:3,000	Sigma Aldrich
Secondary:			
Anti-rabbit IgG Alexa Flour 647+	Goat	1:1,000	Cell Signaling Technology
Anti-rabbit IgG Alexa Flour 555	Goat	1:1,000	Cell Signaling Technology
Anti-rabbit IgG HRP- linked Antibody	Goat	1:2,000	Cell Signaling Technology
Anti-mouse IgG HRP- linked Antibody	Goat	1:2,000	Cell Signaling Technology
DAPI		1:1,000	Sigma Aldrich

2.1.8 Kits

Kit	Company
BCA assay Kit	Thermo Fisher Scientific
Bio-Plex Pro Mouse Chemokine Panel 31-Plex	Bio-Rad
Cytotoxicity Detection Kit (LDH)	Roche Diagnostics
DAB Substrate Kit, Peroxidase (HRP), with Nickel, (3,3'-diaminobenzidine)	Vector Laboratories
ELISA CCL17	R&D systems
ELISA CXCL1	R&D systems
ELISA CXCL2/MIP	R&D systems
ELISA CXCL5/LIX	R&D systems
ELISA IgM	Thermo Fisher Scientific
ELISA IL-33	R&D systems
ELISA IL-6	R&D systems
ELISA Lipocalin 2	R&D systems
ELISA MPO	R&D systems
ELISA Osteopontin1	R&D systems
ELISA SAA3	EMD Millipore
ELISA TNFa	R&D systems
Goat-on-Rodent AP Polymer	Biocare Medical
LightCycler® 480 SYBR® Green I Master	Roche
LDH assay	Roche
Masson's Goldner Trichrome staining Kit	Roth
Nucleospin RNA kit for RNA purification	Macherey-Nagel
RNeasy kit for RNA purification	Qiagen
Quant-iT PicoGreen dsDNA assay Kit	Thermofisher Scientific
Rabbit-on-Rodent AP Polymer	Biocare Medical
Rat-on-Rodent AP Polymer	Biocare Medical
RNA isolation Kit	Macherey&Nagel
RNA isolation Kit	Qiagen

TUNEL assay kit-BrdU-red	Abcam
Vulcan fast red chromogen kit	Zytomed Systems

2.1.9 Primer sequences

Target gene	Forward primer (5'-3')	Reverse primer (5'-3')
<i>Acta2</i>	GCTGGTGATGATGCTCCCA	GCCCATTCCAACCATTACTCC
<i>Actb</i>	TCCATCATGAAGTGTGACGT	GAGCAATGATCTTGATCTTCAT
<i>Ccl2</i>	TTAAAAACCTGGATCGGAACCAA	GCATTAGCTTCAGATTTACGGGT
<i>Ccl5</i>	CTGCTGCTTTGCCTACCTCT	ACACACTTGGCGGTTCTT
<i>Ccl9</i>	ATTTTCCCACCACCCTCCATC	CCCTAACAGCCCAATTTAGCC
<i>Ccl17</i>	CTCTGCTTCTGGGGACTTTTCT	AGTAATCCAGGCAGCACTCTC
<i>Ccl22</i>	TCATGGCTACCCTGCGTGTC	CCTTCACTAAACGTGATGGCAGAG
<i>Ccr4</i>	TCTACAGCGGCATCTTCTTCAT	CAGTACGTGTGGTTGTGCTCTG
<i>Ccr5</i>	ATGGATTTTCAAGGGTCAGTTCC	CTGAGCCGCAATTTGTTTCAC
<i>Igae</i>	GGGTCCTACTTTGGCTCTGT	GTGTGTGTGCCAAGGAGAAG
<i>Cd19</i>	GAACAAAGCCTGTATGTGCCCC	AAGCAGAAGAGACCCCCAAACC
<i>Cd247</i>	AGTGTCTGTTCTCGCCTGCATC	TCTGCTGTTTGCCTCCCATCTC
<i>Cd3d</i>	CTTGGGCAAAGGCGTTCTG	CAGTTCTGGCACATTTCGGTAAT
<i>Cd3e</i>	GCTGGGACATTGCTGACTCAAC	AAGGAACTGAGGCAGAGAGGAC
<i>Cd3g</i>	TTGGTACAAGTGGATGGCAGC	CCTTGACACTGATACGTGCCTC
<i>Cd4</i>	AGGTGATGGGACCTACCTCTC	GGGGCCACCACCTTGAACCTAC
<i>Cd8a</i>	CCGTTGACCCCGCTTTCTGT	CGGCGTCCATTTTCTTTGGAA
<i>Cd8b</i>	TCCTTCTACAACCTGCCCAAC	GCAGAAGCAGGATGCAGACTAC
<i>Col1a1</i>	ACGGCTGCACGAGTCACAC	GGCAGGCGGGAGGTCTT
<i>Cxcl1</i>	GCTGGGATTCACCTCAAGAA	TCTCCGTTACTTGGGGACAC
<i>Cxcl9</i>	GGAGTTCGAGGAACCCTAGTG	GGGATTTGTAGTGGATCGTGC
<i>Cxcl10</i>	ATGACGGGCCAGTGAGAATGAG	TGGGTAAAGGGGAGTGATGGAG
<i>Cxcl11</i>	GAAGGTCACAGCCATAGCCC	CTTTGTCGCAGCCGTTACTC
<i>Cxcl16</i>	AACAAAGAGCACACCCAACCC	GAGTGTACCAGAGCTGCAAACC
<i>Cx3cl1</i>	ATTGGAAGACCTTGCTTTGG	GCCTCGGAAGTTGAGAGAGA
<i>Cx3cr1</i>	CTGTTATTTGGGCGACATTG	AACAGATTTCCCACCAGACC
<i>Cxcr3</i>	CCAGCCAAGCCATGTACCTT	TCGTAGGGAGAGGTGCTGTT
<i>Cxcr5</i>	ACTCCTCTCCATCCACATCACC	CACCATCCCATCACAAGCATCG
<i>Cxcr6</i>	TGTGTTTCTGCTGAACTTGCCC	CACATGACTGTGCCAAAGACCC
<i>Fn1</i>	AATGGAAAAGGGGAATGGAC	CTCGGTTGTCTTCTTGCTC

Materials and Methods

<i>Gpmb</i>	AGAAATGGAGCTTTGTCTACGTC	CTTCGAGATGGGAATGTATGCC
<i>Gzmk</i>	GCCCACTGCTACTCTTGGTTTC	ACCTGGCATTGTTGGTCCCATCTC
<i>Gzmm</i>	AGAAAGCCCCGATCCAAGC	AAGCGGCTGTTGTTACACATT
<i>Hprt</i>	GTTGGATACAGGCCAGACTTTGT	CACAGGACTAGAACACCTGC
<i>Ifng</i>	AAAGAGATAATCTGGCTCTGC	GCTCTGAGACAATGAACGCT
<i>Klrd1</i>	ATGCTGTGTTTGCCTGGACAA	GCTCTGGCCTGATAACTGAGAAT
<i>Klrg1</i>	GGCTCACATCTCCTTACATTTCC	CAAGCCGATCCAGTAAAAGTCC
<i>Il4</i>	GGCATTGGAACGAGGTCAC	AAATATGCGAAGCACCTTGG
<i>Il6</i>	TAGTCCTTCCTACCCCAATTTCC	TTGGTCCTTAGCCACTCCTTC
<i>Il7r</i>	AAAGTCGATCCATTCCCCAT	CCATCCTCCTTGATTCTTGGGT
<i>Il10</i>	CCAAGCCTTATCGGAAATGA	TTTTCACAGGGGAGAAATCG
<i>Il12b</i>	TTGAACTGGCGTTGGAAGCAC	TCTTGGGCGGGTCTGGTTTG
<i>Mmp2</i>	TGGCACCACCGAGGACTATG	GTTGCCCAGGAAAGTGAAGGG
<i>Mmp9</i>	CTATTCGGCCTGCACCACAG	CTTCTCCGTTGCCGTGCTC
<i>Mmp12</i>	CAATTGGAATATGACCCCCTGT	AGCAAGCACCCCTTCACTACAT
<i>Muc5ac</i>	GTCTCCACGTCACAGTAGT	CTGAAGGTGGATGACCAG
<i>Orf50</i>	GGAATTTCTGCAGCGATGGCCTCT	CCTCTTTTGTTCAGCAGAGACTC CA
<i>Orf73</i>	CTGGACTCCTCATCACCTT	TGTCTGAGCGTCTTCCAC
<i>Retnla</i>	GCTAACTATCCCTCCACTGTAACG	CAAGCACACCCAGTAGCAGTC
<i>Saa3</i>	GAAGCTGGTCAAGGGTCT	GTCAGCTCTTGAGTCCTC TG
<i>Spp1</i>	AGCTCAGAGGAGAAGCTT	CTTCAGAGGACACAGCAT
<i>Tff2</i>	GCCCAGGTCCAGTGGAG	GAACCTTCTTCTGGCTTGCAG
<i>Tgfb</i>	GACTCTCCACCTGCAAGACCA	GGGACTGGCCGAGCCTTAGTT
<i>Thy1</i>	GTCATTCTCAGCCACCACACAC	TACCCCTTTCCCATCATTCCC
<i>Tnf</i>	CACCACGCTCTTCTGTCT	GGCTACAGGCTTGTCACTC
<i>Tnfrsf25</i>	GGCTGGTGTGTTGACTGCT	GTTGGAGCCTCATGGACTGG
<i>Wfdc17</i>	CCAGAGCCAACATGAAGAC	CACAGCTATTGCTACAGCAC

2.1.10 Equipment and General Consumables

Equipment Name	Company
ALICE chamber (commercial)	Vitrocell
ALICE chamber (Prototype)	Lab made in the Institute of Lung Health and Immunity at Helmholtz center Munich

Autoclave machine	Systec
Brightfield Microscope	Olympus
Bioruptor Probe sonication	Diagenode SA
Cannulas	Braun
Centrifuge 5430	Eppendorf
Centrifuge universal 32R	Hettich
Centrifuge 1k15	Sigma Laborzentrifugen
Centrifuge	Eppendorf
Cell culture T75, T150 flasks	Greiner Bio-One
Cell culture incubator	Thermo Fisher Scientific,
Cell culture workflow – HERA Safe KS	Thermo Fisher Scientific
Cell scraper	Sarstedt
Chemical workflow hood	Köttermann
ChemiDoc XRS+	Bio-Rad
Confocal Microscope	Zeiss
Cover Slips 24x50mm	Menzel-Gläser
Cuvettes for Mastersizer analysis	Brand
Cytospin Centrifuge	Shandon, PA
Decloating chamber	Biocare Medical
Easypet® automatic pipette	Eppendorf
Einbettmaschine	Thermo Scientific
Falcon Tubes (15 mL, 50 mL)	Corning Science
Fluorescence Microscope	Olympus
Glass plates for SDS Gel	Bio-Rad Laboratories
Gloves	Kleenex Kimtech
Gloves	Nitril NextGen
Glass bottle (5 mL) and lid for nanoparticle preparation	Carl Roth
Histological cassette	Leica Microsystems GmbH
Ice machine	Buchner Labortechnik
Light Cyclor 480	Roche
Luminex 200	Luminex Corporation
Mastersizer 2000 Laser Particle Size Analyzer	Malvern

Materials and Methods

Micro-Dismembrator S	Sartorius
Microscope Axiovert 135	Zeiss
Microtome Hyrax M55	Zeiss
Mirax Desk Scanner	Zeiss
Multipipette	Eppendorf
NanoDrop® ND-1000 spectrometer	Thermo Fisher Scientific,
Optically Clear Adhesive Seal Sheets	Thermo Scientific
PCR Cycler nexus gradient	Eppendorf
Pipette (10 µl, 20 µl, 100 µl, 1000 µl)	Eppendorf
PVDF membrane	Thermo Scientific
QCM	Scientific Instruments GmbH
qPCR LightCycler® 480 II	Roche
Shaker	Coulter Electronics
S-Monovette	Sarstedt
Sonication water bath	Bandelin
Spin tissue processor	Leica
Syringe	Braun
Tecan Reader NanoQuant infinite M200 Pro	Tecan Group
Tecan Safire 2	Tecan Group
Thermo Cycler	Eppendorf
Tips (10 µl, 20 µl, 200 µl, 1000 µl)	Starlab
Tips with filters (10 µl, 20 µl, 200 µl, 1000 µl)	Biozol; Starlab
Ventilation hood	Thermo Fisher Scientific
Vibrating mesh nebulizer (Aeroneb Pro)	Aeroneb Inc.
Vortex mixer	Scientific Industries
Water bath for cell culture	Lauda, Koenigshofen, Germany
Western blot bands detection machine	Bio-Rad Laboratories
Zetasizer AT	Malvern
15 mL and 50 mL Tubes	Falcon
0.5, 1.5 mL and 2ML Tubes	Eppendorf
6-well transwell insert plate #3450	Corning
96 well LightCycler plate	Sarstedt

96 well plate for WST-1, LDH and BCA assay	Greiner Bio-One
96 well plate for ELISA	Thermo Scientific
96 well plate black for dsDNA measurement	Greiner Bio-One

2.1.11 Softwares

Product	Company
BioPlex Manager 6.1 software	Luminex Corporaion
Computer Assisted Stereological Toolbox (newCAST) software	Visiopharm
GraphPad Prism 6	GraphPad
Image Lab Software, Version 5.2.1	Bio-Rad
Light Cyclser 480 software	Roche
Magellan Software	Tecan Group
Tecan Safire 2 Software	Tecan Group
ZEN 2010-Digital Imaging for Lightmicroscopy Software	Zeiss

2.2 Methods

2.2.1 *in vivo* mice experiments

Mice were treated humanely and with consideration to reduce suffering, according to the German law of protection of animal life. All animal experiments followed approved protocols by the local Animal Care and Use Committee (District Government of Upper Bavaria; permit numbers: 55 2-1-54-2532-67-2015). C57BL/6 mice were purchased from Charles River Laboratories (Sulzfeld, Germany) and housed in individual ventilated cages (IVC). 148 female mice were divided into 18 groups anesthetized by intraperitoneal injection of a mixture of Medetomidine (0.5 mg/kg body mass), Midazolam (5.0 mg/kg body mass) and Fentanyl (0.05 mg/kg body mass) (MMF) prior to intranasal (i.n.) infection with 5×10^4 PFU MHV-68. After infection mice were antagonized by subcutaneous injection of a mixture of Atipamezole (2.5 mg/kg body mass), Flumazenil (0.5 mg/kg body mass) and Naloxone (1.2 mg/kg body mass) to guarantee their awakening and well-being.

After 6 days, in acute virus infection, 8 mice were sacrificed for tissue harvest. After establishing of virus latency infection at day 28 post infection, mice were either left untreated for control, instilled with 50 μ g of spherical or double-walled fiber-shaped carbon nanoparticles or instilled with 0,1 μ g LPS as a positive control with intratracheal instillation. Following the anesthetizing with MMF the animals were intubated for the instillation by a nonsurgical technique, using a cannula inserted 10 mm into the trachea, a particle dispersion containing 50 μ g CNPs, DWCNTs and a suspension 0,1 μ g LPS in 50 μ L ultra-pure water (Gibco) was instilled. After instillation, mice were antagonized by subcutaneous injection.

After the first instillation of 24 hours, mice for analyzing 1 particle dosing and LPS response, mice were anesthetized by intraperitoneal injection of a mixture of xylazine (4.1 mg/kg body mass) and ketamine (188.3 mg/kg body mass) and killed by exsanguination. Therefore, blood was drawn from the retroorbital plexus by a capillary and collected in non EDTA-covered tubes to gain blood serum.

55 days after the first instillation, mice were instilled a second time with 50 μ g CNPs or DWCNTs in 50 μ L ultra-pure water described before. 24hours and 6 days post

instillation mice were over injected with Ketamine and Xylazine for harvesting the tissue samples.

2.2.2 Harvesting mice lungs for histology

From each treatment group three mice were chosen for histological examination. As described before mice were injected with Ketamine and Xylazine for anesthetizing and exsanguinated after opening the abdominal region. For histological examinations especially for immunofluorescence staining of the lung, it is recommended to perfuse the organ with PBS to remove all erythrocytes which influence the autofluorescence with a high background fluorescence. After opening the chest, a 10 mL Syringe filled with PBS was used to inject the buffer into the right ventricle of the heart to infiltrate the blood vessels in the lung and remove the remaining blood. For inflating of the lung tissue to retain the alveolar structure an indwelling venous cannula was inserted to the trachea. Trachea and cannula were connected by a thread to avoid leakage of PFA from the lung. After setting the cannula in the correct way 1 mL of 4% PFA was injected over the cannula into the lung. The lung was carefully removed out of the chest with avoiding the loss of PFA from inner lumen and collected in a 50 mL falcon tube filled with 4% PFA over night at 4°C. For embedding the lungs into paraffin blocks, the lung lobes were separated into the four right lobes and one left lobe. Right and left lobes were separately poured later into blocks. After separation, the lobes were cut into 2-3 mm thick slices and placed into a cassette to avoid losing tissue during dehydration process in the spin tissue processor. The tissues were dehydrated and paraffinized in the spin tissue processor over night for about 16 hours. The tissue slices were placed into holders and filled with paraffin in the tissue embedding machine. After cooling of the paraffin, blocks were stored at 4°C until cutting on the microtome.

2.2.3 Harvesting serum from mice

From each treatment group five mice were chosen for taking serum, bronchoalveolar lavage and lung tissue collection for protein and RNA isolation. As described before mice were intraperitoneal injected with Ketamine and Xylazine for anesthetizing. Blood was collected by puncture of the peri-orbital vein with a glass capillary into a serum vial (S-Monovette). Blood was incubated in the vials for complete coagulation for 30 minutes at room temperature, following by centrifugation for 10 minutes at 4°C with

1500 g. The yellowish clear supernatant (serum) was removed and collected in a new 1.5 mL reaction tube. Serum was snap frozen in liquid nitrogen and stored until further analysis at -80°C.

2.2.4 Bronchoalveolar Lavage (BAL)

To analyze cell types and proteins in the alveolar space a bronchoalveolar lavage (BAL) was performed to harvest cells for cytopsin and subsequent BAL cell differentiation and lavage fluid to analyze cytokines and proteins with ELISA and protein quantification. As described before mice were intraperitoneal injected with and overdose of Ketamine and Xylazine for anesthetizing and blood was collected. An indwelling venous canula was inserted to the trachea and lung was flushed with 1 mL PBS for two times. BALF was collected in a 15 mL falcon tube. Additionally, lungs were flushed four more times with 1 mL PBS and liquid was collected in a second tube. BALF was separately centrifuged for 20 minutes at 4°C with 400 x g. The first two mL supernatant from first tube was aliquot in three 1.5 mL reaction tubes and snap frozen in liquid nitrogen. BALF samples were stored at -80°C for long time till ELISA, BCA and LDH analysis. Supernatant from the second tube was discarded and cell pellet from tube one and two was resuspended and collected in total of 1 mL BAL cell medium. Cell numbers were determined with counting in a Neubauer chamber and the volume for 30,000 cells/slide was used for BAL cytopsin centrifugation. Residual cell suspension was centrifuged for 10 minutes at 4°C with 1500 rpm. Supernatant was discarded and cell pellets were snap frozen in liquid nitrogen and stored for long term at -80°C.

2.2.5 BAL cytopsin

To analyze cell types in bronchoalveolar lavage, the volume for 30,000 cells/slide (or a maximum volume of 200 µL) was used for cytopsin. For each mouse 2 microscope slides for subsequent freezing to -80°C and 2 slides for subsequent May-Gruenwald-Giemsa staining were load up with cells. Frozen BAL cells were stored till IF or IHC staining for specific protein analysis. May-Gruenwald-Giemsa-stained BAL cells were further analyzed for cell type identification. After centrifugation, cells were dried for several minutes at room temperature.

2.2.6 BAL cell staining – May-Gruenwald-Giemsa staining

BAL cells on microscope slide were stained as followed:

- 10 minutes in May-Gruenwald stain
- 2 minutes in tap water
- 15 minutes in Giemsa stain (1:20 dilution from stock solution, diluted with tap water)
- 2 minutes distilled water
- 2 minutes distilled water

Slides were dried after staining and covered with Entellan and cover glass. Slides were stored at room temperature on dry and light protect place until BAL cell differentiation.

2.2.7 BAL cell differentiation

To observe the composition of cell types recruited to the bronchoalveolar region the morphology of cell types was distinguished using a microscope and cell counter. Cell types were separated by Macrophages/Monocytes, Neutrophils, Lymphocytes and multicellular Macrophages. 200 cells were differentiated on two separate slides per animal. Total cell number/percentage of each cell types was calculated with known total cell numbers in BAL fluid.

2.2.8 Harvesting mice lungs for protein and RNA isolation

From each treatment group five mice were chosen for taking serum, bronchoalveolar lavage and lung tissue collection for protein and RNA isolation. As described before mice were intraperitoneal injected with Ketamine and Xylazine for anesthetizing and exsanguinated by collecting blood over peri-orbital vein. The chest of the mice was opened, and lungs were taken out. Lung lobes were separated and snap frozen in liquid nitrogen. Frozen tissue was stored till homogenization in -80°C freezer.

2.2.9 Lung homogenate preparation

Frozen lung lobes were used to prepare homogenates with Micro-Dismembrator S (Sartorius). Lung homogenates were dissolved in TRIzol™ (Thermo Fisher Scientific)

for mRNA isolation and RIPA buffer for protein isolation. Residual tissue homogenates were stored at -80°C.

2.2.10 Preparation of carbon nanoparticle (CNP) and double walled carbon nanotube (DWCNT) dispersions

Carbonaceous spherical nanoparticles (CNP, Printex90, Degussa, Frankfurt, Germany) and double-walled carbon nanotubes (DWCNT; Nanocyl, Auvélais, Belgium) were used in the *in vivo* experiments. In the *in vitro* application only CNP were used because of nebulization issues. For DWCNT it is difficult to nebulize because of their fiber shape. For both, *in vivo* and *in vitro* application CNPs were dispersed in pyrogen-free water. For the application in animals, CNPs were dispersed in 1 mg/mL as followed: sonication for 5 minutes in sonication bath, sonication with sonication lance for 30 seconds at 30% power constant on ice, 5 minutes in sonication bath. For the application in vitro, CNPs were dispersed in 3 mg/mL as followed: 13 minutes in sonication bath, lid covered with ice for protection of heating. DWCNTs were dispersed in a 1% Pluronic in pyrogen-free water (diluted from 10% Pluronic stock solution) to a concentration of 1 mg/mL and dispersed as followed: 5 minutes in sonication bath, 50 seconds in at 30% power constant on ice, 5 minutes in sonication bath. After dispersion, the size and size distribution of CNP and DWCNT in the dispersions was measured with the dynamic laser scatter (DLS) device in a maximum concentration of 1 mg/mL. For nebulization in ALICE-Cloud model, Ions are necessary to form droplets in the vibrating mesh membrane of the nebulizer (Aeroneb). Because of this reason 1:1000 0.9% NaCl (Braun) was added to the CNP dispersion to a final salt concentration of 0.0009% NaCl.

2.2.11 Characterization of particle dispersion

To analyze the dispersion and agglomeration of particles the hydrodynamic size and polydispersity of DWCNTs and CNPs were measured using a Mastersizer 2000 Laser Particle Size Analyzer (Malvern) at 21°C. For this, particle dispersions were diluted to the lowest concentration of 1 mg/mL and 80 µL were measured in appropriate cuvettes.

2.2.12 Cell culture

Cell culture is the growth and maintenance of cells from a multicellular organism outside the body in cell culture dishes and plates. Cells are grown under special conditions of temperature, CO₂ concentration, nutrition and sterile conditions.

All cell lines were kept during growth in 75 cm² cell culture flasks and were maintained at 37°C, 5 % CO₂ in a humidified incubator and routinely passaged at confluency.

Cells were passaged one or twice per week into a new 75 cm² flask with 0.5 – 1.5 x 10⁶ cells per flask. Passaging was performed under sterile conditions under a cell culture workflow hood, which was cleaned on all surfaces before with PureSept A. Passaging of the cells was performed as follows: Growth medium was removed collected in a 50 mL falcon tube in case of suspended cells and discarded in case of adhered cells. Cells remained in the flask were washed with about 10 mL Dulbecco's phosphate buffered saline (Gibco, DPBS, - MgCl₂, - CaCl₂) two mL 0.5 % trypsin/EDTA (Ethylenediaminetetraacetic acid) was given to the cells and incubated for 2 – 5 minutes at 37°C until the cells detached from the surface of flasks. 18 mL complete growth medium + 10 % FBS were added to the trypsin/EDTA-cell suspension, to stop the trypsinization reaction. Cells were centrifuged in 50 mL falcon tubes for 5 minutes, 1400 rpm at RT. Supernatant was removed by vacuum pump and the remaining cell pellet was resuspended in growth medium. Cells were counted and an appropriate number of cells were transferred into a new cell culture flask, containing warm growth medium.

All experiments were performed on cells seeded out 2-24 hours in advance, allowing the cells to attach to the surface of the culture plate or the transwell insert plate membrane for the respective experiments.

2.2.13 Freezing of cells

Cells from continuous cell cultures are under influence of genetic drift and susceptible to microbial contamination. The replacement of established cell lines is expensive and time consuming. For these reasons, it is important that samples are frozen down and prepared for long-term storage. The best storage condition is in liquid nitrogen in growth medium with high serum concentration and in presence of a cryoprotective

agent such as dimethylsulfoxide (DMSO). DMSO reduces the freezing point of the medium and reduces the risk of ice crystal formation, which derogates the cells.

Freezing medium was prepared for the cryo-preservation of cells. The appropriate freezing medium depends on the cell line. Cells were grown to about 90 – 100% confluency. Mammalian adherent cells were washed with DPBS (Dulbecco's phosphate buffered saline, Gibco) and then incubated with 0.05 % Trypsin/EDTA trypsinization medium, until cells detached from tissue culture plated. Trypsinization reaction was stopped with about 8 ml growth medium and cells were centrifuged for 1400 rpm for 5 minutes. The supernatant was discarded, and the cell pellet was resuspended in freezing medium. The cell suspension was pipetted into sterile cryogenic storage vials. The cryovials were placed in a paper towel and aluminum foil and stored at -80°C overnight, for decreasing temperature approximately 1°C per minute. For long-term frozen cells were stored in liquid nitrogen.

2.2.14 Thawing of cells

A sample taken from liquid nitrogen storage was transferred quickly in a 37°C water bath and cells were thawed, for about 1 minute, until only one or two small ice pieces remained. The whole content of the cryovial was pipetted into a cell culture flask, containing 20 mL of pre-warmed growth medium. Cells were incubated at 37°C and 5 % CO₂. It is important to thaw cells correctly to maintain the viability and recovery of the culture.

2.2.15 Counting cells

For the determination of the cell amount a Neubauer chamber (Roth) was used. One chamber contains nine squares with the dimension of 1 x 1 mm and a total volume of each square of 10 µL. adherent cells were washed with DPBS and dissected from the culture vessel with trypsinization medium. The trypsinization reaction was stopped by adding growth medium to the cells. Detached cells were centrifuged and supernatant was discarded. The cell pellet was resuspended in 1 mL growth medium. 10 µl of cell suspension were pipetted to 190 µl Trypan Blue Stain, for the discrimination of viable and death cells. 10 µl of this suspension were counted. The average of four counted quadrants was used to calculate the number of cells per mL in the following equation:

Cell number/mL = average x 20 (dilution factor) x 10,000 (chamber factor)

2.2.16 Alveolar macrophage cell line – ANA-1

Bone marrow derived macrophage cell line ANA-1 (Mouse macrophage; RRID:CVCL_0142), derived from C57BL/6, was grown in complete RPMI-1640 medium supplemented with 15% fetal bovine serum, 2mM L-Glutamine, 1% Non-essential amino acids, 100 U/mL Penicillin and 100µg/mL Streptomycin.

2.2.17 Bone Marrow derived macrophage cell line – latently infected MHV-68/ANA-1

Murine bone marrow derived macrophage cell line ANA-1 (RRID: CVCL_0142), derived from C57BL/6, was latently infected with MHV-68 and called “**ANA-1/MHV-68**” (Sattler et al., 2017).

This cell line was used in the method of ALICE-Cloud treatment with CNPs and for the investigation of MHV-68 reactivation from latency to lytic phase after CNP treatment either under submerged conditions or on ALICE-Cloud treatment with a persistently MHV-68 infected cell line established by C. Sattler [Sattler et al., 2017].

ANA-1 cells were grown in complete RPMI-1640 medium supplemented with 15% fetal bovine serum, 2mM L-Glutamine, 1% Non-essential amino acids, 100 U/mL Penicillin and 100µg/mL Streptomycin. For the maintaining of the latent MHV-68 infection, Hygromycin B resistance was integrated to ensure stable infection of MHV-68. This modification of MHV-68 is the reason to only handle these cells and medium under safety level 2 laboratories. The cells were handled very carefully in order not to reactivate the virus by stressful treatment. 0.05% Trypsin-EDTA was used. During experimental condition, growth medium without the addition of Hygromycin B was applied.

2.2.18 Alveolar macrophage cell line – MHS

Murine alveolar macrophage cell line MHS (RRID: CVCL_3855), derived from BALB/cJ mice, was used for ALICE-Cloud exposure. Cells were grown in complete RPMI-1640 medium supplemented with 10% fetal bovine serum, 0.05 mM β-Mercaptoethanol, 100 U/mL Penicillin and 100µg/mL Streptomycin.

2.2.19 Alveolar epithelial cell line – MLE-12

Murine lung epithelial cell line MLE-12 (RRID: CVCL_ 3751), derived from FVB/N-Tg(SFTPC-TAg)^{5.1Jaw} SV40 transgenic mice, was used for ALICE-Cloud exposure in the co-culture model for virus reactivation analysis. Cells were grown in complete DMEM F12 medium supplemented with 10% fetal bovine serum, 100 U/mL Penicillin and 100µg/mL Streptomycin.

2.2.20 Alveolar epithelial cell line – LA4

Murine lung epithelial cell line LA-4 (RRID: CVCL_ 3535), from lung adenoma, was used for ALICE-Cloud exposure in single culture and in the co-culture model for virus reactivation analysis. Cells were grown in complete Ham's F12K medium supplemented with 15% fetal bovine serum, 1% NEAAs, 100 U/mL Penicillin and 100µg/mL Streptomycin.

2.2.21 Cultivation of non-infected and MHV-68 latently infected ANA-1 cells on transwell insert

To investigate MHV-68 reactivation on ANA-1 cell cultured on air liquid interface, ANA-1 or ANA-1/MHV-68 cells were detached from T75 cell culture plates with first taking of the medium and collecting in a 50 mL falcon tube to keep the suspended macrophages. After washing with 10 mL of DPBS, the washing medium was collected as well. Trypsin was used to remove the cells with 2 mL and 4 minutes incubation at 37°C. The enzymatic reaction was stopped with addition of 18 mL growth medium, and all detached cells were collected together. Cell suspension was centrifuged for 5 minutes with 1400 rpm at RT. Supernatant was discarded and cell pellet was resuspended in 5 mL growth medium. Cells were counted as described before. In each well of the 6-well transwell inserts, 1200 µL medium was given to the basal insert compartment.

2.2.22 Transwell co-culture of alveolar epithelial cells and bone marrow derived macrophages

For the approximation to mimic more the *in vivo* situation, a co-culture of alveolar epithelial cell lines on the apical site of a transwell insert was grown together with the

latently infected bone marrow derived macrophage cell line located on the basal site of the transwell insert. For this co-culture model, ANA-1 cells with a density of 150,000 cells per well in 33 % Matrigel matrix in ANA-1 growth medium was pipette to the basal site of the transwell insert with a volume of 125 μ L cell-Matrigel-suspension per 6 well. Before seeding procedure, everything was done on ice to avoid hardening of the Matrigel matrix. Matrigel matrix was polymerized for 20 minutes in 37°C incubator with transwell insert converted upside down. Transwell insert were placed back to inserts, containing 1,200 μ L growth medium. LA-4 and MLE-12 cells were seeded to the apical site with 1.6×10^6 LA-4 cells per well and 1.0×10^6 MLE-12 cells per well in 600 μ L cell growth medium.

2.2.23 ALICE-Cloud treatment of non-infected cells with carbon nanoparticle dispersion

For treatment of epithelial cells or macrophages growing on air liquid interface (ALI) with nanoparticle dispersion, first the ALICE-CLOUD (Vitrocell) 6-well chamber was cleaned with 80% Ethanol to avoid contaminations with bacteria or fungi. The surface area at the plate site is 145 cm². All connections for the QCM and the control panel for the vibrating mesh nebulizer was set. QCM was run for a while to stabilize measurement baseline for later detection. ALICE-CLOUD was switched on and 18 mL of DPBS was given to all wells and was run for at least 1h to warm the chamber block and DPBS to 37°C. Nebulizer was cleaned with 200 μ L 0.9% NaCl, followed by 2 x 200 μ L 0.0009% NaCl. After cleaning and base setting, transwell inserts were placed to the treatment plate in the ALICE-CLOUD chamber. QCM was started to detect and 200 μ L of in water dispersed CNPs were nebulized onto the cells. CNP dispersions were in different concentration with highest concentration of 1 mg/mL. Too high CNP concentrations lead to clotting the nebulizer mesh. Nebulization took around 25 seconds, to completely nebulize 200 μ L dispersion. CNPs were allowed to settle down in the cloud for 10 minutes. Then the chamber was opened and the QCM was dried. Only with the dry surface of the QCM, the exact CNP deposition could be detected. After the final measurement of CNP deposition, treated transwell inserts were put back to the plate and the incubator. For each experiment with CNP nebulization, sham controls and untreated controls were run, in which the sham control was nebulized with 200 μ L 0.0009% NaCl.

2.2.24 ALICE-Cloud prototype treatment of ANA-1/MHV-68 latently infected cells with carbon nanoparticle dispersion

For treatment of epithelial cells or macrophages growing on air liquid interface (ALI) with nanoparticle dispersion, first the ALICE-Cloud chamber was cleaned with 80% Ethanol to avoid contaminations with bacteria or fungi. All connections for the QCM and the control panel for the vibrating mesh nebulizer was set. QCM was run for a while to stabilize measurement baseline for later detection. As the prototype version of ALICE-Cloud chamber was used for S2 work with infected cell, there was no heating unit integrated into the chamber block. 1.2 mL ANA-1 cell growth medium was added to each well of the sterilized 5-well plate. Nebulizer was cleaned with 200 μ L 0.9% NaCl, followed by 2 x 200 μ L 0.0009% NaCl. After cleaning and base setting, transwell inserts were placed to the treatment plate in the ALICE-CLOUD chamber. QCM was started to detect and 200 μ L of in water dispersed CNPs were nebulized onto the cells. CNP dispersions were in different concentration with highest concentration of 1 mg/mL. Too high CNP concentrations lead to clotting the nebulizer mesh. Nebulization took around 25 seconds, to completely nebulize 200 μ L dispersion. CNPs were allowed to settle down in the cloud for 10 minutes. Then the chamber was opened and the QCM was dried. Only with the dry surface of the QCM, the exact CNP deposition could be detected. After the final measurement of CNP deposition, treated transwell inserts were put back to the plate and the incubator. For each experiment with CNP nebulization, sham controls and untreated controls were run, in which the sham control was nebulized with 200 μ L 0.0009% NaCl.

2.2.25 Sterilization of cut 5-well plates for ALICE-Cloud prototype

For the ALICE-Cloud prototype a 6-well cell culture plate was cut to a 5-well plate, because one well needed to be free for the deposition measurement with the quartz crystal microbalance (QCM) which can measure the nanoparticle deposition after nebulization into the ALICE-Cloud chamber. Under the sterile hood, plates were washed 1 x 10 min. with 10% Penicillin Streptomycin in DPBS followed by 2 x 10 min. 80% Ethanol washing steps. Plates were dried under the sterile hood and UV-light was activated for 20 minutes to finally sterilize the plates. Sterile 5-well plates were placed into sterile autoclaving bags and closed properly before the usage in the ALICE-Cloud prototype.

2.2.26 Immunofluorescence (IF) staining of fixed cell culture cells

IF staining is a technique to visualize the localization of a protein of interest in cells by using a specific primary antibody and a secondary antibody labeled with a fluorophore. For this method, cover slips of transwell insert membrane with cultured cells were fixed with 4 % paraformaldehyde (PFA) in PBS for 15-20 minutes and washed 2 times in 1 x PBS for 5 minutes. After fixation endogenous ... were quenched in 50mM NH₄Cl in 1 x PBS. For blocking, the cells were incubated in blocking solution (PBS-T Triton X-100 0.1 %, 5 % BSA) for 1 hour at room temperature. After blocking, cells were washed two times with 1xPBS for 5 minutes. All antibodies were diluted in PBS-T Triton X-100 0.01 %, 5 % BSA in required dilution and were incubated on cells overnight at 4°C. At the following day, coverslips or membranes were washed three times with PBS-T Triton X-100 0.01 % for 5 minutes at room temperature and incubated with appropriate secondary antibodies conjugate with a fluorophore (Invitrogen) at a concentration of 1:1000 at room temperature for one hour. Cell culture plates were covered with aluminum foil to protect the fluorescent dyes from the light. Cells were stained with DAPI (1:1000 in 1 x PBS) after washing cells 3 times with PBS-T 0.01 % for 5 minutes. Cells were washed at least 2 more times with 1 x PBS after DAPI staining. Membrane and cover slips were prepared on microscope slides and mounted with DAKO fluorescence mounting medium.

2.2.27 Water soluble tetrazolium (WST-1) cell viability assay

The water-soluble tetrazolium (WST-1) assay is used to determine the viability and proliferation of cells in culture. In this method tetrazolium salts get reduced to colored formazan compounds by succinate-tetrazolium reductase, which exists in viable cells. The optical density at 450nm is measured to determine cell viability. Growth medium was taken off from cells in culture plates or transwell inserts and replaced by the associated growth medium of the cell line containing 1:10 or 1:15 dilution of WST-1 reagent. Cells with diluted WST-1 medium were incubated for 30 to 60 minutes in the cell culture incubator, protected from light. After the incubation time, the WST-1 medium was collected in dark tubes and centrifuged for 10 minutes at rpm to sediment the particles to the bottom of the tube. 100µL triplicates were pipette to 96-well-plate and measured in a Tecan plate reader at 450nm. WST-1 medium was used as a blank

control. After subtraction of the blank OD value from OD value of the samples, the value of untreated or vehicle control cells were set to 100% viability. The treatment OD values were calculated to the corresponding % viability in comparison with the untreated or vehicle control.

2.2.28 Lactate Dehydrogenase (LDH) assay – assessment of cytotoxicity in BALF and *in vitro*

To analyze cytotoxic effects of different treatments, LDH assay was performed. The assay is based on measurement of lactate dehydrogenase (LDH) released by cells losing the membrane integrity into the growth medium *in vitro* or into the bronchoalveolar region *in vivo*. For defining 100 % LDH *in vitro*, 1 % Triton X-100 in growth medium was prepared. All supernatants (apical and basal in case of air liquid interface culturing) were collected into 1.5 mL reaction tubes. The volume of collected supernatant was measured and the same volume of 1 % Triton X-100 in medium was added to the cell into the control well to destroy all cell membranes. This medium was also collected into a 1.5 mL reaction tube and defined as the high control (maximum LDH concentration in the experiment). The supernatant collected previously from non-treated cell is defined as low control. All collected samples from *in vitro* experiments were centrifuged for 10 min. at 14,000 rpm to remove the cells and particles left in the medium. For LDH assay for BALF a LDH standard curve was prepared for the fact its not possible to create a high and low control. For pipetting the standard curve, LDH standard (Roche) was diluted in DPBS from dilutions 1:1,600 to 1:102,400. LDH assay was performed in transparent 96-well plates. 100 μ L DPBS was used to measure the blank for the *in vivo* samples. For the *in vitro* samples, 100 μ L of medium without FBS was used as a background or blank control. For the high control, 95 μ L of medium without FBS was preset and 5 μ L lysate was given to the medium. 100 μ L low control, without dilution was added to the 96-well plate. For the samples, 70 μ L medium plus 30 μ L samples supernatant was mixed. LDH working solution was prepared by thawing dye solution and reconstitution of catalyst in 1 mL ultra pure water for 10 min. Dilution of catalyst with dye solution in 1:45 was prepared. 100 μ L of the freshly prepared LDH working solution was added to each well and incubated for 15 minutes at RT, protected from light. After incubation time, 50 μ L of stop solution (1M HCl) was given to each well and plate was immediately measured in the Tecan reader at wavelength of 492 nm.

Either standard curve or the percentage of LDH compared to high control was calculated as shown:

$$\text{Cytotoxicity in \%} = \text{Sample average OD}/(\text{High control} - \text{low control}) * 100$$

2.2.29 Plaque assay

To analyze the production of infectious virus particles in cell culture cells and release into the supernatant plaque assay was performed. For this method BHK21 cells were detached from confluent 75cm² cell culture flask with 0.25% Trypsin in EDTA (Invitrogen, Gibco) and resuspended in 10 mL BHK-21 growth medium. 0.25 mL of cell suspension was mixed with 9.75 mL fresh BHK21 growth medium and 1 mL of diluted cell suspension was pipetted into a 24-well plate. Cells were incubated for 24 hours at 37°C, 5% CO₂ cell culture incubator. On following day, experimental supernatants were taken from -80°C storage and thaw on ice. A 1:10 dilution series was done from 10⁻¹ to 10⁻⁶ by preloading 900 µL of BHK21 medium to the tubes and pipetting 100 µL from first to second tube, properly mixing and repeating the process to the last 10⁻⁶ dilution. Old medium from cell coated plate was removed and 900 µL of each dilution series was added to the wells starting from 10⁻⁶ dilution. Cells were incubated for 90 minutes with dilutions in cell culture incubator. After incubation, dilution series media were removed, and 2 mL of methylcellulose overlay medium was applied to each well. Cells were incubated for 5 days. Methylcellulose medium was removed and 300 µL of a crystal violet stain in 4 % PFA was added for 15 minutes to the cells. After fixation and staining, crystal violet stain was washed with tap water and plates were dried at room temperature. Plaques were counted under the microscope in the dilution range where plaques were clearly separated, and virus titer was calculated with following equation:

$$\text{Number of plaques} \times 1.1 \text{ (input factor)} \times \text{dilution} = \text{virus titer in pfu/mL}$$

$$\text{Where input factor} = \frac{1}{\text{mL inoculum/plate}} = \frac{1}{0.9} = 1.1$$

2.2.30 Enzyme-linked Immunosorbent assay (ELISA)

To determine the concentration or quantity of a specific protein in tissue homogenates protein lysates, BAL fluids and serum ELISA method was used. First a capture

Materials and Methods

antibody specific for the antigen of interest was coated over night to a 96-well-plate according to its specific working concentration diluted in PBS. For coating a volume of 100 μ L per well was added to the plate. On following day, 96-well-plate was washed 3 times with PBS-T and 300 μ L Reagent Diluent per well was pipetted to the plate to block nonspecific binding sites. During the blocking time standard curve was prepared for different concentrations with recombinant protein of interest diluted in Reagent Diluent and samples, which were stored at -80°C were thaw on ice. Reagent Diluent was used as blank. Sample lysate, BALF or serum was either diluted with Reagent Diluent or used undiluted to a final volume of 100 μ L per well. With dilution it was made sure to include all sample concentrations into the concentration range of standard curve. The samples were incubated for 2 hours at room temperature and plate washed again 3 times with PBS-T to remove unbound antigens. Detection antibody was diluted with Reagent Diluent to working concentration and pipetted 100 μ L per well for incubation at room temperature for 2 hours. After incubation with Detection antibody the plate was washed 3 times with PBS-T and incubated with Streptavidin-HRP (prediluted 1:40 in reagent diluent) for 20 minutes at room temperature. After washing again 3 times with PBS-T 100 μ L TMB was pipetted into each well and incubated for maximum of 20 minutes. Depending on the antigen of interest and sample type incubation with TMB substrate was stopped earlier when color was changing. For stopping of the enzymatic reaction, 50 μ L of 2 N H_2SO_4 was added per well. The absorbance of the plate was measured at 450 nm and reference wavelength at 540 nm with the Tecan plate reader. To determine the quantity of antigen in the sample, the blank OD value was subtracted from each standard curve and sample value. With OD values of standard curve and the known recombinant protein concentration, a curve was fitted to the graph and concentrations in the samples were calculated according to the corresponding standard curve equation.

2.2.31 Luminex analysis

To investigate chemokine release in the lung into the bronchoalveolar space, a Bio-Plex Pro Mouse Chemokine Panel 31-Plex was performed.

The following cytokines and chemokines were detected using the Bio-Plex kit (Bio-Rad, CA, USA): CXCL13, CCL27, CXCL5, CCL11, CCL24, CX3CL1, GM-CSF, CL1, IFN- γ , IL-1 β , IL-2, IL-4, IL-6, IL-10, IL-16, CXCL10, CXCL11, CXCL1, CCL2, CCL7,

CCL12, CCL22, CCL3, CCL4, CCL20, CCL5, CCL19, CXCL16, CXCL12, CCL17, TNF- α .

Method was used, following the manufacturer's instructions.

Standard diluent was reconstituted by adding 250 μ L of diluent. Preparation of a fourfold standard dilution series and blank. Sample dilutions were prepared 25 μ L of BAL liquid was used for the analysis. Samples were centrifuged before to remove particulates from the supernatant before use. Vortex and add coupled beads and add 50 μ L to each well of the assay plate. After washing add samples, standard, blank and control to each well. Incubated with the detection antibody for 30 minutes. After several washes, detection antibody was added and incubated for 30 min. After washing, Streptavidin-PE was added to each well and incubated for 10 min. Cytokine and chemokine expression was measured using the Luminex 200 System (Luminex Corporation, Austin, USA).

2.2.32 Measurement of dsDNA in BALF

To quantify double stranded DNA (dsDNA) released to the bronchoalveolar area Quant-iT PicoGreen dsDNA assay kit was used. Λ -DNA was used to pipette a standard curve for dsDNA. All dilutions were used in 1x TE buffer. 50 μ L of 1xTE buffer was added to each well. 50 μ L of standard, blank and BAL fluid was added. Quant-iT PicoGreen Reagent was diluted 1:200 with 1x TE buffer and 100 μ L was added to each well. Plate was measured with Tecan Safire 2 (Tecan Group, Männedorf, Switzerland) and final dsDNA concentration was calculated according to the standard curve.

2.2.33 Protein extraction

To investigate protein expression in treated cell culture cells or lung tissue, protein isolation and Western blot analysis were performed. Cells from cell culture were washed with DPBS and lysed with RIPA lysis buffer containing 1x HALT Protease and Phosphatase Inhibitor Mix. Tissue protein was extracted after homogenization of the tissue. Homogenized tissue was lysed with appropriate amount of RIPA lysis buffer supplemented with 1x HALT Protease and Phosphatase Inhibitor Mix. For protein extraction, all steps were prepared on ice. Cells were lifted from the cell culture dish with RIPA lysis buffer and the mechanical help of a cell scraper. Lysate was incubated for 15 minutes at 4°C. After the incubation, lysate was centrifuged at 14,000 rpm for

15 minutes at 4°C, to sample non-protein parts on the bottom of the reaction tube. Supernatant was transferred into a new 1.5 ml reaction tube and the pellet was discarded. For long term storage, protein lysates were stored at -80°C. The protein concentration of the sample was measured afterwards with the BCA assay.

2.2.34 Protein quantification with BCA assay

The BCA assay was used to determine the protein concentration in cell or tissue lysate samples, which is important for the equal loading of the SDS gel and quantitative comparison of the results. For the reference standard solution, 0.5 mg/mL BSA solution was prepared by solving 75 µL of 2 mg/mL BSA stock solution in 225 µL PBS. The standard curve was prepared as follow:

Concentration µg/mL BSA	0.5 mg/mL BSA standard solution (µL)	PBS (µL)
0	0	80
0.025	4	76
0.05	8	72
0.1	16	64
0.2	32	48
0.3	48	32
0.4	64	16
0.5	80	0

The BCA assay working solution was made with Reagent A and Reagent B from BCA assay kit which were diluted 50:1 (A:B). The BCA assay was performed in 96 well plates with triplicates of standard. In each well contained 20 µL of sample dilution (18 µL PBS + 2 µL protein lysate sample) 200 µL of working solution was added. The mixture was incubated for 30 minutes at 37°C or 1 hour at room temperature. Standard curve and protein samples were read in the Tecan reader at 562 nm. Raw data were used to calculate the protein concentration of the individual samples. All samples were brought to the same concentration by dilution with RIPA lysis buffer. After equalization, 4 x Laemmli buffer (previously dilute 1-part β-ME + 9 parts Laemmli) was added to the protein samples. After vortexing, samples with Laemmli buffer were denatured for 10

minutes at 95°C, cooled down on ice for 5 minutes and centrifuged down for 30 seconds at 6000 x g. Samples were ready for loading on a SDS gel or frozen down at – 80°C for later analysis.

2.2.35 RNA purification from tissue homogenates

To measure genetic expression profiles in whole lung tissue, RNA needs to be purified from frozen lung homogenate powder. For this 1.0 mL of Trizol Reagent was added to the reaction tube containing frozen lung powder. The reaction tube was vortexed for 30 seconds and incubated for 5 minutes on ice. 200 µL Chloroform was added to the reaction tube and vigorously shake for 15 seconds and following incubated for 5 minutes at room temperature. The samples were centrifuged for 20 minutes at 4,000 g and room temperature and colorless, upper phase (around 600 µL) was transferred to a fresh RNase-free tube. RNA isolation continued like in the manufacturers protocol.

Measure the RNA-concentration and purity with the NanoDrop and either directly perform cDNA synthesis or store RNA at least at -20°C until processing to cDNA.

2.2.36 cDNA synthesis

To measure the level of gene expression in tissue and cells with quantitative PCR cDNA was synthesized from tissue or cell isolated mRNA. The RNA was reversed-transcribed with help of the High-Capacity cDNA Reverse-transcription Kit. The working area was cleaned with 80% EtOH or RNase free to avoid RNA digestion from RNases on contaminated surfaces. Either at -20°C stored RNA was frozen on ice or directly used after RNA extraction on ice for cDNA synthesis. 1 µg total RNA was pipet in a fresh 0.5 mL reaction tube and filled up to a volume of 10 µL with RNase free water. For RNA samples with a lower concentration of 100 ng/µL 10 µL of the sample were used without additional water. 1 µL of random nanomers was added to the reaction tube. After the addition of the nanomers to the RNA, everything was incubated for 5 minutes at 70°C for denaturation in the PCR cycler. Directly after the denaturation, samples were cooled down on ice for 5 minutes and incubated additional 5-10 minutes at room temperature. In this incubation times a Master Mix was prepare for later addition to the reaction tube. The master mix was prepared as follow:

Materials and Methods

Master Mix for 1 sample

5 x First Strand Buffer	4 μ L
10 x DTT 0.1M	2 μ L
Superscript II RT 200 U/ μ L	1 μ L
RNase Inhibitor 40 U/ μ L	1 μ L
20 x 4dNTP mix 10 mM each NTP	1 μ L

All components were pipet into one reaction tube, vortexed and centrifuged down to make sure the mixture is sufficient mixed. After room temperature incubation of the samples in the reaction tube, 9 μ L of the master mix was added to the RNA sample. Samples were incubated for 1 hour at 42°C for cDNA synthesis and subsequently incubated for 15 minutes in 70°C to inactivate Superscript. Both incubations were done in PCR cycler. After synthesis and inactivation, samples were shortly centrifuged and dilute 1:5 with distilled water (addition of 80 μ L distilled water to 20 μ L synthesis product). cDNA was stored for long term at -20°C or directly used in the quantified PCR.

2.2.37 quantified PCR (qPCR) – Transcriptome analysis

qPCR is used to quantify the level of gene expression of samples, after mRNA isolation from tissue homogenates or cell lysates and cDNA synthesis. The selective gene expression analysis from cDNA by real time quantitative PCR was done with 45 cycles using TaqMan SYBR green PCR master mix. The used primer sets are specified in Materials (2.1.9). Gene expression analysis was performed with technical duplicates of each sample and gene of interest. The fold gene expression of each target gene was calculated relative to the housekeeper gene *Hprt* (Hypoxanthine-guanine phosphoribosyl transferase of murine cells) expression. Calculations for Normalized Relative Quantity (NRG) were based on the threshold cycle (Ct):

$$\text{NRG: } 2^{-\Delta\text{Ct}}; \text{ where } \Delta\text{Ct} = \text{Ct}_{\text{target gene}} - \text{Ct}_{\text{Hprt}}$$

2.2.38 Sodium dodecyl sulfate polyacrylamide gel electrophoresis (SDS-PAGE)

SDS-PAGE is a technique to separate proteins according to their electrophoretic mobility, which depends on the size of the molecule.

<u>10% SDS resolving gel:</u>		<u>5 % stacking gel:</u>	
H ₂ O	6.7 mL	H ₂ O	5.8 mL
30 % acrylamide mix	5.5 mL	30 % acrylamide mix	1.7 µL
1.5 M Tris (pH 8.8)	4.2 mL	0.5 M Tris (pH 6.8)	2.5 mL
10 % SDS	165 µL	10 % SDS	100 µL
25 % ammonium persulfate (APS)	22 µL	25 % APS	20 µL
TEMED	22 µL	TEMED	20 µL

For one 10 % SDS PAGE gel, 8,3 ml of separating gel was prepared. The separating gel mixture was immediately loaded into the casing with a pipette. Distilled H₂O was gently added on the top of the gel. The leftover mixture was held back for determination when the gel is polymerized. The polymerization takes about half an hour, depending on the amount of APS and TEMED. After the separating gel was set, H₂O was poured off and with the help of a Whatman paper the inside of the casing was dried. 5 ml of stacking gel was prepared for one SDS gel. The stacking gel mixture was pipetted into the casing and a required comb was inserted. The leftover was held back for determination of the polymerization similar as for the separating gel. After polymerization of the gel, it was immediately used for the electrophoresis or stored in water wetted paper towel at 4°C for less than one week. 10 µl of PageRuler prestained protein ladder was used for the marker. Gel was run for 10 minutes at 100V constant followed by 1 – 1.5 hours at 120 V constant with 1 x Running Buffer.

2.2.39 Western blotting transfer

Western blotting is a technique for transferring proteins from a gel matrix to a membrane for the subsequent immunodetection of proteins separated by electrophoresis. First, the SDS-PAGE method was used, to separate proteins by their size. Proteins in the SDS gel were transferred with the wet blotting method.

The transfer sandwich was assembled in the following way:

- Anode side of holder (black)
- Thrush
- 1 x Whatman filter
- SDS gel
- PVDF membrane

Materials and Methods

- 1 x Whatman filter
- Thrush
- Cathode side of holder (white)

PVDF membrane was activated with methanol for 1 minute before inserted to the transfer sandwich. All bubbles in the sandwich were removed and the cassette was put into the transfer tank. Transfer buffer was filled in the tank and an ice battery was placed in the chamber to prevent melting of the gel by the heat of the voltage during transfer. Transfer was carried out for 1 hour with a constant voltage of 100V.

PVDF membranes were blocked in 1x Roti-Block for 1 h at room temperature. Membranes were incubated with primary antibodies in the required concentration in blocking solution overnight at 4°C. After incubation, membranes were washed with PBS-T 3 times for 10 minutes and then incubated with the secondary antibody (linked with HRP) for 1 h at room temperature. After washing with PBS-T 3 times for 10 minutes, signals were made visible by SuperSignal® West Femo Maximum Sensitive Substrate (Thermo Fisher Scientific) or ECL® Prime Western Blotting Detection Reagent (GE Healthcare Life Science) and membranes were developed by using ChemiDoc imaging system (BioRad).

After detection of protein of interest binding antibodies were optionally stripped off from the membrane for the incubation with a second specific antibody. Before the stripping, membranes were washed 3 times 10 minutes with PBS-T to remove residual chemiluminescent substrate. To remove binding antibodies, membranes were incubated with Restore PLUS Western Blot Stripping Buffer (Thermo Scientific) for 15 minutes at RT. After stripping, membranes were washed 3 times 10 minutes with PBS-T and blocked again 1h at room temperature in 1 x Roti-Block. Membranes were incubated with the new primary antibody over night at 4°C or 1h at room temperature. Usually after stripping off the antibodies binding the protein of interest, an HRP-labeled anti- β -actin Antibody was used to use the intensity of this housekeeper protein for analysis of protein intensities of the treatment conditions within the experiment. After incubation of the HRP-labeled β -actin antibody, membranes were washed 3 times 10 minutes with PBS-T and β -actin amount was detected described earlier.

2.2.40 Microtome cutting

Lung tissues embedded into paraffin blocks were cut with microtome into 3 µm thick lung slices. Tissue slices were fixed and dried on microscopic slides (super frost,) with 45°C heating plate.

2.2.41 Immunohistochemistry (IHC) staining of lung tissue sections – Vulcan fast red

IHC staining is a method to specifically detect a protein of interest in tissue sections based on an enzymatic reaction leading to a coloration change on site of the target protein. Lung tissue embedded in paraffin and cut on microtome to 3µm thick slides were placed over night at 60°C for the first deparaffinization. To remove the remaining paraffin and rehydrate the tissue it was placed in Xylol and descending ethanol series:

- Xylene 1 5 min.
- Xylene 2 5 min.
- 100% EtOH 1 min.
- 100% EtOH 1 min.
- 90% EtOH 1 min.
- 80% EtOH 1 min.
- 70% EtOH 1 min.
- distilled water 1 min.

To block endogenous peroxidase activity slides were incubated for 20 minutes in 1.8% H₂O₂-Methanol-solution and dipped briefly afterwards in distilled water. For paraffin embedded tissue, epitopes of interest need to be restored. For this depending on the primary antibody application heat induced epitope retrieval (HIER) needs to be done either with the use of HIER Citrate buffer or HIER EDTA buffer. In case of Citrate retrieval, tissue sections were placed into a cuvette immersed with 1 x HIER Citrate buffer and cooked in the Decloaking chamber (filled with 500 mL distilled water) up to 125°C holding the temperature for 10 seconds and subsequently cooled down to 90°C holding the temperature for 30 seconds. In need of EDTA retrieval, tissue sections were placed into a cuvette immersed with 1 x HIER EDTA buffer. Cuvette was placed into a water bath preheated to 95°C for 45 minutes. After the retrieval processes, cuvettes were cooled down for 10 minutes at room temperature and gradually cooled

Materials and Methods

down by adding little by little TBS wash buffer into the cuvette. Sections were washed 3 times for 2 minutes in TBS wash buffer. After the first washing step, tissue sections were bordered with PapPen (histological hydrophobic pen, DAKO). After washing, samples were blocked for 30 minutes at room temperature with addition of 1 or 2 drops per section of Rodent Block M (BioCare Medical). After blocking tissue sections were washed by rinsing 3 times with TBS buffer. Primary antibody of interest was diluted to the working concentration (depending on primary antibody) in Antibody diluent and add to the sections. Primary antibody was incubated over night at 4°C, placed in an incubation box to maintain moisture surrounding. On following day, lung sections were washed 3 times for 2 minutes in TBS buffer. After washing lung sections were incubated with an AP-Polymer specific binding to the host specimen of the primary antibody (Rabbit on rodent AP-Polymer, Rat on rodent AP-Polymer, Mouse on Mouse AP-Polymer, Goat on Mouse AP-Polymer) and washed again 3 times for 2 minutes with TBS buffer. 2.5 mL of Vulcan fast red buffer were freshly mixed with 1 drop of chromogen dye and added to the tissue section for enzymatic substrate metabolism to visualize protein of interest by a color change to pink. Incubation time depends on intensity of primary antibody. Time varies between 5 and 15 minutes. Enzymatic reaction was stopped by placing slides into distilled water. For counterstain of the tissue structure, sections were dipped briefly (0.5 sec. up to 4 sec. depending on antibody and wanted intensity of counter staining) in Hematoxylin followed by briefly dipping into distilled water and incubated for one minute in tap water for blueing of the sections. After tap water incubation, slides were washed once in distilled water and dried on 60°C heating plate for 15 minutes. For dehydration and mounting, completely dried slides were placed into Xylol for 5 minutes. This step was repeated with fresh Xylol. Slides were mounted with Entellan and covered with a glass cover slide. Because of vapors, Xylol and Entellan is releasing, slides were dried under the chemical hood overnight and stored for long term in histological boxes, protected from light at room temperature.

2.2.42 Immunohistochemistry (IHC) staining of lung tissue sections – DAB

IHC staining is a method to specifically detect a protein of interest in tissue sections based on an enzymatic reaction leading to a coloration change on site of the target protein. Lung tissue embedded in paraffin and cut on microtome to 3µm thick slides

were placed over night at 60°C for the first deparaffinization. To remove the remaining paraffin and rehydrate the tissue it was placed in Xylol and descending ethanol series:

- Xylene 1 5 min.
- Xylene 2 5 min.
- 100% EtOH 1 min.
- 100% EtOH 1 min.
- 90% EtOH 1 min.
- 80% EtOH 1 min.
- 70% EtOH 1 min.
- Running tap water 4 min.

For paraffin embedded tissue, epitopes of interest need to be restored. For this depending on the primary antibody application heat induced epitope retrieval (HIER) needs to be done either with the use of HIER Citrate buffer or HIER EDTA buffer. In case of Citrate retrieval, tissue sections were placed into a cuvette immersed with 1 x HIER Citrate buffer and cooked in the Decloaking chamber (filled with 500 mL distilled water) up to 125°C holding the temperature for 10 seconds and subsequently cooled down to 90°C holding the temperature for 30 seconds. In need of EDTA retrieval, tissue sections were placed into a cuvette immersed with 1 x HIER EDTA buffer. Cuvette was placed into a water bath preheated to 95°C for 45 minutes. After the retrieval processes, cuvettes were cooled down for 10 minutes at room temperature and gradually cooled down by running tap water for 5 minutes. Slides were quickly rinsed in dest. Water and tissue sections were bordered with PapPen (histological hydrophobic pen, DAKO). Slides were rehydrated for 10 minutes in PBS-T (1 x PBS + 0.1% Tween-20). Endogenous peroxidase activity was blocked in the tissue with incubating 10 minutes in 3% H₂O₂ (30% H₂O₂ diluted in PBS). After blocking, slides were washed 3 x 2 minutes in PBS-T and a drop of Avidin solution was add to each section and incubated for 15 min, at RT, followed by 3 x 2 minutes washing in PBS-T. 1 drop of Biotin solution was added to each section and washing step was repeated. Unspecific binging was blocked with 3% BSA in PBS blocking for 1h at RT. Primary antibody was diluted in 3% BSA in PBS, where the dilution was depending on the antibody, and overlayed to the tissue sections. Primary antibody was humidified incubated overnight at 4°C. At the following day, slides were washed 3 x 2 min. in PBS-T and incubated for 30 minutes at RT with biotinylated secondary antibody, where the dilution was depending on the antibody. Peroxidase solution was prepared by adding

Materials and Methods

1 drop of solution A and 1 drop of solution B in 2.5 mL PBS. Prepared solution was protected from light and incubated for 30 minutes at RT in the falcon tube before application. After the usual washing step, peroxidase solution was given to the tissue and incubated for 30 minutes, protected from light. Slides were washed again and substrate solution was prepared by adding 1 drop of DAB to 1 mL of DAB buffer.

After an additional washing step, substrate solution was added to the tissue section for enzymatic substrate metabolism to visualize protein of interest by a color change to brown. Incubation time depends on intensity of primary antibody. Time varies between 30 seconds and 5 minutes. Enzymatic reaction was stopped by placing slides into distilled water. For counterstain of the tissue structure, sections were dipped briefly (4 to 20 sec. depending on antibody and intensity of counter staining) in Hematoxylin followed by briefly dipping into distilled water and placing under running in tap water for blueing of the sections. After tap water incubation, slides were dipped into distilled water and rehydration was performed, by dipping slides in 70% Ethanol, 80% Ethanol, 96% Ethanol and 90% Ethanol followed by 2 x 100% Ethanol for 1 minute and 2 x Xylol for 5 minutes. Slides were mounted with Entellan and covered with a glass cover slide. Because of vapors, Xylol and Entellan is releasing, slides were dried under the chemical hood overnight and stored for long term in histological boxes, protected from light at room temperature.

2.2.43 Immunofluorescence (IF) staining of lung tissue sections

IF staining is a method to specifically detect a protein of interest in tissue sections based on binding of a primary antibody to the target protein and following binding of a fluorophore labelled secondary antibody to the primary antibody. Lung tissue embedded in paraffin and cut on microtome to 3µm thick slides were placed over night at 60°C for the first deparaffinization. To remove the remaining paraffin and rehydrate the tissue it was placed in Xylol and descending ethanol series:

- Xylene 1 5 min.
- Xylene 2 5 min.
- 100% EtOH 1 min.
- 100% EtOH 1 min.
- 90% EtOH 1 min.
- 80% EtOH 1 min.

- 70% EtOH 1 min.
- distilled water 1 min.

For paraffin embedded tissue, epitopes of interest need to be restored. For this depending on the primary antibody application heat induced epitope retrieval (HIER) needs to be done either with the use of HIER Citrate buffer or HIER EDTA buffer. In case of Citrate retrieval, tissue sections were placed into a cuvette immersed with 1 x HIER Citrate buffer and cooked in the Decloaking chamber (filled with 500 mL distilled water) up to 125°C holding the temperature for 10 seconds and subsequently cooled down to 90°C holding the temperature for 30 seconds. In need of EDTA retrieval, tissue sections were placed into a cuvette immersed with 1 x HIER EDTA buffer. Cuvette was placed into a water bath preheated to 95°C for 45 minutes. After the retrieval processes, cuvettes were cooled down for 10 minutes at room temperature and gradually cooled down by adding little by little PBS-T wash buffer into the cuvette. Sections were washed 3 times for 2 minutes in PBS-T wash buffer. After the first washing step, tissue sections were bordered with PapPen (histological hydrophobic pen, DAKO). After washing, samples were blocked for 60 minutes at room temperature with addition of 1 or 2 drops per section of IF Blocking buffer. After blocking tissue sections were washed by rinsing 3 times with PBS-T buffer. Primary antibody of interest was diluted to the working concentration (depending on primary antibody) in Antibody diluent and add to the sections. Primary antibody was incubated over night at 4°C, placed in an incubation box to maintain moisture surrounding. On following day, lung sections were washed 3 times for 2 minutes in PBS-T buffer. After washing lung sections were incubated for 1 hour at room temperature and protected from light with fluorophore labeled secondary antibody binding specific to host specimen of primary antibody. Additionally adding of 1:1000 dilution of DAPI and 1:40 dilution of Phalloidin, to visualize the nuclear structure and cytoplasm. After incubation, slides were washed 3 x 5 minutes in PBS-T and slides were mounted to preserve the staining. For this preservation, 1 drop of fluorescence DAKO mounting medium was added to the tissue and a glass cover slip was gently placed on the slide. After 1h of letting the mounting medium harden at RT, in the dark, the slides were stored at 4°C until microscopical examination.

2.2.44 Detecting DNA fragmentation with TUNEL assay

TUNEL assay is a method to detect DNA fragmentation by labeling the 3'-hydroxyl termini in the double stranded DNA breaks generated during cell death. Lung tissue embedded in paraffin and cut on microtome to 3µm thick slides were placed over night at 60°C for the first deparaffinization. To remove the remaining paraffin and rehydrate the tissue it was placed in Xylol and descending ethanol series:

- Xylene 1 5 min.
- Xylene 2 5 min.
- 100% EtOH 1 min.
- 100% EtOH 1 min.
- 90% EtOH 1 min.
- 80% EtOH 1 min.
- 70% EtOH 1 min.

After rehydration, slides were incubated for 5 min. in 0.85% NaCl, followed by 2 x 5 min. in PBS. Addition of 100 µL proteinase K solution (20µg/mL Proteinase K in Tris-HCl pH 8.0 + 50 mM EDTA) and incubation for 5 minutes at RT. Wash slides 5 minutes in PBS. Fix slides for 5 minutes in 4% PFA and wash again 5 minutes in PBS. Cover slides with Wash buffer for 5 minutes and repeat this step one more time. Cover the slides with 50 µL of the DNA labeling solution, prepared as described:

For 1 test

- TdT Reaction Buffer 10 µL
- TdT Enzyme 0.75 µL
- Br-dUTP 8 µL
- ddH₂O 32.35 µL
- TOTAL VOLUME 51 µL

Gently place a cover slip on the top of the cells to ensure even distribution. Place the slides in a dark humidified 37°C incubator for 1h. Remove the cover slips and wash the slides 3 x 5 minutes in PBS. Cover the slides with 100 µL antibody solution, prepared as described:

For 1 test

- Anti-BrdU-Red antibody 5 µL

- Rinse buffer 95 μ L
- Phalloidin-488 2.5 μ L
- DAPI 1 μ L

Gently place a cover slip on the top of the cells to ensure even distribution. Place the slides in a dark humidified incubation chamber for 30 minutes at RT. Wash the slides 3 x 5 minutes with ddH₂O. Slides were mounted to preserve the staining. For this preservation, 1 drop of fluorescence DAKO mounting medium was added to the tissue and a glass cover slip was gently placed on the slide. After 1h of letting the mounting medium harden at RT, in the dark, the slides were stored at 4°C until microscopical examination.

2.2.45 Hematoxylin and Eosin (H&E) staining

H&E staining is for staining of histological samples to an intense blue nucleus by Hemalum and a pink stain of the cytoplasm by Eosin.

Lung tissue embedded in paraffin and cut on microtome to 3 μ m thick slides were placed over night at 37°C for the first deparaffinization. To remove the remaining paraffin and rehydrate the tissue it was placed in Xylol and descending ethanol series:

- Xylene 1 5 min.
- Xylene 2 5 min.
- 100% EtOH 1 min.
- 100% EtOH 1 min.
- 90% EtOH 1 min.
- 80% EtOH 1 min.
- 70% EtOH 1 min.
- distilled water 1 min.

For the nuclear staining tissues were incubated with Mayer's Hemalum (filtered before usage) for 5 minutes. After the incubation tissues were briefly dipped first into tap water and subsequent in 0.1% HCL-EtOH. Following samples were adequately blued in the sink with running tap water for 10 minutes. After bluing, the tissue was dipped briefly in distilled water and afterwards incubated in 0.5% Eosin (filtered before usage) for 8

minutes for cytoplasm staining. after finishing the staining tissue was dehydrogenated with an ascending ethanol series:

- 70% EtOH 1 x dip briefly
- 80% EtOH 1 x dip briefly
- 90% EtOH 1 x dip briefly
- 96% EtOH 1 x dip briefly
- 100% EtOH 1 min.
- 100% EtOH 1 min.
- Xylene 1 5 min.
- Xylene 2 5 min.

After dehydration, tissues were covered with Entellan and glass cover slips in the corresponding size. The slides were left for hardening overnight under the hood and long term stored in a dry and light protected cover box at room temperature.

2.2.46 Masson's Goldner Trichrome staining

To visualize collagen deposition into the lung tissue, Masson's Goldner Trichrome staining was done with 3 µm thick lung sections using the staining Kit #3459 from Roth. Manufacturer's protocol was change according to the best suitable conditions.

All staining solutions were filtered before usage and except Weigert's iron hematoxylin used for several times.

First deparaffinization was done by putting slides over night at 60°C incubator. To remove the remaining paraffin and rehydrate the tissue it was placed in Xylol and descending ethanol series:

5 minutes Xylene 1

- 5 minutes Xylene 2
- 1 minute 100% Ethanol 1
- 1 minute 100% Ethanol 2
- 1 minute 90% Ethanol
- 1 minute 80% Ethanol
- 1 minute 70% Ethanol

Start with staining directly from 70% Ethanol:

- 10 minutes in Weigert's iron hematoxylin
- 1 x dip briefly in tap water

- 1 x dip briefly in HCl-Ethanol (2 mL 32% HCl + 200 mL 70% Ethanol)
- 12 minutes under running tap water
- 1 x dip briefly in distilled water
- 5 minutes in Goldner Solution I (ponceau acid fuchsin)
- 1x dip briefly in 1% acetic acid and change solution → 30 seconds in 1% acetic acid
- 1 x dip briefly in distilled water
- 8 minutes in Goldner Solution II (phosphomolybdic acid)
- 1x dip briefly in 1% acetic acid and change solution → 30 seconds in 1% acetic acid
- 15 minutes in Goldner Solution III (Light green)
- 1x dip briefly in 1% acetic acid and change solution → 30 seconds in 1% acetic acid
- 1 x dip briefly in distilled water
- 1 x dip briefly sequentially in 70% EtOH, 80% EtOH, 90% EtOH, 96% EtOH
- 1 minute 100% Ethanol 1
- 1 minute 100% Ethanol 2
- 5 minutes Xylene 1
- 5 minutes Xylene 2

After dehydration, tissues were covered with Entellan and glass cover slips in the corresponding size. The slides were left for hardening overnight under the hood and long term stored in a dry and light protected cover box at room temperature.

2.2.47 Imaging of histological stainings

Brightfield and fluorescence images were taken with Olympus BX-51 light microscope (Olympus, Hamburg, Germany). With fluorescence filter for DAPI, AF-488, Cy-3, Cy-5.

2.2.48 Quantitative morphometry of mean linear chord length (MCL), IHC stains and tissue inflammation

In this study, MCL, IHC stains and tissue inflammation were determined using stereology. Computer-assisted stereological toolbox software Visopharm Integrator

Materials and Methods

System (VIS) v6.0.0.1765 (newCAST, Visiopharm) was used for design-based stereology to analyze histological lung sections using an Olympus BX51 light microscope. H&E was used for assessing the airspace enlargement and the tissue inflammation. Air space enlargement was assessed by quantifying mean linear chord length (MCL) on 30 field of view per lung, a line grid was superimposed on lung section images taken with the $\times 20$ objective. Intercepts of lines with alveolar septa and points hitting airspace were counted to calculate MCL applying the formula $MCL = \frac{\sum P_{air} \times L(p)}{\sum I_{septa}} \times 0.5$. P_{air} are the points of the grid hitting air spaces, $L(p)$ is the line length per point, and I_{septa} is the sum of intercepts of alveolar septa with grid lines. To quantify tissue inflammation in the lung, a line grid was superimposed on lung section images taken with the $\times 20$ objective and were analyzed on lung sections across at least 30 random fields per lung. Intercepts of lines crossing with airways and vessels were counted to calculate the tissue inflammation ($\mu m^3/\mu m^2$) = $\frac{\sum P_{inflamed\ area} \times L(p)}{\sum I_{intercept(A+V)}}$. $P_{inflamed\ area}$ are the points of the grid hitting inflammatory tissue area, $L(p)$ is the line length per point, and $I_{intercept(A+V)}$ is the sum of intercepts of airways and vessels to normalize the inflammatory area.

To determine IHC stains, the number of specific antibody positive cells across the lung was used with CAST system. 30 random fields were chosen by the software in the lung sections and with 40x objective was used to take images of AB positive cells, which were count across this random field of views. The mean value per lung was used as a representative “positive cells per field”.

2.2.49 Statistical analysis

In this study, results were presented as mean values \pm standard deviation (SD). Figure legends contain the number of samples as well as number of repeats (“n” numbers) for each graph. To compare the significance between only two groups, student’s unpaired t-test was performed, when comparing more than two groups in one experiment, one-way ANOVA followed by Tukey’s multiple comparisons test was used. Dose dependent analysis was performed with either nonlinear or linear regression.

Correlations between two measured results were tested with GraphPad Prism correlation test. Significance was determined according to *P value* being lower than 0.05. All graphs were generated with the help of GraphPad Prism software version 9.4 (GraphPad Software, Inc. San Diego, CA, USA). “*”, “#” or “\$” was used to show

significant difference, */#/\$ $P < 0.05$, **/##/\$\$ $P < 0.01$, ***/###/\$\$\$ $P < 0.001$, ****/####/\$\$\$\$ $P < 0.0001$.

3. Results

3.1 Characterization of CNP and DWCNT for *in vitro* and *in vivo* application

To study virus reactivation *in vitro* and pulmonary inflammatory and virus reactivation *in vivo*, I used different kinds of carbonaceous nanoparticles (CNP) and fiber shaped double walled carbon nanotubes (DWCNTs). CNP is a soot-like nanoparticle of agglomerates from primary particles with a diameter of 14 nm. Brunauer-Emmett-Teller (BET) analysis revealed the CNP surface area of 272 cm²/g (Stoeger et al., 2009; Sattler et al., 2017). In aqueous dispersions, with a concentration of 1 mg/mL, CNP form agglomerates of 140 nm (+/- 20nm) analyzed by dynamic laser scatter (DLS) measurement. The Polydispersity index (Pdl) is between 0.1 and 0.2 which indicates a stable dispersion in H₂O.

DWCNTs is an engineered nanomaterial with fiber shape similar to asbestos. DWCNT has a 10 nm diameter and a length of 1000 nm with a BET of 660 m²/g (Sattler et al., 2017). DWCNTs easily form aggregations when dispersed in ultrapure water. Dispersion quality can be increased with 1% Pluronic F-127 (Sigma Aldrich, Germany). The dynamic diameter is 1800 to 3200 nm and Pdl is 0.4 to 0.6. DWCNT are less stable in water than CNPs.

Table 3.1 Characterization of nanoparticles used in the study

Nanoparticles	Name	Acronym	Particle Size ^a (nm)	BET ^b (m ² /g)
Carbon black	Printex 90	CNP	14	272
Double walled carbon nanotubes	NC2100 TM	DWCNT	10*1000	660

a Particle Size: primary particle size, not considering agglomerate formation

b BET: Brunauer-Emmett-Teller (BET) surface area analysis of particle surface area based on nitrogen adsorption.

3.2 Repeated CNP and DWCNT instillation trigger MHV-68 reactivation in the lungs

3.2.1 Repeated CNP and DWCNT instillation approaches environmental NP exposure

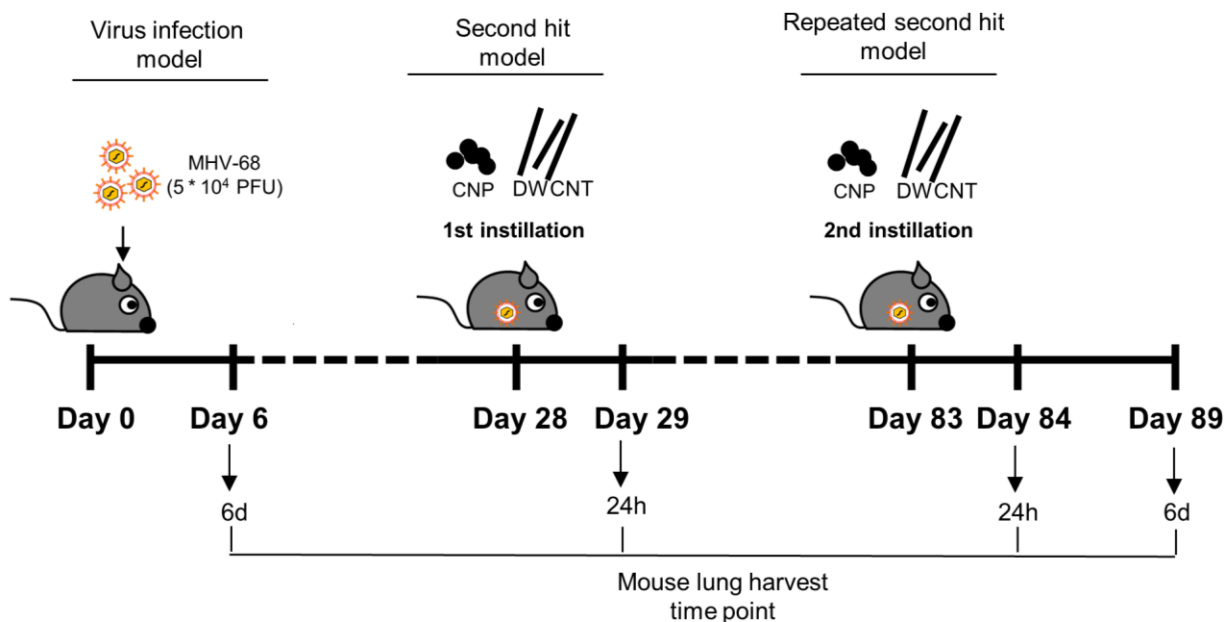


Figure 3.1 Schematic illustration of repeated CNP and DWCNT instillation into MHV-68 infected mice.

C57BL/6 mice were intranasally infected with 5×10^4 PFU MHV-68 for 28 days to establish virus latency. At day 28 and day 83 after virus infection mice were exposed to 50 μg of CNP or DWCNT by intratracheal instillation. 6d after MHV-68 infection, 24h after the first and 24h and 6 days after the second CNP or DWCNT exposure, mouse serum, lung tissue, bronchoalveolar lavage (BAL) fluid and BAL cells were harvested to investigate cytokines and chemokines, free dsDNA, BAL protein and IgM levels as well as structural and inflammatory changes and cell recruitment into the lung tissue and air space. 5 mice per group were treated for the analysis of BAL fluid and protein, RNA in lung tissue and 3 mice per group were treated for the histological examination.

Previous experiments from our group, as described in Sattler et al. 2017, showed that pulmonary exposure to carbon nanoparticles (CNP) and double walled carbon nanotubes (DWCNT) trigger the reactivation of latent virus infection with an increase of lytic virus proteins in mouse lungs of latently infected MHV-68 animals (Sattler et al., 2017). In my project, I was interested, how repeated nanoparticle (NP) exposure effect the lung structure, inflammation and integrity. The repeated NP exposure should mimic

Results

a chronic and more environmental relevant exposure scenario. We performed an *in vivo* experiment (**Fig. 3.1**) with C57BL/6 mice. They were intranasally (i.n.) infected with 5×10^4 PFU MHV-68 for 28 days to establish latency (virus infection model). At day 28, either 50 μ g CNP or DWCNT were intratracheal instilled for the first time (second hit model). 24h later, some mice were sacrificed, and tissue was harvested. 55 days after the first instillation, a second 50 μ g CNP or DWCNT dosing was intratracheal instilled into the lungs (repeated second hit model). 24h and 6 days after the repeated instillation, mice were sacrificed, and lungs were analyzed on histological level for nanoparticle-triggered reactivation of MHV-68 latent infection to its lytic infection phase. To investigate reactivation, lytic virus proteins were stained with Immunohistochemistry (IHC) with polyclonal rabbit serum containing antibodies directed against lytic proteins of MHV-68 (described previously by Steer et al., 2010).

3.2.2 CNP and DWCNT trigger virus reactivation in the lung in first and repeated exposure

During latent virus infection only a limited number of viral proteins are expressed. When latent virus gets triggered to reactivate to its lytic infection phase, more proteins are produced by the virus. In previous work of Sattler and the group, only one time of CNP or DWCNT was instilled to the lungs of infected animals to test virus reactivation (Sattler et al., 2017). In this work, I confirm, that the repeated NP exposure also allows the MHV-68 to reactivate. For this investigation, lung tissue was sectioned and immunohistochemically (IHC) stained for lytic virus proteins with polyclonal rabbit serum containing antibodies directed against lytic proteins of MHV-68. MHV-lytic proteins can be visualized in Vulcan fast red staining in pink, compared to the violet staining for the lung structure. In **Fig. 3.2**, its shown, that the control and virus latency have no positive cells for lytic proteins. In the positive control, the acute virus infection after 6 days, lytic MHV-68 proteins are mainly localized in the alveolar epithelium. In the 2nd hit models, virus latency plus NP exposure, cells positive for the lytic virus proteins are visible. The localization of the virus proteins changed from acute virus infection mainly in the epithelial region to more diffuse localizations in tissue recruited cells. These cells are mainly localized peribronchial and perivascular. Virus reactivation can be observed in both, the first and repeated instillation, with both the CNP and DWCNT particles. Even still in the later time point at 6 days after the repeated

NP exposure, lytic virus protein positive cells can still be observed. These results show that virus can be reactivated for several times, after nanoparticle exposure to the lungs.

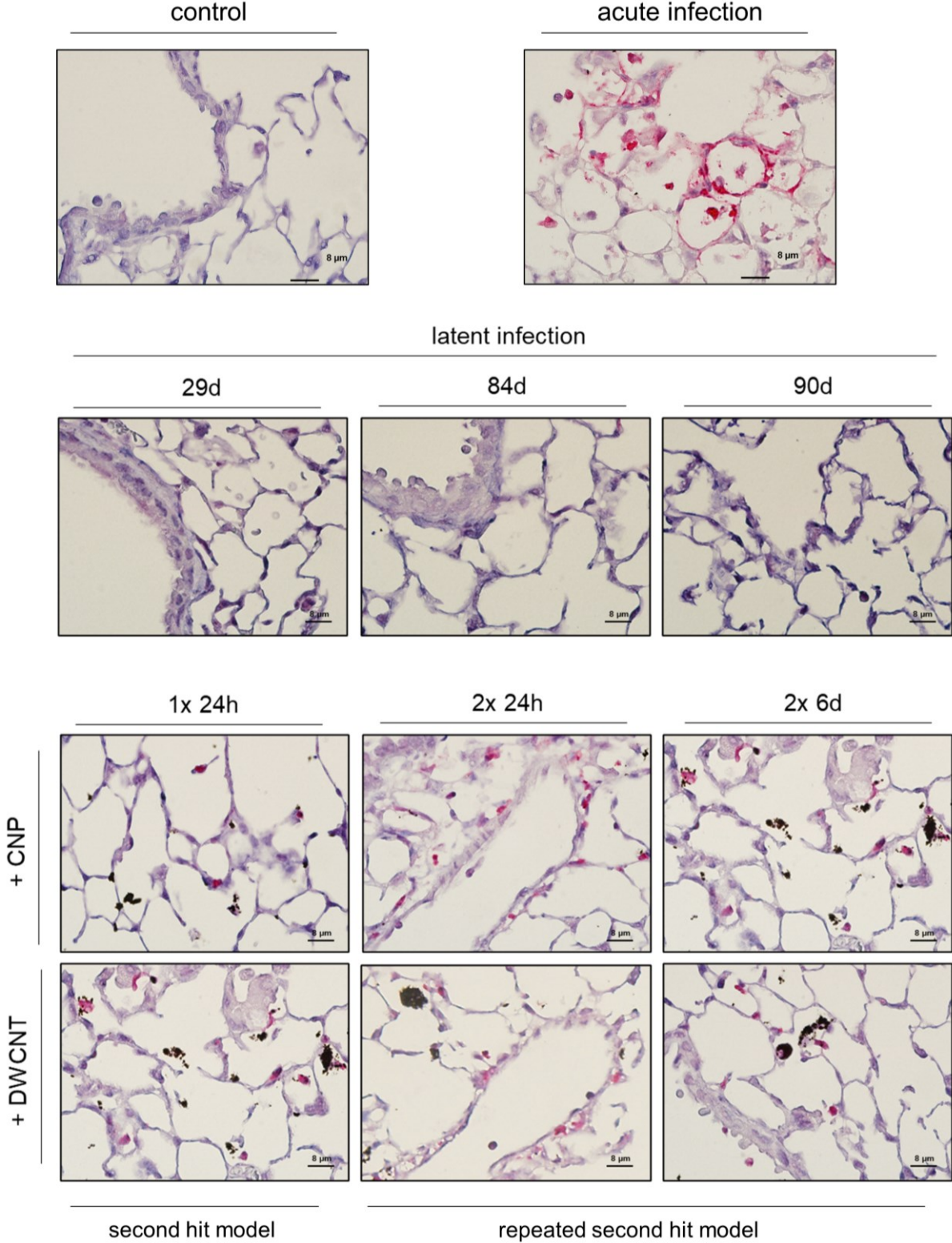


Figure 3.2 Nanoparticles trigger virus reactivation in first and repeated exposure in lung tissue. Mice latently infected with MHV-68 were one and two times instilled with CNP or DWCNT. Lung tissue was isolated and histological analyzed after IHC staining for lytic virus proteins to investigate virus

Results

reactivation. Non-infected control and virus latency shows no lytic virus protein staining. Acute virus infection after 6 days shows lytic virus proteins localized mainly in epithelial cells. IHC stains of lytic virus proteins show reactivation in the 2nd hit model, mainly in infiltrating cells. In all conditions, with CNP and DWCNT in first and repeated NP exposure. Scale bar: 8 μ m.

3.2.3 CD11b and IBA1 positive recruited macrophages are the main cell type for nanoparticle-triggered virus reactivation

As I detected MHV-68 lytic protein expression via IHC in infiltrating cells after particle-triggered reactivation, I want to investigate which cells reactivating latent MHV-68 infection upon the CNP or DWCNT exposure. I used IF co-staining to test different cellular marker to be co-localized with the lytic MHV-68 proteins. MHV-68 lytic proteins were not found to be co-localized with CD3+ T-lymphocytes, CD45r/B220+ B-lymphocytes, MPO+ neutrophils, CCR2+ monocytes or CD11c+ or Siglecf+ alveolar macrophages. I found MHV-68 reactivating in cells positive for both, CD11b and Iba1 (**Fig. 3.3**). CD11b, or integrin alpha M, belongs to integrin family and predominately expressed in monocytes, monocyte derived macrophages and granulocytes. In lung tissue, A high expression of CD11b is mainly detected in inflammatory, recruited macrophages originating from circulating monocytes or interstitial macrophages. Ionized calcium-binding adapter molecule (Iba1), or allograft inflammatory factor 1 (AIF-1), in contrast is expressed in all lung macrophages, except alveolar macrophages. Few cells reactivating MHV-68 were found to be also positive for ARG1 and GPNMB. Both proteins are known to be expressed in inflammatory macrophages. The predominantly co-localization of CD11b and Iba1 with lytic MHV-68 proteins, indicate inflammatory recruited macrophages, not tissue resident alveolar macrophages as the source of MHV-68 reactivating cells in the 2nd hit model.

Table 3.2 Marker co-localization with lytic MHV-68 proteins

Immunohistological marker	Co-localization with MHV-68 lytic proteins	Potential cell type
CD11b	yes	Inflammatory monocyte derived macrophages, interstitial macrophages, dendritic cell subset

IBA1/AIF-1	yes	All macrophages, except alveolar macrophages
Arg1	yes	M2 polarized inflammatory macrophages, monocytes
GPNMB	yes	Inflammatory macrophages
CD11c	no	Alveolar macrophages, dendritic cell subset
Siglecf	no	Alveolar macrophages, Eosinophils
CCR2	no	Classical monocytes and derived macrophages
CD45r/B220	no	B-lymphocytes
CD3	no	T-lymphocytes
CD4	no	T-helper cells
CD8	no	Cytotoxic T-lymphocytes
MPO	no	Neutrophils

Results

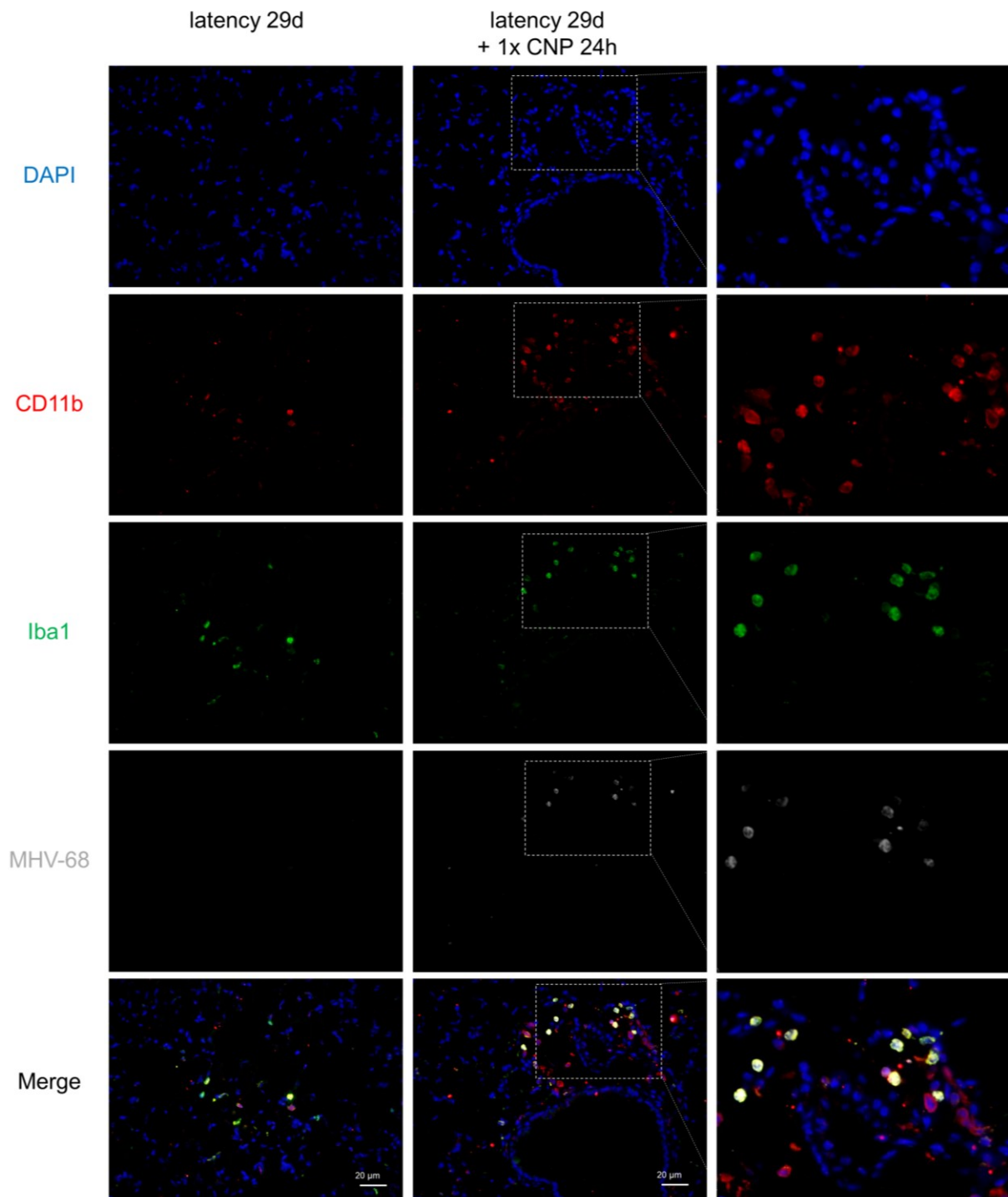


Figure 3.3 NP-triggered MHV-68 reactivation occurs in CD11b+/IBA1+ cells.

Immunofluorescence (IF) staining of CD11b, IBA1 and lytic MHV-68 proteins. Left picture shows IF staining of lung tissue of latent virus infection after 29 days. Right picture shows staining of lung tissue of virus latency plus 1xCNP instillation. Anti-CD11b antibody, anti-Iba1 antibody and anti-lytic MHV-68 protein antibody was used for IF staining followed by Alexa Fluor 555-conjugated, Alexa Fluor 488-conjugated and Alexa Fluor 647-conjugated secondary antibodies, respectively. Image below shows all channels merged. The co-staining show co-localization of all markers, indicating NP-triggered virus reactivation happening in recruited macrophages. All sections were co-stained with DAPI. Scale bar: 20 μm .

3.3 BAL cell differentiation – Airspace accumulation of lymphocytes and neutrophils in repeated CNP exposure of latently infected mice

Mice were infected with MHV-68 and after established latency (day 28 post infection), either with 50µg CNP or DWCNT were instilled intratracheal for one or two repeated times. After different time points, bronchoalveolar lavage was performed to collect cells, which are localized in the airspace. Cells were centrifuged to a microscopic slide and Giemsa staining was performed to differentiate the BAL cells by morphology and staining pattern. A significant increase of total BAL cell numbers in all groups of the second hit model and repeated second hit model, both after CNP and DWCNT and 24h after of the first and repeated CNP exposure was observed (**Fig. 3.4a**). Elevated airspace neutrophil numbers indicating an acute pulmonary inflammation. Neutrophils were observed significantly high 24h after the first and repeated CNP exposure in non-infected animals, 24h after the first DWCNT exposure in non-infected mice and in the second hit model (**Fig. 3.4b**). Furthermore, elevated airspace as well as interstitial lymphocyte numbers indicate chronic pulmonary inflammation. In BAL differentiation staining (Giemsa staining), further discrimination of B-lymphocytes, T-lymphocytes or natural killer cells cannot be investigated. Significantly higher numbers of airspace lymphocytes are found in all latency groups, in NP treatment or without. In both CNP and DWCNT exposure. Besides the infection groups, there is also a significant increase of airspace lymphocytes in the later time point of repeated CNP exposure in non-infected animals (**Fig. 3.4c**). Airspace macrophages are mainly alveolar macrophages and found to be significantly increased in the early phases of virus latency with and without NP exposure. High macrophage numbers last longer in the second hit and repeated second hit model of DWCNTs (**Fig. 3.4d**). Representative Giemsa-stained BAL cell images are shown in **Figure 3.4e**. In the control, mainly alveolar macrophages are found (marked with “M”), and few numbers of neutrophils and lymphocytes (“L”). In virus latency and CNP exposure, there are significantly more neutrophils (“N”) and lymphocytes (“L”) compared to macrophages (“M”). In the right image, CNP uptake of alveolar macrophages are clearly visible (“NP-M”). No eosinophils were observed in BAL cytopins.

Results

Taken together, BAL cell differentiation shows combinatory significant increase of airspace recruited lymphocytes and neutrophils in repeated 2nd hit model with CNP instillation compared to virus latency or NP exposure alone.

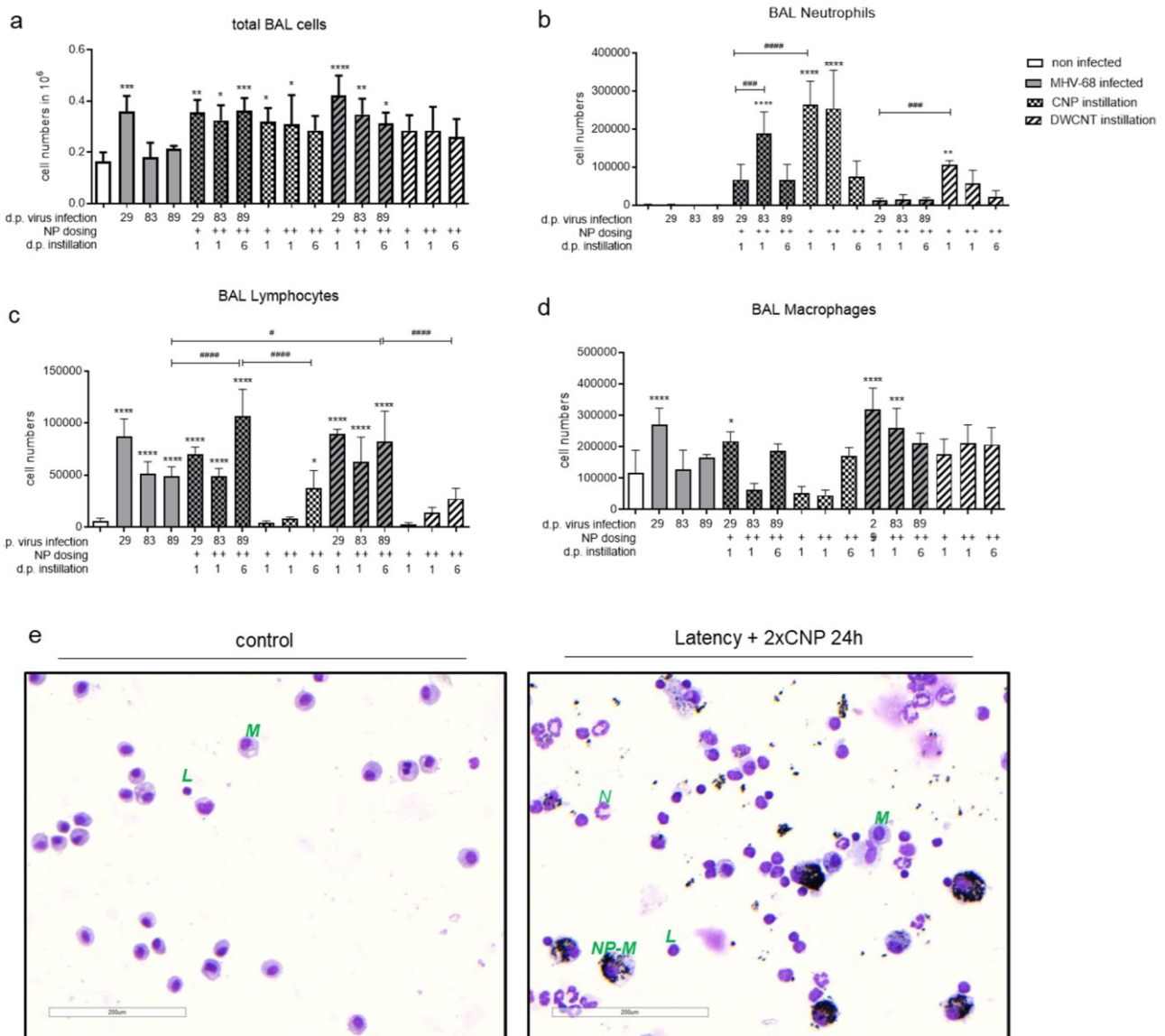


Figure 3.4 Differentiation of BAL cells show significant increase of lymphocytes and neutrophils in 2nd hit model.

BAL cell isolation from mice infected with MHV-68 and treated with CNP or DWCNT. BAL cells were counted and differentiated after cytopsin and Giemsa staining. (a) shows total BAL cells. (b) shows BAL neutrophil numbers which were significantly high in repeated CNP exposure in virus latency, early CNP time points in first and repeated exposure and in the first exposure of DWCNTs. (c) shows BAL lymphocytes with increased numbers in all MHV-68 latency groups with and without CNP or DWCNT, and in the late time point of repeated CNP exposure. Significant higher BAL lymphocytes in later time points in the 2nd hit model after repeated CNP or DWCNT exposure compared to virus latency or NP

only. (d) shows BAL macrophages with increased numbers in virus latency with and without NP exposure. (n = 5-7). (e) shows representative bright field microscopic images of BAL cell cytopins with Giemsa staining. Left image show control with green "M": macrophage and green "L": lymphocyte, right image show MHV-68 latency plus repeated CNP exposure with green "N": neutrophil, green "L": lymphocyte, green "M": macrophage, green "NP-M": nanoparticle laden macrophage. Scale bar: 200 μ m. Data were analyzed by Ordinary one-way ANOVA and Tukey's multiple comparisons test, "*" indicates statistically significant difference to "control". *: indicates *P value* < 0.05. **: indicates *P value* < 0.01. ***: indicates *P value* < 0.001. ****: indicates *P value* < 0.0001. "#" indicates statistically significant difference of two indicated groups. #: indicates *P value* < 0.05. ###: indicates *P value* < 0.001. ####: indicates *P value* < 0.0001.

3.4 Increased lung tissue inflammation in 2nd hit model

As I can see a high recruitment of lymphocytes and neutrophils to the airspace, I wanted to investigate, how the lung tissue inflammation can be validated. For this observation, lungs were harvested, PFA-fixed and embedded into paraffin. After embedding, tissue was cut in slices and stained with hematoxylin and eosin (H&E) to visualize pulmonary structure. In lung tissue, I also observe high numbers of tissue infiltrating cells (**Fig. 3.5a**). Cellular infiltrations mainly localized in peribronchial and perivascular regions. Inflammation level can be assessed by CAST quantification, in which random fields of view are chosen by the software, and inflammatory area is marked. Inflammatory area gets normalized to the bronchial region of all slides. In the quantification I see higher tissue inflammation in the 2nd hit model, with both, CNP and DWCNT exposure. There is also higher pulmonary inflammation in the first exposure to DWCNT in non-infected animals (**Fig. 3.5b**). From H&E staining it was not possible to clearly distinguish the exact cell types infiltrating to the pulmonary area, leading to tissue inflammation. What is only clear with H&E staining, that there are no eosinophil cell recruitments, which confirms also the BAL cell differentiation in which I did not see changes of eosinophilic numbers.

Results

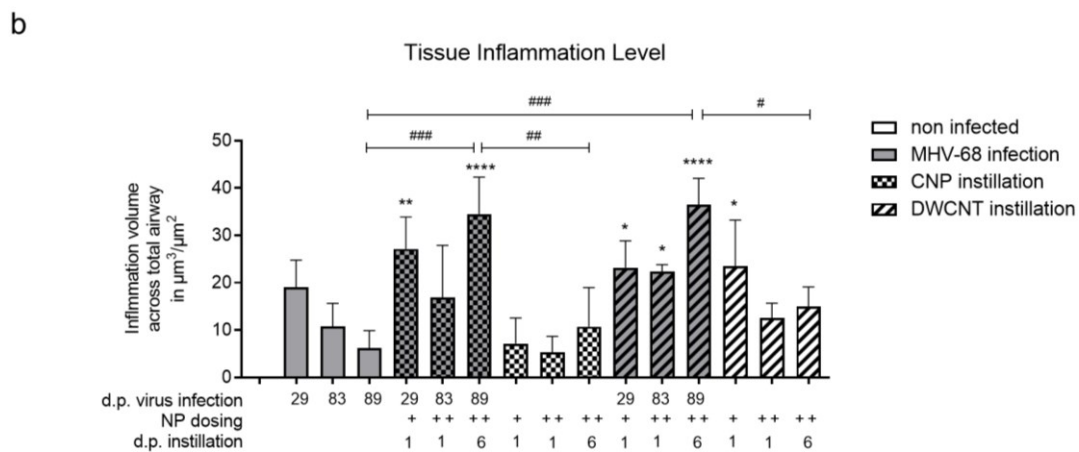
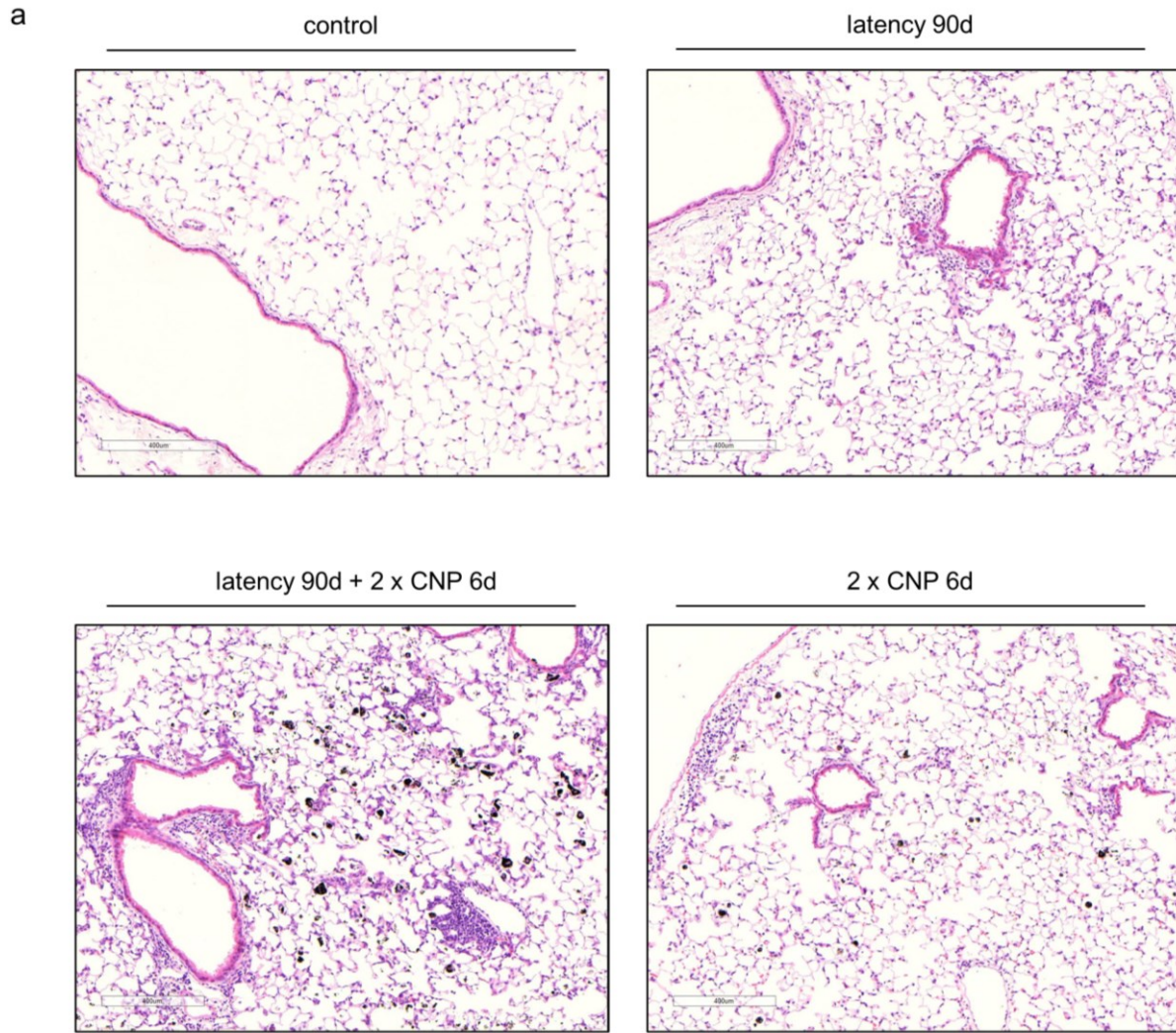


Figure 3.5 Increased tissue inflammation level in 2nd hit model.

Lungs were isolated from mice infected with MHV-68 and instilled with CNP or DWCNT in latency. Histological slides were stained with H&E and analyzed for tissue inflammation with CAST. (a) shows representative brightfield images from lung tissue. (b) Quantification of tissue inflammation shows increased inflammation levels in both 2nd hit models with CNP or DWCNT compared to latency or particle only. (n = 3). Data were analyzed by Ordinary one-way ANOVA and Tukey's multiple comparisons test,

“**” indicates statistically significant difference to “control”. *: indicates *P value* < 0.05. **: indicates *P value* < 0.01. ***: indicates *P value* < 0.001. ****: indicates *P value* < 0.0001. “#” indicates statistically significant difference of two indicated groups. #: indicates *P value* < 0.05. ##: indicates *P value* < 0.01. ###: indicates *P value* < 0.001. ####: indicates *P value* < 0.0001.

3.5 Increased Leakage of Proteins and IgM into bronchoalveolar space

Next, I wanted to investigate whether higher pulmonary inflammation levels in lung tissue can lead to the disruption of the endothelial-epithelial barrier. This can be assessed by measuring the BAL protein and BAL IgM concentration. Upon endothelial-epithelial barrier damage, smaller proteins and eventually even high molecular weight serum proteins, such as IgM, with an average size of 1050 kDa can enter the airspace through these leakages. Measurement of BAL protein and BAL IgM confirms tissue inflammation is significantly higher in the second hit and repeated second hit model, with CNP and with DWCNT exposure (**Fig. 3.6a**). In addition to the high BAL protein content, the IgM concentration is also elevated in the 2nd hit models. But also during the latency and 6 days after the repeated CNP exposure (**Fig. 3.6b**). However, the BAL IgM content remains significantly higher 6 days after the CNP exposure in latently infected animals, compared to CNP exposure alone.

Results

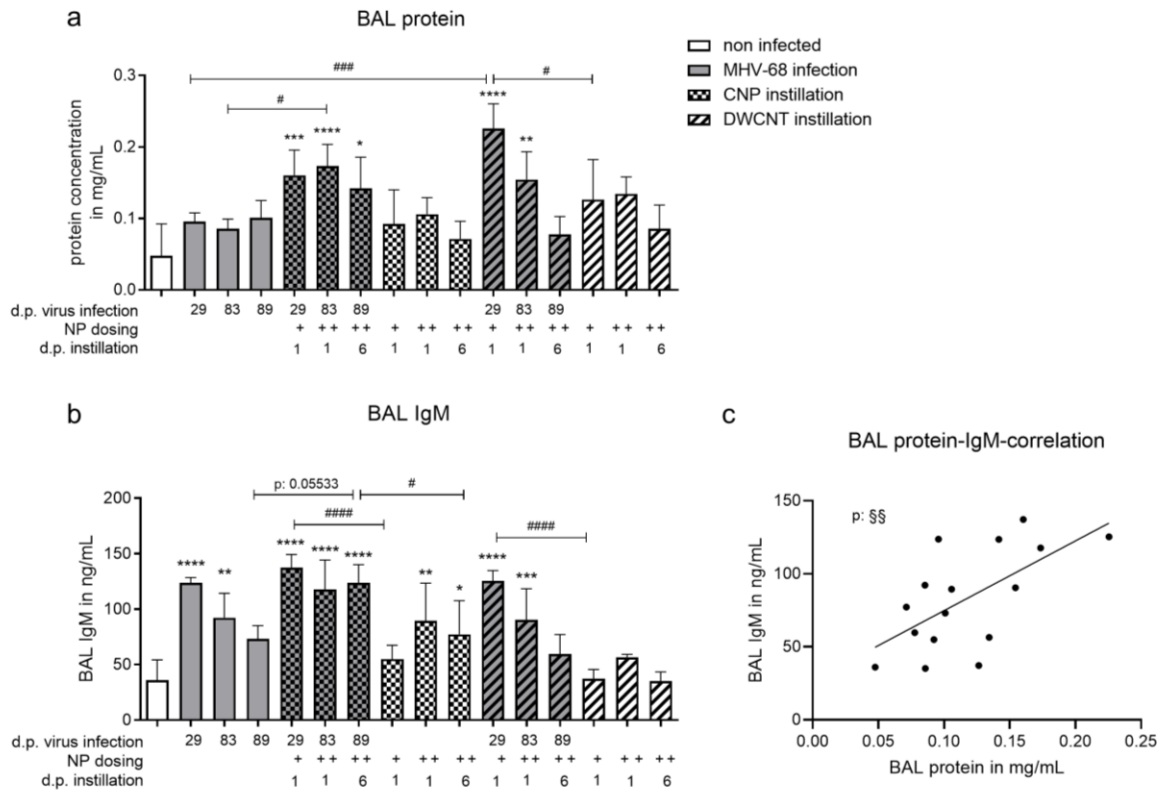


Figure 3.6 Increased BAL protein and BAL IgM levels in 2nd hit model indicate elevated epithelial endothelial barrier damage.

Bronchoalveolar lavage (BAL) was performed on mice infected with MHV-68 and treated with CNP or DWCNT in virus latency. **(a)** BAL protein concentration was measured in mg/mL with BCA and show elevated levels in virus latency plus CNP or DWCNT compared to virus latency or NP instillation alone (n = 3-7). **(b)** BAL IgM content was measured in ng/mL with IgM-ELISA and show significant increased levels in early MHV-68 latency, in repeated CNP exposure, in all MHV-68 latency plus CNP and early MHV-68 latency plus DWCNT time points. (n = 3-7). **(c)** Significant correlation between mean of BAL protein concentrations and mean of BAL IgM levels confirms results. **(a and b)** Data were analyzed by Ordinary one-way ANOVA and Tukey's multiple comparisons test, "*" indicates statistically significant difference to "control". *: indicates *P value* < 0.05. **: indicates *P value* < 0.01. ***: indicates *P value* < 0.001. ****: indicates *P value* < 0.0001. "#" indicates statistically significant difference of two indicated groups. #: indicates *P value* < 0.05. ####: indicates *P value* < 0.001. #####: indicates *P value* < 0.0001. **(c)** Data were analyzed by correlation test, "§" indicated statistically significant correlation of "BAL protein" and "BAL IgM". §§ indicates *P value* < 0.01.

3.6 Elevated levels of neutrophil chemoattractants after repeated CNP exposure in 2nd hit model

As high numbers of neutrophils recruited to the air space of the lungs have been observed, mainly after particle exposure only but also in the repeated second hit model, I investigated the release of neutrophil chemoattractants into the air space region. To investigate this, I collected the BAL fluid and separated the cells for the BAL cyospin from the BAL liquid only. This BAL fluid was used in ELISA to test the concentrations of CXCL2, CXCL1, CXCL5 and myeloperoxidase (MPO), a peroxidase enzyme most abundantly expressed in neutrophil granulocytes (**Fig. 3.7**).

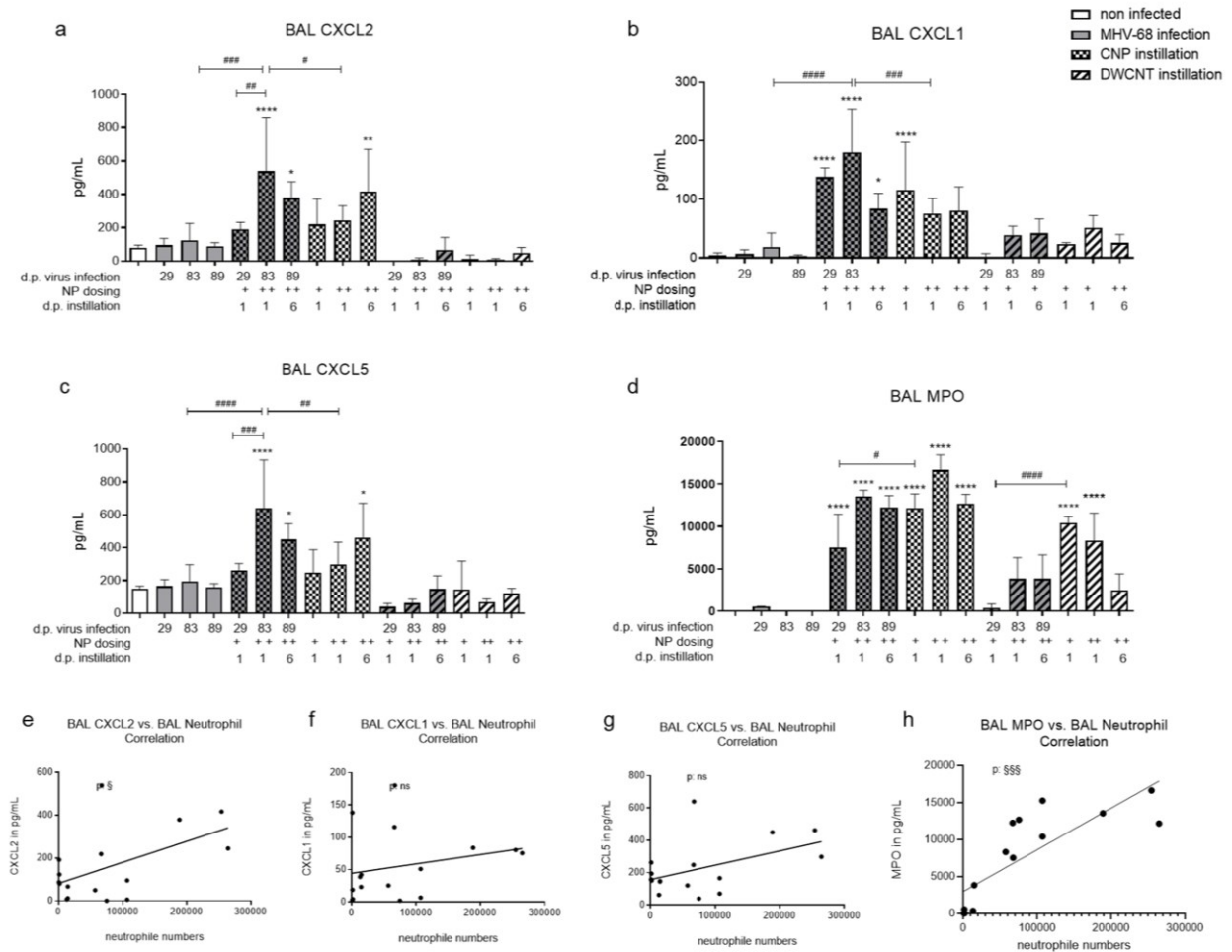


Figure 3.7 Increased neutrophil chemoattractants in BAL fluid after CNP exposure.

Neutrophil chemoattractants were measured with ELISA and correlated to BAL neutrophil numbers. (a) CXCL2 concentrations in BAL fluid in pg/mL measured with CXCL2-ELISA show increased levels in repeated CNP exposure in MHV-68 latency and later timepoint of repeated CNP exposure without MHV-68 infection. (b) CXCL1 concentrations in BAL fluid in pg/mL measured with CXCL1-ELISA show

Results

increased levels in all 2nd hit conditions with CNP exposure and early CNP exposure without infection. (c) CXCL5 concentrations in BAL fluid in pg/mL measured with CXCL5-ELISA show increased levels in repeated CNP exposure in MHV-68 latency and later timepoint of repeated CNP exposure without MHV-68 infection. (d) MPO concentrations in BAL fluid in pg/mL measured with MPO-ELISA show increased MPO levels in all groups with CNP exposure with or without MHV-68 infection. (n = 4 – 5). (e – h) show correlation between CXCL2/CXCL1/CXCL5/MPO vs. BAL neutrophils. (e) indicates a significant correlation between BAL CXCL2 and BAL neutrophils. (f) indicates no significant correlation between BAL CXCL1 and BAL neutrophils. (g) indicates no significant correlation between BAL CXCL5 and BAL neutrophils. (h) indicates a significant correlation between BAL MPO and BAL neutrophils. (a – d) Data were analyzed by Ordinary one-way ANOVA and Tukey's multiple comparisons test, "*" indicates statistically significant difference to "control". *: indicates *P value* < 0.05. **: indicates *P value* < 0.01. ***: indicates *P value* < 0.001. ****: indicates *P value* < 0.0001. "#" indicates statistically significant difference of two indicated groups. #: indicates *P value* < 0.05. ##: indicates *P value* < 0.01. ###: indicates *P value* < 0.001. ####: indicates *P value* < 0.0001. (e – h) Data were analyzed by correlation test, "\$" indicated statistically significant correlation of "neutrophil numbers" and "BAL CXCL2,CXCL1,CXCL5 or MPO". § indicates *P value* < 0.05. §§§ indicates *P value* < 0.001.

The release of all chemokines increases from first repeated instillation of CNP during latency (**Fig. 3.7a-d**). They are still significantly high in the later time point, after 6 days post CNP exposure to latent infection. CXCL2 and CXCL5 were significantly high in the first instillation of CNP in non-infected animals (**Fig. 3.7a, c**). Whereas CXCL1 was significantly high in the late time point after 6 days without virus infection. (**Fig. 3.7b**). MPO was significantly high in all CNP groups, both infected and not infected. As well as in the early time points of first and repeated DWCNT instillation without infection (**Fig. 3.7d**).

CXCL1 and CXCL5 concentrations were not significantly correlated with BAL neutrophil numbers (**Fig. 3.7f, g**). But there was a significant correlation of CXCL2 and MPO release to the BAL neutrophil numbers (**Fig. 3.7e, h**).

3.7 Investigation of lymphocytes in the 2nd hit model

3.7.1 No change in CD45R+ B-lymphocyte numbers after viral infection and NP treatment

Elevated lymphocyte numbers infiltrating the air space, mainly in virus infection but in addition even higher numbers after CNP instillation were observed. To investigate,

which lymphocyte cell types specifically are recruited to the lungs under the respective conditions. Immunohistochemical staining for CD45R, as a marker for B-lymphocytes was performed. No increase of B-lymphocyte numbers in lung tissue with or without infection or NP treatment was observed (**Fig. 3.8**),

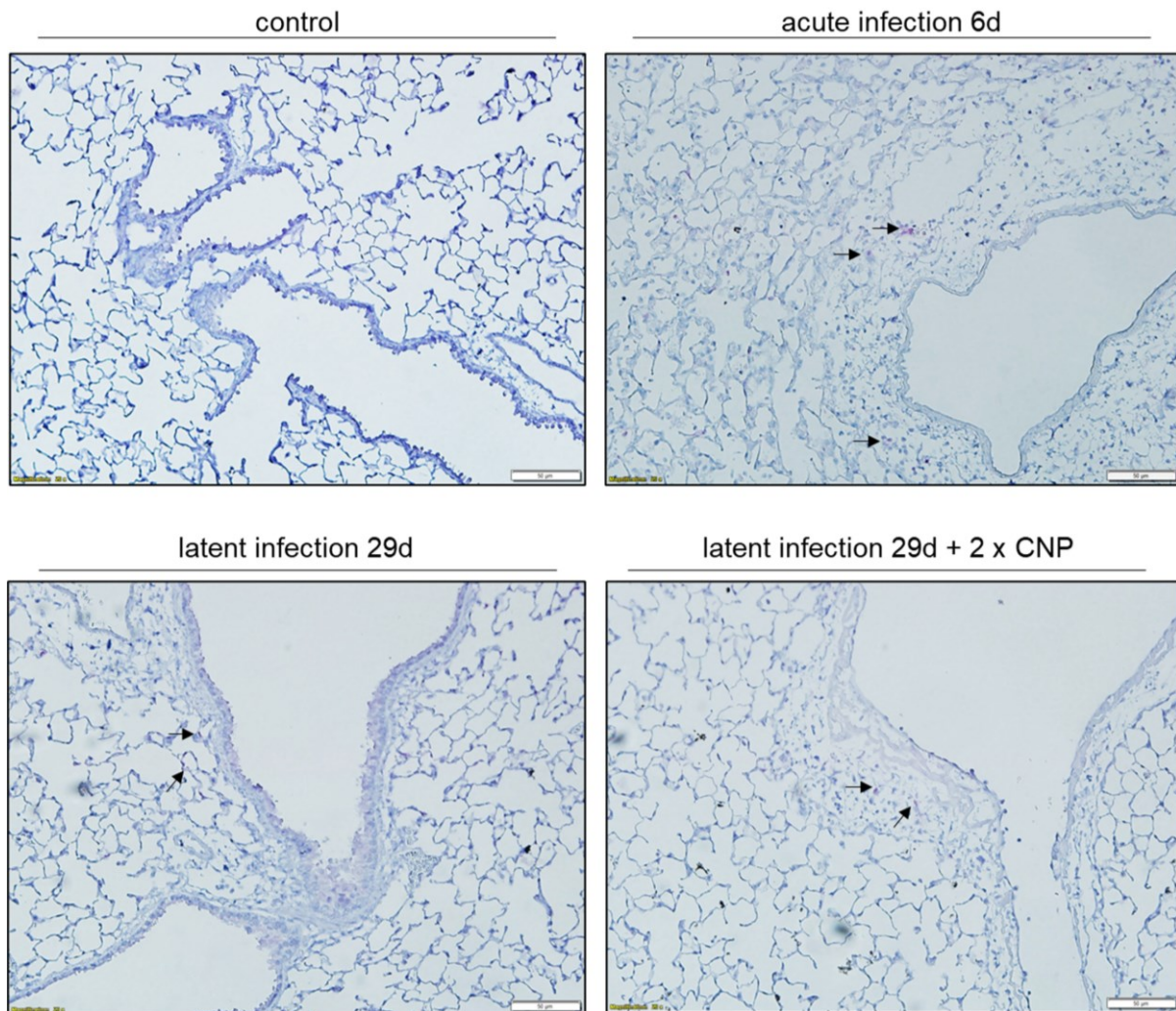


Figure 3.8 B-lymphocytes are not recruited to the lungs after NP exposure into latent virus infection.

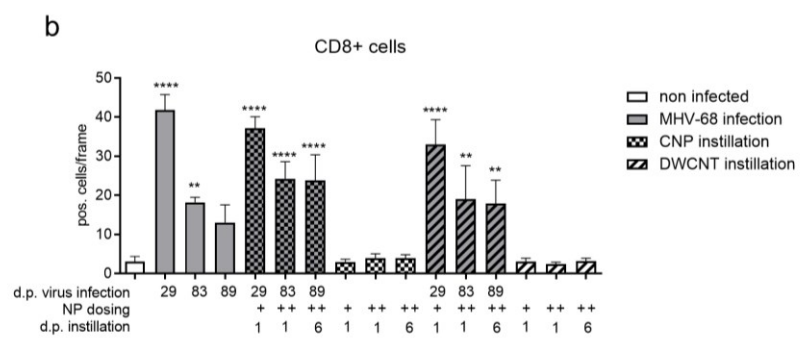
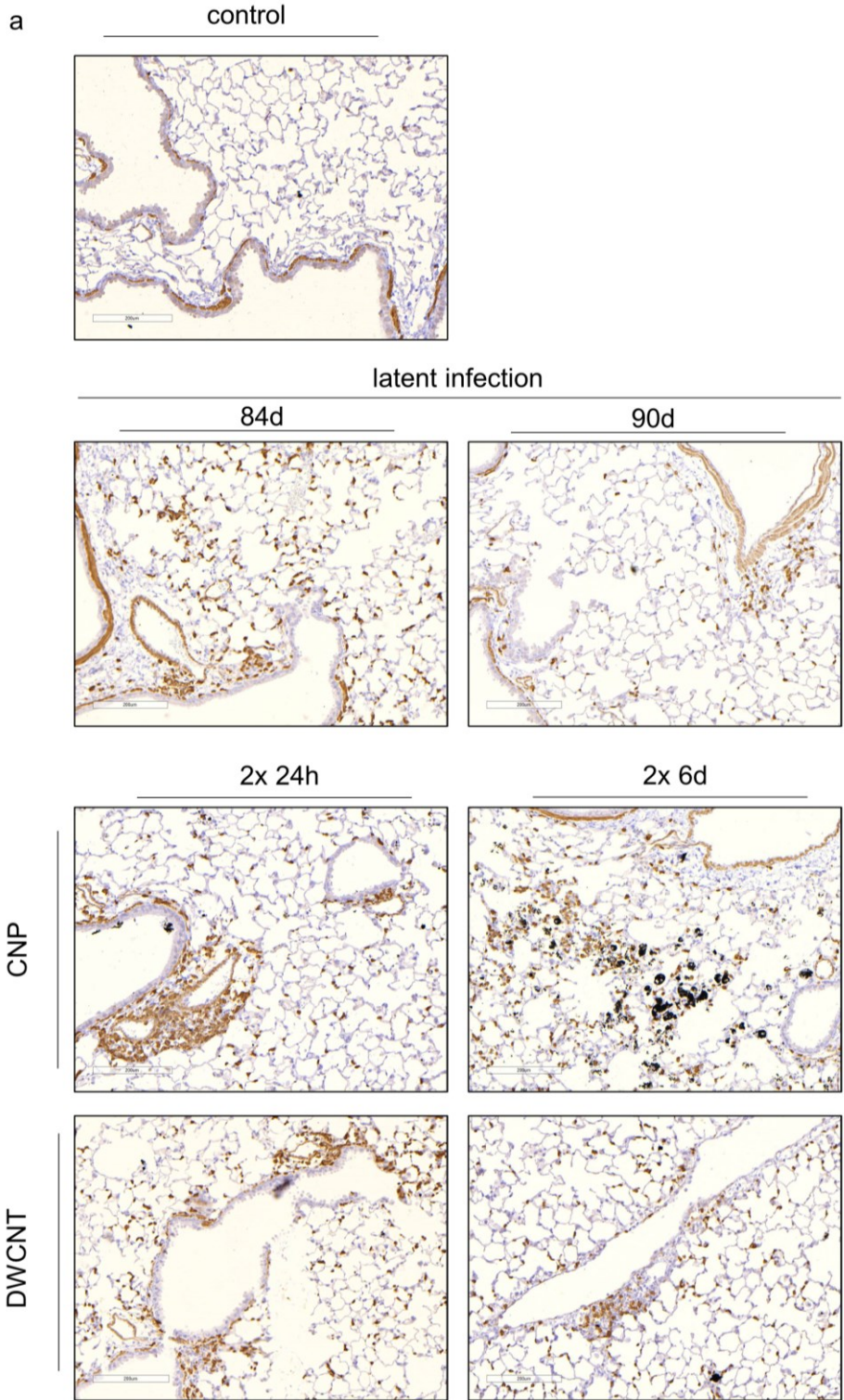
Mice were infected with MHV-68 and either CNP or DWCNT were exposed to the lungs. Lung tissue was isolated, fixed and embedded to paraffin. Lung sections were immunohistochemically stained (vulcan fast red) with anti-CD45R antibody, labelling B-lymphocytes in the lung tissue colored in pink. Images show no changes in B-lymphocyte numbers between different treatments. Scale bars: 50 μ m.

3.7.2 Increased infiltration of CD8+ T-lymphocytes in lungs after viral infection

T-lymphocytes were stained, using the pan-T-lymphocyte marker is CD3. The CD3 complex, as T cell co-receptor is expressed on the plasma membrane virtually all T cells. Whereas the marker for cytotoxic T-lymphocytes is CD8 and for helper T-lymphocytes CD4. Immunohistochemical staining of these T-lymphocyte markers show high numbers of CD3+/CD8+ T-lymphocyte cells in the cell infiltrating area (**Fig. 3.9a**). No changes in CD4+ positive cell numbers indicating steady CD4+ T-lymphocyte numbers. Additionally higher T-cell numbers in BAL cells can be confirmed with significantly higher CD8+ lymphocyte numbers in the repeated second hit model 6 days after both with CNP and DWCNT exposure (**Fig. 3.9b**). CD8+ positive cells were quantified in the pulmonary tissue by CAST, in which random fields of view are chosen by the software, and positive stained cells are marked and counted.

CD8+ T-lymphocytes were localized diffusely over the lung tissue and elevated pulmonary recruitment was detected in the peribronchial and perivascular areas (**Fig. 3.9a**).

CD8+ T-lymphocytes were investigated on their proliferation. Ki67, which production accumulates in the cells are cycling from S to M phases and is an established marker for cell polarization was used to co-stain in immunofluorescence (IF) staining with CD8. Co-immunofluorescence staining of anti-CD8 antibody and anti-Ki67 are detected to co-localization of both markers only in the virus reactivation model, not in virus or CNP exposure alone. These results indicating the proliferation of CD8+ T-lymphocytes in pulmonary tissue in the second hit model (**Fig. 3.10**).



Results

Figure 3.9 CD8 IHC staining, and quantification show elevated T-lymphocyte recruitment to the lungs during MHV-68 infection.

Mice were infected with MHV-68 and either CNP or DWCNT were exposed to the lungs. Lung tissue was isolated, fixed and embedded to paraffin. (a) Lung sections were immunohistochemically stained (DAB) with anti-CD8 antibody, labelling cytotoxic T-lymphocytes in the lung tissue colored in brown. Scale bars: 50 μm . (b) Quantification of CD8 positive cells in lung tissue with CAST, confirms elevated T-lymphocyte numbers in the tissue with still higher numbers after nanoparticle exposure. (n=3). Data were analyzed by Ordinary one-way ANOVA and Tukey's multiple comparisons test, “**” indicates statistically significant difference to “control”. *: indicates P value < 0.05. **: indicates P value < 0.01. ***: indicates P value < 0.001. ****: indicates P value < 0.0001.

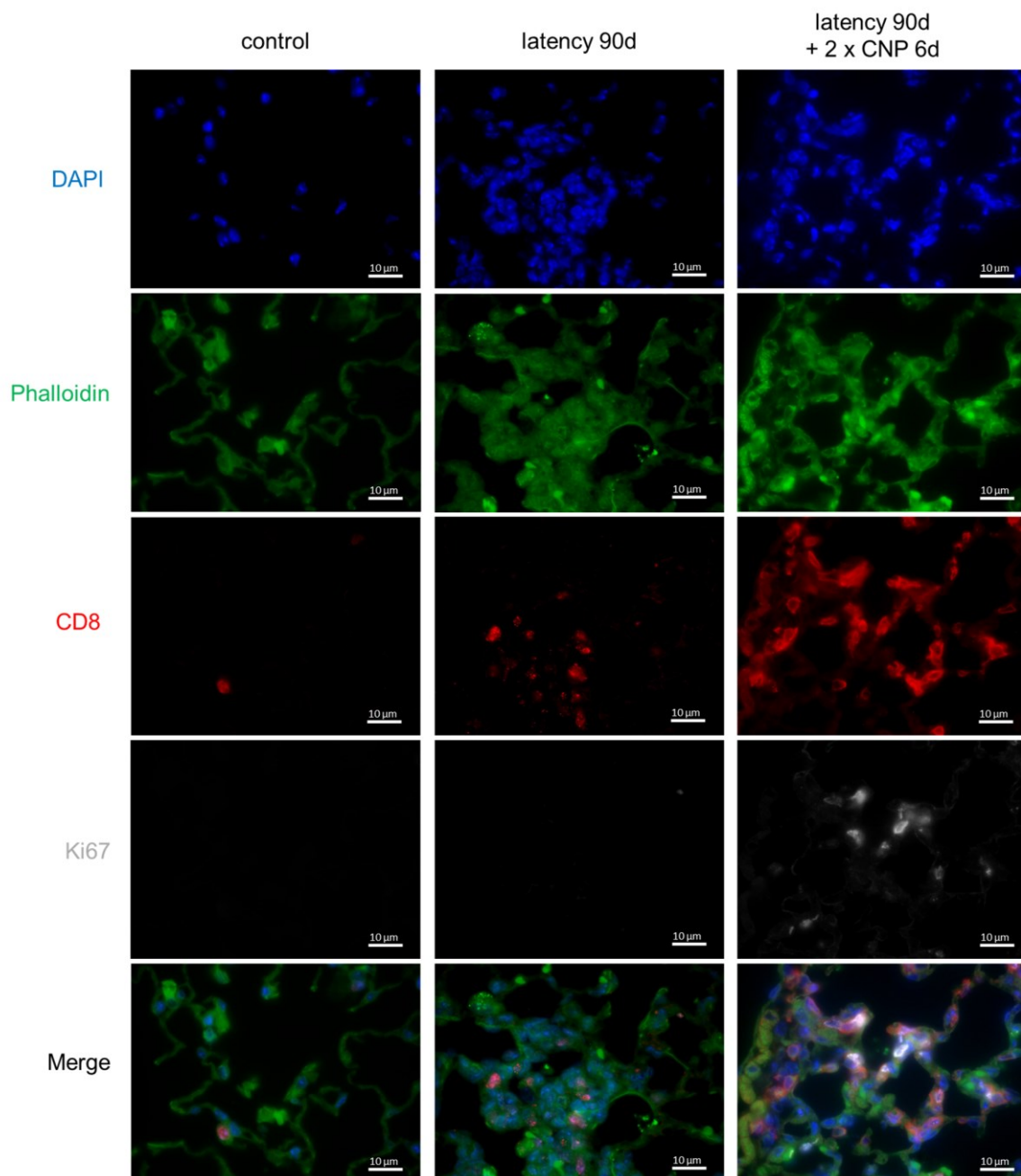


Figure 3.10 CD8+ T-lymphocytes proliferate in 2nd hit model.

Mice were infected with MHV-68 and either CNP or DWCNT were exposed to the lungs. Lung tissue was isolated, fixed and embedded to paraffin. Lung sections were immunofluorescence stained (IF) with anti-CD8 and anti-Ki67 antibodies, labelling cytotoxic T-lymphocytes and cell proliferation, respectively. Proliferation was detected in T-lymphocytes in the 2nd hit model with MHV-68 infection and CNP treatment. Scale bars: 10 µm.

3.7.3 Increased CD8+ T-lymphocytes in BAL cells

Elevated cytotoxic T-lymphocyte recruitment and proliferation in lung interstitium and air space after MHV-68 infection and even more increase in the repeated second hit model after CNP or DWCNT treatment. Lymphocytes types contributing to the elevated numbers in the BAL cell were analyzed. To answer this question, the collected BAL cells were lysed, and RNA was purified. cDNA was synthesized and cell type specific marker expressions was analyzed relative to the housekeeper gene *Hprt*. *Cd19* (for B-lymphocytes), *Klra7* (for natural killer (NK) cells), *Cd247* (pan T-lymphocytes), *Cd4* (for T-helper cells), *Cd8b* (for cytotoxic T-lymphocytes), *Cxcr3* (for effector T-lymphocytes) and *Cxcr6* (for resident memory T-lymphocytes) gene expression were investigated (**Fig. 3.11**). Only a small increase of *Cd19*, the B-lymphocyte marker expression was found in BAL cells in CNP induced second hit model (**Fig. 3.11a**). No significant changes in marker expression of *Klra7* and *Cd4*, for NK-cells and T-helper cells were observed (**Fig. 3.11b, d**). Significant expression of pan-T-lymphocyte, cytotoxic T-lymphocyte, effector T-cell and resident memory T-cell were found by elevated *Cd247*, *Cd8b*, *Cxcr3* and *Cxcr6* expression (**Fig. 3.11c, e – g**), with even higher expression in the CNP induced second hit and repeated second hit model. These results suggest enhanced cytotoxic T-cell recruitment to the alveolar space in the CNP-induced second hit and repeated second hit model compared to MHV-68 latent infection or CNP exposure only.

Results

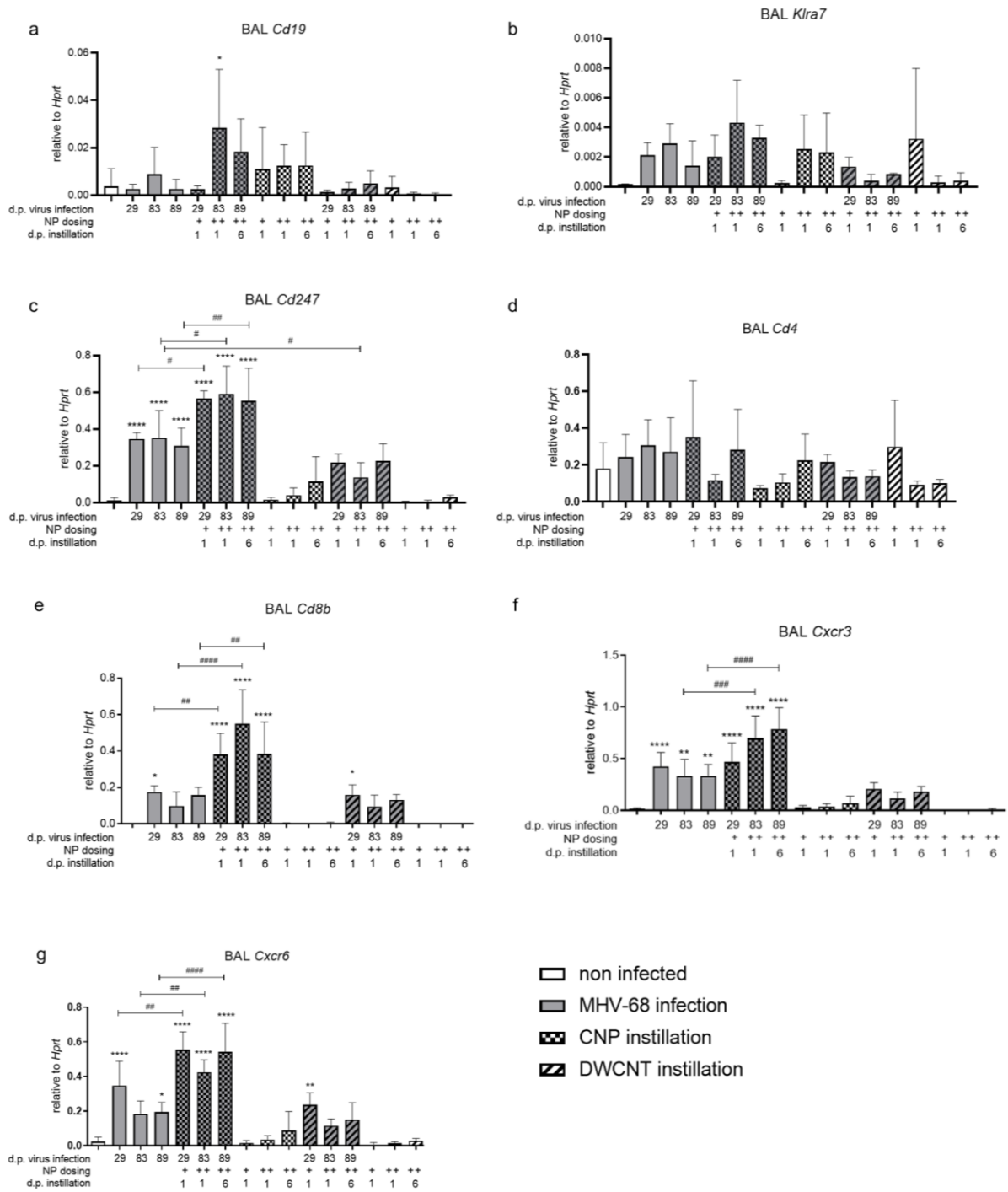


Figure 3.11. High expression of cytotoxic T-lymphocyte markers in BAL cells of CNP induced 2nd hit model.

Mice were infected with MHV-68 and instilled with CNP or DWCNT. Lungs were lavaged and BAL cells isolated. RNA was isolated. cDNA synthesized and the expression of *Cd19*, *Klr7*, *Cd247*, *Cd4*, *Cd8b*, *Cxcr3* and *Cxcr6* was detected by qPCR. *Hprt* was used as a housekeeping gene and used to normalize the expression to the gene of interest. No significant change in NK-cell and T-helper-lymphocyte expression markers, *Klr7* (b) and *Cd4* (d), respectively. (a) shows significant increase of B-lymphocyte

expression marker *Cd19* high in the first CNP exposure in latent infection. (n=5). Data were analyzed by Ordinary one-way ANOVA and Tukey's multiple comparisons test, "*" indicates statistically significant difference to "control". *: indicates *P* value < 0.05. **: indicates *P* value < 0.01. ***: indicates *P* value < 0.001. ****: indicates *P* value < 0.0001. "#" indicates statistically significant difference of two indicated groups. #: indicates *P* value < 0.05. ##: indicates *P* value < 0.01. ###: indicates *P* value < 0.001. ####: indicates *P* value < 0.0001.

3.7.4 Elevated cytotoxic potential of BAL T-lymphocytes in CNP induced 2nd hit model

As cytotoxic T-lymphocytes are defined in the property to express and regulate secretion of potent toxins, including pore-forming protein perforin and serine proteases granzymes, I investigated the cytotoxic potential by analysis of the expression of these genes by qPCR.

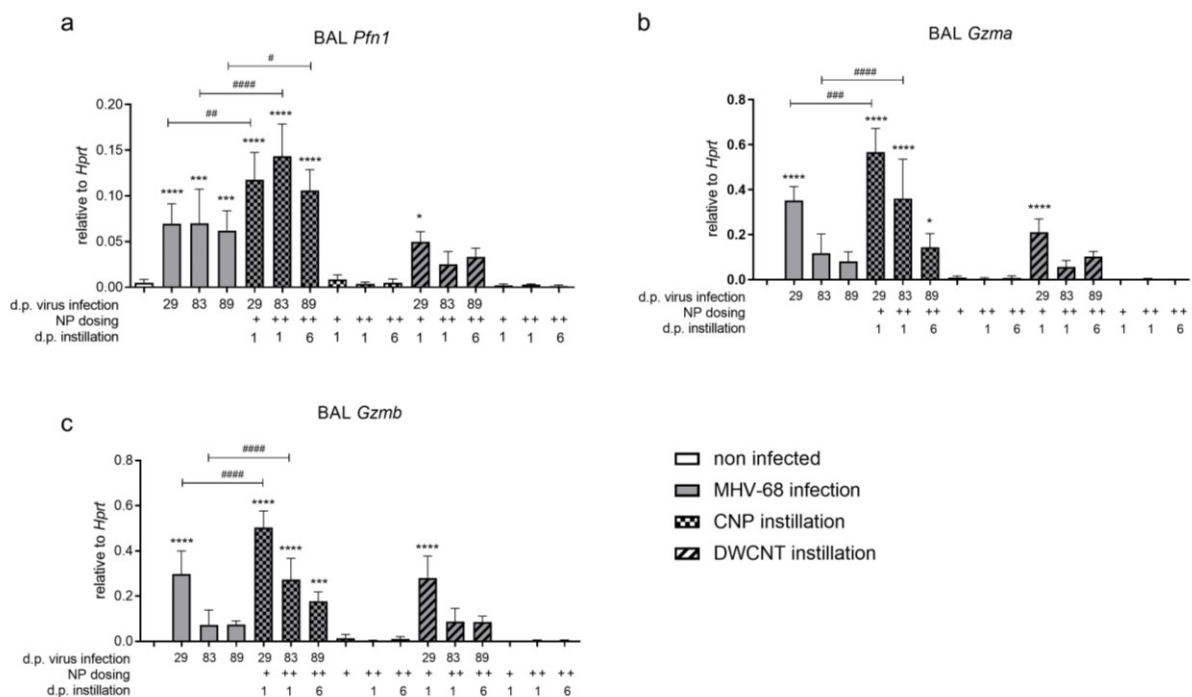


Figure 3.12 Elevated markers for cytotoxic T-lymphocyte potential.

Mice were infected with MHV-68 and instilled with CNP or DWCNT. Lungs were lavaged and BAL cells isolated. RNA was isolated. cDNA synthesized and the expression of *Pfn1*, *Gzma* and *Gzmb* was detected. *Hprt* was used as a housekeeping gene and used to normalize the expression to the gene of interest. (n=5). Data were analyzed by Ordinary one-way ANOVA and Tukey's multiple comparisons test, "*" indicates statistically significant difference to "control". *: indicates *P* value < 0.05. **: indicates

Results

P value < 0.01. ***: indicates *P* value < 0.001. ****: indicates *P* value < 0.0001. “#” indicates statistically significant difference of two indicated groups. #: indicates *P* value < 0.05. ##: indicates *P* value < 0.01. ###: indicates *P* value < 0.001. ####: indicates *P* value < 0.0001.

Increase of cytotoxic T-lymphocyte marker expression was observed and increased cytotoxic potential of the T-lymphocytes in the alveolar region was confirmed by significant higher expression levels of *Pfn1*, *Gzma* and *Gzmb*, marker for perforin, granzyme a and granzyme b respectively (**Fig. 3.12**). Again, even higher expression levels in the repeated second hit model induced by CNP in first and repeated instillation were detected. These results suggest more cytotoxic effector T-lymphocytes in airspace with elevated cytotoxic potential in the CNP induced second hit and repeated second hit model.

3.8 Inflammatory response of virus infection and nanoparticle exposure

Classically inflammatory genes and proteins were investigated to observed potential alterations in inflammatory response to NP exposure with and without latent MHV-68 infection.

3.8.1 The effect of virus infection and CNP or DWCNT exposure on IL-6

IL-6 is a cytokine that plays an important role in host immune defense. It has various functions in immune and hematopoietic activities and IL-6 is able to induce the acute phase response. It acquires the immune response by stimulation of antibody production and of effector T-cell development. It can induce proliferation and promote differentiation of several cells and rather pro-inflammatory in chronic inflammation.

The expression and released of IL-6 during latent infection and NP treatment was observed. Additionally, *Il6* gene expression was investigated from whole lung homogenate relative to the housekeeper gene *Hprt* by qPCR analysis (**Fig. 3.13a**). *Il6* expression in the lung was only significantly increased in the first instillation of CNP in non-infected mice and in the first and repeated DWCNT exposure after 24h also in non-infected mice. However, the expression of *Il6* in whole lung was not increased in

the second hit model, I observed significantly increased IL-6 release into the air space, what was analyzed by Bio-Plex assay (**Fig. 3.13b**). Similar to the *Il6* expression pattern in the lung, there was a significant IL-6 release in 1x CNP and first and repeated DWCNT exposure in non-infected mice. The trend of reduction of *Il6* expression and IL-6 release from the first to the repeated NP exposure without virus infection is reversed in the latent infected mice. Here there is an increase in both CNP and DWCNT from first to repeated exposure in the MHV-68 infection (**Fig. 3.13**).

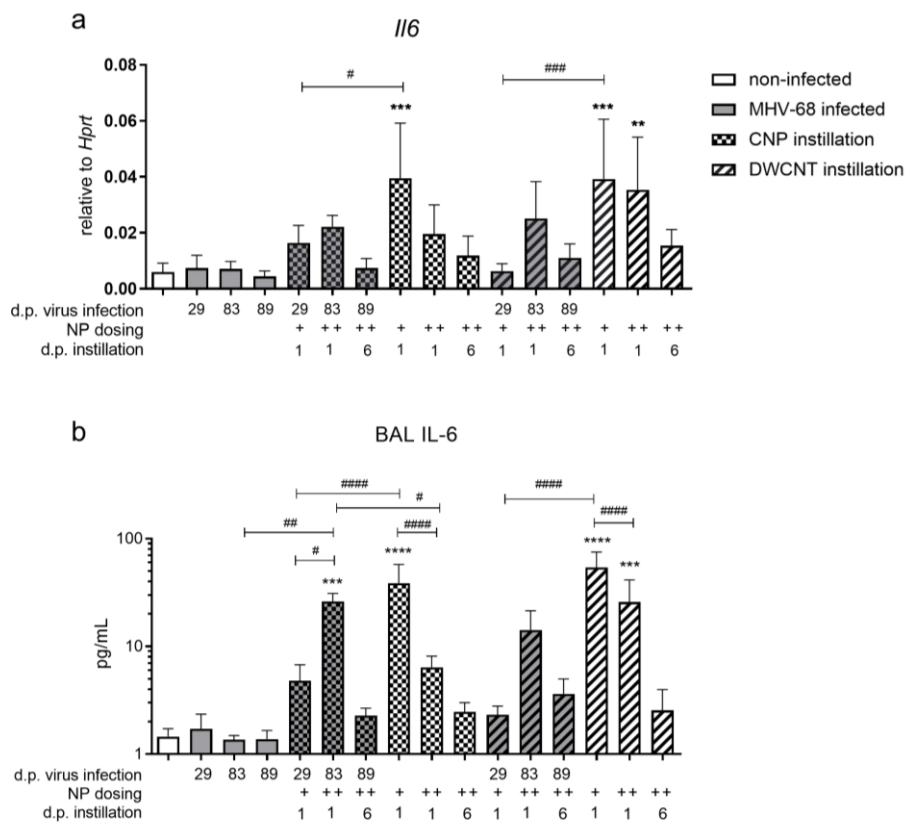


Figure 3.13 Increase of IL-6 release after repeated CNP exposure in virus latency and early NP exposure without virus infection.

Mice were infected with MHV-68 and treated with either CNP or DWCNT during latency. Lungs were lavaged and isolated. BAL fluid was collected for analysis of chemokines released into the airspace and lung tissue was homogenized for RNA purification. RNA was synthesized to cDNA and (a) whole lung gene expression of *Il6* relative to the housekeeper gene *Hprt* was detected. (b) The release of IL-6 into the BAL fluid was measured in pg/mL by Bio-Plex assay. (n = 4-5). Data were analyzed by Ordinary one-way ANOVA and Tukey's multiple comparisons test, "*" indicates statistically significant difference to "control". *: indicates *P* value < 0.05. **: indicates *P* value < 0.01. ***: indicates *P* value < 0.001. ****: indicates *P* value < 0.0001. "#" indicates statistically significant difference of two indicated groups. #: indicates *P* value < 0.05. ##: indicates *P* value < 0.01. ###: indicates *P* value < 0.001. ####: indicates *P* value < 0.0001.

Results

3.8.2 Elevated interferon- γ (*Ifng*) expression in BAL cells in the CNP induced second hit model

Because of the observed increased cytotoxic CD8+ T-lymphocytes in lung tissue and in the air space, Interferon- γ (IFN- γ) expression was investigated. IFN- γ orchestrates early inflammatory events and is also known to play an important role in MHV-68 latency regulation. Gene expression of *Ifng* in the BAL cells by qPCR relative to the housekeeper gene *Hprt* was performed. Analysis of the *Ifng* expression reveal longer significant increased levels in the CNP induced second hit and repeated second hit model compared to the virus latency alone. This response was not visible in the second hit and repeated second model induced by DWCNT (**Fig. 3.14**). These results match the expression data of *Pfn1*, *Gzma* and *Gzmb* (**Fig. 3.12**), which were also elevated in the CNP induced second hit models.

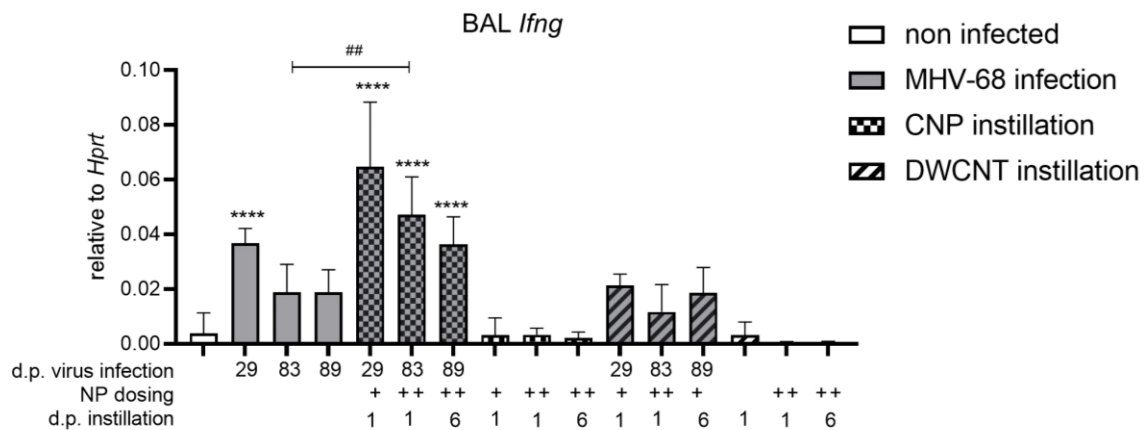


Figure 3.14. Expression of *Ifng* in BAL cells.

Mice were infected with MHV-68 and treated with either CNP or DWCNT during latency. Lungs were lavaged and isolated. BAL cells were collected for RNA purification. RNA was synthesized to cDNA and gene expression of *Ifng* relative to the housekeeper gene *Hprt* was detected. (n = 4-5). Data were analyzed by Ordinary one-way ANOVA and Tukey's multiple comparisons test, "*" indicates statistically significant difference to "control". *: indicates *P* value < 0.05. **: indicates *P* value < 0.01. ***: indicates *P* value < 0.001. ****: indicates *P* value < 0.0001. "#" indicates statistically significant difference of two indicated groups. ##: indicates *P* value < 0.01.

3.8.3 The effect of virus infection and CNP or DWCNT exposure on Lipocalin-2

Lipocalin-2 (LCN2), also known as neutrophil gelatinase-associated lipocalin (NGAL), is a member of the lipocalin family. It is an innate acute-phase protein and an inflammatory mediator. LCN2 plays a role in multiple biological processes, including cell migration and differentiation and its expression is specifically upregulated in the lung in alveolar epithelial type II cells during inflammatory injury. Because of its role in pulmonary inflammation, its regulation in the lung on genetic level, as well as in the release of LCN2 into the air space was analyzed. RNA of whole lung homogenates was purified and synthesized to cDNA. *Lcn2* gene expression was investigated relative to the expression of the housekeeper gene *Hprt* (**Fig. 3.15a**). Significant higher expression was detected 24h after first and repeated CNP and DWCNT exposure in non-infected mice and in the repeated CNP exposure in latently infected mice. Also, here the trend of decreasing expression of *Lcn2* from first to repeated NP in non-infected mice and the increase of first to repeated CNP exposure is similar from the previous expression of *Il6* (**Fig. 3.13**). LCN2 protein release was measured from BAL fluid with LCN2 ELISA (**Fig. 3.15b**). All CNP exposed groups were significantly increased, both with and without MHV-68 infection, in released LCN2. LCN2 levels were significantly elevated in the DWCNT induced repeated second hit model and 24h after the first and repeated DWCNT exposure in non-infected mice.

Results

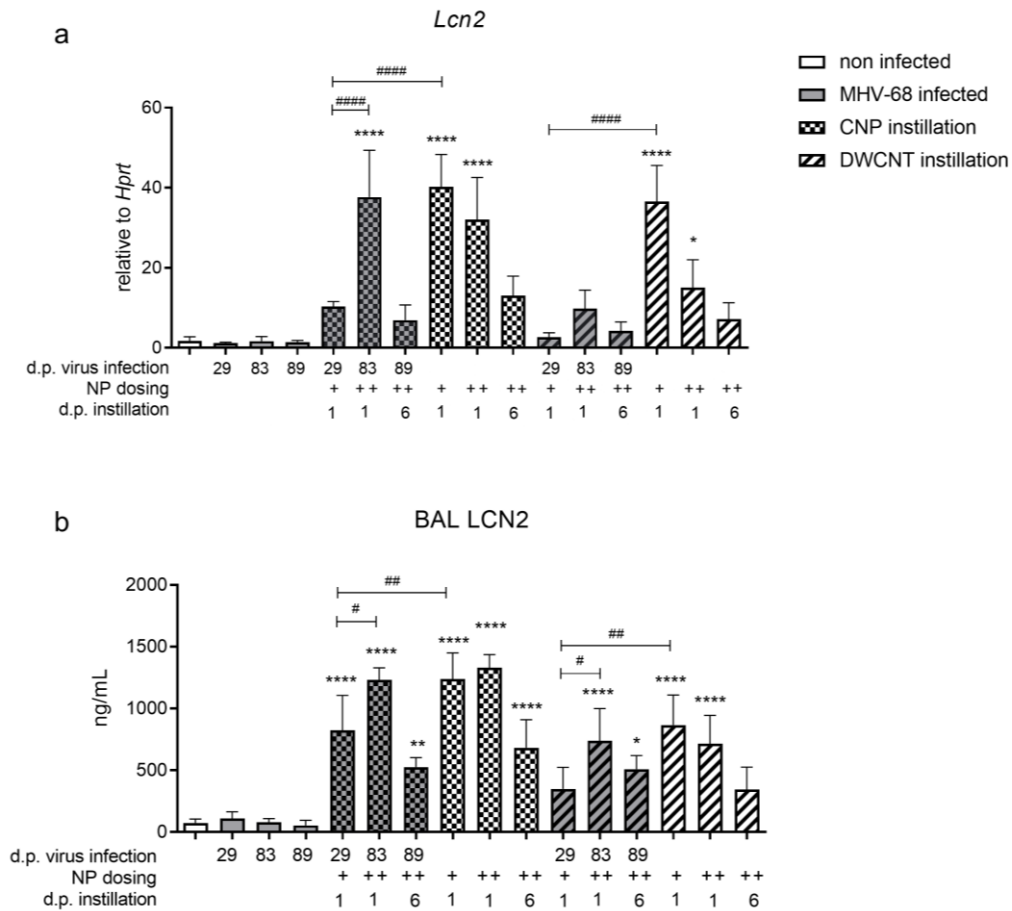
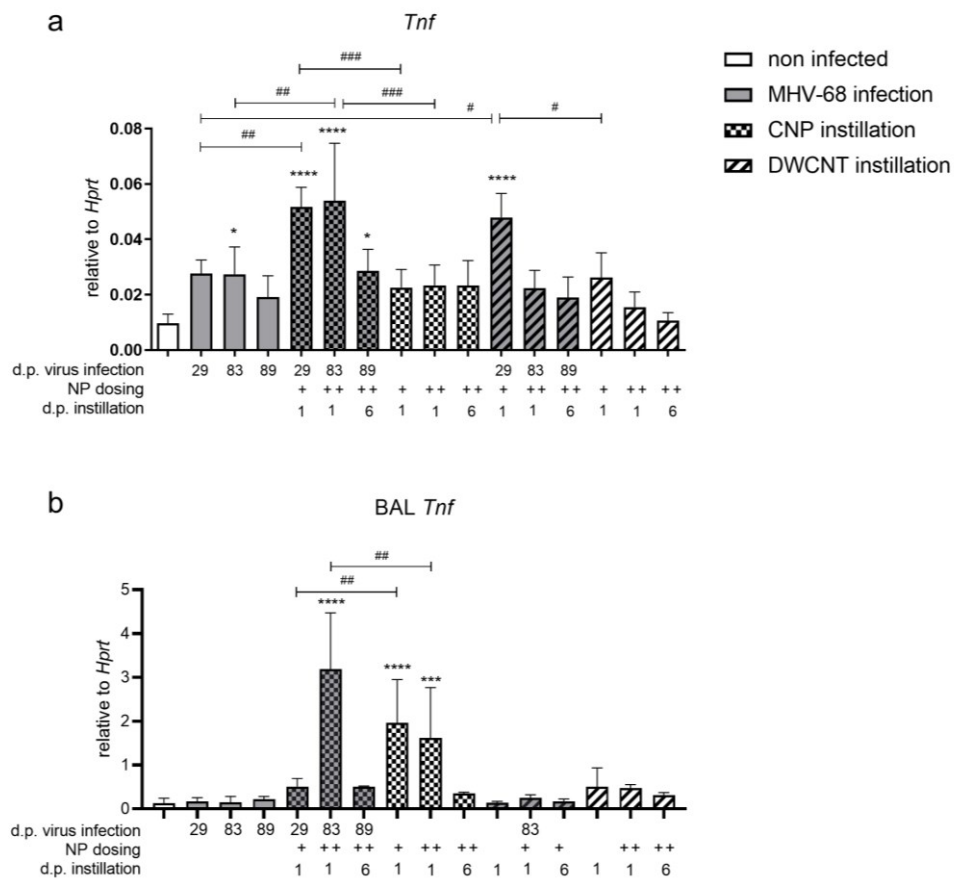


Figure 3.15 Elevated Lipocalin-2 release and gene expression after NP treatment.

Mice were infected with MHV-68 and treated with either CNP or DWCNT during latency. Lungs were lavaged and isolated. BAL fluid was collected for analysis of chemokines released into the airspace and lung tissue was homogenized for RNA purification. RNA was synthesized to cDNA and (a) whole lung gene expression of *Lcn2* relative to the housekeeper gene *Hprt* was detected. The release of LCN2 into the BAL fluid was measured by (b) ELISA assay. (n = 4-5). Data were analyzed by Ordinary one-way ANOVA and Tukey's multiple comparisons test, "*" indicates statistically significant difference to "control". *: indicates *P* value < 0.05. **: indicates *P* value < 0.01. ***: indicates *P* value < 0.001. ****: indicates *P* value < 0.0001. "#" indicates statistically significant difference of two indicated groups. #: indicates *P* value < 0.05. ##: indicates *P* value < 0.01. ###: indicates *P* value < 0.001. ####: indicates *P* value < 0.0001.

3.8.4 The effect of virus infection and CNP or DWCNT exposure on TNF- α

TNF- α is a potent inflammatory cytokine, which plays essential roles in maintenance of immune homeostasis, acute inflammation and is has been implicated in various chronic pulmonary diseases as a driver of pathology. Expression of *Tnf* in the lung and BAL cells was investigated. For this analysis *Tnf* expression was detected by qPCR, relative to the housekeeping gene *Hprt*. Significantly high *Tnf* expression was observed in the CNP induced second hit and repeated second model. Additionally, the gene expression level of *Tnf* in DWCNT induced second hit model was significantly upregulated (**Fig. 3.16a**) compared to virus infection or NP treatment alone. In the BAL cell gene expression, *Tnf* was significantly high expressed in the first and the repeated CNP exposure in non-infected mice and additionally in the CNP induced repeated second hit model (**Fig. 3.16b**). There was no change in the expression induced by DWCNT exposure.



Results

Figure 3.16 Increased lung gene expression of *Tnf* in the 2nd hit model and particle treatment.

After MHV-68 virus infection and CNP or DWCNT instillation during latency, lungs and BAL cells, were isolated and homogenized. Whole lung and BAL cell RNA was isolated. *Tnf* gene expression was investigated from whole lung tissue (a) and from BAL cells (b) by qPCR. Expression results were normalized to the housekeeper gene *Hprt*. Data were analyzed by Ordinary one-way ANOVA and Tukey's multiple comparisons test, "*" indicates statistically significant difference to "control". *: indicates *P value* < 0.05. **: indicates *P value* < 0.01. ***: indicates *P value* < 0.001. ****: indicates *P value* < 0.0001. "#" indicates statistically significant difference of two indicated groups. #: indicates *P value* < 0.05. ##: indicates *P value* < 0.01. ###: indicates *P value* < 0.001. ####: indicates *P value* < 0.0001.

3.8.5 The effect of virus infection and CNP or DWCNT exposure on CCL17

CCL17, also known as TARC, is described to be elevated in many models related to pulmonary inflammation, such as COPD, acute asthma and idiopathic pulmonary fibrosis and plays a role in Th1 and Th2 immune response. *Ccl17* gene expression and release and its regulation during MHV-68 infection and NP exposure was investigated. To answer this question, whole lung homogenates were used to purify RNA, which was synthesized to cDNA for qPCR analysis. *Ccl17* gene expression was detected relative to the housekeeper gene expression *Hprt*. *Ccl17* gene expression levels were significantly elevated in the first and repeated CNP exposure after 24h, in both, virus infected and non-infected mice (**Fig. 3.17a**). Interestingly, the trend here is similar to the *Il6* (**Fig. 3.13a**) and *Lcn2* expression patterns (**Fig. 3.15a**). The gene expression of *Ccl17* is higher in repeated CNP exposure in virus infected compared to the first CNP instillation in the latency. And the trend in the non-infected animals is decreasing in the repeated CNP exposure compared to the first exposure (**Fig. 3.17a**). Similar patterns were observed after DWCNT exposures, even there is no significant increase of *Ccl17* expression levels in DWCNT exposure in latent infected mice, this trend for higher expression from first to repeated instillation was observed. And a trend in the non-infected animals from first to repeated DWCNT exposure in reduction of *Ccl17* expression levels.

Measurement of BAL CCL17 concentration by ELISA demonstrate significantly high CCL17 release into the air space after repeated CNP exposure in infected and non-infected lungs (**Fig. 3.17b**). Whereas CCL17 release was not affected by DWCNT exposure.

These results confirm previous data and amplify the suggestion, about a differential regulated immune response to NP exposure between latent MHV-68 infected and non-infected animals.

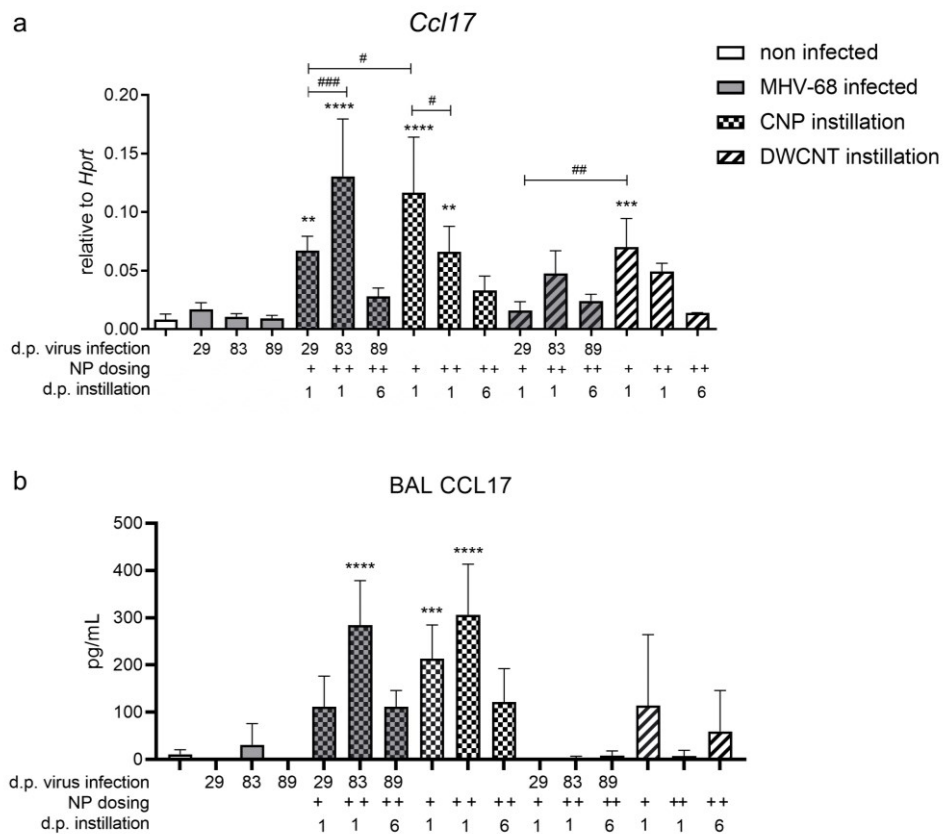


Figure 3.17 Increased CCL17 release and gene expression after CNP exposure in virus infected and not infected lungs.

Mice were infected with MHV-68 and treated with either CNP or DWCNT during latency. Lungs were lavaged and isolated. BAL fluid was collected for analysis of chemokines released into the bronchoalveolar area and lung tissue was homogenized for RNA purification. RNA was synthesized to cDNA and (a) whole lung gene expression of *Ccl17* relative to the housekeeper gene *Hprt* was detected. The release of CCL17 into the BAL fluid was measured by (b) ELISA assay. (n = 4-5). Data were analyzed by Ordinary one-way ANOVA and Tukey's multiple comparisons test, "*" indicates statistically significant difference to "control". *: indicates *P* value < 0.05. **: indicates *P* value < 0.01. ***: indicates *P* value < 0.001. ****: indicates *P* value < 0.0001. "#" indicates statistically significant difference of two indicated groups. #: indicates *P* value < 0.05. ##: indicates *P* value < 0.01. ###: indicates *P* value < 0.001. ####: indicates *P* value < 0.0001.

Results

3.8.6 The effect of virus infection and NP exposure on cell migrating and priming chemokines

Chemokines, regulating monocyte T-lymphocyte and eosinophil recruitment and priming were investigated. These chemokines are known to be essential for eosinophil migration and priming. As eosinophils are a major source of reactive oxygen, metalloproteinases as well as pro-inflammatory cytokines such as TNF- α , TGF- β and IL-6 and play an important role in allergic inflammation. CCL24 (eotaxin-2), CCL11 (eotaxin-1) and CCL5 (RANTES) released into the air space was detected by Bio-Plex assay. Mice lungs were lavaged after MHV-68 and NP exposure and BAL liquid was collected for the analysis.

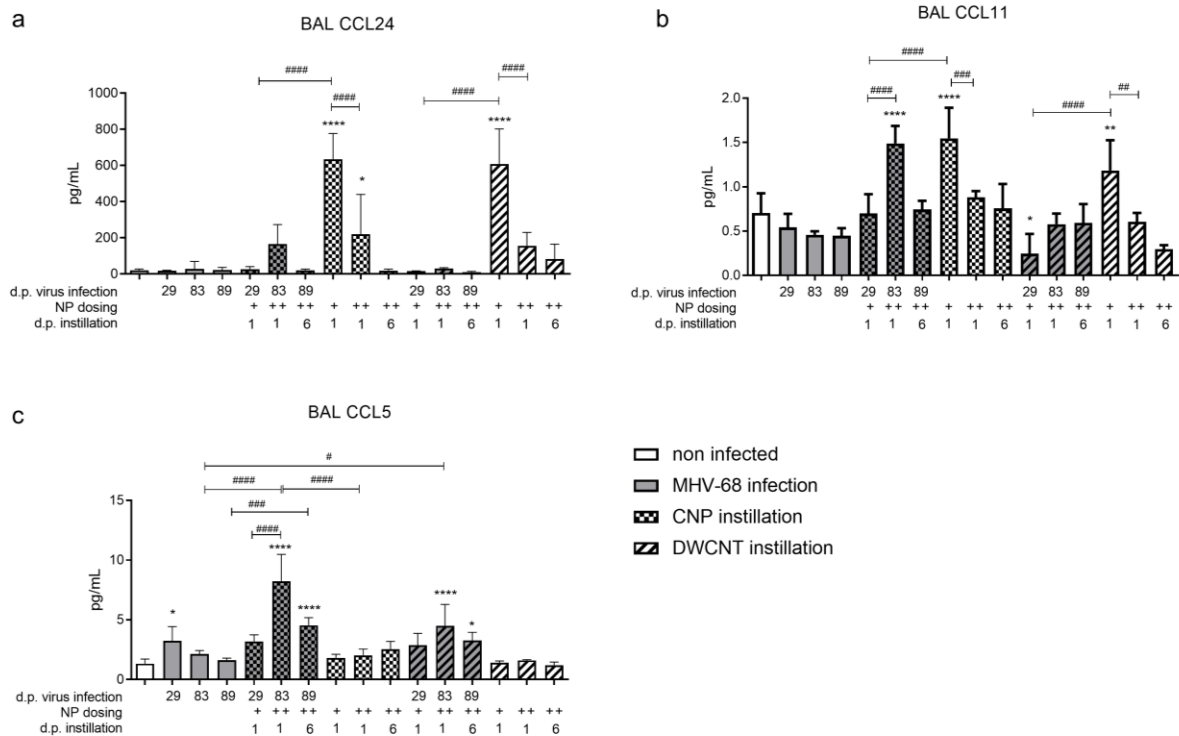


Figure 3.18. Bio-Plex analysis of immune cell migrating, and priming chemokines released into the air space.

CCL24, CCL11 and CCL5 concentrations in pg/mL were measured with a Bio-Plex assay. (a) significant high CCL24 release after CNP and DWCNT exposure in non-infected mice. (b) significant high CCL11 release in repeated CNP exposure in virus infected mice, first CNP exposed group and early single exposure to DWCNT in non-infected mice. (c) significantly high CCL5 release in early virus latency and in the 2nd hit models with CNP and DWCNT (n = 4-5). Data were analyzed by Ordinary one-way ANOVA and Tukey's multiple comparisons test, "*" indicates statistically significant difference to "control". *:

indicates *P value* < 0.05. **: indicates *P value* < 0.01. ***: indicates *P value* < 0.001. ****: indicates *P value* < 0.0001. “#” indicates statistically significant difference of two indicated groups. #: indicates *P value* < 0.05. ##: indicates *P value* < 0.01. ###: indicates *P value* < 0.001. ####: indicates *P value* < 0.0001.

Significant increase of BAL CCL24 levels in first exposure of CNP and DWCNT and in the repeated CNP exposure in non-infected animals were observed (**Fig. 3.18a**). The pattern of CCL11 reflects again the trend of additive release in the repeated CNP exposure in latent infection compared to the first exposure, compared to the non-infected mice, with a decreased release from first to second CNP exposure (**Fig. 3.18b**). Release of CCL5 was significantly elevated in the first group of latent virus infection, as well as elevated in the early and later time point in the exposure of CNP and DWCNT in the repeated second hit model (**Fig. 3.18c**). Especially CCL5 is described to direct T-lymphocytes, monocytes and eosinophils to site of inflammation. This cytokine is only significantly elevated in the repeated second hit model.

3.8.7 Elevated macrophage activation in 2nd hit model

Lung macrophages including alveolar macrophages and interstitial macrophages, are important innate immune cells and play an important role in the destruction of pathogens and in the processing and clearing of inhaled particles. As a next step, the potential of MHV-68 latent infection and NP treatment to alter macrophage inflammation in the lung was investigated.

3.8.8 The effect of virus infection and NP exposure macrophage inflammatory proteins CCL3 and CCL4

Macrophage inflammatory proteins CCL3, also known as MIP-1 α , and CCL4, also known as MIP-1 β , are important chemokines for immune response towards infection and inflammation. To investigate CCL3 and CCL4 content in the airspace, lungs were lavaged, after MHV-68 infection and CNP or DWCNT instillation, to collect the BAL fluid. BAL fluid was analyzed for CCL3 and CCL4 by Bio-Plex assay (**Fig. 3.19**). CCL3 release into airspace was significantly elevated in all repeated NP exposure, with both, CNP and DWCNT exposure in non-infected and in virus infected lungs (**Fig. 3.19a**). However, the expression pattern of CCL4 is different to the pattern of CCL3. CCL4 is

Results

significantly high in all CNP exposed groups without virus infection and high in the first exposure of DWCNT in non-infected mice (**Fig. 3.19b**). In the latent virus infected groups, latency alone, doesn't affect the release of CCL3 and CCL4. But repeated CNP exposure after 24h and repeated DWCNT exposure after 6d in virus infected mice, increase the CCL4 release significantly.

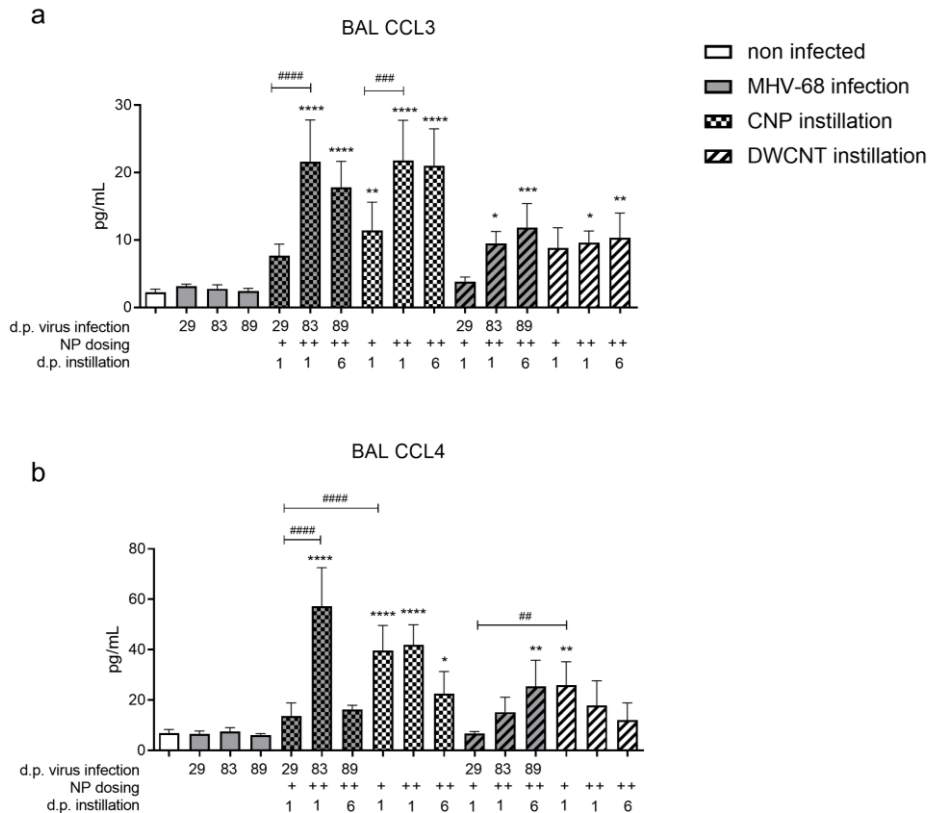


Figure 3.19. Increased CCL3 and CCL4 release to the airspace after nanoparticle exposure.

CCL3 and CCL4 concentrations in pg/mL were measured with a Bio-Plex assay. **(a)** significant high CCL3 release after repeated CNP exposure to the latently infected mice, CNP exposure without virus infection and the repeated dosing of DWCNT in virus infected and non-infected mice. **(b)** significant high CCL 4 release in repeated CNP exposure in virus infected mice, all CNP exposed groups without virus infection, late time point of repeated DWCNT exposure in virus infected animals and early single exposure to DWCNT in non-infected mice. (n = 4-5). Data were analyzed by Ordinary one-way ANOVA and Tukey's multiple comparisons test, "*" indicates statistically significant difference to "control". *: indicates *P value* < 0.05. **: indicates *P value* < 0.01. ***: indicates *P value* < 0.001. ****: indicates *P value* < 0.0001. "#" indicates statistically significant difference of two indicated groups. #: indicates *P value* < 0.05. ##: indicates *P value* < 0.01. ###: indicates *P value* < 0.001. ####: indicates *P value* < 0.0001.

3.8.9 The effect of virus reactivation on the expression of osteopontin in lung

Osteopontin (OPN) is a matricellular protein that drives different biological functions. OPN functions as a cytokine, promotes cell-mediated immune response and plays a role in chronic pulmonary inflammation. Lung diseases are associated with increased OPN expression, since OPN modulates remodeling of the lung structure.

The gene name of OPN is called *Spp1*. *Spp1* expression and OPN release between different treatments were investigated. For this investigation, lungs were lavaged and isolated, RNA was purified from lung homogenates and BAL cells. cDNA was synthesized and *Spp1* gene expression was detected, normalized to the expression of the housekeeper gene *Hprt* (**Fig. 3.20**). Lung *Spp1* gene expression was significantly high in all CNP induced second hit model groups as well as in the repeated DWCNT exposure in virus infection (**Fig. 3.20a**). Repeated DWCNT exposure in non-infected mice also significantly increases *Spp1* expression. However, there is also a significant increase in the repeated DWCNT in non-infected groups, there is even significant higher expression in the DWCNT induced second hit model. Also, all CNP induced second hit model groups are significantly higher in expressing *Spp1* compared to the MHV-68 latency or NP treatment alone.

The *Spp1* expression pattern in BAL cells alters compared to whole lung expression. Significant higher expression 24h after the second hit and repeated second hit model and in non-infected mice, only 24h after the repeated CNP exposure leads to significant higher *Spp1* BAL cell expression (**Fig. 3.20b**). In DWCNT all groups of repeated exposure was expressing higher *Spp1* levels, in both, non-infected and latently infected mice.

Results

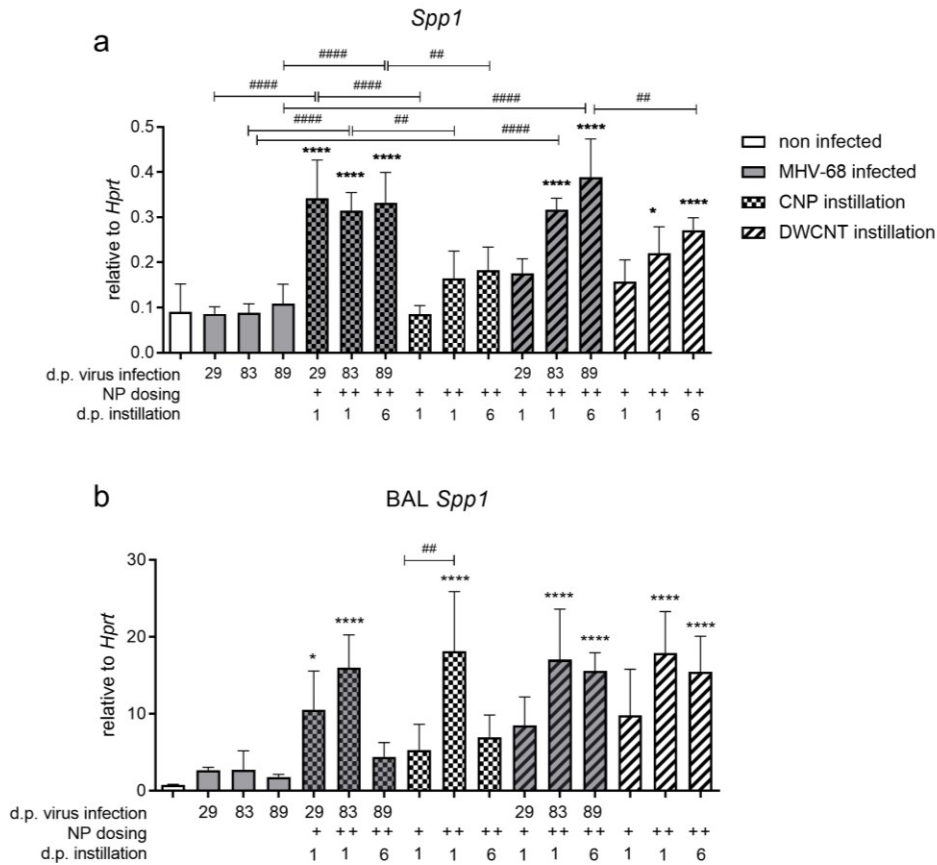


Figure 3.20. Increased lung and BAL cell gene expression of *Spp1* in the 2nd hit model and particle treatment.

After MHV-68 virus infection and CNP or DWCNT instillation during latency, lungs and BAL cells, were isolated and homogenized. Whole lung and BAL cell RNA was isolated. *Spp1* gene expression was investigated from whole lung tissue (a) and from BAL cells (b) by qPCR. Expression results were normalized to the housekeeper gene *Hprt*. (n = 4-5). Data were analyzed by Ordinary one-way ANOVA and Tukey's multiple comparisons test, "*" indicates statistically significant difference to "control". *: indicates *P* value < 0.05. **: indicates *P* value < 0.01. ***: indicates *P* value < 0.001. ****: indicates *P* value < 0.0001. "#" indicates statistically significant difference of two indicated groups. #: indicates *P* value < 0.05. ##: indicates *P* value < 0.01. ###: indicates *P* value < 0.001. ####: indicates *P* value < 0.0001.

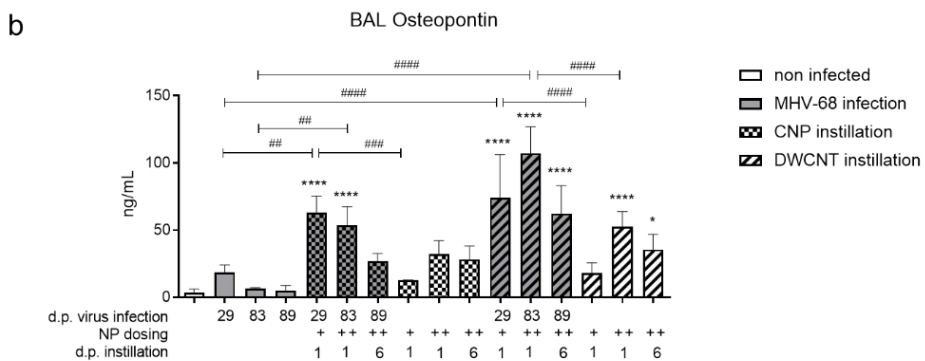
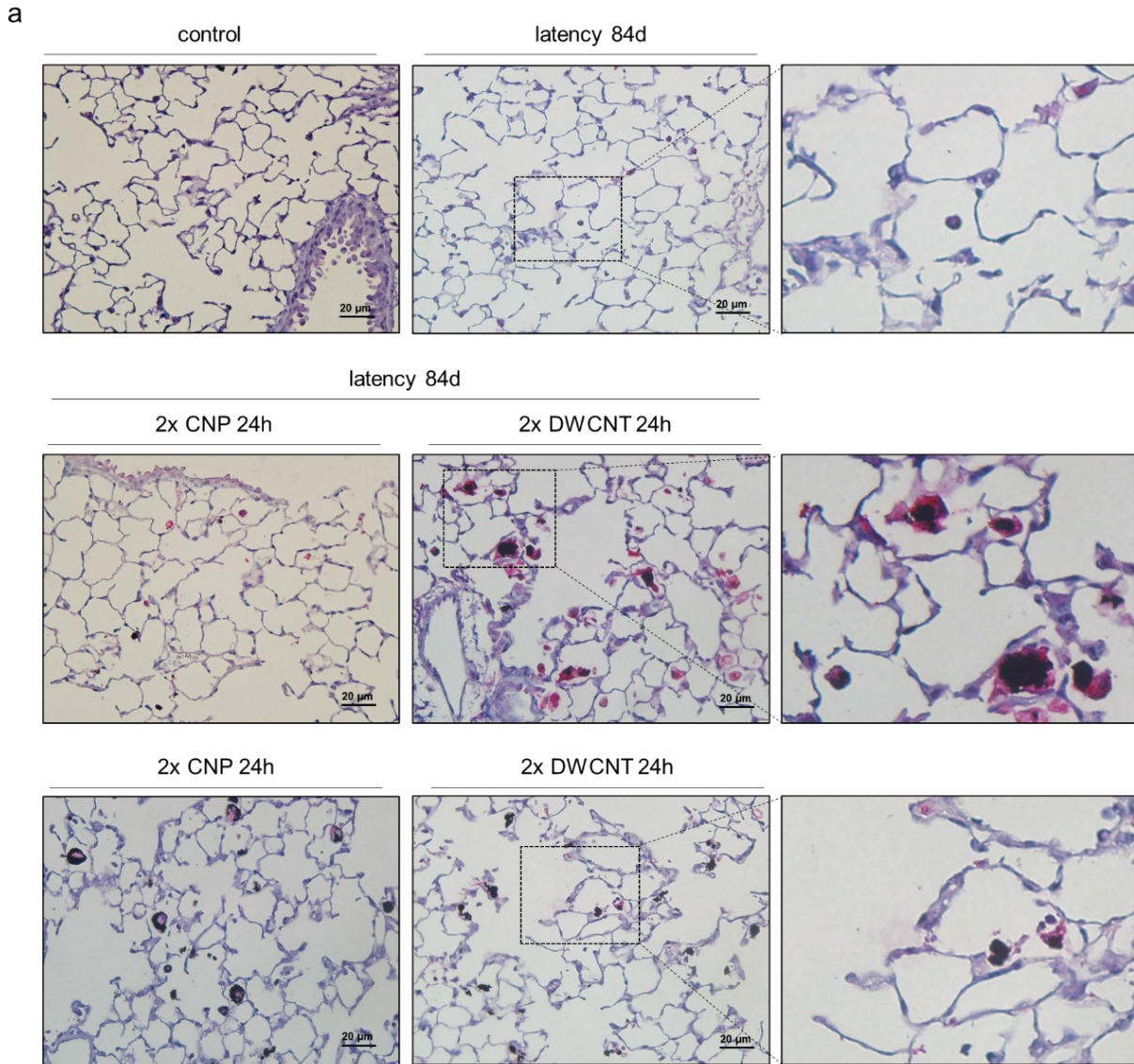


Figure 3.21 Increased Osteopontin in alveolar macrophages and release into airspace after particle treatment.

After MHV-68 virus infection and CNP or DWCNT instillation during latency, lungs and BAL liquid, were isolated. Lung tissue was fixed and embedded into paraffin. Tissue slides were immunohistochemically stained with anti-OPN and images are shown in (a). OPN staining is mainly localized in alveolar

Results

macrophages. BAL OPN concentration was measured by ELISA and **(b)** shows significantly increase mainly in the 2nd hit model induced by CNP and DWCNT. (n = 3-5). Data were analyzed by Ordinary one-way ANOVA and Tukey's multiple comparisons test, "*" indicates statistically significant difference to "control". *: indicates *P value* < 0.05. **: indicates *P value* < 0.01. ***: indicates *P value* < 0.001. ****: indicates *P value* < 0.0001. "#" indicates statistically significant difference of two indicated groups. #: indicates *P value* < 0.05. ##: indicates *P value* < 0.01. ###: indicates *P value* < 0.001. ####: indicates *P value* < 0.0001.

After the analysis of *Spp1* gene expression, the localization of OPN protein in the lung was investigated. OPN was detected localized in alveolar macrophages (**Fig. 3.21a**) in pink after IHC staining of lung tissue slides. These OPN+ alveolar macrophages have uptaken the carbon nanoparticles, which is clearly visible as the black particles in the cells. Released OPN was measure from BAL fluid, performed with ELISA. Significantly high OPN levels were observed 24h after the first and repeated CNP exposure in latently infected mice (**Fig. 3.21b**). All groups of DWCNT induced second hit and repeated second hit model were releasing significantly high OPN levels, whereas in the non-infected mice, only the repeated DWCNT release higher OPN. However, the infected mice release significantly more OPN into the airspace in the first and repeated DWCNT exposure after 24h compared to DWCNT only.

3.8.10 Increased GM-CSF release in CNP exposure

Granulocyte macrophage-colony stimulating factor (GM-CSF) promotes the survival, differentiation, proliferation and function of myeloid progenitors and the differentiation of alveolar macrophages and plays an important role in the pathogenesis of acute and chronic pulmonary inflammation and disease. As the reactivating MHV-68 was mainly detected in recruited inflammatory monocyte derived macrophages and particles were found to be uptaken in alveolar macrophages and releasing pro-inflammatory mediators. Levels of GM-CSF in bronchoalveolar lavage were measured by Bio-Plex assay. GM-CSF release was significantly elevated in first and repeated CNP exposure after 24h in non-infected mice and in the CNP induced repeated second hit model (Fig. 3.22). However, the GM-CSF release in the CNP induced second hit model is significantly lower compared to non-infected mice, GM-CSF levels in BAL fluid are significantly increased in the CNP induced repeated second hit model compared to the non-infected repeated CNP exposure. From first to repeated, GM-CSF significantly

increase in CNP induced second hit model, whereas GM-CSF release significantly reduces from first to repeated CNP exposure in non-infected animals.

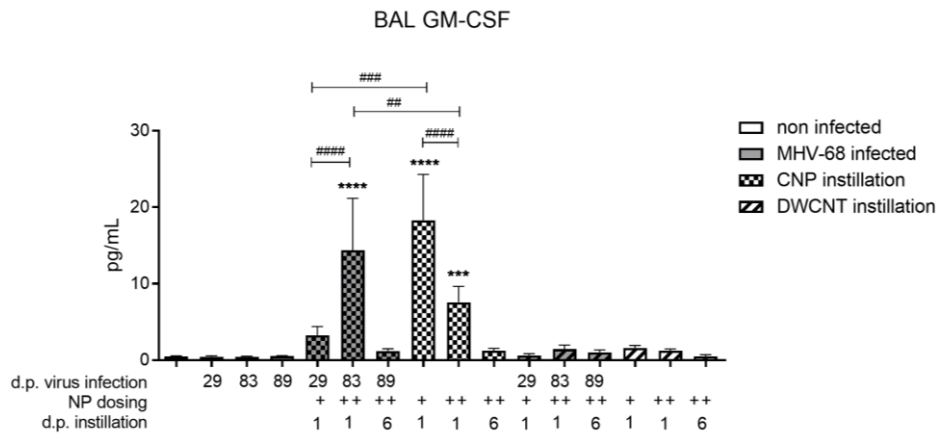


Figure 3.22. Increased GM-CSF release into bronchoalveolar lavage after CNP exposure and CNP induced 2nd hit model with repeated exposure.

After MHV-68 virus infection and CNP or DWCNT instillation during latency, BAL liquid was collected and analyzed with Bio-Plex assay for the concentration of GM-CSF. Figure shows significantly increase in the 2nd hit model induced by repeated CNP and in the first and repeated CNP exposure in non-infected mice. (n = 4-5). Data were analyzed by Ordinary one-way ANOVA and Tukey's multiple comparisons test, "" indicates statistically significant difference to "control". *: indicates *P* value < 0.05. **: indicates *P* value < 0.01. ***: indicates *P* value < 0.001. ****: indicates *P* value < 0.0001. "#" indicates statistically significant difference of two indicated groups. #: indicates *P* value < 0.05. ##: indicates *P* value < 0.01. ###: indicates *P* value < 0.001. ####: indicates *P* value < 0.0001.

3.9 Effect of MHV-68 infection and NP exposure on pulmonary morphology

As chronic pulmonary diseases are defined by different pathophysiological changes in the lung, epithelial regeneration, changes in air space, collagen deposition, alterations in lung cell morphology or cell death after virus infection and NP exposure were highly interested in observations.

3.9.1 Reduction of alveolar epithelial type II (AT2) cell numbers in second hit model

After epithelial injury, alveolar epithelial type II (AT2) cells are essential for epithelial regeneration in the alveoli, due to their specific stem/progenitor cell function. Alveolar epithelial type I (AT1) cells are more sensitive to injury and after AT1 injury, AT2 cells get stimulated to multiply and transdifferentiate into AT1 cells.

To investigate alveolar epithelial recovery in the lungs, pro-SPC was stained in brown with IHC, as a marker for AT2 cells in the lung tissue (**Fig. 3.23a**). AT2 cell numbers were analyzed in lung tissue with CAST quantification of pro-SPC positive IHC stained cells. Significant reduced AT2 cell numbers in the lungs of CNP induced repeated second hit model after 24 hours and 6 days were observed compared to the control. In addition, significantly reduction of AT2 cell numbers were detected in the CNP induced repeated second hit model after 24h in comparison to the latency or CNP exposure alone (**Fig. 3.23b**). Compared to the control, there is only a significant increase in the early latency after 29 days, whereas 29 days after infection plus CNP exposure was significantly reduced compared to the latency only.

Taken together, significantly decreased AT2 cell numbers in the CNP induced repeated second hit model suggest insufficient alveolar epithelial recovery in chronic CNP exposure and prior MHV-68 infection.

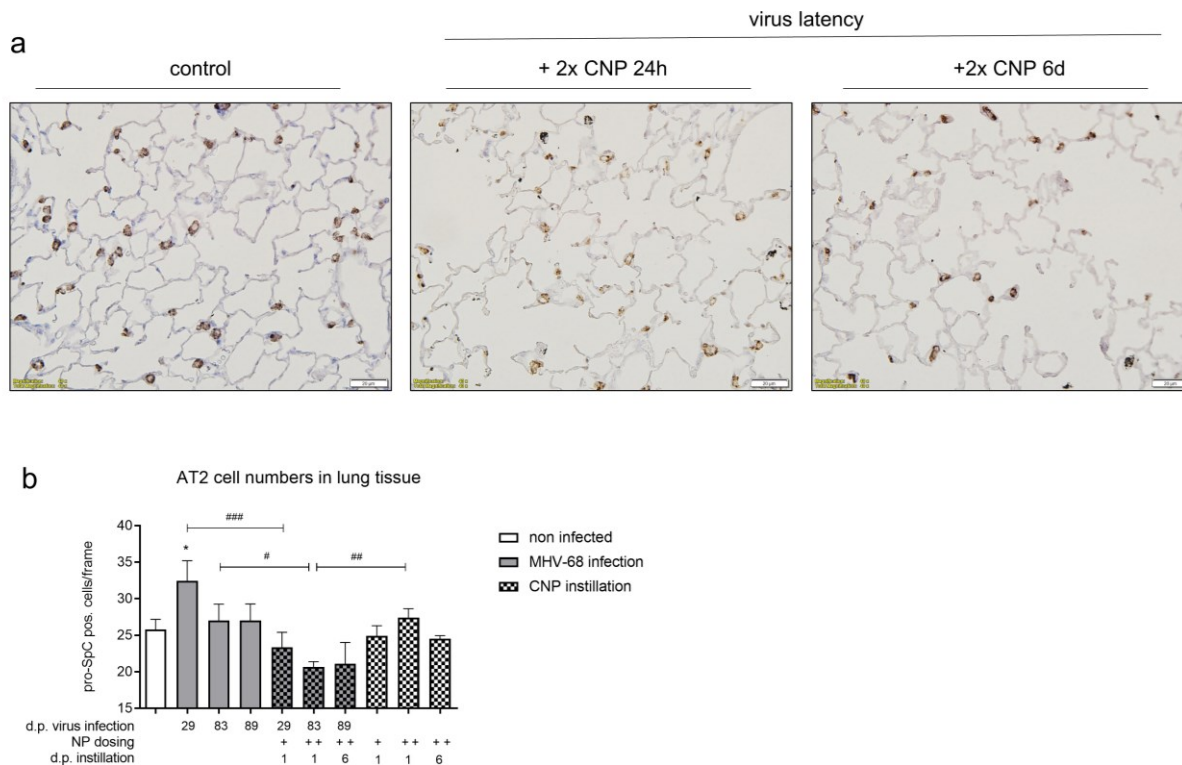


Figure 3.23 Repeated CNP exposure to MHV-68 latency decrease AT2 cell numbers in lung tissue.

pro-SPC was stained with immunohistochemistry in lung tissue as a marker for alveolar epithelial type II (AT2) cells. **(a)** representative bright field images of pro-SPC in lung tissue. Left image: control, middle image: MHV-68 latency plus repeated CNP 24h, right image: MHV-68 latency plus repeated CNP exposure 6d. Scale bar: 20 μ m. **(b)** CAST quantification of pro-SPC IHC staining, shows increased AT2 cell numbers in early latency and reduced AT2 cell numbers of 2nd hit model in repeated CNP exposure compared to virus latency and CNP only. (n = 3). Data were analyzed by Ordinary one-way ANOVA and Tukey's multiple comparisons test, "*" indicates statistically significant difference to "control". #: indicates *P* value < 0.05. "#" indicates statistically significant difference of two indicated groups. #: indicates *P* value < 0.05. ##: indicates *P* value < 0.01. ###: indicates *P* value < 0.001.

3.9.2 Increased alveolar air space in chronic time points of virus reactivation

Pulmonary injury can lead to loss of alveolar epithelial cells and to airspace enlargement with emphysema-like changes, which is also known to play an important role in the developed in the chronic lung disease COPD. Airspace enlargement leads to difficulties of gas exchange, as there is a reduction of alveolar epithelial cells, which are necessary for gas exchange.

Results

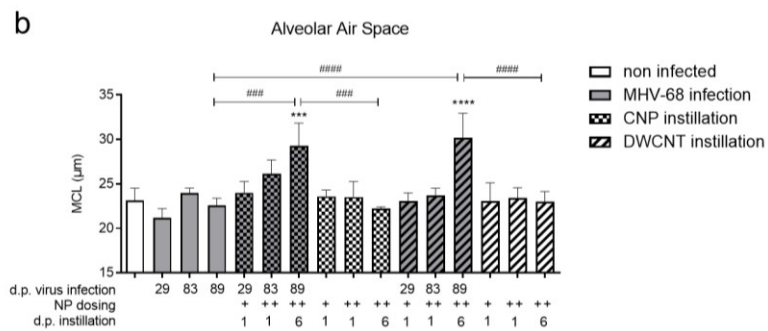
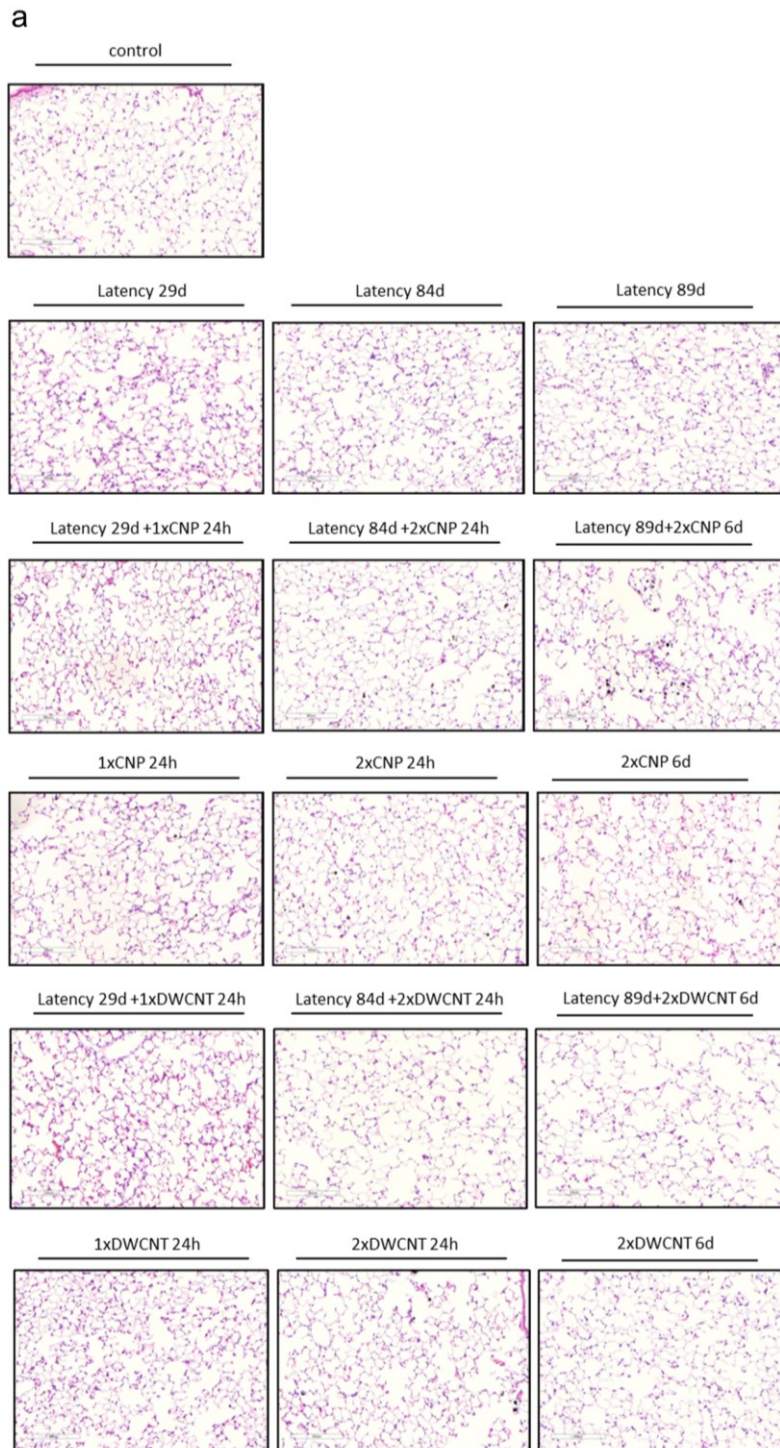


Figure 3.24 Repeated CNP exposure of MHV-68 infected mice increase alveolar air space and lung tissue inflammation.

(a) H&E stained lung tissue show increased air space in lung tissue of mice 89 days MHV-68 and 6 days after 2nd CNP and DWCNT instillation. Scale bar: 300 μ m. (b) quantification of H&E stained slides for mean chord length (MCL) with CAST method verifies significant alveolar air space enlargement in lungs of mice 89 days infected and 6 days after 2nd CNP and DWCNT instillation (n = 3). Data were analyzed by Ordinary one-way ANOVA and Tukey's multiple comparisons test, "" indicates statistically significant difference to "control". *: indicates *P value* < 0.05. **: indicates *P value* < 0.01. ***: indicates *P value* < 0.001. ****: indicates *P value* < 0.0001. "#" indicates statistically significant difference of two indicated groups. #: indicates *P value* < 0.05. ####: indicates *P value* < 0.001. #####: indicates *P value* < 0.0001.

Lungs were isolated, fixed and embedded in paraffin. Lungs were sliced and tissue slides were stained with H&E to visualize the lung structure. Significant elevated airspace enlargement was detected 6 days after both, CNP and DWCNT induced repeated second hit model (**Fig. 3.24a**). Quantification of mean chord length (MCL) with CAST confirms significant enlargement 6 days after NP induced repeated second hit models with both, CNP and DWCNT (**Fig. 3.24b**).

Taken together, co-exposure of MHV-68 infection and repeated NP treatment lead to elevated airspace enlargement compared to only NP exposure or MHV-68 infection challenges.

3.9.3 No changes in pulmonary collagen deposition

The chronic lung disease IPF is characterized by excessive extracellular matrix (ECM) deposition and remodeling. A major component of ECM is collagen, and in healthy lungs, there is a balance between degradation and synthesis of collagen and other ECM proteins. This is disturbed in fibrosis.

To investigate possible alterations in ECM deposition in the lung, lung tissue was isolated, fixed and embedded into paraffin. Lungs were sliced and tissue was stained with Masson's-Goldner-Trichrome (MGT) staining. This staining visualizes collagen deposition in the lungs by blue staining. Observing different treated lungs with MGT staining, no change in collagen deposition was observed (**Fig. 3.25**).

Results

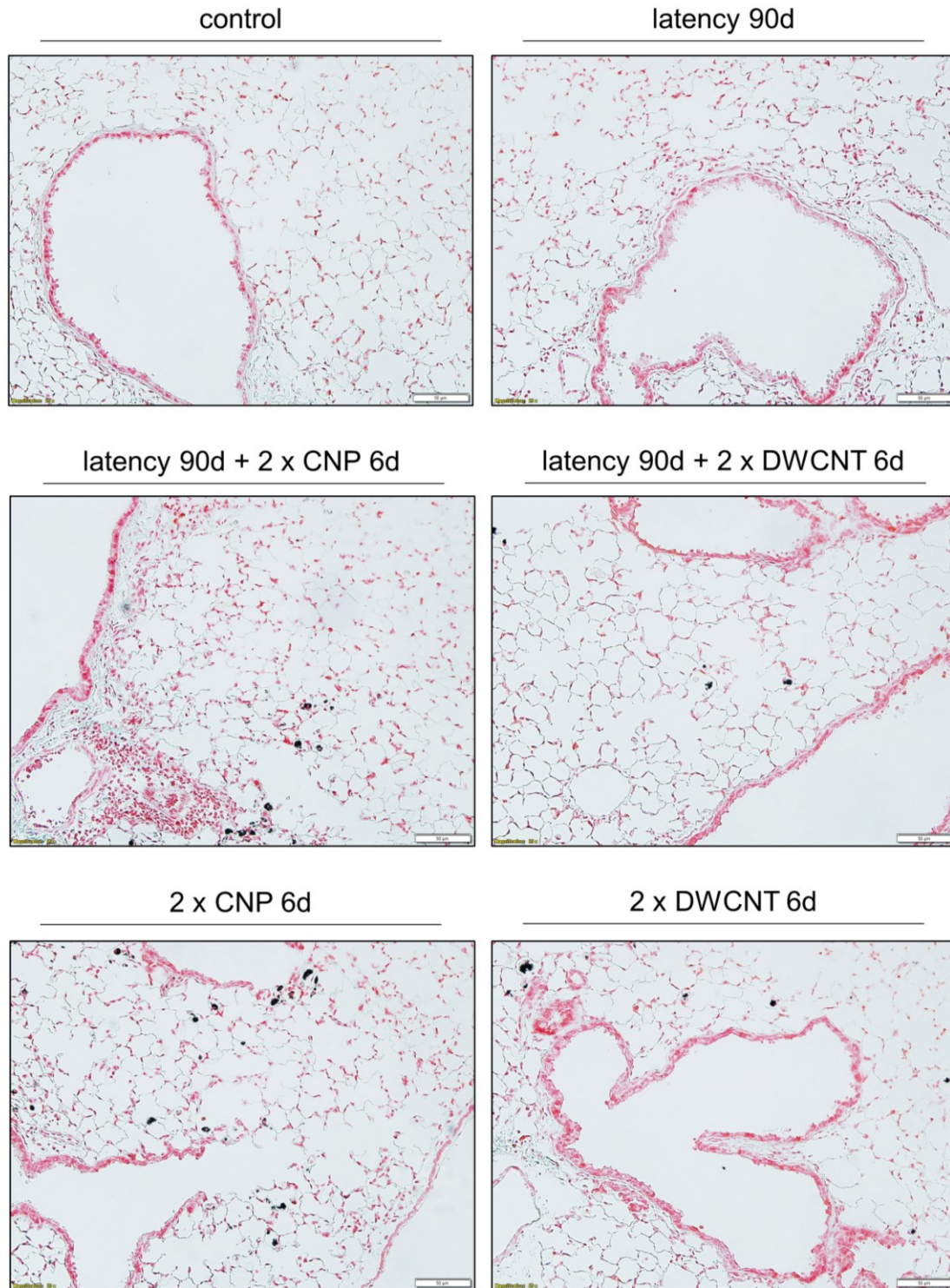


Figure 3.25 Masson's-Goldner-Trichrome staining shows no change in collagen deposition during virus infection or NP treatment.

Mice were infected with MHV-68 and during latent infection either CNP or DWCNT were instilled into the lungs. Lungs were isolated, fixed and in paraffin embedded. Lung sections were stained for Goldner Masson's Trichrome staining. The Trichrome staining shows no changes in collagen deposition in lung tissue of different treatments. Scale bar: 50 μm.

Pro-fibrotic markers for myofibroblasts and ECM were observed by qPCR of whole lung homogenates. The markers for myofibroblast *Acta2*, and lipofibroblast *Fn1* and an ECM marker for collagen1a1 *Col1a1* were detected relative to the housekeeper gene *Hprt* (**Fig. 3.26**). Myofibroblasts and lipofibroblasts secrete excessive amounts of collagen in fibrotic tissue. Additionally, expression of *Fn1* and *Col1a1* is known to be increased under fibrotic conditions. No changes in *Fn1* expression levels were detected with MHV-68 infection or NP exposure (**Fig. 3.26b**). Increased *Col1a1* gene expression level was found only in lung tissue of single DWCNT exposure in non-infected mice, whereas the repeated DWCNT decreases again to no significant change to the control (**Fig. 3.26c**). myofibroblast marker gene *Acta2* was only significantly elevated expressed 24h after the first exposures of CNP or DWCNT in non-infected animals, which declines back to no significant changes compared to the control at the repeated exposure (**Fig. 3.26a**).

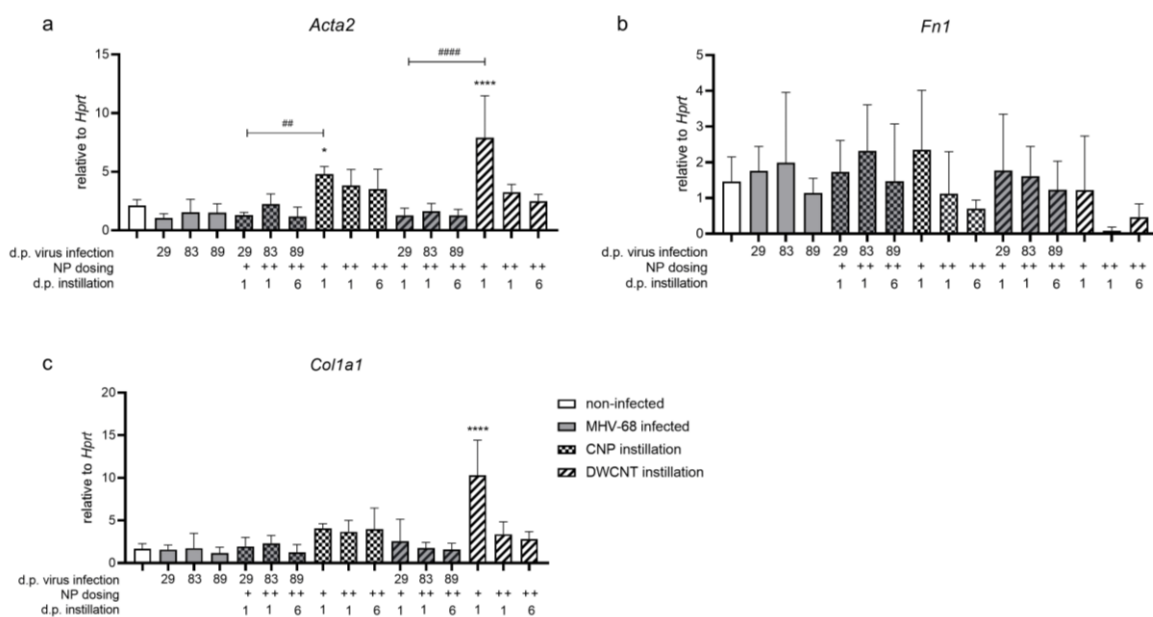


Figure 3.26 Effect of virus and NP treatment to the expression of pro-fibrotic markers.

Mice were infected with MHV-68 and during latent infection either CNP or DWCNT were instilled into the lungs. Lungs were isolated and homogenized and RNA was purified. RNA was synthesized to cDNA and *Acta2*, *Fn1* and *Col1a1* gene expressions of whole lung were analyzed by qPCR. Expression results were normalized to the housekeeper gene *Hprt*. (n = 5). Data were analyzed by Ordinary one-way ANOVA and Tukey's multiple comparisons test, "*" indicates statistically significant difference to "control". *: indicates *P* value < 0.05. **: indicates *P* value < 0.01. ***: indicates *P* value < 0.001. ****: indicates *P* value < 0.0001.

Results

indicates P value < 0.0001 . “#” indicates statistically significant difference of two indicated groups. #: indicates P value < 0.05 . ##: indicates P value < 0.01 . ###: indicates P value < 0.001 . ####: indicates P value < 0.0001 .

3.9.4 No changes in goblet cell morphology and mucus production

Mucus hypersecretion is an important pathophysiological feature in several chronic pulmonary diseases like COPD or asthma. Airway mucus is mainly composed of gel-forming mucins MUC5AC and MUC5B. To investigate, whether MHV-68 virus infection and CNP or DWCNT exposure lead to goblet cell hyperplasia or alterations in mucus production, isolated lung tissue was fixed with PFA and embedded for sectioning in paraffin. Lung slides were stained with periodic acid-Schiff (PAS) staining, to visualize mucus in bronchial area by staining to pink. There was no changes of mucus production or morphological changes observed in all different treatment groups (**Fig. 3.27**).

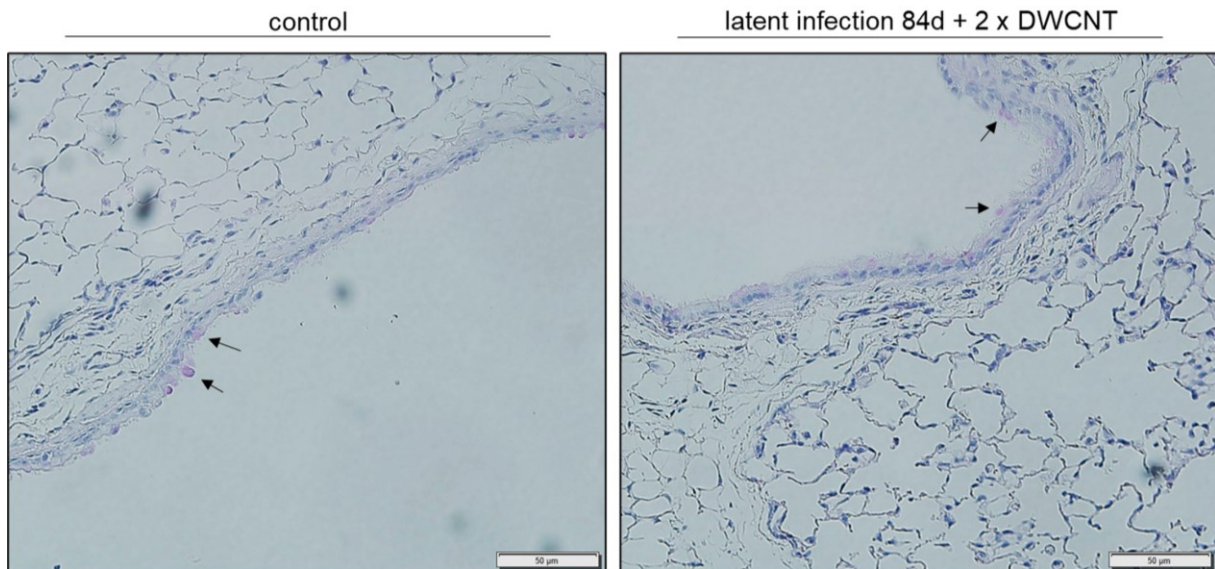


Figure 3.27 PAS staining shows no goblet cell hyperplasia.

Mice were infected with MHV-68 and during latent infection either CNP or DWCNT were instilled into the lungs. Lungs were isolated, fixed and in paraffin embedded. Lung sections were stained for PAS staining to analyze changes in goblet cells. The PAS staining indicates no changes in mucus production in lung tissue of different treatments. Scale bar: 50 μ m.

In addition, to histological lung tissue examination, changes in mucus production were investigated by mucus gene regulation with the marker *Muc5ac* (Fig. 3.28). *Muc5ac* gene expressions was investigated from whole lung homogenates and detected relative to the housekeeper gene *Hprt*. No significant changes in *Muc5ac* gene expression levels were observed between all treatment groups, strengthen the results from histological examination, in which no alterations in mucus production were observed.

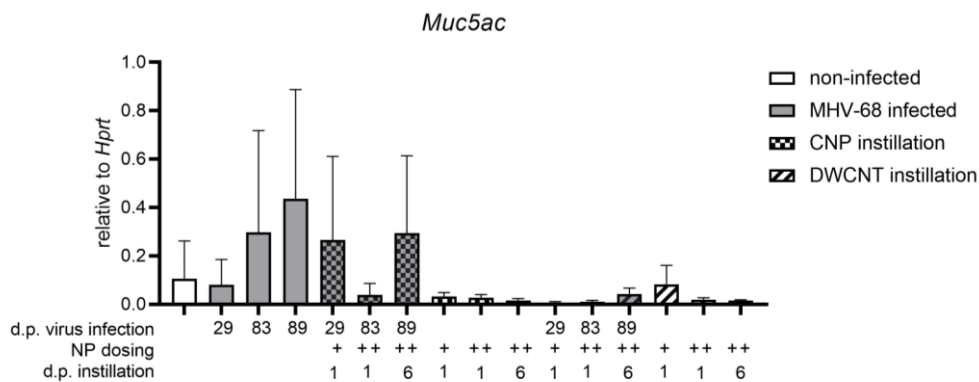


Figure 3.28 No changes of airway mucus gene *Muc5ac*.

Mice were infected with MHV-68 and during latent infection either CNP or DWCNT were instilled into the lungs. Lungs were isolated and homogenized and RNA was purified. RNA was synthesized to cDNA and *Muc5ac* gene expression of whole lung was analyzed by qPCR. Expression results were normalized to the housekeeper gene *Hprt*. No significant changes are observed between different treatment groups. (n = 5). Data were analyzed by Ordinary one-way ANOVA and Tukey's multiple comparisons test, “*” indicates statistically significant difference to “control”. *: indicates *P* value < 0.05. **: indicates *P* value < 0.01. ***: indicates *P* value < 0.001. ****: indicates *P* value < 0.0001. “#” indicates statistically significant difference of two indicated groups. #: indicates *P* value < 0.05. ##: indicates *P* value < 0.01. ###: indicates *P* value < 0.001. ####: indicates *P* value < 0.0001.

3.9.5 DNA damage and dsDNA release increased after nanoparticle exposure

To investigate DNA fragmentation in the lung tissue, TUNEL assay was performed. In this assay, nick ends of DNA fragments is labelled with a fluorescent tag and be imaged under a fluorescence microscope. Comparing different treatment groups, Increased TUNEL positive signals relative to DAPI events were observed after CNP exposure in non-infected and CNP induced second hit model (Fig. 3.29a). Quantification of TUNEL

Results

positive cells compared to DAPI numbers in the tissue revealed even higher elevated DNA fragmentation from CNP induced second hit model to CNP induced repeated second hit model, whereas in non-infected lungs, TUNEL signal declines from first to repeated CNP exposure (**Fig. 3.29b**). TUNEL signals were detected in alveolar epithelial cells in the CNP induced repeated second hit model, as well as in particle-loaden alveolar macrophages. In the repeated CNP exposure in

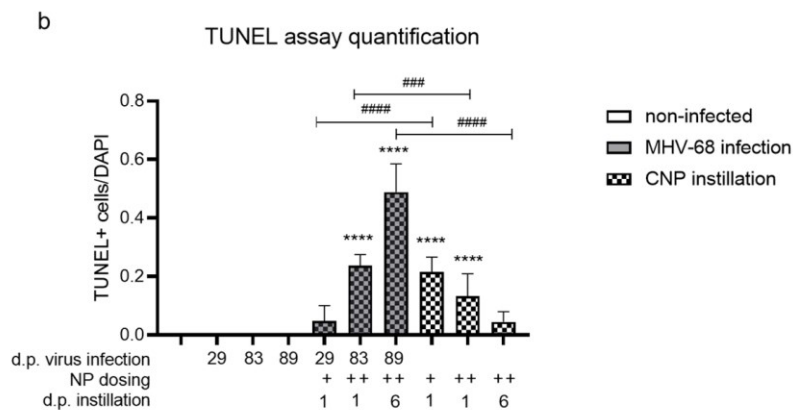
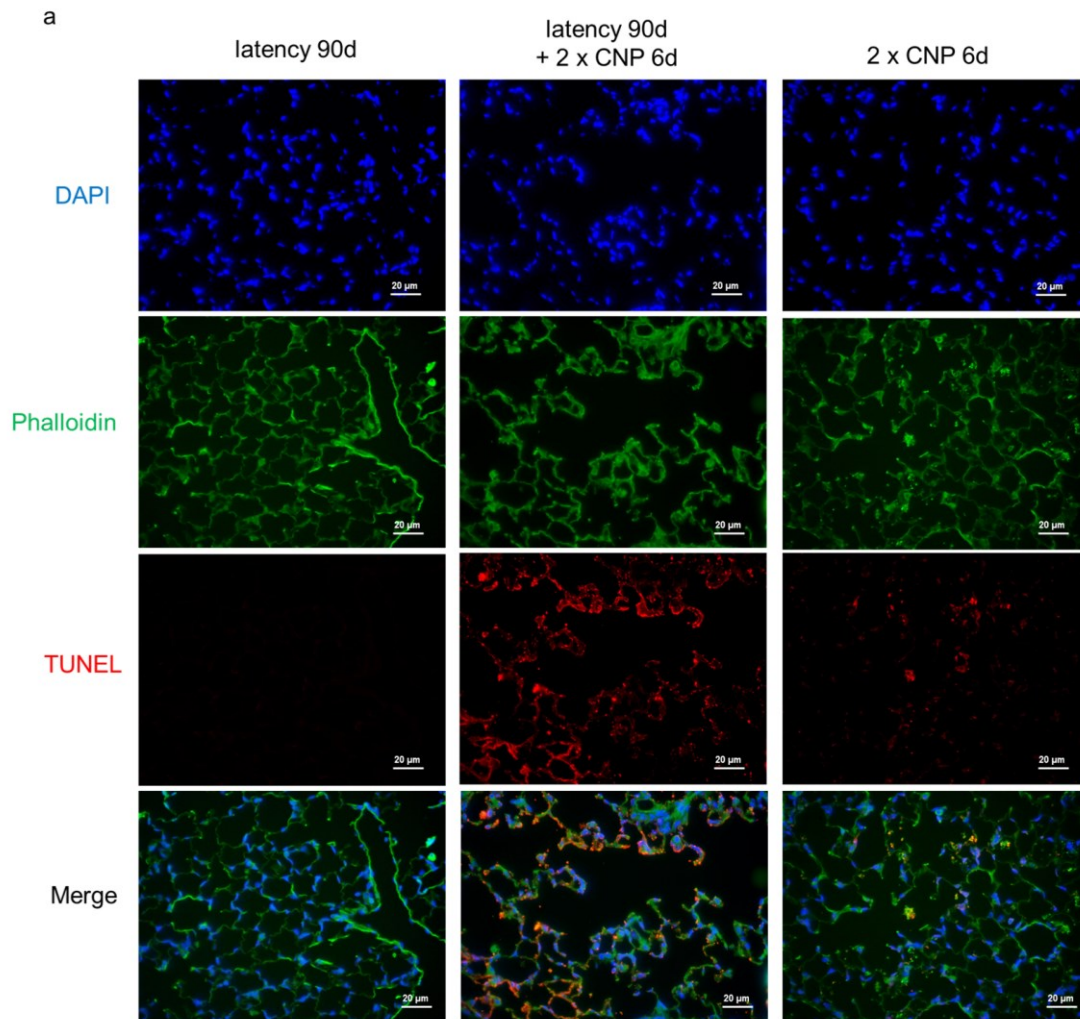


Figure 3.29. Increased DNA fragmentation in repeated CNP exposure in 2nd hit model.

Mice were infected with MHV-68 and during latent infection CNP were instilled into the lungs. Lungs were isolated, fixed and in paraffin embedded. (a) Lung sections were stained with TUNEL assay to visualize DNA fragmentation. Scale bar: 20 μ m. (b) Quantification of TUNEL positive cells normalized to DAPI numbers (n = 3). Data were analyzed by Ordinary one-way ANOVA and Tukey's multiple comparisons test, “*” indicates statistically significant difference to “control”. *: indicates *P* value < 0.05. **: indicates *P* value < 0.01. ***: indicates *P* value < 0.001. ****: indicates *P* value < 0.0001. “#” indicates statistically significant difference of two indicated groups. #: indicates *P* value < 0.05. ##: indicates *P* value < 0.01. ###: indicates *P* value < 0.001. ####: indicates *P* value < 0.0001.

Measurement of free dsDNA release into the air space was significantly increased dsDNA levels in all CNP treated groups. In both, single and repeated exposure and in non-infected and MHV-68 infected animals (Fig. 3.30). Again, a significant increase between first and repeated CNP exposure in infected mice and a decrease of dsDNA level from first to repeated CNP exposure in non-infected mice. This pattern was also observed on a lower detection level in DWCNT treated groups.

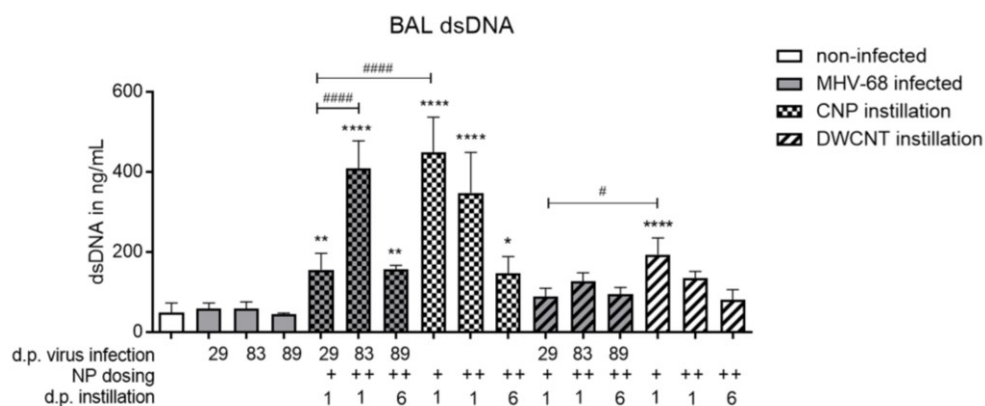


Figure 3.30 dsDNA release into airspace.

Mice were infected with MHV-68 and during latent infection either CNP or DWCNT were instilled into the lungs. Lungs were lavaged and BAL fluid was collected. BAL fluid was measured for free dsDNA. (n = 5). Data were analyzed by Ordinary one-way ANOVA and Tukey's multiple comparisons test, “*” indicates statistically significant difference to “control”. *: indicates *P* value < 0.05. **: indicates *P* value < 0.01. ***: indicates *P* value < 0.001. ****: indicates *P* value < 0.0001. “#” indicates statistically significant difference of two indicated groups. #: indicates *P* value < 0.05. ##: indicates *P* value < 0.01. ###: indicates *P* value < 0.001. ####: indicates *P* value < 0.0001.

Results

Taken together, this increased TUNEL detection, along with similar patterns in dsDNA levels, indicate higher DNA fragmentation and potential cell death in CNP induced repeated second hit model compared to repeated CNP exposure in non-infected lungs. Mainly localized TUNEL events in alveolar epithelial cells strengthened the results of reduced AT2 cell numbers and increased alveolar air space enlargement in the CNP induced repeated second hit model.

4. Discussion

In this study, repeated NP exposure in latently MHV-68-infected mice was shown to cause increased interstitial and air space inflammation and injury with loss of AT2 cell numbers and emphysema-like changes, which was not observed to this extent with viral latency or NP exposure alone.

4.1 NP-triggered MHV-68 reactivation detected in lung recruited inflammatory monocyte-derived macrophages

Gamma herpesviruses are ubiquitous in human society. The best-known gamma herpesviruses in humans include Epstein-Barr virus (EBV or human herpesvirus 4, HHV-4) and Kaposi's sarcoma-associated herpesvirus (KSHV), which infect at least 90% of the adult population worldwide before the age of 30 (de-The et al., 2975; Venkitarama et al., 1985; Levin et al., 2010). Similar to other herpesviruses, gamma herpesviruses also develop lifelong latency after primary infection. During the latency period, the viral genome remains in the cells as an episome (Murata, 2014). In the murine gamma herpesvirus infection model with MHV-68, that initial infection, which peaks at around 6 days after nasal infection, occurred mainly in lung epithelial cells (**Fig. 3.2**). Latency is established after 28 days (Sattler et al., 2017), and has been described to get established from day 14 post infection on (Sunil-Chandra et al. 1992). The exact cell types that carry latent virus infection was not detected in this model because the antiserum only detects lytic MHV-68 proteins. But the lytic MHV-68 proteins and thus the virus in the lytic phase of infection were clearly observed in the lungs by immunohistological examinations. The lytic proteins were detected in immunofluorescence (IF) staining together with other cell-specific markers under the fluorescence microscope, and in single stains in immunohistochemical (IHC) staining, observed under the bright field microscope. Both staining methods were applied to either co-stain cell type specific markers to detect co-localization and identify cell type, or IHC single staining to investigate the localization of virus reactivating cells in the lung tissue.

Conclusion and Outlook

A variety of chemical and biological factors have been described to trigger the reactivation of gammaherpesvirus. These factors could be, for example, infection with other viruses or bacteria, oxidative stress or reactive oxygen species (ROS), and elevated stress hormones (Ye et al., 2011a; Ye et al., 2011b; Coskun et al., 2010; Li et al., 2011). Using IF co-staining, there was no NP-triggered MHV-68 reactivation observed in B-lymphocytes, T-lymphocytes, epithelial cells, monocytes or alveolar macrophages in the lung, as I did not observe co-localization with lytic MHV-68 proteins and the cell type-specific markers for the listed cell types. The main reactivation occurs in macrophages derived from monocytes, as the lytic MHV-68 proteins were co-localized in IBA1- and CD11b-positive cells. IBA1/AIF1 is used as a pan-macrophage marker that stains all macrophages in lung tissue except for alveolar macrophages. The markers CD11b and IBA1 expressing on macrophages have been observed in inflammatory monocyte-derived macrophages (Duan et al., 2015). Alveolar macrophages are derived from fetal liver during embryogenesis and are found to be long-lived, self-renewing resident lung cell population (Yona et al. 2013; Hashimoto et al., 2013; Guilliams et al., 2013). Following pulmonary inflammation, which can be induced by nanoparticle instillation, bone marrow-derived macrophages (BMDM) are recruited to the lungs (Misharin et al., 2017). It has also been described that latently infected blood monocytes can reactivate the latent herpesvirus "human cytomegalovirus" (HCMV) in progenitor cells, as a result of differentiation into macrophages or dendritic cells driven by pro-inflammatory cytokines such as IFN- γ , TNF- α , or GM-CSF (Hahn et al., 1998; Reddehase et al., 2019). Thus, the observed MHV-68 reactivation in my model could also be a consequence of the differentiation of recruited monocytes into macrophages. However, the exact process of whether monocytes recruited by particle exposure reactivate the virus during differentiation or the latently infected recruited macrophages interact with the NP directly or indirectly via epithelial cells and reactivate cannot be clarified in this model and needs to be further investigated by co-staining of MHV-68 lytic proteins and monocyte markers such as CCR2 or isolation of bone marrow monocytes in the future. However, the *in vitro* models, in the ALI model as well as in the submerged treatment, show that the interaction of the latently infected BMDM with the exposed nanoparticles leads to reactivation of the latent virus (Sattler et al., 2017).

Furthermore, carbon nanoparticles are known to cause pulmonary inflammation, oxidative stress, and DNA fragmentation after pulmonary exposure (Jacobsen et al.,

2011; Hadrup et al. 2017; Migliore et al., 2010), which have previously been described to trigger latent herpesvirus reactivations (Sattler et al., 2017). In this study, mice were latently infected with MHV-68 and exposed to either single or repeated CNP or DWCNT. With repeated administration, the environmental situation of not being exposed exclusively to one dose of particulate matter was adapted.

MHV-68 reactivation was confirmed after the first and repeated instillations of CNP or DWCNT only based on the increased lytic viral protein production in the lungs by IHC and IF staining. In addition, the viral reactivation at the level of gene expression based on the expression of open reading frame 50 (ORF50) and open reading frame 73 (ORF73) was sought to be detected. ORF50 is expressed in the lytic phase of infection, whereas ORF73 is continuously expressed in both phases, lytic and latent, and was used as a viral gene to normalize the whole infected cells. However, in contrast to previous studies (Sattler et al., 2017), an increase in the ORF50/ORF73 ratio was not observed. Change in ORF50/ORF73 ratio neither has been observed in whole lung homogenates nor in isolated BAL cells. Either the numbers of infected and reactivating cells are not in a sufficient amount in the lung tissue and the expression change cannot be observed because it may be below the detection limit. Or 24h after NP exposure may be not the time where the reactivation on gene expression can be observed in the lung. In the *in vitro* ALICE cloud exposure model, the ORF50/ORF73 expression ratio has been observed with increase 9 hours after CNP exposure compared with the submerged *in vitro* reactivation model, where the ratio was increased 24 hours after the CNP exposure to ANA-1/MHV-68. Because the ALI treatment is closer to the environmental setting due to direct cell-particle contact, the viral gene expression might be also higher *in vivo* earlier than the 24-hour time point due to this rapid direct cell contact with the nanoparticles. Future studies of nanoparticle-triggered viral reactivation *in vivo* should consider additional sampling of lungs at earlier time points, such as 6 or 12 hours after NP instillation, to investigate the kinetics of viral reactivation at the level of gene expression.

4.2 Elevated cytotoxic T-lymphocyte infiltration into the air space with higher cytotoxic potential in the repeated second hit model

In my repeated NP exposure model and the second hit model or also called reactivation model, together with a previous gammaherpesvirus infection, I was able to distinguish

Conclusion and Outlook

some reactions that were clearly induced by the nanoparticle treatment and reactions that were clearly induced by the MHV-68 infection. One clear NP reaction I found was that neutrophilic infiltrates were present in lung tissue and bronchoalveolar lavage. It is well known that pulmonary exposure to various kinds of NP lead to high levels of neutrophil infiltrations in acute lung inflammation (Bendtsen et al, 2019; Danielsen et al, 2021; Knudsen, et al, 2019; Poulsen et al, 2016; Hadrup et al, 2021; Stoeger et al, 2006; Duan et al., 2015; Cosnier et al, 2021). This elevated neutrophil numbers were in this model with CNP or DWCNT in both uninfected and latently infected animals. A clear response to viral infection is the recruitment of lymphocytes to the tissues. It is well described that viral infections and chronic pulmonary inflammation result in heavy infiltration of lymphocytes into the lungs, particularly CD8+ T-lymphocytes (Connors et al, 2016; Kawasaki et al, 2022; Marshall and Swain, 2011; Patel et al, 2022). Moreover, exposure to nanoparticles is known to lead to recruitment of lymphocytes mainly in the peri-bronchial and perivascular areas (Di Ianni et al., 2022; Bendtsen et al., 2019; Kyjovska et al., 2015), in which I also see many CD8+ T-lymphocytes localized in this model. Repeated exposure to nanoparticles with previous infection shows that even more CD8+ T-cells are recruited to the bronchoalveolar space, suggesting a combined inflammatory effect of viral infection and exposure to nanoparticles, which is even higher with repeated NP dosing and repeated viral reactivation. However, not only was the number of CD8+ T-lymphocytes increased in the 2nd-hit model with repeated CNP exposure, but I also found that markers for effector and memory T-cells were significantly increased. Infants were found to have significantly increased CD8+ T-cells, particularly in acute lung injury induced by viral infection, which were also functionally in the activated and memory phenotype with increased cytotoxic capacity (Connors et al., 2016). In addition, I found significantly increased expression of cytotoxic markers such as perforin, granzyme a, and b in my model. These results suggest a higher cytotoxic T-cell potential after CNP exposure and subsequent increased lung inflammation and injury. This could also lead to an exacerbation of chronic inflammation with more cytotoxicity and less regeneration during disease development in patients with chronic lung disease. The interaction of nanoparticles in the alveoli could lead to greater reactivation in these regions and greater recruitment and activation of T-cells. This recruitment and activation of T-cells in the alveolar region could affect alveolar epithelial cells, which could explain the increased alveolar space with increased mean chord length (MCL) and reduced ATII cell numbers with repeated

CNP administration in virus-infected mice. High numbers of neutrophils and lymphocytes also play a role in chronic lung disease, as they are necessary to control the inflammatory response (Saetta et al. 2001).

In chronic lung diseases such as COPD or asthma, it has been described that ectopic lymphoid tissue can form in the lung after inflammation or infection. This tissue is called inducible bronchus-associated lymphoid tissue (iBALT) and is a tertiary lymphoid structure. The presence of iBALT is thought to exacerbate inflammation in chronic disease and correlates with worsening pathology rather than resolution of inflammation in chronic inflammatory disease (Marin et al., 2019; Kuroda et al., 2016; Roos et al., 2015). In this model, chronic NP exposure was attempted to mimic the environmental condition, accumulation of T-cell infiltrations were observed but no actual iBALT formation.

The assumption arise that further and longer nanoparticle exposure and longer chronic inflammation and virus reactivation may lead to the presence of iBALT structures in the lung. Or even prolong inflammation in already chronic inflammatory disease to worsen the chronic condition. However, not only iBALT formation, but also the increase of CD8⁺ T-lymphocytes in the bronchial area is known to lead to increased epithelial remodeling with COPD-like features, increased airflow limitation, and increased capacity to exert effector functions, supporting the hypothesis that the presence of CD8⁺ T-cells contributes to disease progression (Williams et al., 2021; Ravensberg et al., 2013; O'Shaughnessy et al., 1997). In my model, I did not examine lung function with potential airflow limitations or reduction in diffusing capacity. However, I see emphysema-like changes in the increase in MCL in the second-hit model with repeated CNP or DWCNT exposure, higher expression of cytotoxic T-lymphocyte genes, and possibly lower epithelial recovery indicated by lower numbers of AT2 progenitor cells. IFN- γ expression was significantly high in BAL cells in the CNP-induced reactivation model at both initial and repeated exposure. IFN- γ is known to play a role in cytokine storm and lung tissue inflammation and injury (Zhang et al., 2021; Verma et al., 2022). IFN- γ promotes monocyte-mediated lung injury during IAV infection (Schmit et al., 2022) and plays a role in acute lung injury (Mock et al., 2020).

Further *in vivo* studies should consider lung function tests and further investigation of T-lymphocyte subsets by co-staining in FACS analysis. Currently, I only know that the composition of total CD8⁺ T-lymphocytes is increasing in the BAL cells, but not exactly which markers are colocalized on individual cells.

4.3 Elevated inflammatory response in repeated NP exposure in latently infected vs. adaptive response in non-infected mice

For many inflammatory responses, there was an increase detected from first to repeated exposure in latently MHV-68-infected animals (BAL release of TNF, IL-6, LCN2, CCL17, CCL5, CXCL1, CXCL2, CXCL5, GM-CSF, CCL3, CCL4, CCL11, and CCL24). This pattern was even more evident with exposure to CNP than to DWCNT. In contrast, a rather decreasing inflammatory response in the uninfected animals from the first to the second NP exposure was observed. This suggests that the immune system responds differently to nanoparticle exposure in uninfected mice compared with exposure after prior MHV-68 infection.

Different responses could be explained by trained immunity. Following primary immunological exposure, innate monocytes, macrophages, and NK cells could be programmed to have immune memory that enhances host defense (Cheng et al., 2014; Gourbal et al., 2018). Acute respiratory viral infections induce alveolar macrophages (AMs) with changes in surface markers, gene expression, metabolism, and antimicrobial responsiveness (Yao et al., 2018). This priming of memory AMs requires the help of effector CD8 T-lymphocytes, which are located in the early phase of the antiviral response in the airway mucosa. Effector T cell-derived IFN- γ is necessary to activate memory AMs, which in turn induce significantly greater neutrophil chemotaxis through the release of CXCL2 (Yao et al., 2018). As I have also seen in my viral reactivation model, *Irfn- γ* expression is significantly high in the early latency and CNP-induced second-hit model, as are more effector T-lymphocytes in the bronchoalveolar region, where cells can come into direct contact with alveolar macrophages, which is important for priming to memory AMs.

I can speculate that the immune response after viral infection and after CNP exposures differs from noninfected CNP exposures in the context of trained immunity. Another point is the significant increase in CXCL2 release in BAL fluid from initial to repeated CNP exposure in latently infected mice, highlighting the potential involvement of trained immunity.

4.4 Elevated injury of pulmonary barrier integrity in NP induced second hit model

In healthy lungs, the alveolar epithelial membrane acts as a barrier limiting the entry of fluid and proteins from the interstitial and vascular space into the airspace and is also responsible for the capacity of alveolar fluid clearance (AFC). Both are necessary to maintain the proper air-liquid interface, which is essential for gas exchange and host defense against infection and pathogens and can be distributed in severely injured lungs (Matthay et al., 2005).

There is also evidence that lung permeability increases significantly during terminal senescence (Tankersley et al., 2003). I examined the integrity of the alveolar-capillary membrane by quantifying protein and IgM content in the bronchoalveolar space, which has been described as a valid method (Herrero et al., 2011, 2013). Leakage of protein-rich fluid into the BAL is a consequence of barrier damage, as evident from total protein and the presence of high molecular weight plasma proteins such as IgM (plasma protein or larger size, 900 kDa).

After viral infection and NP exposure alone, significantly increased total protein influx into the air space was observed at the 24-hour time points at DWCNT induced second hit model and repeated second hit model, as well as increased total protein in all CNP-exposed mice with previous MHV-68 infection. Increased IgM levels in BAL were detected in viral latency (29d and 84d), after repeated CNP exposure in uninfected mice, and in the second hit and repeated second hit model induced by CNP and DWCNT. Total protein and IgM levels in BAL fluid correlated significantly with each other. This suggests epithelial-endothelial barrier damage after virus infection and NP exposure, but prolonged and even more severe alveolar-capillary damage in the second hit and repeated second hit model compared with virus or NP alone.

Alveolar epithelial barrier dysfunction has been described as a hallmark of acute respiratory distress syndrome, resulting in the development of edema and diffuse alveolar damage (Huppert et al, 2019; Matthay et al, 2019; Dutra Silva et al, 2021). Dysfunctional epithelial-endothelial barriers and vascular leakage in COVID-19 disease are also a contributing factor to disease severity (Biering et al., 2021).

Alveolar epithelial type 1 (AT1) cells are large squamous cells that cover 95% of the alveolar surface and form the epithelial component of the air-blood barrier (Wang et al., 2017). AT1 cells are described to be more sensitive to injury than AT2 cells (Herzog

et al., 2008). My detection of DNA fragmentation also shows localization of DNA fragmentation in AT1-formed epithelial cells. Nanoparticles have been described to induce DNA damage in epithelial cells (Mroz et al., 2007; Ahmed et al., 2020). This induction of epithelial damage by the combined viral infection and nanoparticle treatment, which I also confirmed by increasing the airspace in the second hit model, suggests increased alveolar-capillary damage.

4.5 CNP and DWCNT exposure differentially activate pulmonary inflammatory response

In this study, the inflammatory response elicited by CNP or DWCNT with or without prior infection was observed to differ between the two particles. CNP appears to be more effective in eliciting inflammatory responses, with higher release of chemoattractants into the air space (GM-CSF, CCL3, CCL4, CXCL2, CXCL1, CXCL5, and MPO) and increased infiltration and proliferation of CD8⁺ lymphocytes in the air space, with elevated T-cell cytotoxicity, and increased *Ifn- γ* expression in BAL cells. Only osteopontin release in the air space was increased with DWCNT exposure compared with CNP exposure. Overall BAL protein concentration was similarly elevated in both CNP and DWCNT exposure in latently infected mice, as well as tissue inflammation levels and increased mean chord length.

Since the dispersion of DWCNT in water can hardly be stabilized, the addition of Pluronic F-127 increases the stabilization of the particle dispersion. Pluronic F-127 is a commercially available polyethylene oxide (PEO)-polypropylene oxide (PPO) copolymer that reduces the hydrophobicity of CNTs, allowing them to form more stable solutions in water, and has been shown to be effective in dispersing CNTs (Ciofani et al., 2009). These additional surface changes result in lower hydrophobicity and thus potential CNT-surface-cell interaction. Pluronic-coated MWCNTs have been described to protect the tube from lysosomal membrane damage and reduce the potential to induce pulmonary fibrosis (Wang et al., 2012). This could result in lower measured inflammatory responses in the bronchoalveolar space compared to those triggered by CNP exposure. This also raises the question of whether the use of Pluronic to disperse CNT is appropriate to study viral reactivation triggered by DWCNT and its possible contribution to the development or exacerbation of chronic lung disease in this model, when some effects of DWCNT exposure could be influenced by particle coating with

Pluronic. Different dispersion media were tested, with the result that water appeared to be the best dispersion medium to mimic carbon black inhalation, while CNT dispersion required the addition of either 2% serum or 0.05% serum albumin (Hadrup et al., 2017). This confirms that dispersion media affect the toxicity of nanomaterials and should be considered when planning intratracheal studies. However, in this study, the effect of Pluronic on the possible containment of CNT-induced inflammatory response cannot be clarified, but MHV-68 reactivation after DWCNT exposure was detected similar to CNP exposure, as well as increased BAL protein and dsDNA levels, neutrophil recruitment, and enlargement of the alveolar airspace.

Parallel investigations in our group suggest that CNP and DWCNTs activate inflammatory and MHV-68 reactivation pathways differently *in vitro*, with DWCNTs not dispersed in Pluronic (data not shown; from Lianyong Han's dissertation, 2022). Even when CNTs are not dispersed in Pluronic, there are differences in pathway activation between DWCNTs and CNPs, suggesting differences in response due to their different structure, shape, and surface area. Long multi-walled carbon nanotubes (MWCNTs) are known to induce frustrated phagocytosis with subsequent induction of a pro-inflammatory and pro-fibrotic immune response, whereas short CNTs do not induce cytotoxicity (Boyles et al., 2015). It has been studied that the larger MWCNTs induce different pathways compared to the smaller SWCNTs (Gosh et al., 2020).

CNTs are biopersistent materials with high aspect ratio, some are rigid and have a length that leads to frustrated phagocytosis and pleural accumulation, which has been associated with fibrosis, neoplastic changes in the lung, and cardiovascular disease (Møller et al., 2014).

In summary, the induction of inflammation depended on the physical properties of the nanoparticles. The spherical CNPs and the fibrous DWCNTs elicit different inflammatory responses simply because of their different structures.

4.6 Effect of MHV-68 infection and nanoparticle exposure on macrophage activation

Prenatal macrophages derived from fetal liver are resistant and self-renewing in lung tissue and are referred to as alveolar macrophages (Hashimoto et al, 2013; Tan et al, 2016; Schneider et al, 2014; Bain et al, 2014; Hashimoto et al, 2013; Hussell et al, 2014; Misharin et al, 2011). Bone marrow macrophages are recruited from the bone

Conclusion and Outlook

marrow to the lungs during inflammation or particle deposition and are essential for stopping the inflammatory response (Misharin et al., 2017). Among others, they release TNF α , IL-6, and CXCL2 (Maruyama et al., 2019). In this model, I also found CD11b-positive macrophages, indicative of bone marrow-derived macrophages that are recruited to the lungs after particle exposure. These cells carry the latent infection and due to the inflammatory or stress response triggered by the particles, the latent MHV-68 is reactivated, leading to even more tissue damage and inflammation. I found that the expression of IFN γ , IL-6, and CXCL2 was significantly increased with repeated CNP exposure in latently infected mice, suggesting increased inflammation in infiltrated bone marrow-derived macrophages carrying potential infection and reactivated after particle infiltration.

Alveolar macrophages, and in this model even more so infiltrating macrophages from bone marrow, have been described to produce extracellular vesicles (EVs) in a dose-dependent manner after their exposure to atmospheric particulate matter. Subsequently, EVs were able to induce a pro-inflammatory phenotype in epithelial cells, triggering the release of IL-6 and TNF α (Martin et al., 2019). In my study, I did not observe EVs production, but I observed increased IL-6 and Tnf expression and therefore can attribute to EV content in the bronchoalveolar space a possible role in the repeated second hit model. The observation of EV production should be considered in this model in the future, as it is also discussed as a potential biomarker of disease activity in COPD (Bazzan et al., 2020) or as a biomarker of acute respiratory distress syndrome (Mahida et al., 2022).

CD11b⁺ IBA1⁺ macrophages are the main cell type, reactivating MHV-68 after nanoparticle exposure. IBA1, or allograft inflammatory factor-1 (AIF-1), has been detected in macrophages during pulmonary fibrosis. AIF-1 increases the production of TGF- β , which plays an important role in the mechanism of fibrosis (Nagahara et al., 2018). Macrophages high in AIF-1 have been observed to increase the production of IL-6, TNF- α , and CXCL1 (Nagahara et al., 2016), which were also increased in this NP-induced second hit and repeated second hit model. This suggests, that recruited AIF-1-positive macrophages in the reactivation model might enhance acute lung injury and the development of chronic pulmonary injury and even further to IPF.

Significant increase in CCL17 release and expression in BAL cells and BAL fluid after CNP exposure in mice latently infected and uninfected with MHV-68 were detected and even higher expression from the first to repeated CNP exposure. CCL17 is known

to influence the pathogenesis of respiratory diseases and is a predictive marker of rapid deterioration of lung function (forced expiratory volume in one second [FEV₁] or percentage of predicted FEV₁) in patients with COPD (Machida et al., 2021; Girkin, 2022; Malaviya et al., 2021). It is highly expressed in epithelial cells and BAL cells of COPD patients, especially in smokers (Ying et al., 2008). This is evidence that CCL17 is dependent on particle-induced activation and exacerbation of COPD. Machida and colleagues (2021) found that CCL17 triggers macrophage recruitment, leading to chronic inflammation and destruction of lung tissue. This inflammatory response may also play a role in this model, as an increase in CCL17 after CNP exposure and subsequent macrophage recruitment carrying and reactivating MHV-68 was observed. Macrophage polarization may also drive inflammation and tissue repair and play a role in the development of chronic lung disease. M1, classically activated pro-inflammatory macrophages, may act as promoters in the pathogenesis of acute lung injury and acute respiratory distress syndrome (Sun et al., 2022). M2, alternatively activated macrophages play a key role in anti-inflammatory responses and are important regulators of fibrogenesis, which exacerbates the progression of pulmonary fibrosis (Cheng et al., 2021; Wynn et al., 2016; Yao et al., 2016; Van Dyken et al., 2013). I did not examine changes in macrophage polarization, but I found increased *Tnf* expression in the lungs of the second hit model and, in addition, high *Tnf* expression in BAL cells upon repeated CNP exposure in latently infected mice, which can be highly expressed by M1 macrophages, among others. In addition, CXCL2 can be highly produced by M1 macrophages, which were significantly released into the bronchoalveolar space after repeated CNP exposure in latently infected mice. Both *Tnf* expression and CXCL2 release were greatly increased upon repeated CNP exposure in the second hit model and exacerbated lung injury (Ciesielska et al., 2021). The role of macrophage polarization in the second hit model is important for future studies. Deficiency of *Ifn-γ* receptor or silencing of this gene in mice was unable to control MHV-68 infection from the lytic to the latent phase of infection, resulting in herpesvirus-induced fibrosis in the lung structure (Mora et al., 2007; Lee et al., 2003; Decman et al., 2005). Not only in mice, but also in humans, it has been described that EBV infection can underline the main pathological features of fibrosis (Farina et al., 2014). Although the virus can be restored to its latent infection, repeated and chronic pulmonary exposure to NPs can chronically reactivate the viral infection and lead to fibrotic changes over time.

Conclusion and Outlook

Depletion of alveolar macrophages increases neutrophil influx in LPS-induced lung injury (Beck-Schimmer et al., 2005). In this model, alveolar macrophages could be lysed by virus or depleted by NP exposure, leading to increased recruitment of neutrophils to the lung due to virus reactivation. Myeloperoxidase (MPO) can be used as a predictor of the presence of neutrophils. In this model, MPO in the BAL and the number of neutrophils in the BAL correlated significantly with each other. MPO is an important component of the innate immune system and is mainly released by neutrophils to defend against pathogens.

Because significantly increased DNA fragmentation with repeated NP exposure compared with single exposure was observed, it may be possible that the alveolar macrophages in this model have impaired efferocytosis. Efferocytosis is the process of clearance of apoptotic cells by phagocytes and is essential for the maintenance of tissue homeostasis. Dead cells can become secondarily necrotic, leading to autoimmunity, tissue necrosis, and pathological inflammation (Doran et al., 2020; Kawano and Nagata, 2018; Szondy et al., 2014). It has been described that excessive production of proinflammatory cytokines such as IL-6, IL-1 β , or IL-8 (human homolog for murine CXCL1, CXCL2, and CXCL5) interferes with the efficient clearance of dead cells required for tissue repair (Matthay et al., 2019). In this model, expression and release of IL-6, CXCL2, CXCL1, and CXCL5 were detected upon repeated NP dosing in latently infected mice, raising the question of efferocytosis efficiency in MHV-68-infected and particle-exposed macrophages. Impaired efferocytosis has been observed in severe COVID-19 immunopathogenesis (Salina et al., 2022).

Kheradmand et al. (2017) found evidence for DNA double-strand breaks after pulmonary exposure to carbon black (CB), and the CB accumulation in the lung immune cells may promote emphysema development. This accumulation of carbon black was confirmed in this model by finding that it is localized and phagocytosed by alveolar macrophages. In addition, an increase in air space was observed, suggesting emphysema development.

Yuan et al. (2020) showed that macrophages exposed to carbon black exhibited necrotic features and were characterized by lysosomal ruptures. Further analysis suggests that mitochondrial DNA (mtDNA) release from necrotic cells acts as a key event in mediating neutrophilic lung inflammation. Although the origin of free double-stranded DNA (dsDNA) cannot be discriminated in this model, a significant increase in dsDNA release after CNP instillation was observed. Elevated dsDNA release was

detected in 24 hours after the first and repeated CNP exposure in uninfected animals. In latently infected mice, a moderate but still significantly high release was observed after the first CNP exposure, increasing more significantly in the CNP induced repeated second hit model. This pattern of dsDNA release can be confirmed by the pattern of neutrophil cell numbers recruited to the air space. Elevated neutrophil numbers at 24h after the first and repeated CNP exposures in uninfected mice, moderate but still significantly elevated neutrophil numbers in the CNP induced second hit model and even more cell numbers from the first to repeated CNP exposures in latently infected mice were observed. Circulating or free dsDNA lacks specificity but has been used as a surrogate for neutrophil extracellular traps (NETs) and associated components (Masuda et al., 2016). The process of NETs release, also called NETosis, is triggered by various granular proteins such as MPO and neutrophil elastase (Zawrotniak, et al., 2013). From these matching results, the free dsDNA in the bronchoalveolar lavage fluid can be part of neutrophilic inflammation after NP exposure. It has been described that excess NET formation damages the epithelium and may lead to lung tissue damage (Storisteanu et al., 2017), which has also been described in patients with COPD (Porto et al., 2016).

Epithelial cells and macrophages are among the first cells to come into contact with nanoparticles. NP uptake of alveolar macrophages has been observed in H&E staining and even more clearly in immunohistochemical staining of OPN. Uptake of CNP and CNTs by phagocytosis may be prolonged and incomplete, which may promote interstitial fibrosis in the long term. High expression levels and release of Spp1/Osteopontin (OPN) at all time points in the second hit and repeated second hit model was detected. Staining demonstrated Spp1/OPN localization in alveolar macrophages that clearly ingested CNP and DWCNT particles. Spp1/OPN has been described an essential regulator of immunity and cell death, and Spp1/OPN was found to increase the expression of necroptosis-related genes and enhance macrophage necroptosis in influenza A virus (IAV)-infected THP1 cells (Wang et al., 2022). Wang et al. (2022) describe that the reduction of Spp1/OPN results in lower IAV viral titers and protects against infection. In addition, osteopontin was found to be increased in expression in the lungs of a mouse model of allergen-induced chronic airway remodeling, suggesting a contribution of OPN to airway remodeling in asthma (Kohan et al., 2007). Spp1/OPN is a consistently observed marker for IPF, and Spp1/OPN-rich

macrophages represent a profibrotic macrophage population in IPF lungs (Morse et al., 2019).

Similar to asbestos fibers, "long" CNTs (mean length of 13 μm) can induce frustrated phagocytosis in macrophages due to their fibrous indigestibility, which can release a variety of reactive oxygen species (ROS) (Jiang et al., 2008, Murphy et al., 2012). The main source of ROS comes from mitochondrial production and contributes to oxidative stress (Climent et al., 2020). Accumulation of ROS has been found in disease progression in asthmatic mice (Wang et al., 2019a). Further investigation of ROS production and oxidative stress and their contribution to chronic lung disease exacerbation is needed in the future.

4.7 Inflammatory response to NP exposure and virus infection and the development of chronic lung diseases

Exposure to nanoparticles has been described to cause acute pneumonia (Wong et al., 2016), and exposure to air pollution and particulate matter has also been found to exacerbate chronic lung diseases such as asthma and COPD (Chatkin et al., 2022; Thurston et al, 2020; Wang et al, 2019b; Li et al, 2016; Cai et al, 2014; Cho et al, 2014; Guan et al, 2016; Guarnieri et al, 2014; Habre et al, 2018; Kurdo et al, 2016). Significant associations have been found between short- and long-term exposure to air pollution and airway remodeling, lower forced expiratory volume in 1 s (FEV_1), increased inflammatory markers, and respiratory disease exacerbations. Carbon black nanoparticles have been described to induce histologic inflammation (Roulet et al., 2012).

The predominant CNT-induced pathology is rapid onset and prolonged pulmonary inflammation and fibrosis (Dong and Ma, 2018; Dong and Ma, 2019; Dong, 2020; Duke and Bonner, 2017; Vietti et al, 2016; Porter et al, 2015). Phenotypic studies show similarities to human pulmonary diseases such as silicosis, idiopathic pulmonary fibrosis, and asbestosis. In this study, long-term exposure with repeated NP exposure was mimicked by repeated particle exposure. Using CNP as a surrogate for combustion-derived nanoparticles in air pollution and DWCNT as fibrous manufactured nanoparticles. Since 50 μg of CNP and DWCNT are high exposures to the lung, more exposures than just two times with a lower NP dosing per treatment that may be needed to adapt to environmental conditions need to be considered in the future.

However, the evidence of increased DNA damage, airspace enlargement, interstitial inflammation and increased expression of inflammatory mediators in the CNP induced repeated second hit model has been observed compared with a single CNP exposure in uninfected mice. Although lung function was not measured, it can be assumed that the lung function may be impaired due to the increase of the mean chord length (Oelsner et al., 2014; McAllister et al., 2014).

It has been described that there is a significant association between long-term exposure to air pollution and increasing emphysema (Wang et al., 2019).

Increased neutrophil numbers in sputum are described in non-Th2 asthma, furthermore extracellular DNA, NET-formation and inflammasome activation was detected in the sputum of patients with more severe asthma (Lachowicz-Scroggins et al., 2019; Hastie et al., 2020). This increase of neutrophil numbers and increased cell free dsDNA in BAL fluid in the second hit model from the first to repeated CNP exposure suggest a worsening and further development of non-Th2 asthma disease. Furthermore, release and expression of CXCL1, CXCL2, CXCL5, IL-6, MPO, TNF- α and IFN- γ have been described to be elevated due to infection, cigarette smoke or air pollution, which lead to neutrophilic inflammation and later to airway hyperresponsiveness (Sze et al., 2019). These inflammatory factors and neutrophil influx were also observed in the repeated second hit model, what might be a factor in the development of this asthmatic phenotype.

The excessive DNA fragmentation, loss of alveolar epithelium, and potential impairment of epithelial cell regeneration, as indicated by a significantly lower AT2 cell numbers, which was observed after 24h in the CNP induced repeated second hit model, might play an important role in the development of pulmonary disease over years. This may eventually lead to scarring and further to fibrotic changes in the lungs. It has been described that AT2 cells from patients suffering from severe pulmonary fibrosis have reduced lung stem cell renewal with distal epithelial stem cell failure, which suggested to be the cause of the disease severity (Liang et al., 2016; Parimon et al., 2020). Clear results of fibrotic changes were not detected, where exposure times and numbers are potential reasons for lacking fibrotic pattern. However, these fibrotic changes were not detected in this model, a significant loss of AT2 cell numbers were observed in the repeated second hit model. In addition, long-term exposure to environmental particles has also been described to induce fibrotic changes and exacerbate the fibrosis process in pre-existing pulmonary fibrosis (Nie et al., 2022;

Conclusion and Outlook

Stermann et al., 2022; Zhang et al., 2022b; Simeonova and Erdely, 2009; Yue et al., 2022).

Increased exposure to air pollution has been described to increase the risk of upper and lower respiratory tract infections (Mehta et al., 213). In 2017, 433 thousand people died from lower respiratory tract infections due to particulate matter pollution (GBD, 2017b). Not only air pollution potentially contributes to the spread of viral infections (Conticini et al., 2020; Setti et al., 2020), but simultaneous exposure to viral infection and high levels of air pollution also exacerbates the severity and outcome of infection, as measured by an increase in the spread and mortality of SARS-CoV-2 (Jerrett et al., 2022; Xiong et al., 2022; Wu et al., 2020; Pozzer et al., 2020; Konstantinoudis et al., 2021). Frontera et al. (2020) use the term "double-hit hypothesis" to propose that regions with high levels of air pollution register more COVID-19 cases with more severe forms of disease due to particle-triggered ACE-2 overexpression, which may increase viral load, which in turn depletes the ACE-2 receptor and impairs host defense, and a second hit from atmospheric NO₂, which worsens disease progression.

The increasing spread of the virus is closely but not causally related, as more air pollution also indicates a higher population. However, we cannot ignore the fact that air pollution is associated with COVID-19 morbidity and thus contributes to the overall worsening of the disease course. Although some publications describe that gamma-herpesviruses are protective against RSV infections with the help of CD8⁺ T cells (Dourcy et al., 2020), emphysema-like changes were observed in this model of repeated NP-triggered reactivation of gamma-herpesviruses, which suggests pathologic changes due to nanoparticles and virus reactivation.

Lower respiratory tract infections are the leading cause of infectious death and the fifth leading cause of death overall, with mortality closely linked to air pollution (Troeger et al., 2017). In recent years, more attention has been paid to the hypothesis that exposure to environmental factors such as air pollution may impair the immune system and limit its ability to cope with infections such as respiratory syncytial virus (RSV) or influenza virus (McCarthy et al., 2022; Vandini et al., 2013; Nenna et al., 2017). Higher airborne NO_x levels have been found to be associated with prolonged exacerbations likely of viral etiology, with COPD exacerbations occurring most severely 2-4 days after elevated airborne NO_x levels (Pfeffer et al., 2019). This supports the toxicological effects of air pollution on increased susceptibility to respiratory infections.

Among all the particle effects on lung inflammation and potential exacerbation of chronic lung disease, MHV-68 infections have been shown to highly express IL-6 in their lytic phase, which exacerbates oxidative stress and soluble type I collagen (Bortz et al., 2018). We can assume that MHV-68 reactivated during the lytic phase of infection may exacerbate pre-existing lung disease and play a role in the development of chronic lung disease, depending on the particle exposure concentration and type, as well as the number of reactivations of latent viruses.

Mohan et al (2010) showed that respiratory viral infections are strongly associated with acute exacerbation of COPD. Human gammaherpesvirus "Epstein-Barr virus" (EBV) DNA has been associated with both idiopathic pulmonary fibrosis (Kelly et al., 2002; Tang et al., 2003) and COPD (McManus et al., 2008). Although NP exposure is known to induce fibrotic changes, only increased expression levels of *Acta2* and *Col1a1* at the single dose of DWCNT without viral infection were observed. ECM deposition with collagen content in the lungs was not detected. The exposure time or nanoparticle dosage may not have been sufficient to induce fibrotic changes. In addition, EBV has been detected in patients with respiratory failure and is thus associated with higher mortality in the intensive care unit (He et al., 2017). In recent years, EBV infection in patients has been described to be closely associated with lymphoproliferative disorders after transplantation in the transplanted lung due to COPD with relatively poor prognosis (Li et al., 2021).

It has been described that sequential exposure of single-walled carbon nanotubes (SWCNT) and bacterial infection increased lung inflammation and collagen formation, where alveolar macrophages are unable to cope with bacterial phagocytosis, and increased neutrophil and lymphocyte numbers and elevated lactate dehydrogenase levels were detected in the air space compared to SWCNT or bacterial infection alone (Shvedova et al., 2008).

The findings in this repeated second hit model, in which exposure of NP to prior latent MHV-68 infection prolongs inflammation through prolonged lymphocyte infiltration and prolonged elevated IgM levels in BAL fluid, as well as increased interstitial lung inflammation, suggesting injury of the epithelial and endothelial barrier. The increased expression and release of proinflammatory cytokines, such as TNF α , IL-6, and INF- γ , in the repeated second hit model, as well as elevated interstitial inflammation and significant loss of both, AT1 and AT2 cell numbers were observed. Epithelial regeneration and maintenance of alveolar structure is essential for maintaining the

Conclusion and Outlook

healthy lung function. Taken together, the results of repeated NP exposure in latently infected mice clearly highlight the strong potential in the exacerbation of chronic lung disease. With population growth and urbanization, greater control of air pollution is necessary and will become even more important in the future.

5. Conclusion and Outlook

5.1 Conclusion

Repeated NP exposure to latently MHV-68 infected mice was elevating emphysema-like changes with increased air space, accompanied with AT2 loss, and alveolar epithelial DNA fragmentation. indicating increased lung inflammation and injury and inadequate epithelial cell recovery in the repeated second hit model compared to NP or MHV-68 challenge only.

In addition, this study of repeated particle exposure in latent infection detected an additive inflammatory effect on neutrophil and lymphocyte infiltration into the lung and bronchoalveolar space. Increased neutrophil chemoattractants are released into the bronchoalveolar space. Lymphocytes recruited to the air space exhibit a signature of CD8⁺ effector memory T lymphocytes with increased cytotoxic potential, as well as increased proliferation and cytotoxic potential. Pro-inflammatory mediators such as SAA3, CXCL1, CXCL2, CXCL5, IL-17, LCN2, Tnf, SpP1/OPN, IL-6, CCL11, CCL5, CCL24, CCL4, and GM-CSF were even more elevated expressed, and the release of dsDNA was more pronounced in mice from second hit to repeated second hit model. This suggests an additional inflammatory effect in the repeated second hit model, which was not observed in uninfected animals. An adaptive inflammatory response with decreasing expression from first to repeated NP exposure was detected. Particle-loaded alveolar macrophages were detected to highly express OPN, which may contribute to airway remodeling.

In addition to the enhanced immune response in the lung *in vivo*, an increased SAA3 expression in the lung was observed, as well as increased SAA3 serum levels after repeated exposure to the nanoparticle treatment in infected mice. Both the increased inflammatory responses in the lungs and the increased acute phase response in the serum demonstrate that repetitive particle-triggered viral reactivation contribute to the development and exacerbation of chronic lung disease, as well as concomitant diseases such as cardiovascular disease.

A single-culture cell exposure system at the air-liquid interface with CNP exposure in ALICE-CLOUD was established to test MHV-68 reactivation in the BMDM macrophage

Conclusion and Outlook

cell line, which may be used in the future to test the potential to trigger viral reactivation of a variety of environmentally relevant airborne particles.

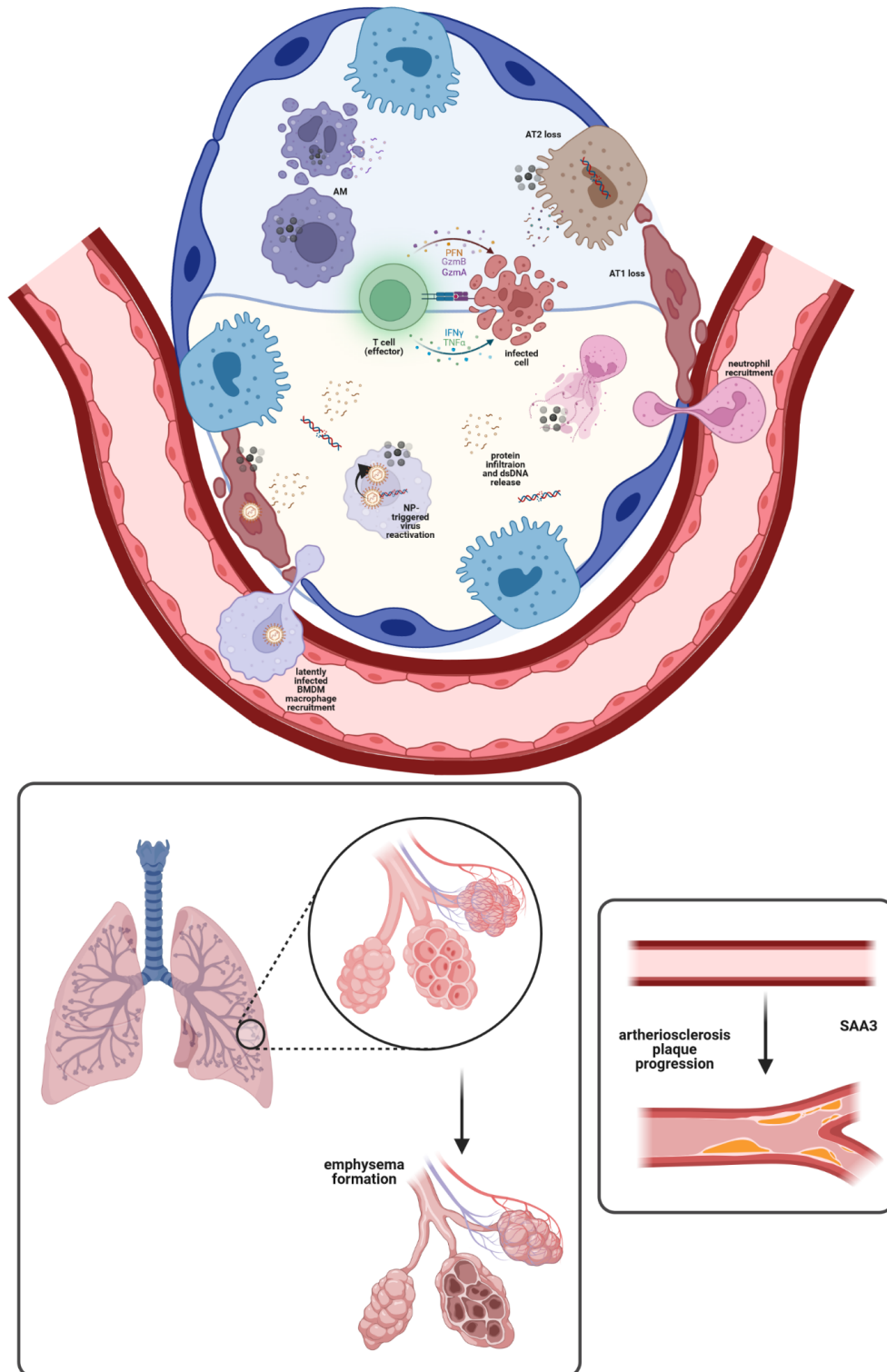


Figure 5.1 Graphical presentation of the proposed response to NP-triggered virus reactivation and the contribution to chronic lung disease and cardiovascular disease.

Created in BioRender.com

5.2 Outlook

CNP nebulization to latently infected cells to investigate the CNP-triggered virus reactivation was investigated. Several environmental relevant particle on ALICE-Cloud system or equal air liquid interface exposure systems, can be used for investigating potential ability to reactivate MHV-68 in the bone marrow derived macrophage cell line ANA-1. These environmental relevant particles could be, freshly generated Diesel exhaust, diesel exhaust particles dispersed and nebulized or bioparticles like pollen. Additionally, an improvement of the co-culture exposure system attempt with primary epithelial cells or epithelial organoids can be established in the future, to approximate the *in vivo* condition more in a culture with several cell types.

For the *in vivo* investigations, nanoparticle exposure should be considered for more repetitive exposures with lower dosing to create a more relevant exposure scenario for investigating the effect on chronic lung diseases (CLD). Additionally, previous establishment of a chronic lung disease model (asthma, COPD or pulmonary fibrosis model) and on top an MHV-68 infection and CNP exposure in latent infection phase could be a closer attempt to study the influence of NP-triggered reactivation to the exacerbation of CLD.

Further analysis with novel methods like single cell RNA sequencing would bring more insights to investigate cell-cell communication in particle triggered virus reactivation and pathways leading to emphysema-like changes and AT2 cell loss. Additionally, the analysis of lung function and diffusion capacity in the chronic and repeated second hit model should be investigated in the future.

References

- AGUILERA, R., LUO, N., BASU, R., WU, J., CLEMESHA, R., GERSHUNOV, A., BENMARHNI, T. 2022. A novel ensemble-based statistical approach to estimate daily wildfire-specific PM_{2.5} in California (2006-2020). *Environ Int*, 24;171:107719.
- AHMED, S., KOBAYASHI, H., AFROZ, T., MA, N., OIKAWA, S., KAWANISHI, S., MURATA, M., HIRAKU, Y. 2020. Nitrate DNA damage in lung epithelial cells exposed to indium nanoparticles and indium ions. *Scientific Reports*, 10,10741.
- ALANIO, C., VERMA, A., MATHEW, D., GOUMA, S., LIANG, G., DUNN, T., OLDRIDGE, D.A., WEAVER, J., KURI-CERVANTES, L., PAMPENA, M.B., BETTS, M.R., COLLMAN, R.G., BUSHMAN, F.D., MEYER, N.J., HENSLEY, S.E., RADER, D., WHERRY, E.J. 2022. Cytomegalovirus Latent Infection is Associated with an Increased Risk of COVID-19-Related Hospitalization. *J Infect Dis*, 26;226(3):463-473.
- ALDER, J.K., CHEN, J.J., LANCASTER, L., DANOFF, S., SU, S.-C., COGAN, J.D., VULTO, I., XIE, M., QI, X., TUDER, R.M., PHILLIPS 3RD, J.A., LANSDROP, P.M., LOYD, J.E., ARMANIOS, M.Y. 2008. Short telomeres are a risk factor for idiopathic pulmonary fibrosis. *Proc Natl Acad Sci USA*, 105(35):13051–13056.
- ALESSANDRINI, F., SCHULZ, H., TAKENAKA, S., LENTNER, B., KARG, E., BEHRENDT, H., JAKOB, T. 2006. Effects of ultrafine carbon particle inhalation on allergic inflammation of the lung. *J Allergy Clin Immunol*, 117(4):824-30.
- ALESSANDRINI, F., BECK-SPEIER, I., KRAPPMANN, D., WEICHENMEIER, I., TAKENAKA, S., KARG, E., KLOO, B., SCHULZ, H., JAKOB, T., MEMPEL, M., BEHRENDT, H. 2009. Role of oxidative stress in ultrafine particle-induced exacerbation of allergic lung inflammation. *Am J Respir Crit Care Med*, 1;179(11):984-91.
- ALESSANDRINI, F., WEICHENMEIER, I., VAN MIERT, E., TAKENAKA, S., KARG, E., BLUME, C., MEMPEL, M., SCHULZ, H., BERNARD, A., BEHRENDT, H. 2010. Effects of ultrafine particles-induced oxidative stress on Clara cells in allergic lung inflammation. *Part Fibre Toxicol*, 26;7:11.
- ALIGO, J., WALKER, M., BUGELSKI, P., WEINSTOCK, D. 2014. Is murine gammaherpesvirus-68 (MHV-68) a suitable immunotoxicological model for examining immunomodulatory drug-associated viral recrudescence? *J Immunotoxicol*, 2015;12(1):1-15.
- ALOISI, F., PUJOL-BORRELL, R. 2006. Lymphoid neogenesis in chronic inflammatory diseases. *Nat Rev Immunol*, 6: 205–217.
- ANDRÉ, E., STOEGER, T., TAKENAKA, S., BAHNWEG, M., RITTER, B., KARG, E., LENTNER, B., REINHARD, C., SCHULZ, H. & WJST, M. 2006. Inhalation of ultrafine carbon particles triggers biphasic pro-inflammatory response in the mouse lung. *Eur Respir J*, 28, 275-85.
- ARMANIOS, M. 2012. Telomerase and idiopathic pulmonary fibrosis. *Mutat Res*, 730(1–2):52–58.
- ATHER, J.L., CKLESS, K., MARTIN, R., FOLEY, K.L., SURATT, B.T., BOYSON, J.E., FITZGERALD, K.A., FLAVELL, R.A., EISENBARTH, S.C., POYNTER, M.E. 2011. Serum amyloid A activates the NLRP3 inflammasome and promotes Th17 allergic asthma in mice.
- BAAN, R.A. 2007. Carcinogenic hazards from inhaled carbon black, titanium dioxide, and talc not containing asbestos or asbestiform fibers: recent evaluations by an IARC Monographs Working Group. *Inhal. Toxicol*, 19(1):213–228.
- BAIN, C.C., BRAVO-BLAS, A., SCOTT, C.L., PERDIGUERO, E.G., GEISSMANN, F., HENRI, S., MALISSEN, B., OSBORNE, L.C., ARTIS, D., MCL MOWAT, A. 2014. Constant replenishment from circulating monocytes maintains the macrophage pool in the intestine of adult mice. *Nat Immunol*. (2014) 15:929–37.

- BALASUBRAMANIAN, A., MACINTYRE, N.R., HENDERSON, R.J., JENSEN, R.L., KINNEY, G., STRINGER, W.W., HERSH, C.P., BOWLER, R.P., CASABURI, R., HAN, M.K., et al. 2019. Diffusing Capacity of Carbon Monoxide in Assessment of COPD. *Chest*, 156, 1111-1119.
- BALFOUR, H.H., JR., ODUMADE, O.A., SCHMELING, D.O., MULLAN, B.D., ED, J.A., KNIGHT, J.A., VEZINA, H.E., THOMAS, W., HOGQUIST, K.A. 2013. Behavioral, virologic, and immunologic factors associated with acquisition and severity of primary Epstein-Barr virus infection in university students. *J Infect Dis*, 207:80–88.
- BAPTISTA, E.A., DEY, S., PAL, S. 2021. Chronic respiratory disease mortality and its associated factors in selected Asian countries: evidence from panel error correction model. *BMC Public Health*, 21, 53.
- BARNES, P.J., SHAPIRO, S.D., PAUWELS, R.A. 2003. Chronic obstructive pulmonary disease: molecular and cellular mechanisms. *Eur Respir J*, 22: 672–688.
- BARTON, E., MANDAL, P., SPECK, S.H. 2011. Pathogenesis and host control of gammaherpesviruses: Lessons from the mouse. *Annu Rev Immunol*, 29:351–397.
- BAUMGARTNER, K.B., SAMET, J.M., STIDLEY, C.A., et al. 1997. Cigarette smoking: a risk factor for idiopathic pulmonary fibrosis. *Am J Respir Crit Care Med*, 155(1):242-8.
- BAZZAN, E., RADU, C.M., TINÈ, M., NERI, T., BIONDINI, D., SEMENZATO, U., CASARA, A., BALESTRO, E., SIMIONI, P., CELI, A., COSIO, M.G., SAETTA, M. 2021. Microvesicles in bronchoalveolar lavage as a potential biomarker of COPD. *Am J Physiol Lung Cell Mol Physiol*, 320: L241–L245.
- BENDTSEN, K.M., BROSTRØM, A., KOIVISTO, A.J., KOPONEN, I., BERTHING, T., BERTRAM, N., KLING, K.I., DAL MASO, M., KANGASNIEMI, O., POIKKIMÄKI, M., LOESCHER, K., CLAUSEN, P.A., WOLFF, H., JENSEN, K.A., SABER, A.T., VOGEL, U. 2019. Airport emission particles: exposure characterization and toxicity following intratracheal instillation in mice. *Part Fibre Toxicol* 11;16(1):23.
- BETENSLEY, A., SHARIF, R., KARAMICHOS, D. 2016. A Systematic review of the role of dysfunctional wound healing in the pathogenesis and treatment of idiopathic pulmonary fibrosis. *J Clin Med*, 6(1):2.
- BIERING, S.B., DE SOUSA, F.T.G., TJANG, L.V., PAHMEIER, F., RUAN, R., BLANC, S.F., PATEL, T.S., WORTHINGTON, C.M., GLASNER, D.R., CASTILLO-ROJAS, B., SERVELLITA, V., LO, N.T.N., WONG, M.P., WARNES, C.M., SANDOVAL, D.R., CLAUSEN, T.M., SANTOS, Y.A., ORTEGA, V., AGUILAR, H.C., ESKO, J.D., CHUI, C.Y., PAK, J.E., BEATTY, P.R., HARRIS, E. 2021. SARS-CoV-2 Spike triggers barrier dysfunction and vascular leak via integrins and TGF- β signaling. *bioRxiv*, 13:2021.12.10.472112.
- BORTHWICK L. A., WYNN T. A., FISHER A. J. 2013. Cytokine mediated tissue fibrosis. *Biochim Biophys Acta*, 1832 1049–1060.
- BORTZ, E., WU, T.-T., PATEL, P., WHITELEGGE, J.P., SUN, R. 2018. Proteomics of bronchoalveolar lavage fluid reveals a lung oxidative stress responses in murine herpesvirus-68 infection. *Viruses. Respiratory*, 15(3):536-42.
- BOSHOF C., WEISS R. A. 2001. Epidemiology and pathogenesis of Kaposi's sarcoma-associated herpesvirus. *Philos Trans R Soc Lond B Biol Sci*, 356, 517–534.
- BOURDON, J. A., SABER, A. T., JACOBSEN, N. R., JENSEN, K. A., MADSEN, A. M., LAMSON, J. S., WALLIN, H., MØLLER, P., LOFT, S., YAUK, C. L. & VOGEL, U. B. 2012. Carbon black nanoparticle instillation induces sustained inflammation and genotoxicity in mouse lung and liver. *Part Fibre Toxicol*, 9, 5.
- BOYLES, M.S., YOUNG, L., BROWN, D.M., MACCALMAN, L., COWIE, H., MOISALA, A., SMAIL, F., SMITH, P.J.W., PROUDFOOT, L., WINDLE, A.H., STONE, V. 2015. Multi-walled carbon nanotube induced frustrated phagocytosis, cytotoxicity and pro-inflammatory conditions in macrophages are length dependent and greater than that of asbestos. *Toxicol In Vitro*, 29(7):1513–28.
- BRUCKENSTEIN, S., SHAY, M. 1985. Experimental aspects of use of the quartz crystal microbalance in solution. *Electrochimica Acta*, 30(10):1295-1300.

References

- BRUSSELLE, G.G., DEMOOR, T., BRACKE, K.R., BRANDSMA, C.A., AND TIMENS, W. 2009. Lymphoid follicles in (very) severe COPD: beneficial or harmful? *Eur Respir J*, 34, 219-230.
- CAI, J., ZHAO, A., ZHAO, J., CHEN, R., WANG, W., HA, S., XU, X., KAN, H. 2014. Acute effects of air pollution on asthma hospitalization in shanghai, china. *Environ Pollut*, 191:139-44.
- CANAGARATNA, M.R., ONASCH, T.B., WOOD, E.C., HERNDON, S.C., JAYNE, J.T., CROSS, E.S., MAIKE-LYE, R.C., KOLB, C.E., WORSNOP, D.R. 2010. Evolution of vehicle exhaust particles in the atmosphere. *J Air Waste Manag Assoc*, 60(10):1192–203.
- CANDEIAS, J., ZIMMERMANN, E.J., BISIG, C., GAWLITTA, N., OEDER, S., GRÖGER, T., ZIMMERMANN, R., SCHMIDT-WEBER, C.B., BUTERS, J. 2022. The priming effect of diesel exhaust on native pollen exposure at the air-liquid interface. *Environ Res*, 211:112968.
- CAPPELLINI, F., DI BUCCHIANICO, S., KARRI, V., LATVALA, S., MALMLÖF, M., KIPPLER, M., ELIHN, K., HEDBERG, J., ODNEVALL WALLINDER, I., GERDE, P., KARLSSON, H.L. 2020. Dry Generation of CeO₂ Nanoparticles and Deposition onto a Co-Culture of A549 and THP-1 Cells in Air-Liquid Interface-Dosimetry Considerations and Comparison to Submerged Exposure. *Nanomaterials (Basel)*, 10(4):618.
- CARBON NANOTUBES MARKET, 2021. (2023, January 26). Carbon Nanotube Market by Type (Single Walled & Multi Walled), End-use Industry (Electronics & Semiconductors, Chemical Material & Polymers, Structural Composites, Energy & Storage, Medical), Method, and Region – Global Forecast to 2026. <https://www.marketsandmarkets.com/Market-Reports/carbon-nanotubes-139.html>.
- CARRAGHER, D.M., RANGEL-MORENO, J., RANDALL, T.D. 2008. Ectopic lymphoid tissues and local immunity. *Semin Immunol*, 20: 26–42.
- CARRE, P.C, MORTENSON, R.L., KING, T.E., NOBLE, P.W., SABLE, C.L., RICHES, D.W. 1991. Increased expression of the interleukin-8 gene by alveolar macrophages in idiopathic pulmonary fibrosis. A potential mechanism for the recruitment and activation of neutrophils in lung fibrosis. *J Clin Invest*, 88(6):1802–1810.
- CARUGNO, M. , DENTALI F., MATHIEU G., et al. 2018. PM10 exposure is associated with increased hospitalizations for respiratory syncytial virus bronchiolitis among infants in Lombardy, Italy. *Environ Res*, 166: 452–457.
- CERVENA, T., VOJTISEK-LOM, M., VRBOVA, K., AMBROZ, A., NOVAKOVA, Z., ELZEINOVA, F., SIMA, M., BERANEK, V., PECHOUT, M., MACOUN, D., KLEMA, J., ROSSNEROVA, A., CIGANEK, M., TOPINKA, J., ROSSNER, P.Jr. 2020. Ordinary Gasoline Emissions Induce a Toxic Response in Bronchial Cells Grown at Air-Liquid Interface. *Int J Mol Sci*, 23;22(1):79.
- CHA, C., SHIN, S.R., ANNABI, N., DOKMECI, M.R., KHADEMHOSEINI, A. 2013. Carbon-based nanomaterials: multifunctional materials for biomedical engineering. *ACS Nano*, 7:2891–2897.
- CHANG, C.C., TSAI, M.L., HUANG, H.C., CHEN, C.Y., DAI, S.X. 2012. Epithelial-Mesenchymal Transition Contributes to SWCNT-Induced Pulmonary Fibrosis. *Nanotoxicology*, 6(6): 600–610.
- CHANG, Y., CESARMAN, E., PESSIN, M.S., et al. 1994. Identification of herpesvirus-like DNA sequences in AIDS-associated Kaposi's Sarcoma. *Science*, 266:1865–1869.
- CHATKIN, J., CORREA, L., SANTOS, U. 2022. External environmental pollution as a risk factor for asthma. *Clin Rev Allergy Immunol*, 62(1):72-89.
- CHEN F., WU W., MILLMAN A., CRAFT J.F., CHEN E., PATEL N., BOUCHER J.L., URBAN JR., J.F.J., KIM C.C., GAUSE W.C. 2014. Neutrophils prime a long-lived effector macrophage phenotype that mediates accelerated helminth expulsion. *Nat. Immunol*, 15: 938-946.
- CHEN, S., YIN, R., MUTZE, K., YU, Y., TAKENAKA, S., KÖNIGSHOFF, M., STOEGER, T. 2016. No involvement of alveolar macrophages in the initiation of carbon nanoparticle induced acute lung inflammation in mice. *Part Fibre Toxicol*, 13:13.
- CHEN, G. , ZHANG W., LI S., et al. 2017a. The impact of ambient fine particles on influenza transmission and the modification effects of temperature in China: a multi-city study. *Environ. Int.* 98: 82–88.
- CHEN, G. , ZHANG W., LI S., et al. 2017b. Is short-term exposure to ambient fine particles associated

- with measles incidence in China? A multi-city study. *Environ Res*, 156: 306–311.
- CHENG, P., LI, S., CHEN, H. 2021. Macrophages in lung injury, repair, and fibrosis. *Cells*, 10(2):436.
- CHERNOVA, T., MURPHY, F.A., GALAVOTTI, S., SUN, X.-M., POWLEY, I.R., GROSSO, S., SCHINWALD, A., et al. 2017. Long-Fiber Carbon Nanotubes Replicate Asbestos-Induced Mesothelioma with Disruption of the Tumor Suppressor Gene *Cdkn2a* (*Ink4a/Arf*). *Current Biology*, 27 (21): 3302–3314.
- CHO, J., CHOI, Y.J., SUH, M., SOHN, J., KIM, H., CHO, S.-K., HA, K.H., KIM, C., SHIN, D.C. 2014. Air pollution as a risk factor for depressive episode in patients with cardiovascular disease, diabetes mellitus, or asthma. *J Affect Disord*, 157:45-51.
- CHRISTOPHERSEN, D.V., JACOBSEN, N.R., JENSEN, D.M., KERMANIZADEH, A., SHEYKHZADE, M., LOFT, S., VOGEL, U., WALLIN, H., MØLLER, P. 2016. Inflammation and vascular effects after repeated intratracheal instillations of carbon black and lipopolysaccharide. *PLoS One*, 11(8): e0160731.
- CIENIEWICZ, B., SANTANA, A.L., MINKAH, N., KRUG, L.T. 2016. Interplay of murine gammaherpesvirus 68 with NF-kappaB signaling of the host. *Front Microbiol*, 7,1202.
- CIESIELSKA, A., MATYJEK, M., KWIATKOWSKA, K. 2021. TLR4 and CD14 trafficking and its influence on LPS-induced pro-inflammatory signaling. *Cell Mol Life Sci*, 78(4):1233-1261.
- CIOFANI, G., RAFFA, V., PENSABENE, V., MENCIASSI, A., DARIO, P. 2009. Dispersion of multi-walled carbon nanotubes in aqueous pluronic F127 solutions for biological applications. *Fuller Nanotub Car N*, 17:11.
- CONLON, T.M., JOHN-SCHUSTER, G., HEIDE, D., PFISTER, D., LEHMANN, M., HU, Y., ERTÜZ, Z., LOPEZ, M.A., ANSARI, M., STRUNZ, M., MAYR, C., ANGELIDIS, I., CIMINIERI, C., COSTA, R., KOHLHEPP, M.S., GUILLOT, A., GÜNES, G., JERIDI, A., FUNK, M.C., BEROSHVILI, G., PROKOSCH, S., HETZER, J., VERLEDEN, S.E., ALSAFADI, H., LINDNER, M., BURGSTALLER, G., BECKER, L., IRMLER, M., DUDEK, M., JANZEN, J., GOFFIN, E., GOSENS, R., KNOLLE, P., PIROTTE, B., STOEGER, T., BECKERS, J., WAGNER, D., SINGH, I., THEIS, F.J., DE ANGELIS, M.H., O'CONNOR, T., TACKE, F., BOUTROS, M., DEJARDIN, E., EICKELBERG, O., SCHILLER, H.B., KÖNIGSHOFF, M., HEIKENWALDER, M., YILDIRIM, A.Ö. 2020. Inhibition of LTβR signalling activates WNT-induced regeneration in lung. *Nature*, 588(7836):151-156.
- COSIO PIQUERAS, M.G., AND COSIO, M.G. 2001. Disease of the airways in chronic obstructive pulmonary disease. *European Respiratory Journal*, 18, 41s-49s.
- COULTAS, D.B., ZUMWALT, R.E., BLACK, W.C., et al. 1994. The epidemiology of interstitial lung diseases. *Am J Respir Crit Care Med*, 150 (4): 967-72
- CROFT, D.P. , ZHANG W., LIN S., et al. 2019. The association between respiratory infection and air pollution in the setting of air quality policy and economic change. *Ann. Am. Thorac. Soc.* 16: 321–330.
- CUSTOVIC, A., JOHNSTON, S.L., GAGA, M.G., FABBRI, L., BEL, E.H., SOUËF, LÖTVALL, J., DEMOLY, P., AKDIS, C.A., RYAN, D., MÄKELÄ, M.J., MARTINEZ, F., HOLLOWAY, J.W., SAGLANI, S., O'BYRNE, P., PAPI, A., SERGEJEVA, S., MAGNAN, A., DEL GIACCO, S., KALAYCI, O., HAMELMANN, E., PAPADOPOULOS, N.G. 2013. EAACI position statement on asthma exacerbations and severe asthma. *Allergy* 68, 1520–1531.
- CZANDERNA, A.W., LU, C. 1984. Chapter 1 – Introduction, history, and overview of applications of piezoelectric quartz crystal microbalances. *Methods and Phenomena*, 7, 1-18.
- DE HAAR, C., HASSING, I., BOL, M., BLEUMINK, R., AND PIETERS, R. 2006. Ultrafine but not fine particulate matter causes airway inflammation and allergic airway sensitization to co-administered antigen in mice. *Clin Exp Allergy*, 36,1469–1479.
- DISEASE, G.B.D., INJURY, I., AND PREVALENCE, C. 2018. Global, regional, and national incidence, prevalence, and years lived with disability for 354 diseases and injuries for 195 countries and territories, 1990 to 2017: a systematic analysis for the Global Burden of Disease Study 2017. *Lancet*, 392,1789-1858.
- DONG, J. 2020. Microenvironmental Alterations in Carbon Nanotube-Induced Lung Inflammation and Fibrosis. *Front Cell Dev Biol*, 8:126.

References

- DONG, J, MA Q. 2019. Integration of inflammation, fibrosis, and cancer induced by carbon nanotubes. *Nanotoxicology*, 13(9):1244–74.
- DONG, J, MA Q. 2018. Type 2 Immune Mechanisms in Carbon Nanotube-Induced Lung Fibrosis. *Front Immunol*, 9:1120.
- DORAN, A.C., JR, A.Y., TABAS, I. 2020 Efferocytosis in health and disease. *Nature Reviews Immunology*, 20,254-267.
- CLIMENT, M., VIGGIANI, G., CHEN, Y.-W., COULIS, G., CASTALDI, A. 2020. MicroRNA and ROS crosstalk in cardiac and pulmonary disease. *Int J Mol Sci*, 21(2):4370.
- CONNORS, T.J., RAVINDRANATH, T.M., BICKHAM, K.L., GORDON, C.L., ZHANG, F., LEVIN, B., BAIRD, J.S., FARBER, D.L. 2016. Airway CN8+ T cells are associated with lung injury during infant viral respiratory tract infection. *Am J Respir Cell Mol Biol*, 54(6):822-830.
- CONTICINI, E., FREDIANI, B., CARO, D. 2020. Can atmospheric pollution be considered a co-factor in extremely high level of SARS-CoV-2 lethality in Northern Italy . *Environ. Pollut*, 261:114465–114465.
- COSKUN, O., SENER, K., KILIC, S., ERDEM, H., YAMAN, H., BESIRBELLIOGLU, A.B., GUL, H.C., EYIGUN, C.P. 2010. Stress-related Epstein-Barr virus reactivation. *Clin Exp Med*, 10(1):15-20.
- COSNIER, F., SEIDEL, C., VALENTINO, S., SCHMID, O., BAU, S., VOGEL, U., DEVOY, J., GATÉ, L. 2021. Retained Particle Surface Area Dose Drives Inflammation in Rat Lungs following Acute, Subacute, and Subchronic Inhalation of Nanomaterials. *Particle and Fibre Toxicology*, 18 (1): 29.
- DANIELSEN, P.H., BENDTSEN, K.M., KNUDSEN, K.B., POULSEN, S.S., STOEGER, T., VOGEL, U. 2021. Nanomaterial- and shape-dependency of TLR2 and TLR4 mediated signaling following pulmonary exposure to carbonaceous nanomaterials in mice. *Part Fibre Toxicol*, 30;18(1):40.
- DECMAN, V., KINCHINGTON, P.R., HARVEY, S.A.K., HENDRICKS, R.L. 2005. Gamma interferon can block herpes simplex virus type 1 reactivation from latency, even in the presence of late gene expression. *J Virol*, 79(16):10339-47.
- DEGHANI, S., VALI, M., JAFARIAN, A., OSKOEI, V., MALEKI, Z., HOSEINI, M. 2022. Ecological study of ambient air pollution exposure and mortality of cardiovascular diseases in elderly. *Sci Rep*, 9;12(1):21295.
- DE LUNA, L.A.V., LORET, T., FORDHAM, A., ARSHAD, A., DRUMMOND, M., DODD, A., LOZANO, N., KOSTARELOS, K., BUSSY, C. 2022. Lung recovery from DNA damage induced by graphene oxide is dependent on size, dose and inflammation profile. *Part Fibre Toxicol*, 21;19(1):62.
- DE-THE, G., DAY, N.E., GESER, A., LAVOUE, M.F., HO, J.H., SIMONS, M.J., SOHIER, R., TUKEI, P., VONKA, V., ZAVADOVA, H. 1975. Sero-epidemiology of the Epstein-Barr virus: preliminary analysis of an international study - a review. *IARC Sci Publ*, 1975:3–16.
- D'HULST, A.I., VERMAELEN, K.Y., BRUSSELLE, G.G., JOOS, G.F., PAUWELS, R.A. 2005. Time course of cigarette smoke-induced pulmonary inflammation in mice. *Eur Respir J*, 26: 204–213.
- DI IANNI, E., MØLLER, P., CHOLAKOVA, T., WOLFF, H., JACOBSEN, N.R., VOGEL, U. 2022. Assessment of primary and inflammation-driven genotoxicity of carbon black nanoparticles in vitro and in vivo. *Nanotoxicology*, 16(4):526-546.
- DOIRON, D., DE HOOGH, K., PROBST-HENSCH, N., FORTIER, I., CAI, Y., DE MATTEIS, S., HANSELL, A.L. 2019. Air pollution, lung function and COPD: results from the population-based UK biobank study. *Eur Respir J*. 25;54(1):1802140.
- DOMINICI, F., PENG, R.D., BELL, M.L., PHAM, L., MCDERMOTT, A., ZEGER, S.L., SAMET, J.M. 2006. Fine particulate air pollution and hospital admission for cardiovascular and respiratory diseases. *JAMA*, 295:1127–1134.
- DONG J., MA Q. 2019. Integration of inflammation, fibrosis, and cancer induced by carbon nanotubes. *Nanotoxicology*, 13 1244–1274.
- DONG J., MA Q. 2017. Osteopontin enhances multi-walled carbon nanotube-triggered lung fibrosis by promoting TGF-beta1 activation and myfibroblast differentiation. *Part Fibre Toxicol*, 14 18.

- DONG J., MA Q. 2016. Myofibroblasts and lung fibrosis induced by carbon nanotube exposure. *Part Fibre Toxicol*, 13 60.
- DOURCY, M., MAQUET, C., DAMS, L., GILLIAUX, G., JAVAUX, J., DESMECHT, D., MACK, M., DEWALS, B.G., MACHIELS, B., GILLET, L. 2020. A gammaherpesvirus licenses CD8 T cells to protect the host from pneumovirus-induced immunopathologies. *Mucosal Immunol*, 13(5):799-813.
- DUKE, K.S., BONNER, J.C. 2017. Mechanisms of carbon nanotube-induced pulmonary fibrosis: a physicochemical characteristic perspective. *Wiley Interdiscip Rev Nanomed Nanobiotechnol*, 10(3):e1498.
- DUNMIRE, S.K., HOGQUIST, K.A., BALFOUR, H.H. 2015. Infectious mononucleosis. *Curr Top Microbiol Immunol*, 390(1):211-40.
- DUPONT, L., REEVES, M. B. 2016. Cytomegalovirus latency and reactivation: recent insights into an age old problem. *Rev. Med. Virol.* 26, 75–89.
- DUTRA SILVA, J., SU, Y., CALFEE, C.S., DELUCCHI, K.L., WEISS, D., MCAULEY, D.F., O'KANE, C., KRASNODEMBSKAYA, A.D. 2021. Mesenchymal stromal cell extracellular vesicles rescue mitochondrial dysfunction and improve barrier integrity in clinically relevant models of ARDS. *Eur Respir J*, 1;58(1):2002978.
- ELDER, A., GELEIN, R., FINKELSTEIN, J.N., DRISCOLL, K.E., HARKEMA, J., OBERDÖRSTER, G. 2005. Effects of subchronically inhaled carbon black in three species. I. Retention kinetics, lung inflammation, and histopathology. *Toxicol Sci*, 88(2):614-629.
- EPA (United States Environmental Protection Agency). 2022. Particulate Matter (PM) Pollution.
- EHTISHAM, S., SUNIL-CHANDRA, N. P., NASH, A. A. 1993. Pathogenesis of murine gamma-herpesvirus infection in mice deficient in CD4 and CD8 T-cells. *J Virol*, 67:5247–5252.
- FARINA, A., CIRONE, M., YORK, M., LENNA, S., PADILLA, C., MCLAUGHLIN, S., FAGGIONI, A., LAFYATIS, R., TROJANOWSKA, M., FARINA, G.A. 2014. Epstein-Barr virus infection induces aberrant TLR activation pathway and fibroblast-myofibroblast conversion in scleroderma. *J Invest Dermatol*, 134(4):954-964.
- FEENSTRA, T.L., VAN GENUGTEN, M.L., HOOGENVEEN, R.T., WOUTERS, E.F., AND RUTTEN-VAN MOLKEN, M.P. 2001. The impact of aging and smoking on the future burden of chronic obstructive pulmonary disease: a model analysis in the Netherlands. *Am J Respir Crit Care Med*, 164, 590-596.
- FENG, C. , LI J., SUN W., et al. 2016. Impact of ambient fine particulate matter (PM2.5) exposure on the risk of influenza-like-illness: a time-series analysis in Beijing, China. *Environ. Health*, 15: 17.
- FLOOD-PAGE, P., SWENSON, C., FAIFERMAN, I., MATTHEWS, J., WILLIAMS, M., BRANNICK, L., ROBINSON, D., WENZEL, S., BUSSE, W., HANSEL, T.T., BARNES, N.C., INTERNATIONAL MEPOLIZUMAB STUDY GROUP. 2007. A study to evaluate safety and efficacy of mepolizumab in patients with moderate persistent asthma. *Am J Respir Crit Care Med*, 176,1062–1071.
- FREY, H.C., GRIESHOP, A.P., KHLYSTOV, A., BANG, J.J., ROUPHAIL, N., GUINNESS, J., RODRIGUEZ, D., FUENTES, M., SAHA, P., BRANTLEY, H., SNYDER, M., TANVIR, S., KO, K., NOUSSI, T., DELAVARRAFIEE, M., SINGH, S. 2022. Characterizing Determinants of Near-Road Ambient Air Quality for an Urban Intersection and a Freeway Site. *Res Rep Health Eff Inst*, (207):1-73.
- FRISCIC, J., BÖTTCHER, M., REINWALD, C., BRUNS, H., WIRTH, B., POPP, S.-J., WALKER, K.I., ACKERMANN, J.A., CHEN, X., TURNER, J., ZHU, H., SEYLER, L., EULER, M., KIRCHNER, P., KRÜGER, R., EKICI, A.B., MAJOR, T., AUST, O., WEIDNER, D., FISCHER, A., ANDES, F.T., STANOJEVIC, Z., TRAJKOVIC, V., HERRMANN, M., KORB-PAP, A., WANK, I., HESS, A., WINTER, J., WIXLER, V., DISTLER, J. 2021. The complement system drives local inflammatory tissue priming by metabolic reprogramming of synovial fibroblasts. *Immunity* 54, 1002-1021.
- FRONTERA, A., CIANFANELLI, L., VLACHOS, K., LANDONI, G., CREMONA, G. 2020. Severe air

References

- pollution links to higher mortality in COVID-19 patients: the “double-hit” hypothesis. *J Infect*, 81(2):255-259.
- FU, C., KUANG, D., ZHANG, H., REN, J., CHEN, J. 2022a. Different components of air pollutants and neurological disorders. *Front Public Health*, 10:959921.
- FU, J., LIU, S., TAN, Q., LIU, Z., QIAN, J., LI, T., DU, J., SONG, B., LI, D., ZHANG, L., HE, J., GUO, K., ZHOU, B., CHEN, H., FU, S., LIU, X., CHENG, J., HE, T., FU, J. 2022b. Impact of TMPRSS2 Expression, Mutation Prognostics, and Small Molecule (CD, AD, TQ, and TQFL12) Inhibition on Pan-Cancer Tumors and Susceptibility to SARS-CoV-2. *Molecules*, 1;27(21):7413.
- FUKUDA, K. , HIDER P.N., EPTON M.J., et al. 2011. Including viral infection data supports an association between particulate pollution and respiratory admissions. *Aust. N. Z. J. Public Health*, 35: 163–169.
- FUKUDA, Y., AKIMOTO, K., HOMMA, T., BAKER, J.R., ITO, K., BARNES, P.J., SAGARA, H. 2020. Virus-induced asthma exacerbations: SIRT1 target approach. *J Clin Med*, 9(8),2623.
- FULLER, R., LANDRIGAN, P.J., BALAKRISHNAN, K., BATHAN, G., BOSE-O'REILLY, S., BRAUER, M., CARAVANOS, J., CHILES, T., COHEN, A., CORRA, L., CROPPER, M., FERRARO, G., HANNA, J., HANRAHAN, D., HU, H., HUNTER, D., JANATA, G., KUPKA, R., LANPHEAR, B., LICHTVELD, M., MARTIN, K., MUSTAPHA, A., SANCHEZ.TRIANA, E., SANDILYA, K., SCHAEFLI, L., SHAW, J., SEDDON, J., SUK, W., TÉLLEZ-ROJO, M.M., YAN, C. 2022. Pollution and health: a progress update. *The Lancet Planetary Health*, 6(6)E535-E547.
- FYFE, A.I., ROTHENBERG, L.S., DEBEER, F.C., CANTOR, R.M., ROTTER, J.I., LUSIS, A.J. 1997. Association between serum amyloid A proteins and coronary artery disease: Evidence from two distinct arteriosclerotic processes. *Circulation*, 96:2914–9.
- GABAY, C., KUSHNER, I. 1999. Acute-phase proteins and other systemic responses to inflammation. *N Engl J Med*, 340:448–54.
- GANEM, D., (Ed.). 2005. Kaposi's Sarcoma-associated herpesvirus. In:Field's Virology. Philadelphia, PA: Lippincott Williams and Wilkins,pp. 2875–2888.
- GANEM, D. 2010. KSHV and the pathogenesis of Kaposi Sarcoma:Listening to human biology and medicine. *J Clin Invest* 120:939–949.
- GANGULY, K., ETTEHADIEH, D., UPADHYAY, S., TAKENAKA, S., ADLER, T., KARG, E., KROMBACH, F., KREYLING, W. G., SCHULZ, H., SCHMID, O. & STOEGER, T. 2017. Early pulmonary response is critical for extra-pulmonary carbon nanoparticle mediated effects: comparison of inhalation versus intra-arterial infusion exposures in mice. *Part Fibre Toxicol*, 14, 19
- GBD 2017a. Disease and Injury Incidence and Prevalence Collaborators. Global, regional, and national incidence, prevalence, and years lived with disability for 354 diseases and injuries for 195 countries and territories, 1990–2017: a systematic analysis for the Global Burden of Disease Study 2017. *Lancet*. 2018;392(10159):1789–858.
- GBD 2017b. Risk Factor Collaborators Global, regional, and national comparative risk assessment of 84 behavioural, environmental and occupational, and metabolic risks or clusters of risks for 195 countries and territories, 1990–2017: a systematic analysis for the Global Burden of Disease Study 2017.*Lancet*, 2019;393(10167):132–132.
- GEISER, M., KREYLING, W.G., 2010. Deposition and biokinetics of inhaled nanoparticles. *Part Fibre Toxicol*, 20;7:2.
- GEORGE, P.M., WELLS, A.U., JENKINS, R.G. 2020. Pulmonary fibrosis and COVID-19: the potential role for antifibrotic therapy. *Lancet Respir Med*, 8(8):807-815.
- GINA. 2015. Global Initiative for Asthma. Global strategy for asthma management and prevention.

- GIRKIN, J. 2022. Is CC chemokine ligand 17 (TARC) driving disease progression in chronic obstructive pulmonary disease? *ATS Journals*, 66:4.
- GHOSH M, MURUGADOSS S, JANSSEN L, COKIC S, MATHYSSEN C, VAN LANDUYT K, JANSSENS W, CARPENTIER S, GODDERIS L, HOET P. 2020. Distinct autophagy-apoptosis related pathways activated by Multi-walled (NM 400) and Single-walled carbon nanotubes (NIST-SRM2483) in human bronchial epithelial (16HBE14o-) cells. *J Hazard Mater*, 5:387:121691.
- GLOBAL INITIATIVE FOR CHRONIC OBSTRUCTIVE LUNG DISEASE. 2020 report. Global strategy for the diagnosis, management, and prevention of chronic obstructive pulmonary disease.
- GOLD. 2021. Global Strategy for the Diagnosis, Management, and Prevention of Chronic Obstructive Pulmonary Disease. Global Initiative for Chronic Obstructive Lung Disease—GOLD. 2021.
- GORIAINOVA, V., AWADA, C., OPOKU, F., ZELIKOFF, J.T. 2022. Adverse Effects of Black Carbon (BC) Exposure during Pregnancy on Maternal and Fetal Health: A Contemporary Review. *Toxics*, 13;10(12):779.
- GOURBAL, B., PINAUD, S., BECKERS, G.J.M., VAN DER MEER, J.W.M., CONRATH, U., NETEA, M.G. 2018. Innate immune memory: An evolutionary perspective. *Immunol Rev*, 283: 21-40.
- GREENBURG, L. , FIELD F., ERHARDT C.L., et al. 1967. Air pollution, influenza, and mortality in New York City; January–February 1963. *Arch Environ Health*, 15: 430–438.
- GUAN, W.-J., ZHENG, X.-Y., CHUNG, K.F., ZHONG, n.-s. 2016. Impact of air pollution on the burden of chronic respiratory disease in china: time for urgent action. *Lancet*, 15;388(10054):1939-1951.
- GUARNIERI, M., BARMES, J.R. 2014. Outdoor air pollution and asthma. *Lancet*, 383(9928):1581-1592.
- GUILLIAMS, M., DE KLEER, I., HENRI, S., POST, S., VANHOUTTE, L., DE PRIJCK, S., DESWARTE, K., MALISSEN, B., HANNAD, H., LAMBRECHT, B.N. 2013. Alveolar macrophages develop from fetal monocytes that differentiate into long-lived cells in the first week of life via GM-CSF. *J Exp Med*, 210(10):1977–1992.
- GÜNES GÜNSEL, G., CONLON, T.M., JERIDI, A., KIM, R., ERTÜZ, Z., LANG, N.J., ANSARI, M., NOVIKOVA, M., JIANG, D., STRUNZ, M., GAIANOVA, M., HOLLAUER, C., GABRIEL, C., ANGELIDIS, I., DOLL, S., PESTONI, J.C., EDELMANN, S.L., KOHLHEPP, M.S., GUILLOT, A., BASSLER, K., VAN EECKHOUTTE, H.P., KAYALAR, Ö., KONYALILAR, N., KANASHOVA, T., RODIUS, S., BALLESTER-LÓPEZ, C., GENES ROBLES, C.M., SMIRNOVA, N., REHBERG, M., AGARWAL, C., KRIKKI, I., PIAVAUX, B., VERLEDEN, S.E., VANAUDENAERDE, B., KÖNIGSHOFF, M., DITTMAR, G., BRACKE, K.R., SCHULTZE, J.L., WATZ, H., EICKELBERG, O., STOEGER, T., BURGSTALLER, G., TACKE, F., HEISSMEYER, V., RINKEVICH, Y., BAYRAM, H., SCHILLER, H.B., CONRAD, M., SCHNEIDER, R., YILDIRIM, A.Ö. 2022. The arginine methyltransferase PRMT7 promotes extravasation of monocytes resulting in tissue injury in COPD. *Nat Commun*, 14;13(1):1303.
- HABRE, R., GIRGUIS, M., URMAN, R., FRUIN, S., LURMANN, F., SHAFER, M., GORSKI, P., FRANKLIN, M., MCCONNELL, R., AVOL, E., GILLILAND, F. 2021. Contribution of tailpipe and non-tailpipe traffic sources to quasi-ultrafine, fine and coarse particulate matter in southern California. *J Air Waste Manag Assoc*, 71(2):209-230.
- HABRE, R., ZHOU, H., ECKEL, S.P., ENEBISH, T., FRUIN, S., BASTAIN, T., RAPPAPORT, E., GILLILAND, F. 2018. Short-term effects of airport-associated ultrafine particle exposure on lung function and inflammation in adults with asthma. *Environ Int*, 118:48-59.
- HADRUP, N., BENGTON, S., JACOBSEN, N.R., JACKSON, P., NOCUN, M., SABER, A.T., JENSEN, K.A., WALLIN, H., VOGEL, U. 2017. Influence of Dispersion Medium on Nanomaterial-Induced Pulmonary Inflammation and DNA Strand Breaks: Investigation of Carbon Black, Carbon Nanotubes and Three Titanium Dioxide Nanoparticles. *Mutagenesis* 32 (6): 581–597.
- HADRUP, N., AIMONEN, K., ILVES, M., LINDBERG, H., ATLURI, R., SAHLGREN, N.M., JACOBSEN, N.R., BARFOD, K.K., BERTHING, T., LAWLOR, A., NORPPA, H., WOLFF, H., JENSEN, K.A., HOUGAARD, K.S., ALENIUS, H., CATALAN, J., VOGEL, U. 2021. Pulmonary Toxicity of

References

- Synthetic Amorphous Silica–Effects of Porosity and Copper Oxide Doping. *Nanotoxicology*, 15 (1): 96–113.
- HADRUP N, ZHERNOVKOV V, JACOBSEN NR, VOSS C, STRUNZ M, ANSARI M, SCHILLER HB, HALAPPANAVAR S, POULSEN SS, KHOLODENKO B, STOEGER T, SABER AT, VOGEL U. 2020. Acute Phase Response as a Biological Mechanism-of-Action of (Nano)particle-Induced Cardiovascular Disease. *Small*, 16(21):e1907476.
- .HAHN G., JORES R., MOCARSKI E.S. 1998. Cytomegalovirus remains latent in a common precursor of dendritic and myeloid cells. *Proc. Natl. Acad. Sci. USA*, 95:3937–3942.
- HAKKARAINEN, H., SALO, L., MIKKONEN, S., SAARIKOSKI, S., AURELA, M., TEINILÄ, K., IHALAINEN, M., MARTIKAINEN, S., MARJANEN, P., LEPISTÖ, T., KUITTINEN, N., SAARNIO, K., AAKKO-SAKSA, P., PFEIFFER, T.V., TIMONEN, H., RÖNKKÖ, T., JALAVA, P.I. 2022. Black carbon toxicity dependence on particle coating: Measurements with a novel cell exposure method. *Sci Total Environ*, 10;838(Pt 4):156543.
- HALAPPANAVAR, S., JACKSON, P., WILLIAMS, A., JENSEN, K.A., HOUGAARD, K.S., VOGEL, U., YAUK, C.L., WALLIN, H. 2011. Pulmonary response to surface-coated nanotitanium dioxide particles includes induction of acute phase response genes, inflammatory cascades, and changes in microRNAs: a toxicogenomic study. *Environ Mol Mutagen*, 52(6):425-39.
- HALPIN, D.M.G., CELLI, B.R., CRINER, G.J., FRITH, P., VARELA, M.V.L., SALVI, S., VOGELMEIER, C.F., CHEN, R., MORTIMER, K., DE OCA, M.M., AISANOV, Z., OBASEKI, D., DECKER, R., AUGUSTI, A. 2019. The GOLD Summit on chronic obstructive pulmonary disease in low- and middle-income countries. *Int J Tuberc Lung Dis*, 23, 1131–1141.
- HAO, J. , YANG Z., HUANG S., et al. 2019. The association between short-term exposure to ambient air pollution and the incidence of mumps in Wuhan, China: a time-series study. *Environ Res*, 177: 108660.
- HARNUNG SCHOLTEN, R., MØLLER, P., JOVANOVIC ANDERSEN, Z., DEHLENDORFF, C., KHAN, J., BRANDT, J., KETZEL, M., KNUDSEN, L.E., MATHIESEN, L. 2020. Telomere length in newborns is associated with exposure to low levels of air pollution during pregnancy *Environ Int*. 146:106202..
- HASHIMOTO, D., CHOW, A., NOIZAT, C., TEO, P., BEASLEY, M.B., LEBOEUF, M., BECKER, C.D., SEE, P., PRICE, J., LUCAS, D., GRETER, M., MORTHA, A., BOYER, S.W., FORSBERG, E.C., TANAKA, M., VAN ROOIJEN, N., GARCÍA-SASTRE, A., STANLEY, E.R., GINHOUX, F., FRENETTE, P.S., MERAD, M. 2013. Tissue-resident macrophages self-maintain locally throughout adult life with minimal contribution from circulating monocytes. *Immunity*. (2013) 38:792–804.
- HASTIE, A.T., MAUGER, D.T., DENLINGER, L.C., COVERSTONE, A., CASTRO, M., ERZURUM, S., JARJOUR, N., LEVY, B.D., MEYERS, D.A., MOORE, W.C., PHILLIPS, B., WENZEL, S.E., FAHY, J.V., ISRAEL, E., BLEECKER, E.R., NHLBI SARP 3 INVESTIGATORS. 2020. Baseline sputum eosinophil + neutrophil subgroups' clinical characteristics and longitudinal trajectories for NHLBI Severe Asthma Research Program (SARP 3) cohort. *J Allergy Clin Immunol*, 146:222–226.
- HAUTEKIET, P., NAWROT, T.S., JANSSEN, B.G., MARTENS, D.S., DE CLERCQ, E.M., DADVAND, P., PLUSQUIN, M., BIJNENS, E.M., SAENEN, N.D. 2021. Child buccal telomere length and mitochondrial DNA content as biomolecular markers of ageing in association with air pollution. *Environ Int*, 147:106332.
- HE, H., WANG, Y., WU, M., SUN, B. 2017. Positive Epstein-Barr virus detection and mortality in respiratory failure patients admitted to the intensive care unit. *Clin Respir J*, 11(6):895-900.
- HERRERO, R., TANINO, M., SMITH, L.S., KAJIKAWA, O., WONG, V.A., MONGOVIN, S., MATUTE-BELLO, G., MARTIN, T.R. 2013. The Fas/FasL pathway impairs the alveolar fluid clearance in mouse lungs. *Am. J. Physiol. Lung Cell Mol. Physiol*, 305:L377-L388.
- HERZOG, E.L., BRODY, A.R., COLBY, T.V., MASON, R., WILLIAMS, M.C. 2008. Knowns and unknowns of the alveolus. *Pro. Am. Thor. Soc.* 5, 778–782.
- HESLOP, H.H. 2020. Sensitizing Burkitt lymphoma to EBV-CTLs. *Blood*, 135(21):1822-1823.

- HOGG, J.C. 2004. Pathophysiology of airflow limitation in chronic obstructive pulmonary disease. *Lancet*, 364: 709–721.
- HORNE, B.D. , JOY E.A., HOFMANN M.G., et al. 2018. Short-term elevation of fine particulate matter air pollution and acute lower respiratory infection. *Am J Respir Crit Care Med*, 198: 759–766.
- HUIZAR, I., MALUR, A., MIDGETTE, Y. A., KUKOLY, C., CHEN, P., KE, P. C., et al. 2011. Novel murine model of chronic granulomatous lung inflammation elicited by carbon nanotubes. *Am J Respir Cell Mol Biol*, 45 858–866.
- HUPPERT, L.A., MATTHAY, M.A., WARE, L.B. 2019. Pathogenesis of acute respiratory distress syndrome. *Semin Respir Crit Care Med*, 40: 31–39.
- HUSSAIN, S., VANOIRBEEK, J.A., LUYTS, K., DE VOOCHT, V., VERBEKEN, E., THOMASSEN, L.C., MARTENS, J.A., DINSDALE, D., BOLAND, S., MARANO, F., NEMERY, B., AND HOET, P.H. 2010. Lung exposure to nanoparticles modulates an asthmatic response in a mouse model of asthma. *Eur Respir J*, 37(2):299-309.
- HUSSELL, T., BELL, T.J. 2014. Alveolar macrophages: plasticity in a tissue-specific context. *Nat Rev Immunol*, 14:81–93.
- HWANG, S., WU, T. T., TONG, L. M., et al. 2008. Persistent gammaherpesvirus replication and dynamic interaction with the host *in vivo*. *J Virol*, 82:12498–12509.
- HWANG, J.-S. & CHAN C.-C.. 2002. Effects of air pollution on daily clinic visits for lower respiratory tract illness. *Am. J. Epidemiol.* 155: 1–10.
- IHRIE, M.D., DUKE, K.S., SHIPKOWSKI, K.A., YOU, D.J., LEE, H.Y., TAYLOR-JUST, A.J., BONNER, J.C. 2021. STAT6-dependent exacerbation of house dust mite-induced allergic airway disease in mice by multi-walled carbon nanotubes. *NanoImpact*, 22:100309.
- INOUE, K., TAKANO, H., YANAGISAWA, R., SAKURAI, M., ICHINOSE, T., SADAKANE, K., AND YOSHIKAWA, T. 2005. Effects of nano particles on antigen-related airway inflammation in mice. *Respir Res*, 6, 106.
- INOUE, K., TAKANO, H., YANAGISAWA, R., SAKURAI, M., ABE, S., YOSHINO, S., YAMAKI, K., AND YOSHIKAWA, T. 2007. Effects of nanoparticles on lung physiology in the presence or absence of antigen. *Int J Immunopathol Pharmacol*, 20, 737–744.
- INOUE, K., KOIKE, E., YANAGISAWA, R., HIRANO, S., NISHIKAWA, M., AND TAKANO, H. 2009. Effects of multi-walled carbon nanotubes on a murine allergic airway inflammation model. *Toxicol Appl Pharmacol*, 237, 306–316.
- INOUE, K., YANAGISAWA, R., KOIKE, E., NISHIKAWA, M., AND TAKANO, H. 2010a. Repeated pulmonary exposure to singlewalled carbon nanotubes exacerbates allergic inflammation of the airway: possible role of oxidative stress. *Free Radic Biol Med*, 48, 924–934.
- INOUE, K., KOIKE, E., TAKANO, H. 2010b. Comprehensive analysis of elastase-induced pulmonary emphysema in mice: effects of ambient existing particulate matters. *Int Immunopharmacol*, 10(11):1380-9.
- INOUE, K., YANAGISAWA, R., KOIKE, E., NAKAMURA, R., ICHINOSE, T., TASAKA, S., KIYONO, M., TAKANO, H. 2011. Effects of carbon black nanoparticles on elastase-induced emphysematous lung injury in mice. *Basic Clin Pharmacol Toxicol*, 108(4):234-40.
- INOUE, K.-I., YAMADA, K., SUZUKI, W., TAKANO, H., SHIMADA, A. 2021. Effect of 95nm carbon black nanoparticles on inflammatory conditions in the murine lung – controversy to size dependent efficacy. *J Respir Dis Med*, 2633-1063.
- ISAEVSKA, E., MOCCIA, C., ASTA, F., CIBELLA, F., GAGLIARDI, L., RONFANI, L., RUSCONI, F., STAZI, M.A., RICHIARDI, L. 2021. Exposure to ambient air pollution in the first 1000 days of life and alterations in the DNA methylome and telomere length in children: A systematic review. *Environ Res.* 93:110504.
- JACOBSEN, N.R., WHITE, P.A., GINGERICH, J., MØLLER, P., SABER, A.T., DOUGLAS, G.R., VOGEL, U., WALLIN, H. 2011. Mutation Spectrum in FE1-Muta-Mouse Lung Epithelial Cells Exposed to Nanoparticulate Carbon Black. *Environmental and Molecular Mutagenesis* 52 (4): 331–337.

References

- JARTTI, T., LEHTINEN, P., VUORINEN, T., RUUSKANEN, O. 2009. Bronchiolitis: age and previous wheezing episodes are linked to viral etiology and atopic characteristics. *Pediatr Infect Dis J*, 28(4):311–317.
- JEGASOTHY, E., HANIGAN, I.C., VAN BUSKIRK, J., MORGAN, G.G., JALALUDIN, B., JOHNSTON, F.H., GUO, Y., BROOME, R.A. 2022. Acute health effects of bushfire smoke on mortality in Sydney, Australia. *Environ Int*, 10;171:107684.
- JERRETT, M., NAU, C.L., YOUNG, D.R., BUTLER, R.K., BATTEATE, C.M., SU, J., BURNETT, R.T., KLEEMAN, M.J. 2022. Air pollution and meteorology as risk factors for COVID-19 death in a cohort from Southern California. *Environ Int*, 2;171:107675.
- JEONG, B.O., KWON, S.W., KIM, T.J., LEE, E.H., JEONG, S.H., JUNG, Y. 2013. Effect of carbon black materials on the electrochemical properties of sulfur-based composite cathode for lithium-sulfur cells. *J Nanosci Nanotechnol*, 13(12):7870–4.
- JHA, H.C., MEHTA, D., LU, J., EL-NACCACHE, D., SHUKLA, S.K., KOVACSICS, C., KOLSON, D., ROBERTSON, E.S. 2015. Gammaherpesvirus infection of human neuronal cells. *American Society for Microbiol*, 6(6):e01844-15.
- JIANG L, AKATSUKA S, NAGAI H, et al. 2012. Iron overload signature in chrysotile-induced malignant mesothelioma. *J Pathol*, 228:366–377.
- JIANG, L., H. NAGAI, H. OHARA, S. HARA, M. TACHIBANA, S. HIRANO, Y. SHINOHARA, N. KOHYAMA, S. AKATSUKA, S. TOYOKUNI. 2008. Characteristics and modifying factors of asbestos-induced oxidative DNA damage. *Cancer Sci*, 99,2142-2151.
- JOHN, G., KOHSE, K., ORASCHE, J., REDA, A., SCHNELLE-KREIS, J., ZIMMERMANN, R., SCHMID, O., EICKELBERG, O., YILDIRIM, A.Ö. 2014. The composition of cigarette smoke determines inflammatory cell recruitment to the lung in COPD mouse models. *Clin Sci (Lond)*, 126(3):207-21.
- JOHN-SCHUSTER, G., HAGER, K., CONLON, T.M., IRMLER, M., BECKERS, J., EICKELBERG, O., YILDIRIM, A.Ö. 2014. Cigarette smoke-induced iBALT mediated macrophage activation in a B cell-dependent manner in COPD. *AJP-Lung Cell Mol Physiol*, 307(9):L692-L706.
- KAMATA, H., TASAKA, S., INOUE, K., MIYAMOTO, K., NAKANO, Y., SHINODA, H., KIMIZUKA, Y., FUJIWARA, H., ISHII, M., HASEGAWA, N., TAKAMIYA, R., FUJISHIMA, S., TAKANO, H., ISHIZAKA, A. 2011. Carbon black nanoparticles enhance bleomycin-induced lung inflammatory and fibrotic changes in mice. *Exp Biol Med (Maywood)*, 236(3):315-24.
- KARR, C. , LUMLEY T., SHEPHERD K., et al. 2006. A case-crossover study of wintertime ambient air pollution and infant bronchiolitis. *Environ. Health Perspect.* 114: 277–281.
- KARR, C.J. , RUDRA C.B., MILLER K.A., et al. 2009. Infant exposure to fine particulate matter and traffic and risk of hospitalization for RSV bronchiolitis in a region with lower ambient air pollution. *Environ. Res.* 109: 321–327.
- KAWANO, M., NAGATA, S. 2018. Efferocytosis and autoimmune disease. *Int. Immunol.* 30,551–558.
- KELLY, G.L., MILNER, A.E., BALDWIN, G.S., BELL, A.I., RICKINSON, A.B. 2006. Three restricted forms of Epstein-Barr virus latency counteracting apoptosis in c-myc-expressing Burkitt lymphoma cells. *Proc Natl Acad Sci U.S.A.*, 103, 14935–14940.
- KELLY, F., ANDERSON, H.R., ARMSTRONG, B., ATKINSON, R., BARRATT, B., BEEVERS, S., DERWENT, D., GREEN, D., MUDWAY, I., WILKINSON, P.; HEI HEALTH REVIEW COMMITTEE. 2011. The impact of the congestion charging scheme on air quality in London. Part 1. Emissions modeling and analysis of air pollution measurements. *Res Rep Health Eff Inst*, (155):5-71.
- KELLY, F.J., FUSSELL, J.C. 2012. Size, source and chemical composition as determinants of toxicity attributable to ambient particulate matter. *Atmos Environ*, 60: 504–26.
- KELLY, B.G., LOK, S.S., HASLETON, P.S., EGAN, J.J., STEWART, J.P. 2002. A rearranged form of Epstein–Barr virus DNA is associated with idiopathic pulmonary fibrosis. *Am J Respir Crit Care Med*, 166:510–513.

- KHAIRALLAH, C., NETZER, S., VILLACRECES, A., JUZAN, M., ROUSSEAU, B., DULANTO, S., et al. 2015. $\gamma\delta$ T cells confer protection against murine cytomegalovirus (MCMV). *PLoS Pathog*, 11:e1004702.
- KHERADMAN, F., YOU, R., GU, B.H., CORRY, D.B. 2017. Cigarette smoke and DNA cleavage promote lung inflammation and emphysema. *Trans Am Clin Climatol Assoc*, 128:222-233.
- KIM, V., AND CRINER, G.J. 2013. Chronic bronchitis and chronic obstructive pulmonary disease. *Am J Respir Crit Care Med*, 187, 228-237.
- KIM, H.Y., DEKRUYFF, R.H. & UMETSU, D.T. 2010. The many paths to asthma: phenotype shaped by innate and adaptive immunity. *Nat. Immunol.* 11, 577–584.
- KLEIN, G., ROTBARD, J., GOTCH, F.M., BAHADUR, G., WRAITH, D., MCMICHAEL, A.J., et al.. 1989. Viral latency and transformation: the strategy of Epstein-Barr virus. *Cell*, 58, 5–8.
- KNUDSEN, K.B., BERTHING, T., JACKSON, P., POULSEN, S.S., MORTENSEN, A., JACOBSEN, N.R., SKAUG, V., SZAREK, J., HOUGAARD, K.S., WOLFF, H., WALLIN, H., VOGEL, U. 2019. Physicochemical Predictors of Multi-Walled Carbon Nanotube–Induced Pulmonary Histopathology and Toxicity One Year after Pulmonary Deposition of 11 Different Multi-Walled Carbon Nanotubes in Mice. *Basic & Clinical Pharmacology & Toxicology*, 124 (2): 211–227.
- KO, F.W., CHAN, K.P., HUI, D.S., GODDARD, J.R., SHAW, J.G., REID, D.W., YANG, I.A. 2016. Acute exacerbation of COPD. *Respirology*, 21(7):1152-65.
- KOHAN, M., BADER, R., PUXEDDU, I., LEVI-SCHAFFER, F., BREUER, R., BERKMAN, N. 2007. Enhanced osteopontin expression in a murine model of allergen-induced airway remodeling. *Clin Exp Allergy*, 37(10):1444-54.
- KOŁODZIEJ, M., DE VEER, M.J., CHOLEWA, M., EGAN, G.F., AND THOMPSON, B.R. 2017. Lung function imaging methods in Cystic Fibrosis pulmonary disease. *Respir Res*, 18, 96.
- KONSTANTINOUDIS, G., PADELLINI, T., BENNETT, J., DAVIES, B., EZZATI, M., BLANGIARDO, M. 2021. Long-term exposure to air-pollution and COVID-19 mortality in England: a hierarchical spatial analysis. *Environ Int*, 146:106316.
- KURODA, E., OZASA, K., TEMINZOZ, B., OHATA, K., KOO, C.X., KANUMA, T., KUSKABE, T., KOBARI, S., HORIE, M., MORIMOTO, Y., NAKAJIMA, S., KABASHIMA, K., ZIEGLER, S.F., IWAKURA, Y., ISE, W., KUROSAKI, T., NAGATAKE, T., KUNISAWA, J., TAKEMURA, N., UEMATSU, S., HAYASHI, M., AOSHI, T., KOBIYAMA, K., COBAN, C., ISHII, K.J. 2016. Inhaled fine particles induce alveolar macrophage death and interleukin-1 α release to promote inducible bronchus associated lymphoid tissue formation. *Immunity*, 45(6)1299-1310.
- KYJOVSKA, Z.O., JACOBSEN, N.R., SABER, A.T., BENGSTON, S., JACKSON, P., WALLIN, H., VOGEL, U. 2015a. DNA damage following pulmonary exposure by instillation to low doses of carbon black (Printex90) nanoparticles in mice. *Environ Mol Mutagen* 56(1):41-9.
- KYJOVSKA, Z.O., JACOBSEN, N.R., SABER, A.T., BENGSTON, S., JACKSON, P., WALLIN, H., VOGEL, U. 2015b. DNA strand breaks, acute phase response and inflammation following pulmonary exposure by instillation to the diesel exhaust particle NIST1650b in mice. *Mutagenesis*, 30(4):499-507.
- LABAKI, W.W., ROSENBERG, S.R. 2020. Chronic obstructive pulmonary disease (COPD). *Ann Intern Med*, 173, ITC17-ITC32.
- LABAKI, W.W., HAN, M.K. 2020. Chronic respiratory diseases: a global view. *The Lancet Respir Med*, 8(6)P531-533.
- LACHOWICZ-SCROGGINS, M.E., DUNICAN, E.M., CHARBIT, A.R., RAYMOND, W., LOONEY, M.R., PETERS, M.C., GORDON, E.D., WOODRUFF, P.G., LEFRANCAIS, E., PHILLIPS, B.R., MAUGER, D.T., COMHAIR, S.A., ERZURUM, S.C., JOHANSSON, M.W., JARJOUR, N.N., COVERSTONE, A.M., CASTRO, M., HASTIE, A.T., BLEECKER, E.R., FAJT, M.L., WENZEL, S.E., ISRAEL E., LEVY, B.D., FAHY, J.V. 2019. Extracellular DNA, neutrophil extracellular traps, and inflammasome activation in severe asthma. *Am J Respir Crit Care Med*, 1;199(9):1076-1085.

References

- LANGE, P., PARNER, J., VESTBO, J., SCHNOHR, P. & JENSEN, G. 1998. A 15-year follow-up study of ventilatory function in adults with asthma. *N. Engl. J. Med.* 339, 1194–1200.
- LANGE, P., CELLI, B., AGUSTI, A., BOJE JENSEN, G., DIVO, M., FANER, R., GUERRA, S., MAROTT, J.L., MARTINEZ, F.D., MARTINEZ-CAMBLOR, P., MEEK, P., OWEN, C.A., PETERSEN, H., PINTO-PLATA, V., SCHNOHR, P., SOOD, A., SORIANO, J.B., TESFAIGZI, Y., VESTBO, J. 2015. Lung-function trajectories leading to chronic obstructive pulmonary disease. *N Engl J Med*, 373: 111-122
- LE, T.G. , NGO L., MEHTA S., et al. 2012. Effects of short-term exposure to air pollution on hospital admissions of young children for acute lower respiratory infections in Ho Chi Minh City, Vietnam. *Res. Rep. Health Eff. Inst.* 5–72;73–83.
- LEE, B.J., KOSZINOWSKI, U.H., SARAWAR, S.R., ADLER, H. 2003. A gammaherpesvirus g protein-coupled receptor homologue is required for increased viral replication in response to chemokines and efficient reactivation from latency. *J Immunol*, 170(1):243-251.
- LENZ, A.G., STOEGER, T., CEI, D., SCHMIDMEIR, M., SEMREN, N., BURGSTALLER, G., LENTNER, B., EICKELBERG, O., MEINERS, S., SCHMID, O. 2014. Efficient bioactive delivery of aerosolized drugs to human pulmonary epithelial cells cultured in air-liquid interface conditions. *Am J Respir Cell Mol Biol*, 51(4):526-35.
- LENZ, A.G., KARG, E., LENTNER, B., DITTRICH, V., BRANDENBERGER, C., ROTHENRUTISHAUSER, B., SCHULZ, H., FERRON, G.A., SCHMID, O. 2009. A dose-controlled system for air-liquid interface cell exposure and application to zinc oxide nanoparticles. *Part Fibre Toxicol*, 6.
- LEVIN, L.I., MUNGER, K.L., O'REILLY, E.J., FALK, K.I., ASCHERIO, A. 2010. Primary infection with the Epstein-Barr virus and risk of multiple sclerosis. *Ann Neurol.* 67:824–830.
- LEY, B., COLLARD, H.R. 2013. Epidemiology of idiopathic pulmonary fibrosis. *Clin Epidemiol*, 5(1):483–492.
- LI, H., GE, M., PEI, Z., HE, J., WANG, C. 2022. Associations of environmental factors with total cholesterol level of middle-aged and elderly people in China. *MC Public Health*, 23;22(1):2423.
- LI, X., ZOU, B.Q., ZHOU, J., SHI, L.Z., FAN, L., YANG, H., YANG, S.D. 2021. Epstein-Barr virus infection-related post-transplant lymphoproliferative disorders in transplanted lung: a clinicopathological analysis. *Zhonghua Bing Li Xue Za Zhi*, 50(5):465-469.
- LI, J., SUN, S., TANG, R., QIU, H., HUANG, Q., MASON, T.G., TIAN, L. 2016. Major air pollutants and risk of COPD exacerbations: a systemic review and meta-analysis. *Int J Chron Obstruct Pulmon Dis*, 12;11:3079-3091.
- LI, X., FENG, J., SUN, R. 2011 Oxidative stress induces reactivation of Kaposi's sarcoma-associated herpesvirus and death of primary effusion lymphoma cells. *J Virol*, 85(2):715-24.
- LIANG, J., ZHANG, Y., XIE, T., LIU, N., CHEN, H., GENG, Y., KURKCIYAN, A., MENA, J.M., STRIPP, B.R., JIANG, D., NOBLE, P.W. 2016. Hyaluronan and TLR4 promote surfactant-protein-C-positive alveolar progenitor cell renewal and prevent severe pulmonary fibrosis in mice. *Nat Med*, 22(11):1285–1293.
- LIANG, Y. , FANG L., PAN H., et al. 2014. PM2.5 in Beijing — temporal pattern and its association with influenza. *Environ. Health* 13: 102–102.
- LIANYONG, H., 2022. Mechanism underlying environmental nanoparticle exposure triggered gammaherpesvirus reactivation. Helmholtz Zentrum München, LMU, Dissertation
- LIEBERMAN, P.M. 2016. Epigenetics and genetics of viral latency. *Cell Host Microbe*, 19, 619–628.
- LIN, M. , STIEB D.M. & CHEN Y.. 2005. Coarse particulate matter and hospitalization for respiratory infections in children younger than 15 years in Toronto: a case-crossover analysis. *Pediatrics*, 116: e235–e240.
- LIU, X.-X. , LI Y., QIN G., et al. 2019. Effects of air pollutants on occurrences of influenza-like illness and laboratory-confirmed influenza in Hefei, China. *Int J Biometeorol*, 63: 51–60.

- LIU, X.F., WANG, X., YAN, S., ZHANG, Z., ABECASSIS, M., HUMMEL, M. 2013. Epigenetic control of cytomegalovirus latency and reactivation. *Viruses*, 5, 1325–1345.
- LIU, L., POON, R., CHEN, L., CHEN, L., FRESCURA, A.-M., MONTUSCHI, P., CIABATTONI, G., WHEELER, A., DALES, R. 2009. Acute effects of air pollution on pulmonary function, airway inflammation, and oxidative stress in asthmatic children. *Environ Health Perspect*, 117: 668–74.
- LONG, C.M., NASCARELLA, M.A., VALBERG, P.A. 2013. Carbon black vs. black carbon and other airborne materials containing elemental carbon: physical and chemical distinctions. *Environ Pollut*, 181:271–86.
- LORET, T., ROGERIEUX, F., TROUILLER, B., BRAUN, A., EGLES, C., LACROIX, G. 2018. Predicting the in Vivo Pulmonary Toxicity Induced by Acute Exposure to Poorly Soluble Nanomaterials by Using Advanced in Vitro Methods. *Particle and Fibre Toxicology* 15 (1): 1–20.
- LORET, T., PEYRET, E., DUBREUIL, M., AGUERRE-CHARIOL, O., BRESSOT, C., LE BIHAN, O., AMODEO, T., TROUILLER, B., BRAUN, A., EGLES, C., LACROIX, G. 2016. Air-liquid interface exposure to aerosols of poorly soluble nanomaterials induces different biological activation levels compared to exposure to suspensions. *Part Fibre Toxicol*, 13(1).
- LUO, H., ZHANG, Q., NIU, Y., KANN, H., CHEN, R. 2022. Fine particulate matter and cardiorespiratory health in China: a systemic review and meta-analysis of epidemiological studies. *J Environ Sci*, 123:306-316.
- MA, P., ZHOU, N., WANG, X., ZHANG, Y., TANG, X., YANG, Y., MA, X., WANG, S. 2022. Stronger susceptibilities to air pollutants of influenza A than B were identified in subtropical Shenzhen, China. *Environ Res*, 21;219:115100.
- MACHIDA, H., INOUE, S., SHIBATA, Y., KIMURA, T., SATO, K., ABE, K., MURANO, H., YANG, S., NAKANO, H., SATO, M., NEMOTO, T., SATO, C., NISHIWAKI, M., YAMAUCHI, K., IGARASHI, A., TOKAIRIN, Y., WATANABE, M. 2021. Thymus and activation-regulated chemokine (TARC/CCL17) predicts decline of pulmonary function in patients with chronic obstructive pulmonary disease. *Allergol Int*, 70:81–88.
- MAHIDA, R.Y., PRICE, J., LUGG, S.T., LI, H., PAREKH, D., SCOTT, A., HARRISON, P., MATTHAY, M.A., THICKETT, D.R. 2022. CD-14 extracellular vesicles in bronchoalveolar lavage fluid as a new biomarker of acute respiratory distress syndrome. *Am J Physiol Lung Cell Mol Physiol*, 1;322(4):L617-L624.
- MALAVIYA, R., ZHOU, Z., RAYMOND, H., WERTHEIMER, J., JONES, B., BUNTING, R., WILKINSON, P., MADIREDDY, L., HALL, L., RYAN, M., RAO, T.S. 2021. Repeated exposure of house dust mite induces progressive airway inflammation in mice: differential roles of CCL17 and IL-13. *Pharmacol Res Perspect*, 9(3): e00770.
- MANEECHOTESUWAN, K., YAO, X., ITO, K., JAZRAWI, E., USMANI, O.S., ADCOCK, I.M., BARNES, P.J. 2009. Suppression of GATA-3 nuclear import and phosphorylation: a novel mechanism of corticosteroid action in allergic disease. *PLoS Med*, 6(5):e1000076.
- MANNINO, D.M., DOHERTY, D.E., BUIST, S.A. 2006. Global Initiative on Obstructive Lung Disease (GOLD) classification of lung disease and mortality: findings from the Atherosclerosis Risk in Communities (ARIC) study. *Respir Med*, 100, 115-122.
- MARIN, N.D., DUNLAP, M.D., KAUSHAL, D., KHADER, S.A. 2019. Friend or Foe: The Protective and Pathological Roles of Inducible Bronchus-Associated Lymphoid Tissue in Pulmonary Diseases. *J Immunol*, 1;202(9):2519-2526.
- MARSHALL, N.B., SWAIN, S.L. 2011. Cytotoxic CD4 T cells in antiviral immunity. *J Biomed Biotechnol*, 2011:954602.
- MARTIN, P.J., HÉLIOT, A., TRÉMOLET, G., LANDKOCZ, Y., DEWAELE, D., CAZIER, F., LEDOUX, F., COURCOT, D. 2019. Cellular response and extracellular vesicles characterization of human macrophages exposed to fine atmospheric particulate matter. *Environ Pollut*, 254(PtA):112933.
- MARTINS, L.C., LATORRE MDO R., CARDOSO M.R., et al. 2002. [Air pollution and emergency room visits due to pneumonia and influenza in Sao Paulo, Brazil]. *Rev. Saude Publica*, 36: 88–94.

References

- MARUYAMA, K., NEMOTO, E., YAMADA, S. 2019. Mechanical regulation of macrophage function – cyclist tensile force inhibits NLRP3 inflammasome-dependent IL-1 β secretion in murine macrophages. *Inflamm Regen*, 29:3.
- MASUDA, S., NAKAZAWA, D., SHIDA, H., MIYOSHI, A., KUSUNOKI, Y., TOMARU, U., ISHIZU, A. 2016. NETosis markers: Quest for specific, objective, and quantitative markers. *Clin Chim Acta*, 1;459:89-93.
- MATHERS, C.D., LONCAR, D. 2006. Projections of Global Mortality and Burden of Disease from 2002 to 2030. *PLoS Med*, 3, e442.
- MATTHAY, M.A., LANDOLT, C.C., STAUB, N.C. 1982. Differential liquid and protein clearance from the alveoli of anesthetized sheep. *J Appl Physiol Respir Environ Exerc Physiol*. 53:96-104.
- MATTHAY, M.A., ZEMANS, R.L., ZIMMERMAN, G.A., ARABI, Y.M., BEITLER, J.R., MERCAT, A., HERRIDGE, M., RANDOLPH, A.G., CALFEE, C.S. 2019. Acute respiratory distress syndrome. *Nat Rev Dis Primers*, 14;5(1):18.
- MAZZOLI-ROCHA F, FERNANDES S, EINICKER-LAMAS M, ZIN WA. 2010. Roles of oxidative stress in signaling and inflammation induced by particulate matter. *Cell Biol Toxicol*, 26(5):481-98.
- MCALLISTER, D.A., AHMED, F.S., AUSTIN, J.H., HENSCHKE, C., KELLER, B.M., LEMESHOW, A., REEVES, A.P., MESIA-VELA, S., PEARSON, G.D.N., SHIAU, M.C., SCHWARTZ, J.E., YANKELEVITZ, D.F., BARR, R.G. 2014. Emphysema predicts hospitalisation and incident airflow obstruction among older smokers: a prospective cohort study. *PLoS One*. 2014;9(4):e93221.
- MCCARTHY, C.E., DUFFNEY, P.F., NOGALES, A., POST, C.M., LAWRENCE, B.P., MARTINEZ-SOBRIDO, L., THATCHER, T.H., PHIPPS, R.P., SIME, P.J. 2022. Dung biomass smoke exposure impairs resolution of inflammatory responses to influenza infection. *Toxicol Appl Pharmacol*, 1;450:116160.
- MCMANUS, T.E., MARLEY, A.M., BAXTER, N., CHRISTIE, S.N., ELBORN, J.S., O'NEILL, H.J., COYLE, P.V., KIDNEY, J.C. 2008. High levels of Epstein-Barr virus in COPD. *Eur Respir J*, 31(6):1221-6.
- MEDALIA, A.I., RIVIN, D., SANDERS, D.R. 1983. A comparison of carbon black with soot. *Sci Total Environ*, 31(1):1–22.
- MEHTA, S., SHIN, H., BURNETT, R., NORTH, T., COHEN, A.J. 2013. Ambient particulate air pollution and acute lower respiratory infections a systematic review and implications for estimating the global burden of disease. *Air Qual Atmos Health*, 6(1):69–83.
- MIGLIORE, L., SARACINO, D., BONELLI, A., COLOGNATO, R., D'ERRICO, M.R., MAGRINI, A., BERGAMASCHI, A., BERGAMASCHI, E. 2010. Carbon Nanotubes Induce Oxidative DNA Damage in RAW 264.7 Cells. *Environmental and Molecular Mutagenesis* 51 (4): NA–303.
- MILLS, N.L., TÖRNQVIST, H., GONZALES, M.C., VINK, E., ROBINSON, S.D., SÖDERBERG, S., BOON, N.A., DONALDSON, K., SANDSTRÖM, T., BLOMBERG, A., NEWBY, D.E. 2007. Ischemic and thrombotic effects of dilute diesel-exhaust inhalation in men with coronary heart disease. *N Engl J Med*, 357:1075-1082.
- MISHARIN, A.V., SCOTT BUDINGER, G.R., PERLMAN, H. 2011. The lung macrophage: a Jack of all trades. *Am J Respir Crit Care Med*, 184:497–8.
- MISHARIN, A.V., MORALES-NEBREDA, L., REYFMAN, P.A., CUDA, C.M., WALTER, J.M., MCQUATTIE-PIMENTEL, A.C., CHEN, C.I., ANEKALLA, K.R., JOSHI, N., WILLIAMS, K.J.N., ABDALA-VALENCIA, H., YACOUB, T.J., CHI, M., CHIU, S., GONZALEZ-GONZALEZ, F.J., GATES, K., LAM, A.P., NICHOLSON, T.T., HOMAN, P.J., SOBERANES, S., DOMINGUEZ, S., MORGAN, V.K., SABER, R., SHAFFER, A., HINCHCLIFF, M., MARSHALL, S.A., BHARAT, A., BERDNIKOV, S., BHORADE, S.M., BARTOM, E.T., MORIMOTO, R.I., BALCH, W.E., SZNAJDER, J.I., CHANDEL, N.S., MUTLU, G.M., JAIN, M., GOTTARDI, C.J., SINGER, B.D., RIDGE, K.M., BAGHERI, N., SHILATIFARD, A., BUDINGER, G.R.S., PERLMAN, H. 2017.

- Monocyte-derived alveolar macrophages drive lung fibrosis and persist in the lung over the life span. *J Exp Med*, 214(8):2387-2404.
- MOCK, J.R., TUNE, M.K., DIAL, C.F., TORRES-CASTILLO, J., HAGAN, R.S., DOERSCGUK, C.M. (2020). Effects of IFN- γ on immune cell kinetics during the resolution of acute lung injury. *Physiol Rep*, 8(3): e14368.
- MOHAN, A.; CHANDRA, S.; AGARWAL, D.; GULERIA, R.; BROOR, S.; GAUR, B.; PANDEY, R.M. 2010. Prevalence of viral infection detected by PCR and RT-PCR in patients with acute exacerbation of COPD: A systematic review. *Respirology*, 15,536–542.
- MØLLER, P., CHRISTOPHERSEN, D.V., JENSEN, D.M., KERMANIZADEH, A., ROURSGAARD, M., JACOBSEN, N.R., HEMMINGSEN, J.G., DANIELSEN, P.H., CAO, Y., JANTZEN, K., KLINGBERG, H., HERSOUG, L.G., LOFT, S. 2014. Role of oxidative stress in carbon nanotube-generated health effects. *Arch Toxicol*, 88(11):1939-64.
- MORA, A.L., TORRES-GONZÁLEZ, E., ROJAS, M., XU, J., RITZENTHALER, J., SPECK, S.H., ROMAN, J., BRIGHAM, K., STECENKO, A. 2007. Control of virus reactivation arrests pulmonary herpesvirus-induced fibrosis in IFN-gamma receptor-deficient mice. *Am J Respir Crit Care Med*, 1;175(11):1139-50.
- MORIMOTO, Y., OGAMI, A., KOCHI, I., UCHIYAMA, T., IDE, R., MYOJO, T., HIGASHI, T. 2010. Continuing investigation of effect of toner and its by-product on human health and occupational health management of toner. *Sangyo Eiseigaku Zasshi*, 52:201–208.
- MORSE, C., TABIB, T., SEMBRAT, J., BUSCHUR, J.S., BITTAR, H.T., VALENZI, E., JIANG, Y., KASS, D.J., GIBSON, K., CHEN, W., MORA, A., BENOS, P.V., ROJAS, M., LAFYATIS, R. 2019. *European Respiratory Journal*, 54:1802441.
- MOSTOVENKO, E., YOUNG, T., MULDOON, P.P., BISHOP, L., CANAL, C.G., VUCETIC, A., ZEIDLER-ERDELY, P.C., ERDELY, A., CAMPEN, M.J., OTTENS, A.K. 2019. Nanoparticle exposure driven circulating bioactive peptidome causes systemic inflammation and vascular dysfunction. *Part Fibre Toxicol*, 29;16(1):20.
- MOTALLEBZADEH, R., REHAKOVA, S., CONLON, T.M., WIN, T.S., CALLAGHAN, C.J., GODDARD, M., BOLTON, E.M., RUDDLE, N.H., BRADLEY, J.A., PETTIGREW, G.J. 2012. Blocking lymphotoxin signaling abrogates the development of ectopic lymphoid tissue within cardiac allografts and inhibits effector antibody responses. *FASEB J*, 26: 51–62.
- MROZ, R.M., SCHINS, R.P.F., DROST, E.M., MACNEE, W., DONALDSON, K. 2007. Nanoparticle carbon black driven DNA damage induces growth arrest and AP-1 and NFkappaB DNA binding in lung epithelial A549 cell line. *J Physiol Pharmacol*, 58(2):461-70.
- MÜLLER, L., RIEDIKER, M., WICK, P., MOHR, M., GEHR, P., ROTHEN-RUTISHAUSER, B. 2010. Oxidative stress and inflammation response after nanoparticle exposure: differences between human lung cell monocultures and an advanced three-dimensional model of the human epithelial airways. *J R Soc Interface*, 6;7(1):S27-40.
- MURATA, T. 2014. Regulation of Epstein-Barr virus reactivation from latency. *Microbiol Immunol*, 58, 307-17.
- MURPHY, F.A., SCHINWALD, A., POLAND, C.A., DONALDSON, K. 2012. The mechanism of pleural inflammation by long carbon nanotubes: interaction of long fibres with macrophages stimulates them to amplify pro-inflammatory responses in mesothelial cells. *Part Fibre Toxicol*, 9:8.
- MURRAY, P.G., YOUNG, L.S. 2019. An etiological role for the Epstein-Barr virus in the pathogenesis of classical Hodgkin lymphoma. *Blood*, 134(7):591-596.
- MURTAS, R., RUSSO, A.G. 2019. Effects of pollution, low temperature and influenza syndrome on the excess mortality risk in winter 2016-2017. *BMC Publ. Health*, 19:1445.
- NABI, S.U., ALI, S.I., RATHER, M.A., SHEIKH, W.M., ALTAF, M., SINGH, H., MUMTAZ, P.T., MISHRA, N.C., NAZIR, S.U., BASHIR, S.M. 2022. Organoids: A new approach in toxicity testing of nanotherapeutics. *J Appl Toxicol*, 42(1):52-72.
- NAGAHARA, H., SENO, T., YAMAMOTO, A., OBAYASHI, H., INOUE, T., KIDA, T., NAKABAYASHI, A., KUKIDA, Y., FUJIOKA, K., FUJII, W., MURAKAMI, K., KOHNO, M., KAWAHITO, Y. 2018.

References

- Role of allograft inflammatory factor-1 in bleomycin-induced lung fibrosis. *Biochem Biophys Res Commun*, 8;495(2):1901-1907.
- NAGAHARA, H., YAMAMOTO, A., SENO, T., OBAYASHI, H., KIDA, T., NAKABAYASHI, A., KUKIDA, Y., FUJIOKA, K., FUJII, W., MURAKAMI, K., KOHNO, M., KAWAHITO, Y. 2016. Allograft inflammatory factor-1 in the pathogenesis of bleomycin-induced acute lung injury. *Biosci Trends*, 10(1):47-53.
- NAGAI H, TOYOKUNI S. 2012. Differences and similarities between carbon nanotubes and asbestos fibers during mesothelila carcinogenesis. *Cancer Sci*, 103:1378–1390.
- NAGAI H, OKAZAKI Y, CHEW S, MISAWA, N., YAMASHITA, Y., AKATSUKA, S., ISHIHARA, T., YAMASHITA, K., YOSHIKAWA, Y., YASUI, H., JIANG, L., OHARA, H., TAKAHASHI, T., ICHIHARA, G., KOSTARELOS, K., MIYATA, Y., SHINOHARA, H., TOYOKUNI, S. 2011. Diameter of multi-walled carbon nanotubes is a critical factor in mesothelial injury and subsequent carcinogenesis. *Proc Natl Acad Sci USA*, 108:E1330–E1338.
- NAGAI H, TOYOKUNI S. 2010. Biopersistent fiber-induced inflammation and carcinogenesis: lessons learned from asbestos toward safety of fibrous nanomaterials. *Arch Biochem Biophys*, 502:1–7.
- NALYSNYK L, CID-RUZAFI, J., ROTELLA, P., ESSER, D. 2012. Incidence and prevalence of idiopathic pulmonary fibrosis: review of the literature. *Eur Respir Rev*, 21(126):355–361.
- NASH, A. A., DUTIA, B. M., STEWART, J. P., DAVISON, A. J. 2001. Natural history of murine gamma-herpesvirus infection. *Philos Trans Royal Soc London*, B356:569–579.
- NEMMAR, A., VANBILLOEN, H., HOYLAERTS, M.F., HOET, P.H., VERBRUGGEN, A., NEMERY, B. 2001. Passage of intratracheally instilled ultra-fine particles from the lung into the systemic circulation in hamster. *Am J Respir Crit Care Med*, 164(9):1665–1668.
- NEMMAR, A., HOET, P.H., VANQUICKENBORNE, B., DINSDALE, D., THOMEER, M., HOYLAERTS, M.F., VANBILLOEN, H., MORTELMANS, L., NEMERY, B. 2002a. Passage of inhaled particles into the blood circulation in humans. *Circulation*, 105(4):411–414.
- NEMMAR, A., HOYLAERTS, M.F., HOET, P.H., DINSDALE, D., SMITH, T., XU, H., VERMYLEN, J., NEMERY, B. 2002b. Ultrafine particles affect experimental thrombosis in an in vivo hamster model. *Am J Respir Crit Care Med*, 166(7):998–1004.
- NEMMAR, A., HOYLAERTS, M.F., HOET, P.H., VERMYLEN, J., NEMERY, B. 2003. Size effect of intratracheally instilled particles on pulmonary inflammation and vascular thrombosis. *Toxicol Appl Pharmacol*, 186(1):38–45.
- NETKUEAKUL, W., CHORTAREA, S., KULTHONG, K., LI, H., QIU, G., JOVIC, M., GAAN, S., HANNIG, Y., BUERKI-THURNHERR, T., WICK, P., WANG, J. 2022. Airborne emissions from combustion of graphene nanoplatelet/epoxy composites and their cytotoxicity on lung cells via air-liquid interface cell exposure in vitro. *NanoImpact*, 27:100414.
- NIE, H., LIU, H., SHI, Y., LAI, W., LIU, X., XI, Z., LIN, B. 2022. Effects of Different Concentrations of Oil Mist Particulate Matter on Pulmonary Fibrosis In Vivo and In Vitro. *Toxics*, 28;10(11):647.
- NIKOTA, J., BANVILLE, A., GOODWIN, L. R., WU, D., WILLIAMS, A., YAUK, C. L., et al. 2017. Stat-6 signaling pathway and not Interleukin-1 mediates multi-walled carbon nanotube-induced lung fibrosis in mice: insights from an adverse outcome pathway framework. *Part Fibre Toxicol*, 14:37.
- NOBLE, P.W. 2008. Epithelial fibroblast triggering and interactions in pulmonary fibrosis. *Eur Respir Rev*, 17(109):123–129.
- NYGAARD, U.C., HANSEN, J.S., SAMUELSEN, M., ALBERG, T., MARIOARA, C.D., AND LOVIK, M. 2009. Single-walled and multi-walled carbon nanotubes promote allergic immune responses in mice. *Toxicol Sci*, 109, 113–123.
- OEDER, S., KANASHOVA, T., SIPPULA, O., SAPCARIU, S.C., STREIBEL, T., ARTEAGA-SALAS, J.M., PASSIG, J., DILGER, M., PAUR, H.R., SCHLAGER, C., MÜLHOPT, S., DIABATÉ, S., WEISS, C., STENGEL, B., RABE, R., HARNDORF, H., TORVELA, T., JOKINIEMI, J.K., HIRVONEN, M.R., SCHMIDT-WEBER, C., TRIDL-HOFFMANN, C., BÉRUBÉ, K.A., WLODARCZYK, A.J., PRYTHERCH, Z., MICHALKE, B., KREBS, T., PRÉVÔT, A.S., KELBG, M., TIGGESBÄUMKER, J., KARG, E., JAKOBI, G., SCHOLTES, S., SCHNELLE-KREIS, J.,

- LINTELMANN, J., MATUSCHEK, G., SKLORZ, M., KLINGBEIL, S., ORASCHE, J., RICHTHAMMER, P., MÜLLER, L., ELSASSER, M., REDA, A., GRÖGER, T., WEGGLER, B., SCHWEMER, T., CZECH, H., RÜGER, C.P., ABBASZADE, G., RADISCHAT, C., HILLER, K., BUTERS, J.T., DITTMAR, G., ZIMMERMANN, R. 2015. Particulate matter from both heavy fuel oil and diesel fuel shipping emissions show strong biological effects on human lung cells at realistic and comparable in vitro exposure conditions. *PLoS One*, 3;10(6):e0126536.
- OELSNER, E.C., SMITH, B.M., HOFFMAN, E.A., FOLSOM, A.R., KAWUT, S.M., KAUFMAN, J.D., MANICHAIKUL, A., LEDERER, D.J., SCHWARTZ, J.E., WATSON, K.E., ENRIGHT, P.L., AUSTIN, J.H.M., LIMA, J.A.C., SHEA, S.J., BARR, R.G. 2018. Associations between emphysema-like lung on CT and incident airflow limitation: a general population-based cohort study. *Thorax*, 73(5):486-488.
- O'SHAUGHNESSY, P.T., ADAMCAKOVA-DODD, A., ALTMAIER, R., THORNE, P.S. 2014. Assessment of the aerosol generation and toxicity of carbon nanotubes. *Nanomaterials (Basel)*, 12;4(2):439-453.
- O'SHAUGHNESSY, T.C., ANSARI, T.W., BARNES, N.C., JEFFREY, P.K. 1997. Inflammation in bronchial biopsies of subjects with chronic bronchitis: inverse relationship of CD8+ T lymphocytes with FEV1. *Am J Respir Crit Care Med*, 155:852-857.
- PAN, Q., TANG Z., YU Y., et al. 2016. Haze and influenza A virus: coincidence or causation? *Am. J. Infect. Control*, 44: 959–960.
- PAN, Q., YU Y., TANG Z., et al. 2014. Haze, a hotbed of respiratory-associated infectious diseases, and a new challenge for disease control and prevention in China. *Am. J. Infect. Control* 42: 688–688.
- PARIMON, T., YAO, C., STRIPP, B.R., NOBLE, P.W., CHEN, P. 2020. Alveolar epithelial type II cells as drivers of lung fibrosis in idiopathic pulmonary fibrosis. *Int J Mol Sci*, 21(7):2269.
- PARRA, E.R., KAIRALLA, R.A., RIBEIRO DE CARVALHO, C.R., EHER, E., CAPELOZZI, V.L. 2007. Inflammatory cell phenotyping of the pulmonary interstitium in idiopathic interstitial pneumonia. *Respir*, 74(2):159-69.
- PARRISH C. R., HOLMES E. C., MORENS D. M., PARK E.-C., BURKE D. S., CALISHER C. H., ET AL.. 2008. Cross-species virus transmission and the emergence of new epidemic diseases. *Microbiol Mol Biol Rev*, 72, 457–470.
- PATEL, D., RINEHART, R., ABRAHAM, R.G. 2022. A Case of Lymphomatoid Granulomatosis in a Lymph Node with Unique Clinical and Histopathologic Features. *Am J Case Rep*, 3;23:e936862.
- PEEL, J.L., TOLBERT P.E., KLEIN M., et al. 2005. Ambient air pollution and respiratory emergency department visits. *Epidemiology (Cambridge, Mass.)*, 16: 164–174.
- PETERS, A., VON KLOT, S., HEIER, M., TRENTINAGLIA, I., HÖRMANN, A., WICHMANN, E., LÖWEL, H. 2004. Exposure to traffic and the onset of myocardial infarction. *N Engl J Med*, 351:1721-1730.
- PFEFFER, P.E., DONALDSON, G.C., MACKAY, A.J., WEDZICHA, J.A. 2019. Increased chronic obstructive pulmonary disease exacerbations of likely viral etiology follow elevated ambient nitrogen oxides. *Am. J. Respir. Crit. Care Med*, 199:581–591.
- POLAND, C.A., DUFFIN, R., KINLOCH, I., MAYNARD, A., WALLACE, W.A.H., SEATON, A., STONE, V., BROWN, S., MACNEE, W., DONALDSON, K. 2008. Carbon nanotubes introduced into the abdominal cavity of mice show asbestos-like pathogenicity in a pilot study. *Nat nanotechnol*, 3:423–428.
- PORSBJERG, C., LANGE, P. & ULRİK, C. S. 2015. Lung function impairment increases with age of diagnosis in adult onset asthma. *Respir. Med.* 109, 821–827.
- PORTO, B.N., STEIN, R.T. 2016. Neutrophil extracellular traps in pulmonary diseases: too much of a good thing? *Front Immunol*, 7:311.
- POPE, C.A., BURNETT, R.T., TURNER, M.C., COHEN, A., KREWSKI, D., JERRETT, M., GAPSTUR, S.M., THUN, M.J. 2011. Lung cancer and cardiovascular disease mortality associated with ambient air pollution and cigarette smoke: shape of the exposure-response relationships. *Environ Health Perspect*, 119(11):1616–21.

References

- POTHIRAT, C., CHAIWONG, W., LIWSRISAKUN, C., BUMROONGKIT, C., DEESOMCHOK, A., THEERAKITTIKUL, T., LIMSUKON, A., TAJARERNMUANG, P., PHETSUK, N. 2019. Acute effects of air pollutants on daily mortality and hospitalizations due to cardiovascular and respiratory diseases. *J. Thorac. Dis*, 11:3070–3083.
- POULSEN, S.S., SABER, A.T., MORTENSEN, A., SZAREK, J., WU, D., WILLIAMS, A., ANDERSEN, O., JACOBSEN, N.R., YAU, C.L., WALLIN, H., HALAPPANAVAR, S., VOGEL, U. 2015. Changes in cholesterol homeostasis and acute phase response link pulmonary exposure to multi-walled carbon nanotubes to risk of cardiovascular disease. *Toxicol Appl Pharmacol*, 15;283(3):210-22.
- POULSEN, S.S., JACKSON, P., KLING, K., KNUDSEN, K.B., SKAUG, V., KYJOVSKA, Z.O., THOMSEN, B.L., CLAUSEN, P.A., ATLTUI, R., BERTHING, T., BENGSTON, S., WOLFF, H., JENSEN, K.A., WALLIN, H., VOGEL, U. 2016. Multi-Walled Carbon Nanotube Physicochemical Properties Predict Pulmonary Inflammation and Genotoxicity. *Nanotoxicology*, 10 (9): 1263–1275.
- PORTER, D.W., HUBBS, A.F., CHEN, B.T., MCKINNEY, W., MERCER, R.R., WOLFARTH, M.G., BATTELLI, L., WU, N., SRIRAM, K., LEONARD, S., ANDREW, M., WILLARD, P., TSURUOKA, S., ENDO, M., TSUKADA, T., MUNEKANE, F., FRAZER, D.G., CASTRANOVA, V. 2013. Acute pulmonary dose-responses to inhaled multi-walled carbon nanotubes. *Nanotoxicology*, 7(7):1179–94.
- POZZER, A., DOMINICI, F., HAINES, A., WITT, C., MÜNZEL, T., LELIEVELD, J. 2020. Regional and global contributions of air pollution to risk of death from COVID-19. *Cardiovasc Res*, 116(14):2247–2253.
- RAASCHOU-NIELSEN, O., ANTONSEN, S., AGERBO, E., HVIDTFELDT, U.A., GEELS, C., FROHN, L.M., CHRISTENSEN, J.H., SIGSGAARD, T., BRANDT, J., PEDERSEN, C.B. 2022. PM_{2.5} air pollution components and mortality in Denmark. *Environ Int*, 171:107685.
- RAGHU, G., CHEN, S.-Y., HOU, Q., YEH, W.-S., COLLARD, H.R. 2016. Incidence and prevalence of idiopathic pulmonary fibrosis in US adults 18-64 years old. *Eur Respir J*, 48(1):179–186.
- RAGHU G., COLLARD H.R., EGAN J.J., MARTINEZ F.J., BEHR J., BROWN K.K., COLBY T.V., CORDIER J.F., FLAHERTY K.R., LASKY J.A., LYNCH, D.A., RYU, J.H., SWIGRIS, J.J., WELLS, A.U., ANCOCHEA, J., BOUROS, D., CARVALHO, C., COSTABEL, U., EBINA, M., HANSELL, D.M., JOHKOH, T., KIM, D.S., KING JR, T.E., KONDOH, Y., MYERS, J., MÜLLER, N.L., NICHOLSON, A.G., RICHELDI, L., SELMAN, M., DUDDEN, R.F., GRISS, B.S., PROTZKO, S.L., SCHÜNEMANN, H.J.; ATS/ERS/JRS/ALAT COMMITTEE ON IDIOPATHIC PULMONARY FIBROSIS. 2011. An official ATS/ERS/JRS/ALAT statement: Idiopathic pulmonary fibrosis: Evidence-based guidelines for diagnosis and management. *Am J Respir Crit Care Med*, 183:788–824.
- RAVENSBERG, A.J., SLATS, A.M., VAN WETERING, S., JANSSEN, K., VAN WIJNGAARDEN, S., DE JEU, R., RABE, K.F., STERK, P.J., HIEMSTRA, P.S. 2013. CD8(+) T cells characterize early smoking-related airway pathology in patients with asthma. *Respir Med*, 107(7):959-66.
- RAY, A., KOLLS, J.K. 2017. Neutrophilic inflammation in asthma and association with disease severity. *Trends Immunol*, 38:942–954.
- RECHE, C., VIANA, M., BRINES, M., PÉREZ, N., BEDDOWS, D., ALASTUEY, A., QUEROL, X. 2015. Determinants of aerosol lung-deposited surface area variation in an urban environment. *Sci Total Environ*, 1;517:38-47.
- REDDEHASE, M.J., LEMMERMANN, N.A.W. 2019. Cellular reservoirs of latent cytomegaloviruses. *Med. Microbiol. Immunol*, 208:391–403.
- REESE, T.A. 2016. Coinfections: another variable in the herpesvirus latency-reactivation dynamic. *J. Virol*. 90, 5534–5537.
- REESE, T.A., WAKEMAN, B.S., CHOI, H.S., HUFFORD, M.M., HUANG, S.C., ZHANG, X., et al. 2014. Helminth infection reactivates latent gamma-herpesvirus via cytokine competition at a viral promoter. *Science*, 345, 573–577.
- RENNARD, S.I., TOGO, S., AND HOLZ, O. 2006. Cigarette smoke inhibits alveolar repair: a mechanism for the development of emphysema. *Proc Am Thorac Soc*, 3, 703-708.

- RENWICK, L. C., BROWN, D., CLOUTER, A., DONALDSON, K. 2004. Increased inflammation and altered macrophage chemotactic responses caused by two ultrafine particle types. *Occup Environ Med*, 61, 442-7.
- RIVERA, G.A., WAKELEE, H. 2016. Lung Cancer in Never Smokers. *Adv Exp Med Biol*, 893:43-57.
- RODRIGUES, S.D.O., CUNHA, C.M.C.D., SOARES, G.M.V., SILVA, P.L., SILVA, A.R., GONÇALVES-DE-ALBUQUERQUE, C.F. 2021. Mechanisms, Pathophysiology and Currently Proposed Treatments of Chronic Obstructive Pulmonary Disease. *Pharmaceuticals*, 14(10):979.
- ROIZMAN, B., WHITLEY, R.J. 2013. An inquiry into the molecular basis of HSV latency and reactivation. *Annu. Rev. Microbiol.* 67, 355–374.
- ROOS, A.B., SANDEN, C., MORI, M., BJERMER, L., STAMPFLI, M.R., ERJEFALT, J.S. 2015. IL-17A Is Elevated in End-Stage Chronic Obstructive Pulmonary Disease and Contributes to Cigarette Smoke-induced Lymphoid Neogenesis. *Am J Respir Crit Care Med*, 191: 1232–1241.
- ROULET, A., ARMAND, L., DAGOUASSAT, M., ROGERIEUX, F., SIMON-DECKERS, A., BELADE, E., VAN NHIEU, J.T., LANONE, S., PAIRON, J.-C., LACROIX, G., BOCZKOWSKI, J. 2012. Intratracheally administered titanium dioxide or carbon black nanoparticles do not aggravate elastase-induced pulmonary emphysema in rats. *BMC Pulmonary Medicine* 12:38.
- RYDMAN E. M., ILVES M., VANHALA E., VIPPOLA M., LEHTO M., KINARET P. A., et al. 2015. A single aspiration of rod-like carbon nanotubes induces asbestos-like pulmonary inflammation mediated in part by the IL-1 receptor. *Toxicol Sci*, 147 140–155.
- RYMAN-RASMUSSEN, J.P., TEWKSBURY, E.W., MOSS, O.R., CESTA, M.F., WONG, B.A., AND BONNER, J.C. 2009. Inhaled multiwalled carbon nanotubes potentiate airway fibrosis in murine allergic asthma. *Am J Respir Cell Mol Biol*, 40,349–358.
- SABER, A.T., HALAPPANAVAR, S., FOLKMANN, J.K., BORNHOLDT, J., BOISEN, A.M., MØLLER, P., WILLIAMS, A., YAUK, C., VOGEL, U., LOFT, S., WALLIN, H. 2009. Lack of acute phase response in the livers of mice exposed to diesel exhaust particles or carbon black by inhalation. *Part Fibre Toxicol*, 20;6:12.
- SABER, a.T., LAMSON, J.S., JACOBSEN, N.R., RAVN-HAREN, G., HOUGAARD, K.S., NYENDI, A.N., WAHLBERG, P., MADSEN, A.M., JACKSON, P., WALLIN, H. ,VOGEL, U. 2013. PARTICLE-INDUCED PULMONARY ACUTE PHASE RESPONSES CORRELATES WITH NEUTROPHIL INFLUX LINKING INHALED PARTICLES AND CARDIOVASCULAR RISK. *PLOS ONE*, 24;8(7):E69020.
- SAETTA, M. 1999. Airway inflammation in chronic obstructive pulmonary disease. *Am J Respir Crit Care Med*, 160, S17-20.
- SAETTA, M., TURATO, G., MAESTRELLI, P., MAPP, C.E., FABBRI, L.M. 2001. Cellular and structural bases of chronic obstructive pulmonary disease. *Am J Respir Crit Care Med*, 163:1304-1309.
- SAGER, T.M., WOLFARTH, M.W., BATTELLI, L.A., LEONARD, S.S., ANDREW, M., STEINBACH, T., ENDO, M., TSURUOKA, S., PORTER, D.W., CASTRANOVA, V. 2013. Investigation of the pulmonary bioactivity of double-walled carbon nanotubes. *J Toxicol Environ Health A*, 76(15):922-36.
- SAHIN, H., WASMUTH, H. E. 2013. Chemokines in tissue fibrosis. *Biochim Biophys Acta*, 1832 1041–1048.
- SAKAMOTO, Y., NAKAE, D., FUKUMORI, N., TAYAMA, K., MAEKAWA, A., IMAI, K., HIROSE, A., NISHIMURA, T., OHASHI, N., OGATA, A. 2009. Induction of mesothelioma by a single intrascrotal administration of multi-wall carbon nanotube in intact male Fischer 344 rats. *J Toxicol Sci*, 34:65–76.
- SALEH, D.M., LUO, S., AHMED, O.H.M., ALEXANDER, D.B., ALEXANDER, W.T., GUNASEKARA, S., EL-GAZZAR, A.M., ABDELGIED, M., NUMANO, T., TAKASE, H., OHNISHI, M., TOMONO, S., ABD EL HADY, R.H., FUKAMACHI, K., KANNO, J., HIROSE, A., XU, J., SUZUKI, S., NAIKI-ITO, A., TAKAHASHI, S., TSUDA, H. 2022. Assessment of the toxicity and carcinogenicity of double-walled carbon nanotubes in the rat lung after intratracheal instillation: a two year study. *Part Fibre Toxicol*, 22;19(1):30.
- SATTLER, C., MORITZ, F., CHEN, S., STEER, B., KUTSCHKE, D., IRMLER, M., BECKERS, J., EICKELBERG, O., SCHMITT-KOPPLIN, P., ADLER, H. & STOEGER, T. 2017. Nanoparticle

References

- exposure reactivates latent herpesvirus and restores a signature of acute infection. *Part Fibre Toxicol*, 14, 2.
- SAULEDA, J., NÚÑEZ, B., SALA, E., SORIANO, J.B. 2018. Idiopathic Pulmonary Fibrosis: Epidemiology, Natural History, Phenotypes. *Med Sci*, 6:110.
- SCHMIT, T., GUO, K., TRIPATHI, J.K., WANG, Z., MCGREGOR, B., KLOMP, M., AMBIGAPATHY, G., MATHUR, R., HUR, J., PICHICHERO, M., KOLLS, J., M. KHAN, N. (2022). Interferon (IFN)- γ promotes monocyte-mediated lung injury during influenza infection. *Cell Rep*, 1; 38(9): 110456.
- SCHNEIDER, C., NOBS, S.P., KURRER, M., REHRAUER, H., THIELE, C., KOPF, M. 2014. Induction of the nuclear receptor PPAR- γ by the cytokine GM-CSF is critical for the differentiation of fetal monocytes into alveolar macrophages. *Nat Immunol*, 15:1026–37.
- SELMAN, M., THANNICKAL, V.J., PARDO, A., ZISMAN, D.A., MARTINEZ, F.J., LYNCH, J.P. 3RD. 2004. Idiopathic pulmonary fibrosis: pathogenesis and therapeutic approaches. *Drugs*, 64(4):405-30.
- SELMAN, M., KING, T.E., PARDO, A; AMERICAN THORACIC SOCIETY; EUROPEAN RESPIRATORY SOCIETY; AMERICAN COLLEGE OF CHEST PHYSICIANS. 2001. Idiopathic pulmonary fibrosis: prevailing and evolving hypotheses about its pathogenesis and implications for therapy. *Ann Intern Med*, 134(2):136–151.
- SENIOR, R.M., ANTHONISEN, N.R. 1998. Chronic Obstructive Pulmonary Disease (COPD). *Am J Respir Crit Care Med*, 157, S139–S147.
- SETTI, L., PASSARINI, F., GENNARO, G., DI GILIO, A., PALMISANI, J., BUONO, P., FORNARI, G., PERRONE, M.G., PIAZZALUNGA, A., BARBIERI, P., RIZZO, E., MIANI, A. 2020. Evaluation of the potential relationship between Particulate Matter (PM) pollution and COVID-19 infection spread in Italy. *Società Italiana di Medicina Ambientale*, 1-6.
- SHAH, R.U., PADILLA, L.E., PETERS, D.R., DUPUY-TODD, M., FONSECA, E.R., MA, G.Q., POPOOLA, O.A.M., JONES, R.L., MILLS, J., MARTIN, N.A., ALVAREZ, R.A. 2023. Identifying Patterns and Sources of Fine and Ultrafine Particulate Matter in London Using Mobile Measurements of Lung-Deposited Surface Area. *Environ Sci Technol*, 10;57(1):96-108.
- SHENDEROV, K., COLLINS, S.L., POWELL, J.D., HORTON, M.R. 2021. Immune dysregulation as a driver of idiopathic pulmonary fibrosis. *J Clin Invest*, 131(2):e143226.
- SHINJI TAKENAKA, 2010. Transmission electron microscopic images of nanoparticles. Helmholtz Zentrum München.
- SHVEDOVA, A.A., FABISIAK, J.P., KISIN, E.R., MURRAY, A.R., ROBERTS, J.R., TYURINA, Y.Y., ANTONINI, J.M., FENG, W.H., KOMMINENI, C., REYNOLDS, J., BARCOWSKY, A., CASTRANOVA, V., KAGAN, V.E. 2008. Sequential exposure to carbon nanotubes and bacteria enhances pulmonary inflammation and infectivity. *Am J Respir Cell Mol Biol*, 38(5):579–90.
- SHVEDOVA A. A., KISIN E. R., MERCER R., MURRAY A. R., JOHNSON V. J., POTAPOVICH A. I., et al. 2005. Unusual inflammatory and fibrogenic pulmonary responses to single-walled carbon nanotubes in mice. *Am J Physiol Lung Cell Mol Physiol*, 289 L698–L708.
- SIELSKI, J., JÓŹWIAK, M.A., KAZIRÓD-WOLSKI, K., SIUDAK, Z., JÓŹWIAK, M. 2022. Impact of Air Pollution and COVID-19 Infection on Periprocedural Death in Patients with Acute Coronary Syndrome. *Int J Environ Res Public Health*, 11;19(24):16654.
- SIELSKI, J., KAZIRÓD-WOLSKI, K., JÓŹWIAK, M.A., JÓŹWIAK, M. 2021. The influence of air pollution by PM_{2.5}, PM₁₀ and associated heavy metals on the parameters of out-of-hospital cardiac arrest. *Sci. Total Env.* 788:147541.
- SILVA, D.R. , VIANA V.P., MÜLLER A.M., et al. 2014. Respiratory viral infections and effects of meteorological parameters and air pollution in adults with respiratory symptoms admitted to the emergency room. *Influenza Other Respir. Viruses*, 8: 42–52.
- SIMEONOVA, P.P., ERDELY, A. 2009. Engineered nanoparticle respiratory exposure and potential risks for cardiovascular toxicity: predictive tests and biomarkers. *Inhal Toxicol*, 21 Suppl 1:68-73.
- SIMOES, E.A., CARBONELL-ESTRANY, X., RIEGER, C.H., MITCHELL, I., FREDRICK, L., GROOTHUIS, J.R. 2010. Palivizumab Long-Term Respiratory Outcomes Study G The effect of

- respiratory syncytial virus on subsequent recurrent wheezing in atopic and nonatopic children. *J Allergy Clin Immunol*, 126(2):256–262.
- SIMPSON, J.L., SCOTT, R., BOYLE, M.J., GIBSON, P.G. 2006. Inflammatory subtypes in asthma: assessment and identification using induced sputum. *Respirology*, 11, 54-61.
- SINCLAIR, J., SISSONS, P. 2006. Latency and reactivation of human cytomegalovirus. *J Gen Virol*, 87, 1763–1779.
- SINGH, D., MARROCCO, A., WOHLLEBEN, W., PARK, H.R., DIWADKAR, A.R., HIMES, B.E., LU, Q., CHRISTIANI, D.C., DEMOKRITOU, P. 2022. Release of particulate matter from nano-enabled building materials (NEBMs) across their lifecycle: Potential occupational health and safety implications. *J Hazard Mater*, 15;422:126771.
- SINGH, P., MADDEN, M., GILMOUR, M.I. 2004. Effects of diesel exhaust particles and carbon black on induction of dust mite allergy in brown norway rats. *J Immunol*, 2:41-49.
- SNIDER, G.L. 1985. Distinguishing among asthma, chronic bronchitis, and emphysema. *Chest*, 87:1, 35S–39S.
- SLOBEDMAN, B., MOCARSKI, E.S. 1999. Quantitative analysis of latent human cytomegalovirus. *J Virol*, 73, 4806–4812.
- SNYDER-TALKINGTON, B.N., DONG, C., PORTER, D.W., DUCATMAN, B., WOLFARTH, M.G., ANDREW, M., BATTELLI, L., RAESE, R., CASTRANOVA, V., GUO, N.L., QIAN, Y. 2016. Multiwalled carbon nanotube-induced pulmonary inflammatory and fibrotic responses and genomic changes following aspiration exposure in mice: a 1-year postexposure study. *J Toxicol Environ Health A*, 79(8):352-66.
- SORIANO, J.B., KENDRICK, P., PAULSON, K., GUPTA, V., VOS, T. 2020. Prevalence and attributable health burden of chronic respiratory diseases, 1990–2017: a systematic analysis for the Global Burden of Disease Study 2017. *Lancet Respir Med*, 8: 585-596.
- SPECK, S.H., GANEM, D. 2010. Viral latency and its regulation: Lessons from the gamma-herpesviruses. *Cell Host Microbe*, 8:100–115.
- STAUDT, M.R., DITTMER, D.P. 2007. The RTA/ORF50 transactivator proteins of the gamma-herpesviridae. *Curr Topics Microbiol Immunol*, 312:71–100.
- STEER, B., ADLER, B., JONJIC, S., STEWART, J.P., ADLER, H. 2010. A gammaherpesvirus complement regulatory protein promotes initiation of infection by activation of protein kinase Akt/PKB. *Plos. one*, 5:e11672.
- STERMANN, T., NGUYEN, T., STAHLMECKE, B., TODEA, A.M., WOESTE, S., HACHENEY, I., KRUTMANN, J., UNFRIED, K., SCHINS, R.P.F., ROSSI, A. 2022. Carbon nanoparticles adversely affect CFTR expression and toxicologically relevant pathways. *Sci Rep*, 22;12(1):14255.
- STEVENS, J.G. 1989. Human herpesviruses: a consideration of the latent state. *Microbiol Rev*, 53, 318–332.
- STEVENSON, P.G., CARDIN, R.D., CHRISTENSEN, J.P., DOHERTY, P.C. 1999. Immunological control of a murine gammaherpesvirus independent of CD8+T-cells. *J Gen Virol*, 80:477–483.
- STEWART, J.P., EGAN, J.J., ROSS, A.J., KELLY, B.G., LOK, S.S., HASLETON, P.S., WOODCOCK, A.A. 1999. The detection of Epstein-Barr virus DNA in lung tissue from patients with idiopathic pulmonary fibrosis. *Am J Respir Crit Care Med*, 159(4 pt 1):1336–1341.
- STOEGER, T., ADLER, H. 2018. “Novel” Triggers of Herpesvirus Reactivation and Their Potential Health Relevance. *Front Microbiol*, 9: 3207.
- STOEGER, T., TAKENAKA, S., FRANKENBERGER, B., RITTER, B., KARG, E., MAIER, K., SCHULZ, H., SCHMID, O. 2009. Deducing in vivo toxicity of combustion-derived nanoparticles from a cell-free oxidative potency assay and metabolic activation of organic compounds. *Environ Health Perspect*, 117:54-60.

References

- STOEGER, T., SCHMID, O., TAKENAKA, S., SCHULZ, H. 2007. Inflammatory response to TiO₂ and carbonaceous particles scales best with BET surface area. *Environ Health Perspect*, 115(6):A290–291.
- STOEGER, T., REINHARD, C., TAKENAKA, S., SCHROEPEL, A., KARG, E., RITTER, B., HEYDER, J., SCHULZ, H. 2006. Instillation of six different ultrafine carbon particles indicates a surface area threshold dose for acute lung inflammation in mice. *Environmental Health Perspectives*, 114 (3): 328–333.
- STORISTEANU, D.M., POCOCCO, J.M., COWBURN, A.S., JUSS, J.K., NADESALINGAM, A., NIZET, V., CHILVERS, E.R. 2017. Evasion of neutrophil extracellular traps by respiratory pathogens. *Am J Respir Cell Mol Biol*, 56:423–431.
- SU, W., WU X., GENG X., et al. 2019. The short-term effects of air pollutants on influenza-like illness in Jinan, China. *BMC Public Health*, 19: 1319–1319.
- SUN S, YAO Y, HUANG C, XU H, ZHAO Y, WANG Y, ZHU Y, MIAO Y, FENG X, GAO X, ZHENG J, ZHANG Q. 2022. CD36 regulates LPS-induced acute lung injury by promoting macrophages M1 polarization. *Cell Immunol*, 372:104475.
- SUNIL-CHANDRA, N. P., ARNO, J., FAZAKERLEY, J., NASH, A. A. 1994. Lymphoproliferative disease in mice infected with murine gammaherpesvirus 68. *Am J Pathol*, 145:818–826.
- SUNIL-CHANDRA, N.P., EFSTATHIOU, S., NASH, A.A. 1992. Murine gamma-herpesvirus 68 establishes a latent infection in mouse B lymphocytes in vivo. *J. Gen. Virol*, 73:3275–3279
- SZE, E., BHALLA, A., NAIR, P. 2019. Mechanisms and therapeutic strategies for non-T2 asthma. *Europ J Allergy Clin Immunol*, 75(2):311-325.
- SZONDY, Z., GARABUCZI, E., JOOS, G., TSAY, G. J., SARANG, Z. 2014. Impaired clearance of apoptotic cells in chronic inflammatory diseases: therapeutic implications. *Front. Immunol*. 5,354.
- TAGER, A.M., LACAMERA, P., SHEA, B.S., CAMPANELLA, G.S., SELMAN, M., ZHAO, Z., POLOSUKHIN, V., WAIN, J., KARIMI-SHAN, B.A., KIM, N.D., HART, W.K., PARDO, A., BLACKWELL, T.S., XU, Y., CHUN, J., LUSTER, A.D. 2008. The lysophosphatidic acid receptor lpa1 links pulmonary fibrosis to lung injury by mediating fibroblast recruitment and vascular leak. *Nat Med*, 14: 45–54.
- TAKAGI, A., HIROSE, A., NISHIMURA, T., FUKUMORI, N., OGATA, A., OHASHI, N., KITAJIMA, S., KANNO, J. 2008. Induction of mesothelioma in p53^{+/-} mouse by intraperitoneal application of multi-wall carbon nanotube. *J Toxicol Sci*, 33:105–116.
- TAN, S.Y., KRASNOW, M.A. 2016. Developmental origin of lung macrophage diversity. *Development*, 143:1318–27.
- TANKERSLEY, C.G., SHANK, J.A., FLANDERS, S.E., SOUTIERE, S.E., RABOLD, R., MITZNER, W., WAGNER, E.M. 2003. Changes in lung permeability and lung mechanics accompany homeostatic instability in senescent mice. *J Appl Physiol*, 95(4):1681-7.
- TAYLOR, G.S., LONG, H.M., BROOKS, J.M., RICKINSON, A.B., HISLOP, A.D. 2015. The immunology of Epstein-Barr virus-induced disease. *Annu Rev Immunol*, 33(1):787-821.
- THURSTON, G.D., BALMES, J.R., GARCIA, E., GILLILAND, F.D., RICE, M.B., SCHIKOWSKI, T., VAN WINKLE, L.S., ANNESI-MAESANO, I., BURCHARD, E.G., CARLSTEN, C., HARKEMA, J.R., KHREIS, H., KLEEBERGER, S.R., KODAVANTI, U.P., LONDON, S.J., MCCONNELL, R., PEDEN, D.B., PINKERTON, K.E., REIBMAN, J. 2020. Outdoor air pollution and new-onset airway disease. An official american thoracic society workshop report. *Ann Am Thorac Soc*, 17(4):387-398.
- THOMSON, N.C., CHAUDHURI, R. 2009. Asthma in smokers: challenges and opportunities. *Curr Opin Pulm Med*, 15(1):39-45.
- THOMSON, N.C., CHAUDHURI, R., LIVINGSTON, E. 2004. Asthma and cigarette smoking. *Eur Respir J*, 24(5):822-33.
- TIAN, F., HABEL, N.C., YIN, R., HIRN, S., BANERJEE, A., ERCAL, N., TAKENAKA, S., ESTRADA, G., KOSTARELOS, K., KREYLING, W., STOEGER, T. 2013. Pulmonary DWCNT exposure causes

- sustained local and low-level systemic inflammatory changes in mice. *Eur J Pharm Biopharm*, 84(2):412-20.
- TOMOS, I., DIMAKOPOULOU, K., MANALI, E.D., PAPIRIS, S.A., KARAKATSANI, A. 2021. Long-term personal air pollution exposure and risk for acute exacerbation of idiopathic pulmonary fibrosis. *Environ Health*, 20: 99.
- TOMOS, I., KARAKATSANI, A., MANALI, E.D., KOTTARIDI, C., SPATHIS, A., ARGENTOS, S., PAPIRIS, S.A. 2020. Telomere length across different UIP fibrotic-Interstitial Lung Diseases: A prospective Greek case-control study. *Pulmonology*, S2531–0437(20):30248–30258.
- TOYOKUNI, S. 2013. Genotoxicity and carcinogenicity risk of carbon nanotubes. *Adv Drug Deliv Rev*, 65:2098–2110.
- TOYOKUNI, S. 2009. Mechanisms of asbestos-induced carcinogenesis. *Nagoya J Med Sci*, 71:1–10.
- TROEGER, C., FOROUZANFAR, M., RAO, P.C., KHALIL, I., BROWN, A., SWARTZ, S., FULLMAN, N., MOSSER, J., THOMPSON, L.R., REINER, R.C., ABAJOBIR, A., ALAM, N., ALEMAYOHU, M.A., AMARE, A.T., ANTONIO, C.A., ASAYESH, H., AVOKPAHO, E., BARAC, A., BESHIR, M.A., BONEYA, D.J., BRAUER, M., DANDONA, L., DANDONA, R., FITCHETT, J.R.A., GEBREHIWOT, T.T., HAILU, G.B., HOTEZ, P.J., KASAEIAN, A., KHOJA, T., KISSOON, N., KNIBBS, L., KUMAR, A.G., RAI, R.K., ABD EL RAZEK, H.M., MOHAMMED, M.S.K., NIELSON, K., OREN, E., OSMAN, A., PATTON, G., QORBANI, M., ROBA, H.S., SARTORIUS, B., SAVIC, M., SHIGEMATSU, M., SYKES, B., SWAMINATHAN, S., TOPOR-MADRY, R., UKWAJA, K., WERDECKER, A., YONEMOTO, N., EL SAYED ZAKI, M., LIM, S.S., NAGHAVI, M., VOS, T., HAY, S.I., MURRAY, C.J.L., MOKDAD, A.H. 2017. Estimates of the global, regional, and national morbidity, mortality, and aetiologies of lower respiratory tract infections in 195 countries: a systematic analysis for the Global Burden of Disease Study 2015. *The Lancet Infectious Diseases*, 17(11)1133-1161.
- TSENG, C.H., TSUANG, B.J., CHIANG, C.J., KU, K.C., TSENG, J.S., YANG, T.Y., HSU, K.H., CHEN, K.C., YU, S.L., LEE, W.C., LIU, T.W., CHAN, C.C., CHANG, G.C. 2019. The Relationship Between Air Pollution and Lung Cancer in Nonsmokers in Taiwan. *J Thorac Oncol*, 14(5):784-792.
- TURUNEN, R., JARTTI, T., BOCHKOV, Y.A., GERN, J.E., VUORINEN, T. 2016. Rhinovirus species and clinical characteristics in the first wheezing episode in children. *J Med Virol*, 88(12):2059–2068.
- UMETSU, D.T., DEKRUYFF, R.H. 2006. The regulation of allergy and asthma. *Immunol Rev*, 212:238–255.
- UPPAL, T., BANERJEE, S., SUN, Z., VERMA, S.C., ROBERTSON, E.S. 2014. KSHV LANA—the master regulator of KSHV latency. *Viruses*, 6, 4961–4998.
- URAL, B.B., CARON, D.P., DOGRA, P., WELLS, S.B., SZABO, P.A., GRANOT, T., SENDA, T., POON, M.M.L., LAM, N., THAPA, P., LEE, Y.S., KUBOTA, M., MATSUMOTO, R., FARBER, D.L. 2022. Inhaled particulate accumulation with age impairs immune function and architecture in human lung lymph nodes. *Nat Med*, 28:2622-2632.
- VALAVANIDIS A, FIOTAKIS K, VLACHOGIANNI T. 2008. Airborne particulate matter and human health: toxicological assessment and importance of size and composition of particles for oxidative damage and carcinogenic mechanisms. *J Environ Sci Health C Environ Carcinog Ecotoxicol Rev*, 26(4):339-62.
- VALBERG, P.A., LONG, C.M., SAX, S.N. 2006. Integrating studies on carcinogenic risk of carbon black: epidemiology, animal exposures, and mechanism of action. *J. Occup. Environ. Med*, 48:1291–1307.
- VAN DER STRATE, B.W., POSTMA, D.S., BRANDSMA, C.A., MELGERT, B.N., LUNGE, M.A., GEERLINGS, M., HYLKEMA, M.N., VAN DEN BERG, A., TIMENS, W., KER-STJENS, H.A. 2006. Cigarette smoke-induced emphysema: a role for the B cell? *AmJ Respir Crit Care Med*, 173: 751–758.
- VAN DYKEN, S.J., LOCKSLEY, R.M. 2013. Interleukin-4- and Interleukin-13-Mediated Alternatively Activated Macrophages: Roles in Homeostasis and Disease. *Annu. Rev. Immunol.* 31:317–343.

References

- VEMPILLY, J., ABEJIE B., DIEP V., et al. 2013. The synergetic effect of ambient PM_{2.5} exposure and rhinovirus infection in airway dysfunction in asthma: a pilot observational study from the Central Valley of California. *Exp. Lung Res*, 39: 434–440.
- VENKITARAMAN, A.R., LENOIR, G.M., JOHN, T.J. 1985. The seroepidemiology of infection due to Epstein-Barr virus in southern India. *J Med Virol*, 15(1):11-6.
- VERMA, A.K., MCKELVEY, M., UDDIN, M.B., PALANI, S., NIU, M., BAUER, C., SHAO, S., SUN, K. 2022. IFN- γ transforms the transcriptomic landscape and triggers myeloid cell hyperresponsiveness to cause lethal lung injury. *Front Immunol*, 20;13:1011132.
- VIEGI, G., PAOLETTI, P., PREDILETTO, R., DI PEDE, F., CARROZZI, L., CARMIGNANI, G., MAMMINI, U., LEBOWITZ, M.D., GIUNTINI, C. 1990. Carbon monoxide diffusing capacity, other indices of lung function, and respiratory symptoms in a general population sample. *Am Rev Respir Dis*, 141, 1033-1039.
- VIETTI, G., LISON, D., VAN DEN BRULE, S. 2016. Mechanisms of lung fibrosis induced by carbon nanotubes: towards an Adverse Outcome Pathway (AOP). *Part Fibre Toxicol*, 13:11.
- VIRGIN, H.W., WHERRY, E.J., AHMED, R. (2009). Redefining chronic viral infection. *Cell*, 138, 30–50.
- WANG, J., LI, X., WANG, Y., LI, Y., SHI, F., DIAO, H. 2022. Osteopontin aggravates acute lung injury in influenza virus infection by promoting macrophages necroptosis. *Cell Death Discov*, 4;8(1):97.
- WANG, Y., ADAMCAKOVA-DODD, A., STEINES, B.R., JING, X., SALEM, A.K., THORNE, P.S. 2020. Comparison of *in vitro* toxicity of aerosolized engineered nanomaterials using air-liquid interface mono-culture and co-culture models. *NanoImpact*, 18:100215.
- WANG, L., BAO, S., LIU, X., WANG, F., ZHANG, J., DANG, P., WANG, F., LI, B., LIN, Y. 2021. Low-dose exposure to black carbon significantly increase lung injury of cadmium by promoting cellular apoptosis. *Ecotox Environ Safety*, 224, 112703.
- WANG, L., XU, J., LIU, H., LI, J., HAO, H. 2019a PM_{2.5} inhibits SOD1 expression by up-regulating microRNA-206 and promotes ROS accumulation and disease progression in asthmatic mice. *Int. Immunopharmacol*, 76:105871.
- WANG, M., AARON, C.P., MADRIGANO, J., HOFFMAN, E.A., ANGELINI, E., YANG, J., LAINE, A., VETTERLI, T.M., KINNEY, P.L., SAMPSON, P.D., SHEPPARD, L.E., SZIPRO, A.A., ADAR, S.D., KIRWA, K., SMITH, B., LEDERER, D.J., DIEZ-ROUX, A.V., VEDAL, S., KAUFMAN, J.D., BARR, G. 2019b. Association Between Long-term Exposure to Ambient Air Pollution and Change in Quantitatively Assessed Emphysema and Lung Function. *JAMA*, 322(6):546-556.
- WANG, Y., THANG, Z., HUANG, H., LI, J., WANG, Z., YU, Y., ZHANG, C., LI, J., DAI, H., WANG, F., CAI, T. 2017. Pulmonary alveolar type I cell population consists of two distinct subtypes that differ in cell fate. *PNAS*, 115(10)2407-2412.
- WANG, X., XIA, T., DUCH, M.C., JI, Z., ZHANG, H., LI, R., SUN, B., LIN, S., MENG, H., LIAO, Y.P., WANG, M., SONG, T.B., YANG, Y., HERSAM, M.C., NEL, A.E. 2012. Pluronic F108 coating decreases the lung fibrosis potential of multiwall carbon nanotubes by reducing lysosomal injury. *Nano Lett*, 12(6):3050-61.
- WARDEN, C., TANG, Q., ZHU, H. 2011. Herpesvirus BACs: past, present, and future. *J Biomed Biotechnol*, 2011:124595.
- WECK, K.E., BARKON, M.L., YOO, L.I., et al. 1996. Mature B-cells are required for acute splenic infection, but not for establishment of latency, by murine gammaherpesvirus 68. *J Virol*, 70:6775–6780.
- WECK, K. E., KIM, S.S., VIRGIN, H.I., SPECK, S.H. 1999. Macrophages are the major reservoir of latent murine gammaherpes-virus 68 in peritoneal cells. *J Virol*, 73:3273–3283.
- WEINREICH, U.M., THOMSEN, L.P., BROCK, C., KARBING, D.S., AND REES, S.E. 2015. Diffusion capacity of the lung for carbon monoxide - A potential marker of impaired gas exchange or of systemic deconditioning in chronic obstructive lung disease? *Chron Respir Dis*, 12, 357-364.
- WEN, K. W., DAMANIA, B. 2010. Kaposi Sarcoma-associated herpesvirus(KSHV): Molecular biology and oncogenesis. *Cancer Lett*, 289:140–150.

- WENZEL, S.E. 2012. Asthma phenotypes: the evolution from clinical to molecular approaches. *Nature America*, 18(5), 716–725.
- WHITLEY, R.J. (1996). Herpesviruses. University of Texas Medical Branch at Galveston.
- WHO (World Health Organization). 2023. Air pollution.
- WHO (World Health Organization). 2007. Global surveillance, prevention and control of chronic respiratory diseases: a comprehensive approach.
- WICHMANN, J., FOLKE, F., TORP-PEDERSEN, C., LIPPERT, F., KETZEL, M., ELLERMANN, T., LOFT, S. 2013. Out-of-hospital cardiac arrests and outdoor air pollution exposure in Copenhagen, Denmark. *PLoS ONE*, 8:e53684.
- WILLIAMS, M., TODD, I., FAIRCLOUGH, L.C. 2021. The role of CD8+ T lymphocytes in chronic obstructive pulmonary disease: a systematic review. *Inflamm Res*, 70(1): 11–18.
- WONG, J., MAGUN, B.E., WOOD, L.J. 2016. Lung inflammation caused by inhaled toxicants: a review. *Int J Chron Obstruct Pulmon Dis*, 23;11:1391-401.
- WONG, C.M. , YANG L., THACH T.Q., et al. 2009. Modification by influenza on health effects of air pollution in Hong Kong. *Environ. Health Perspect*. 117: 248–253.
- WROTEK, A., JACKOWSKA, T. 2022. Molecular mechanisms of RSV and air pollution interaction: a scoping review. *Int J Mol Sci*, 21;23(20):12704.
- WU, W., JIN, Y., CARLSTEN, C. 2018. Inflammatory health effects of indoor and outdoor particulate matter. *J Allergy Clin Immunol*, 141(3), 833-844.
- WU, X., NETHERY, R.C., SABATH, M.B., BRAUN, D., DOMINICI, F. 2020. Air pollution and COVID-19 mortality in the United States Strengths and limitations of an ecological regression analysis. *Sci Adv*, 6(45)
- WU, T. T., USHERWOOD, E. J., STEWART, J. P., et al. 2000. RTA of murine gammaherpesvirus 68 re-activates the complete lytic cycle from latency. *J Virol*, 74:3659–3667.
- XIA, R., ZHOU, G., ZHU, T., LI, X., WANG, G. 2017. Ambient Air Pollution and Out-of-Hospital Cardiac Arrest in Beijing, China. *Int. J. Environ. Res. Public Health*, 14:423.
- XIONG, J., LI, J., WU, X., WOLFSON, J.M., LAWRENCE, J., STERN, R.A., KOUTRAKIS, P., WEI, J., HUANG, S. 2022. The association between daily-diagnosed COVID-19 morbidity and short-term exposure to PM₁ is larger than associations with PM_{2.5} and PM₁₀. *Environ Res*, 210:113016.
- YANG, L., LIU, G., FU, L., ZHONG, W., LI, X., PAN, Q. 2020. DNA repair enzyme OGG1 promotes alveolar progenitor cell renewal and relieves PM_{2.5}-induced lung injury and fibrosis. *Ecotoxicol Environ Saf*, 1;205:111283.
- YANG, H.M., NAM, W.K., PARK, D.W. 2007. Production of nanosized carbon black from hydrocarbon by a thermal plasma. *J. Nanosci. Nanotechnol*. 7:3744–3749.
- YAO, Y., WANG, Y., ZHANG, Z., HE, L., ZHU, J., ZHANG, M., HE, X., CHENG, Z., AO, Q., CAO, Y., YANG, P., SU, W., ZHAO, J., ZHANG, S., YU, Q., NING, Q., XIANG, X., XIONG, W., WANG, C.-Y., XU, Y. 2016. Chop Deficiency Protects Mice Against Bleomycin-induced Pulmonary Fibrosis by Attenuating M2 Macrophage Production. *Mol. Ther*. 2016;24:915–925.
- YAO, Y., JEYANATHAN, M., HADDADI, S., BARRA, N.G., VASEGHI-SHANJANI, M., DAMJANOVIC, D., LAI, R., AFKHAMI, S., CHEN, Y., DVORKIN-GHEVA, A., ROBBINS, C.S., SCHERTZER, J.D., XING, Z. 2018. Induction of autonomous memory alveolar macrophages requires T cell help and is critical to trained immunity. *Cell* 175, 1634–1650.
- YARILIN, D. A., VALIANDO, J., AND POSNETT, D. N. 2004. A mouse herpesvirus induces relapse of experimental autoimmune arthritis by infection of the inflammatory target tissue. *J Immunol*, 173:5238–5246.
- YE, T., XU, R., YUE, X., CHEN, G., YU, P., COELHO, M.S.Z.S., SALDIVA, P.H.N., ABRAMSON, M.J., GUO, Y., LI, S. 2022. Short-term exposure to wildfire-related PM_{2.5} increases mortality risks and burdens in Brazil. *Nat Commun*, 10;13(1):7651.

References

- YE, F., ZHOU, F., BEDOLLA, R.G., JONES, T., LEI, X., KANG, T., GUADALUPE, M., GAO, S.-J. 2011a. Reactive oxygen species hydrogen peroxide mediates Kaposi's sarcoma-associated herpesvirus reactivation from latency. *PLoS Pathog*, 7(5):e1002054.
- YE, F., LEI, X., GAO, S.-J. 2011b. Mechanisms of Kaposi's Sarcoma-Associated herpesvirus latency and reactivation. *Adv Virol*, 2011:193860.
- YING, S., O'CONNOR, B., RATOFF, J., MENG, Q., FANG, C., COUSINS, D., ZHANG, G., GU, S., GAO, Z., SHAMJI, B., EDWARDS, M.J., LEE, T.H., CORRIGAN, C.J. 2008. Expression and cellular provenance of thymic stromal lymphopoietin and chemokines in patients with severe asthma and chronic obstructive pulmonary disease. *J Immunol*, 181:2790–2798.
- YONA, S., KIM, K.-W., WOLF, Y., MILDNER, A., VAROL, D., BREKER, M. STRAUSS-AYALI, S., VIUKOV, S., GUILLIAMS, M., MISHARIN, A., HUME, D.A., PERLMAN, H., MALISSEN, B., ZELZER, E., JUNG, S. 2013. Fate mapping reveals origins and dynamics of monocytes and tissue macrophages under homeostasis. *Immunity*, 38(1):79–91.
- YOU R., LU W., SHAN M., BERLIN J. M., SAMUEL E. L. G., MARCANO D. C., SUN Z., SIKKEMA W. K. A., YUAN X., SONG L., HENDRIX A. Y., TOUR J. M., CORRY D. B., KHERADMAND F. 2015. Nanoparticulate carbon black in cigarette smoke induces DNA cleavage and Th17-mediated emphysema. *eLife* 4, e09623.
- YUAN, X., NIE, W., HE, Z., YANG, J., SHAO, B., MA, X., ZHANG, X., BI, Z., SUN, L., LIANG, X., TIE, Y., LIU, Y., MO, F., XIE, D., WEI, Y., WEI, X. 2020. Carbon black nanoparticles induce cell necrosis through lysosomal membrane permeabilization and cause subsequent inflammatory response. *Theranostics*, 15;10(10):4589-4605.
- YUE, D., ZHANG, Q., ZHANG, J., LIU, W., CHEN, L., WANG, M., LI, R., QIN, S., SONG, X., JI, Y. 2022. Diesel exhaust PM2.5 greatly deteriorates fibrosis process in pre-existing pulmonary fibrosis via ferroptosis. *Environ Int*, 19;171:107706.
- YUWONO, A.S., LAMMERS, P.S. 2004. Odor Pollution in the environment and the detection instrumentation. *Agricultural Engineering International: the CIGR Journal of Scientific Research and Development*. Invited Overview Paper. Vol. VI.
- ZAWROTNIAK, M. & RAPALA-KOZIK, M. 2013. Neutrophil extracellular traps (NETs) - formation and implications. *Acta Biochim. Pol.* 60,277–284.
- ZHANG, F., MEARS, J.R., SHAKIB, L., BEYNOR, J.I., SHANAJ, S., KORSUNSKY, I., NATHAN, A.; ACCELERATING MEDICINES PARTNERSHIP RHEUMATOID ARTHRITIS AND SYSTEMIC LUPUS ERYTHEMATOSUS (AMP RA/SLE) CONSORTIUM, DONLIN, L.T., RAYCHAUDHURI, S. 2021. IFN- γ and TNF- α drive a CXCL10+ CCL2+ macrophage phenotype expanded in severe COVID-19 lungs and inflammatory diseases with tissue inflammation. *Genome Med*, 20;13(1):64.
- ZHANG, J., LI, X., CHENG, W., LI, Y., SHI, Y., JIANG, Y., WANG, T., WANG, H., REN, D., ZHANG, R., ZHENG, Y., TANG, J. 2022a. Chronic carbon black nanoparticles exposure increases lung cancer risk by affecting the cell cycle via circulating inflammation. *Environ Pollut*, 15;305:119293.
- ZHANG, R., CHEN, S., CHEN, L., YE, L., JIANG, Y., PENG, H., GUO, Z., LI, M., JIANG, X., GUO, P., YU, D., ZHANG, R., NIU, Y., ZHUANG, Y., ASCHNER, M., ZHENG, Y., LI, D., CHEN, W. 2022b. Single-cell transcriptomics reveals immune dysregulation mediated by IL-17A in initiation of chronic lung injuries upon real-ambient particulate matter exposure. *Part Fibre Toxicol*, 23;19(1):42.
- ZHAO, B., VO, H.Q., JOHNSTON, F.H., NEGISHI, K. 2018. Air pollution and telomere length: a systematic review of 12,058 subjects. *Cardiovasc Diagn Ther*, 8(4):480–492.
- ZHEN, X., NG, W.C., FENDY, TONG, Y.W., DAI, Y., NEOH, K.G., WANG, C.H. 2017. Toxicity assessment of carbon black waste: A by-product from oil refineries. *J Hazard Mater*, 5;321:600-610.

6. Appendix A:

6.1 Background – Inhaled particles influence systemic inflammation

Reports, about particulate matter triggered health effects are not limited to respiratory health, in fact particularly systemic effects are reported to be initiated after air pollution or nanoparticle exposure such as related to traffic emissions (Peters et al., 2004; Mills et al., 2007). In this context, it has been reported that nanoparticles can translocate from the pulmonary side into the blood circulation (Nemmar et al., 2001, 2002a, 2002b, 2003; Geiser and Kreyling, 2010) and recently nanoparticles were found to persist in the lymph nodes accumulating over lifetime and impairs immune function in decreased activation, phagocytic capacity and altered phagocytosis in macrophages in the lymph nodes (Ural et al., 2022). Pulmonary exposure to multiwalled carbon nanoparticles were found to induce diverse profile of matrix proteases and complex peptidomic response also in the blood compartments (Mostovenko et al., 2019). And stroke, cardiovascular and lung cancer mortality increased after exposure with PM_{2.5} with adverse changes in blood pressure, systemic inflammation, heart rate variability and blood lipids in short-term and long-term PM_{2.5} exposure (Luo et al., 2022).

The acute phase response plays a role in systemic inflammation and is defined as physiological and systemic alterations induced by infection and tissue injury. Serum Amyloid A (SAA) and C-reactive protein (CRP) are the major regulated acute phase proteins and already observed for several years to be upregulated during acute phase response (Gabay et al., 1999). And significant association between SAA3 proteins and coronary artery diseases like arteriosclerosis were found (Fyfe et al., 1997). In mice, in contrast to humans, only SAA not CRP is regulated followed by acute phase response. Inhalation of particulate air pollution has been described to be associated with cardiovascular diseases. It is known that the SAA3 gene and protein is increased in the lung after CNP instillation (Kyjovska et al, 2015a, Kyjovska et al, 2015b).

It has been shown that SAA3 mRNA expression in the lung is positively correlated with blood levels of SAA3 following pulmonary exposure to carbon black, diesel

exhaust and engine particles (Bourdon et al., 2012.; Bendtsen et al., 2019) which is associated with development of cardiovascular diseases.

In summary, nanoparticle inhalation may not only effect development and exacerbation of chronic lung disease but also effect disease progression in secondary organs that may lead to cardiovascular disease.

6.2 Results – Indication for elevated systemic inflammation after repeated particle instillation

Serum amyloid A 3 (SAA3) is known to be a robust biomarker of infection, inflammation and injury. It predicts cardiovascular events. In increased SAA expression, the development of atherosclerosis, rheumatic arthritis and Type 2 diabetes is higher.

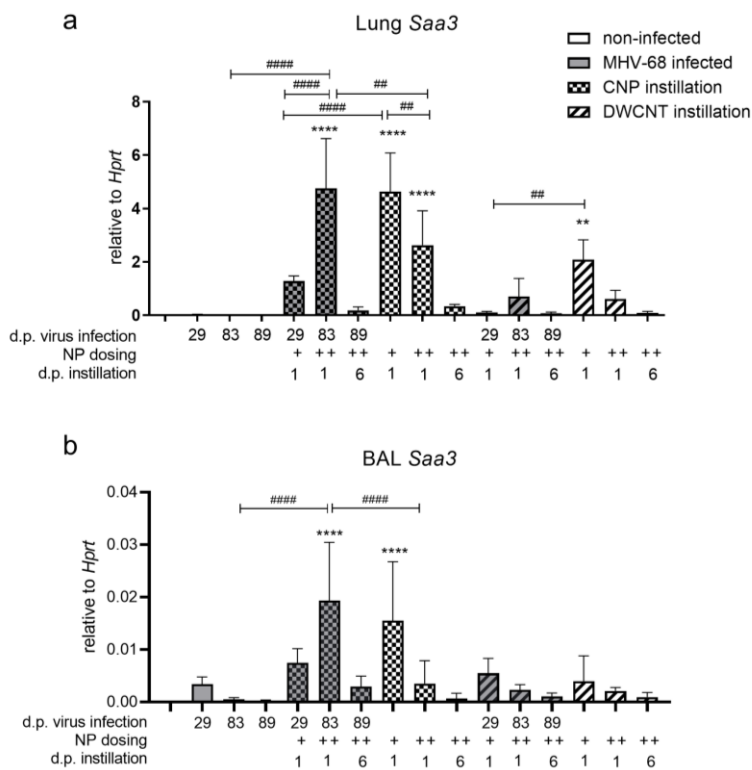


Figure 6.1. Increased lung and BAL cell gene expression of Saa3 in CNP exposure.

Lung tissue was isolated and homogenized and BAL cells were collected after virus infection and NP treatment. RNA was isolated and cDNA was synthesized. Saa3 gene expression was analyzed normalized to the expression of the housekeeper gene Hprt. (a) shows gene expression of Saa3 in whole lung homogenate. (b) shows gene expression of Saa3 in BAL cells. (n = 5). Data were analyzed by Ordinary one-way ANOVA and Tukey’s multiple comparisons test, “*” indicates statistically significant difference to “control”. *: indicates P value < 0.05. **: indicates P value < 0.01. ***: indicates P value <

0.001. ****: indicates P value < 0.0001. “#” indicates statistically significant difference of two indicated groups. #: indicates P value < 0.05. ##: indicates P value < 0.01. ###: indicates P value < 0.001. ####: indicates P value < 0.0001.

To investigate the *Saa3* expression in the lung tissue and BAL cells, I isolated the RNA and synthesized cDNA. With qPCR the *Saa3* gene expression was detected and normalized to the housekeeper gene *Hprt*. Here I found significant increased *Saa3* expression in the lung tissue in first and repeated CNP exposure in non-infected lungs, in the repeated CNP exposure in infected lungs and in the first DWCNT exposure in non-infected lungs (**Fig. 6.31a**). In the BAL cells, *Saa3* expression is significantly high in the first CNP exposure in non-infected animals and in the repeated CNP exposure in MHV-68 infected (**Fig. 6.31b**). Similar to previous results, the same trend can be observed where the expression increases in virus infected mice from first to repeated CNP exposure, whereas the expression decreases from first to repeated CNP exposure in non-infected mice. This trend can also be seen in the lung expression after DWCNT exposure (**Fig. 6.31a**).

To investigate the SAA3 protein content in the lungs, proteins from whole lung homogenate were isolated. Proteins were separated according to the size by SDS-PAGE and blotted to a membrane. SAA3 concentration was measured by detecting the protein on the membrane by anti-SAA3 staining (**Fig. 6.32a**). SAA3 intensity on the membrane was measured and analyzed relative to the housekeeper protein β -actin (**Fig. 6.32b**). SAA3 protein concentration significantly increase in the first CNP exposure in uninfected lungs and in the repeated CNP exposure in MHV-68 infected lungs. This confirms the trend, what was observed in the whole lung gene expression before. Increased *Saa3* expression and SAA3 protein content in the lungs were observed, which lead to the question, how the SAA3 concentration in the serum of mice change depending on the treatment. To answer this question, blood was collected from orbital vein and serum was isolated. SAA3 ELISA was performed to measure the SAA3 concentration in the serum in $\mu\text{g/mL}$. In the exposure to CNP, the same pattern was observed in the serum with significantly increased SAA3 in first CNP exposure in non-infected mice and increased serum SAA3 in the repeated CNP exposure in MHV-68 infected mice (**Fig. 6.33**).

Appendix A

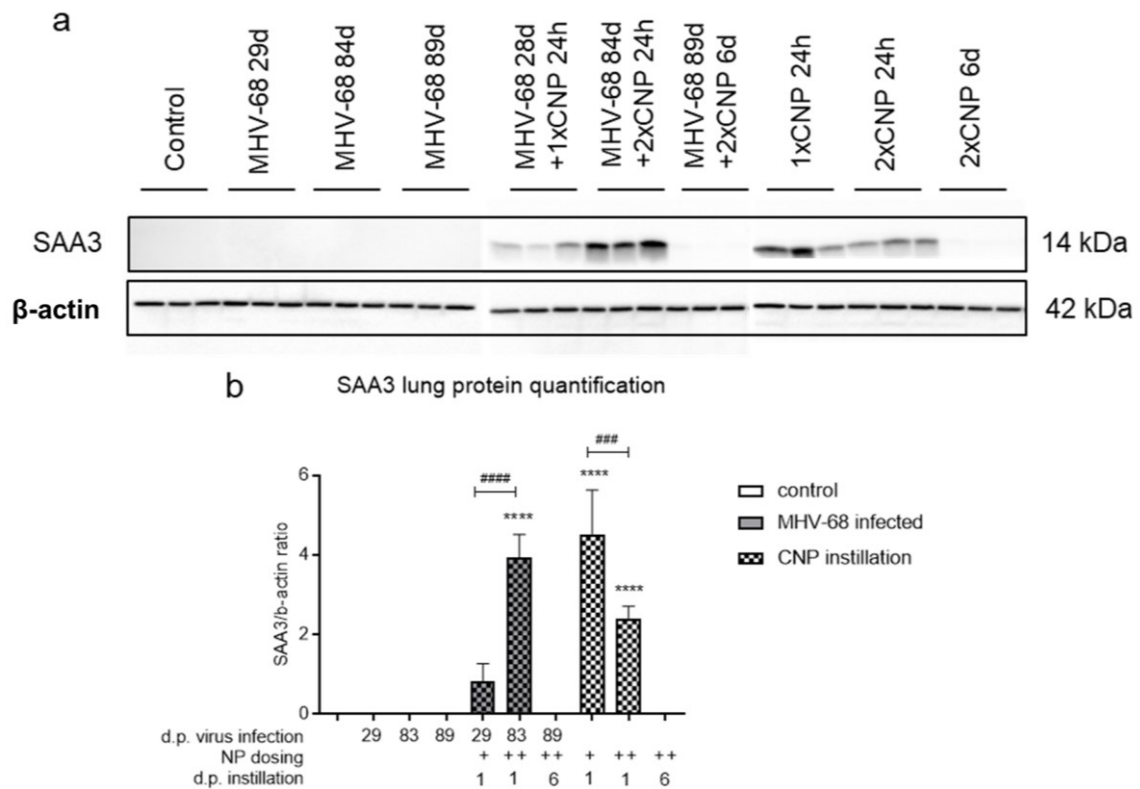


Figure 6.2. Increasing SAA3 protein in lung after repeated CNP instillation in MHV-68 latency and decreasing SAA3 protein in non-infected lungs.

Mice were latently infected with MHV-68 and double treated with CNP. Whole lung protein was extracted. Total protein expression of SAA3 was detected. b-actin was used as a loading control. In (a) western blots of SAA3 and b-actin were shown. In (b) Densitometry analysis of western blot after virus infection and CNP exposure from (a) relative to β -actin. $n=3$. Data was analyzed with One-Way ANOVA and Tukey's multiple comparisons test. "*" indicates statistically significant difference between "control" whereas "#" indicates statistically significant difference between the two groups indicated with the line. ****: $P < 0.0001$, ###: $P < 0.001$, #####: $P < 0.0001$.

These results suggest higher systemic inflammation in the virus infected and repeated NP treated mice compared to the decreasing concentration in the repeated exposure in non-infected animals.

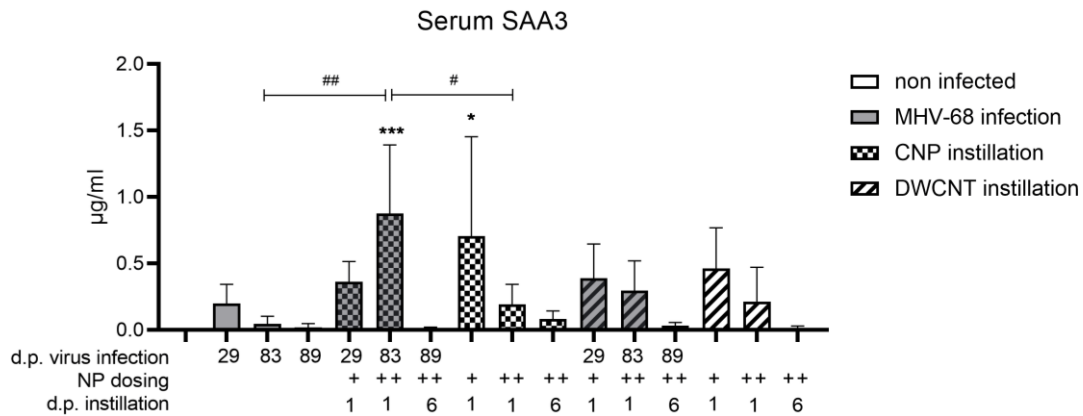


Figure 6.3. Elevated serum SAA3 level in CNP-induced repeated second hit model.

Serum SAA3 concentration was measured in µg/mL with SAA3 ELISA. Significantly increased SAA3 levels in repeated CNP exposure in MHV-68 latency and single CNP exposure in non-infected animals. Significantly higher SAA3 in repeated CNP in latency compared to latency or CNP alone. (n = 5). Data were analyzed by Ordinary one-way ANOVA and Tukey's multiple comparisons test, "*" indicates statistically significant difference to "control". *: indicates *P value* < 0.05. **: indicates *P value* < 0.01. ***: indicates *P value* < 0.001. ****: indicates *P value* < 0.0001. "#" indicates statistically significant difference of two indicated groups. #: indicates *P value* < 0.05. ##: indicates *P value* < 0.01. ###: indicates *P value* < 0.001. ####: indicates *P value* < 0.0001.

6.3 Discussion – Systemic inflammation and extrapulmonary effects of pulmonary nanoparticle exposure and respiratory virus infection

Air pollution and respiratory infections are associated with several health effects. Acute effects and chronic effects resulting from prolonged exposure. The damage caused by particulate matter depends on the concentration and duration of inhalation, as well as the protection of the respiratory system. Air pollution has been shown to have an impact on cardiac arrest (Sielski et al., 2021; Wichmann et al., 2013; Xia et al., 2017). Air pollution and COVID-19 infections impact the pathogenesis of cardiovascular disease and predict the occurrence of perioperative deaths (Sielski et al., 2022; Alanio et al., 2022). In addition, higher total cholesterol levels have been measured in middle-aged and elderly populations as a key factor for cardiocerebrovascular disease in urban areas in southern, southwestern, and northern China (Li et al., 2022). In the study by Dehghani et al. (2022), a positive association was found between exposure

Appendix A

to ozone, particulate matter, and air pollution and cardiovascular disease mortality, as well as a positive association between air pollution and high systolic blood pressure, high LDL cholesterol levels, high body mass index, and type 2 diabetes mellitus. MWCNT exposure is described to affect cholesterol homeostasis, which is important in cardiovascular disease (Poulsen et al., 2015; Simeonova and Erdely, 2009). Cho et al. (2014) found a significant association between cardiovascular disease and air pollution.

Short-term increases in hospitalization rates associated with PM_{2.5} were found for all of the following conditions: cerebrovascular, peripheral, and ischemic heart disease, heart rhythm, COPD, heart failure, respiratory infections and injuries, with the greatest association for heart failure (Dominici et al., 2006). In addition, acute effects of seasonal air pollution were observed in association with higher mortality in hospitalized patients, with variable effects on severe cardiovascular, acute respiratory, and cerebrovascular disease. Only PM_{2.5} has been associated with increased daily mortality in hospitalized patients (Pothirat et al., 2019). Murtas et al. (2019) also detected significant associations between PM₁₀ and cardiovascular related deaths to influenza infection. Exposure to black carbon (CB) during pregnancy increases the risk of preeclampsia, preterm birth, and low birth weight. CB has been shown to induce oxidative stress and placental tissue inflammation, and subsequent placental inflammation has been associated with delays in neurological development (Goriainova et al., 2022). Fu et al. (2022a) found that air pollution increases neuroinflammation, particularly microglial activation, which may be a key mechanism in air pollution-induced Alzheimer's and Parkinson's disease.

Wildfires represent a short-term high exposure to particulate matter and are associated with increased risk of death from cardiovascular and respiratory causes (Ye et al., 2022).

In addition, chronic exposure to air pollution is described to be associated with reduced telomere length and mitochondrial DNA content in children (Hautekiet et al., 2021; Isaevka et al., 2021), and maternal exposure to air pollution during the second and third trimesters of pregnancy impairs fetal telomere length (Harnung Scholten et al., 2020).

Particle-induced SAA3 correlates with neutrophil influx, linking inhaled particles to cardiovascular risk (Saber et al., 2013). For example, inhalation of graphene oxide induces an inflammatory profile with high SAA3 levels (de Luna et al., 2022). SAA3 has

cytokine-like proinflammatory activities and can stimulate the NLRP3 inflammasome of phagocytes to produce high levels of TNF α , IL1 α , IL-1 β , and IL-6, important cytokines for the acute phase response described to promote allergic asthma in mice (Ather et al., 2011). I also found increased Tnf and IL-6 expression and release in bronchoalveolar lavage fluid in the CNP-induced second-beat model. SAA3 is a predictor of the risk of developing cardiovascular disease (Hadrup et al., 2020). My data show that SAA3 levels decrease in uninfected mice and increase in infected mice from first to repeated CNP exposure. This suggests an adaptive effect of the inflammatory response in uninfected animals and an additional inflammatory response in animals latently infected with MHV-68, which I have also seen with various inflammatory markers. Elevated serum SAA3 after repeated CNP exposure in MHV-68 infection suggests a contribution to the development of comorbidities such as cardiovascular disease originating in the lung. Repeated particle dosing in infected animals not only plays a role in exacerbating or developing chronic lung disease, but also has an impact on systemic inflammation. Future experiments with more than two replicates of nanoparticle dosing may lead to a better understanding of immune modulation following latent viral infection and exposure to environmentally relevant nanoparticles

7. Appendix B:

7.1 Background - *In vitro* models to test environmental particles

In previous MHV-68 reactivation work, nanoparticles were tested *in vitro* under submerged conditions for its potential to reactivate the latent MHV-68 infection (Sattler et al., 2017). Approximating lung *in vitro* models to the *in vivo* situation, the usage of air liquid interface culturing and exposure with the commercially available air liquid interface cell (ALICE-CLOUD) exposure chamber rises (Lenz et al., 2009, 2014; Loret et al., 2016).

This model allows the homogenous spreading of nebulized material onto the cell growing on the surface of a membrane on the air. This membrane in the transwell inserts contains pores, which are necessary to supply the cells on the apical site with medium, which is on the basal site of the insert. The nebulized material can be online measured for instance with the deposition using the quartz crystal microbalance (QCM) (Czanderna and Lu, 1984; Bruckenstein and Shay, 1985).

7.2 Results – Establishing of an air liquid exposure system - CNP nebulization trigger MHV-68 reactivation in ANA-1 cell line cultured on air liquid interface

In the lungs of second hit model, the MHV-68 reactivation was observed to be mainly in CD11b positive recruited macrophages. An air liquid interface (ALI) cell exposure (ALICE) system was established to investigate the MHV-68 reactivation *in vitro* under the condition of direct contact of the particles with the cells, which should mimic the more environmental situation. For this system, latently MHV-68 infected and non-infected ANA-1 cells were cultures in a transwell insert and apical medium was removed before the exposure. ANA-1 cells is a murine BMDM cell line, which mimic the CD11b inflammatory macrophages *in vivo*.

7.2.1 CNP exposure effect cell viability in dose dependent manner on non-infected ANA-1, MHS and LA4

To investigate how CNP exposure in the ALICE-Cloud system affect the viability and cytotoxicity of non-infected ANA-1, MHS and LA4 cells were growing on the apical site of a transwell insert for growing the cells on the air liquid interface, exposed with different deposition concentrations of CNP. After CNP ALICE-Cloud exposure to the different cell lines, medium was removed, and new cell culture medium, containing WST-1 reagent was added to the cells. Cell viability, or metabolic activity was measured by WST-1 assay to investigate the effect of CNP deposition on the cell viability. With several depositions of CNP in $\mu\text{g}/\text{cm}^2$ measured with the quartz crystal microbalance (QCM), I normalized the metabolic activity to the activity of the sham controls, defined as 100%. **Figure 7.34a, c and e** show metabolic activity measured by viability assay WST-1. Already in all three graphs, I observed a significant correlation between metabolic activity and CNP deposition in $\mu\text{g}/\text{cm}^2$. Data were fit into a nonlinear regression curve and IC50 of CNP deposition was found in all cell lines, indicated with the green dotted lines (**Fig. 7.34b, d, f**).

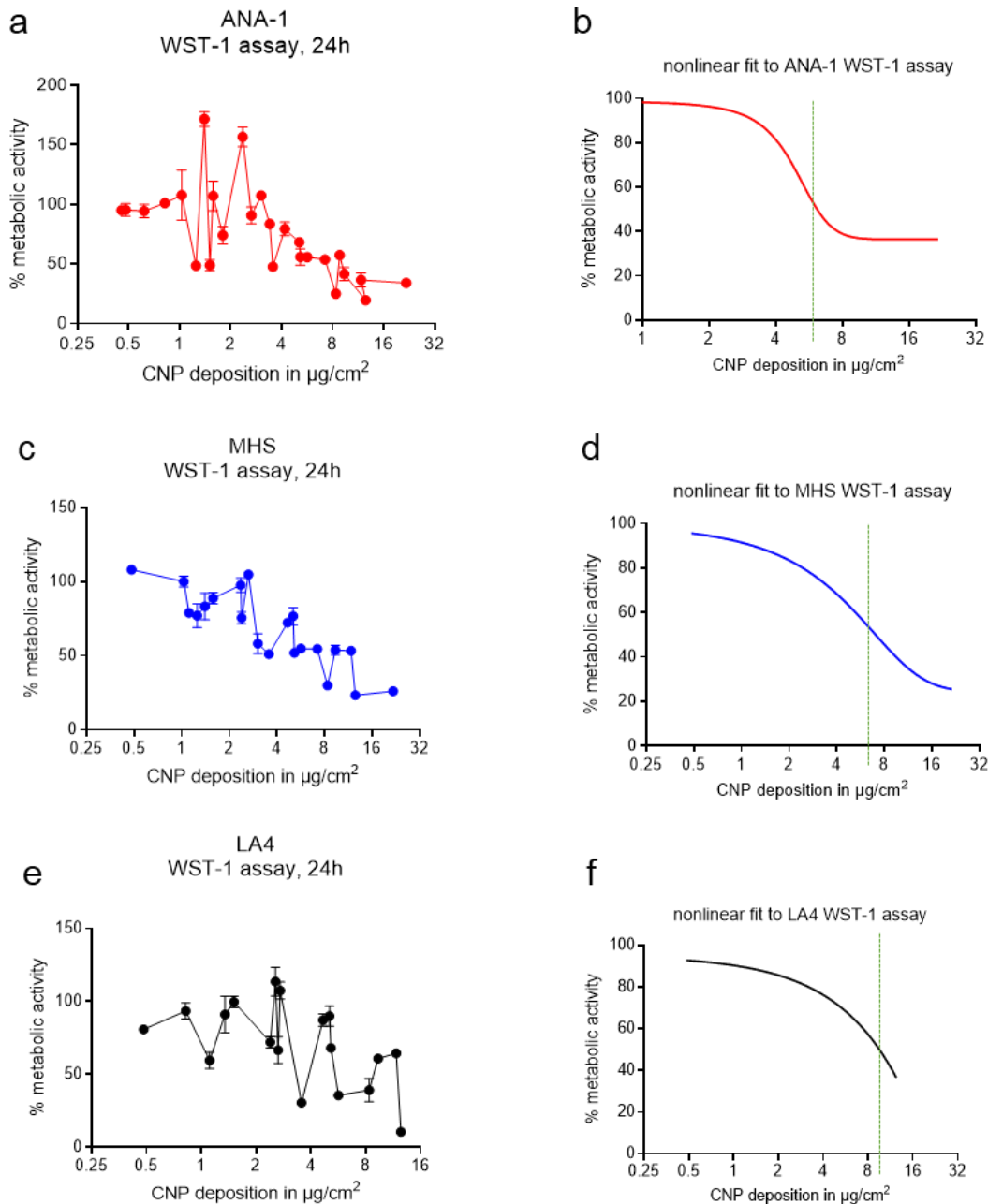


Figure 7.1. ANA-1, MHS, LA4 cell viability alteration induced by CNP exposure at air liquid interface.

ANA-1, MHS and LA4 cells were exposed from 0 up to 22 $\mu\text{g}/\text{cm}^2$ CNP in the ALICE-Cloud exposure chamber. Cell viability was investigated with WST-1 assay after 24h of exposure. 5 independent experiments were performed and included for statistical analysis ($n=4 - 12$). Data was analyzed by nonlinear fit regression. (a, c and e) show % metabolic activity in (a) graph. (b, d and f) show nonlinear regression. Results of ANA-1 cells (a and b) show nonlinear regression with R^2 of 0.5015, a correlation of % cell viability vs. CNP deposition in $\mu\text{g}/\text{cm}^2$ of P-value (two tailed) = 0.0004. Results of MHS cells (c and d) show nonlinear regression with R^2 of 0.7286, a correlation of % cell viability vs. CNP deposition in $\mu\text{g}/\text{cm}^2$ of P-value (two tailed) = <0.0001. Results of LA4 cells (e and f) show nonlinear regression

with R^2 of 0.3382, a correlation of % cell viability vs. CNP deposition in $\mu\text{g}/\text{cm}^2$ of P-value (two tailed) = 0.0038. Green dotted line in (b, d and f) indicates IC50, which is for ANA-1 cells around $6 \mu\text{g}/\text{cm}^2$, for MHS cells around $7 \mu\text{g}/\text{cm}^2$ and for LA4 cells around $11 \mu\text{g}/\text{cm}^2$.

As I observed a reduction of metabolic activity, I was interested in the release of the enzyme lactate dehydrogenase (LDH) into the medium. It is known to be released during cell damage. The release of LDH was not affected in any amount of CNP deposition (Fig. 7.35).

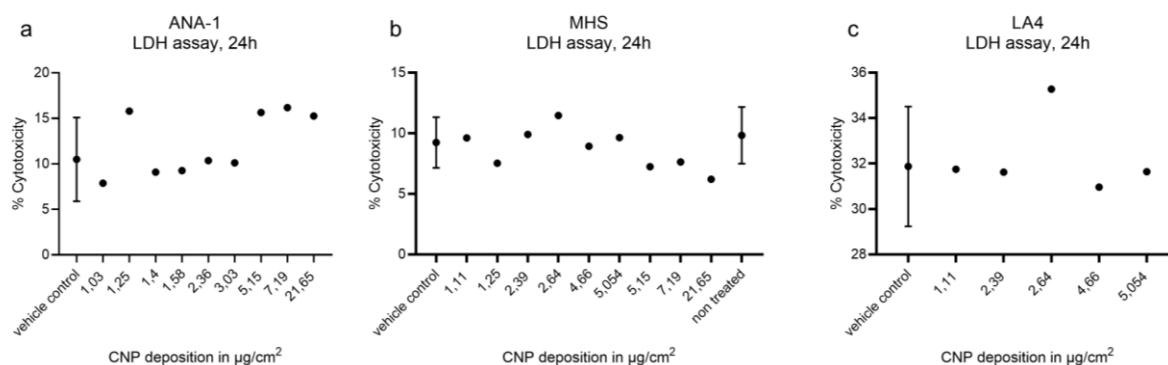


Figure 7.2. No alteration of LDH release depending on CNP deposition.

(a) ANA-1 cells, (b) MHS cells and (c) LA4 cells were cultured and treated on air liquid interface. LDH release was measured with LDH assay after different CNP depositions. % Cytotoxicity was calculated by calculation with high and low control. (a-c) no significant correlation between % Cytotoxicity vs. CNP deposition in $\mu\text{g}/\text{cm}^2$. Data from 3 independent experiments. Correlation was measured with GraphPad Prism.

Taken together, CNP exposure to ANA-1, MHS and LA4 cells effect cell viability or metabolic activity in a dose dependent manner but does not affect the release of LDH.

7.2.2 CNP exposure on ANA-1/MHV-68 affect the virus reactivation on gene in dose dependent manner

In previous *in vitro* reactivation studies (Sattler et al., 2017), nanoparticles were used for the treatment of the cells, growing under submerged conditions. To model a more realistic scenario, I established the NP-triggered MHV-68 reactivation in cells growing at the air-liquid interface (ALI). A schematic illustration of the *in vitro* testing of

Appendix B

dispersed CNPs in the ALICE-Cloud exposure can be seen in **Figure 7.36**. latently infected ANA-1 cells (ANA-1/MHV-68) were seeded on the apical site of a transwell insert. At the following day, apical medium was removed, that cells get only supplied by the basal medium, through the pores in the transwell insert membrane. Dispersed CNPs were nebulized with a nebulizer into the ALICE-Cloud chamber and after ALICE-Cloud treatment, a little bit of medium was added to the cells. After 9h cells were lysed to investigate MHV-68 reactivation on gene expression level and the cell culture medium was collected to detect the numbers of infectious particles by plaque assay. After 9h I observed a significant correlation between CNP deposition in $\mu\text{g}/\text{cm}^2$ and the ratio of Open Reading Frame 50 (ORF50) and Open Reading Frame 73 (ORF73) (**Fig. 3.37a**). ORF50 is expressed in the lytic phase of virus infection cycle, whereas ORF73 is continuously expressed in all infection phases of virus cycle. Increasing ORF50/ORF73 ratio indicates an increase of lytic virus expression and so the reactivation of MHV-68 on the genetic level.

With plaque assay, infectious virus particles were measured at different timepoints, and 48 hours after CNP exposure, I detected a significant correlation between CNP deposition in $\mu\text{g}/\text{cm}^2$ and the virus titer in plaque forming units (PFU) per mL medium (**Fig. 7.37b**).

Taken together, CNP exposure at ALI trigger the upregulation of lytic MHV-68 gene expression in ANA-1 cells as well as the increase of the infectious virus titer, which confirms CNP-triggered virus reactivation in this ALICE-Cloud exposure model.

Experimental Setting to ALICE-Cloud

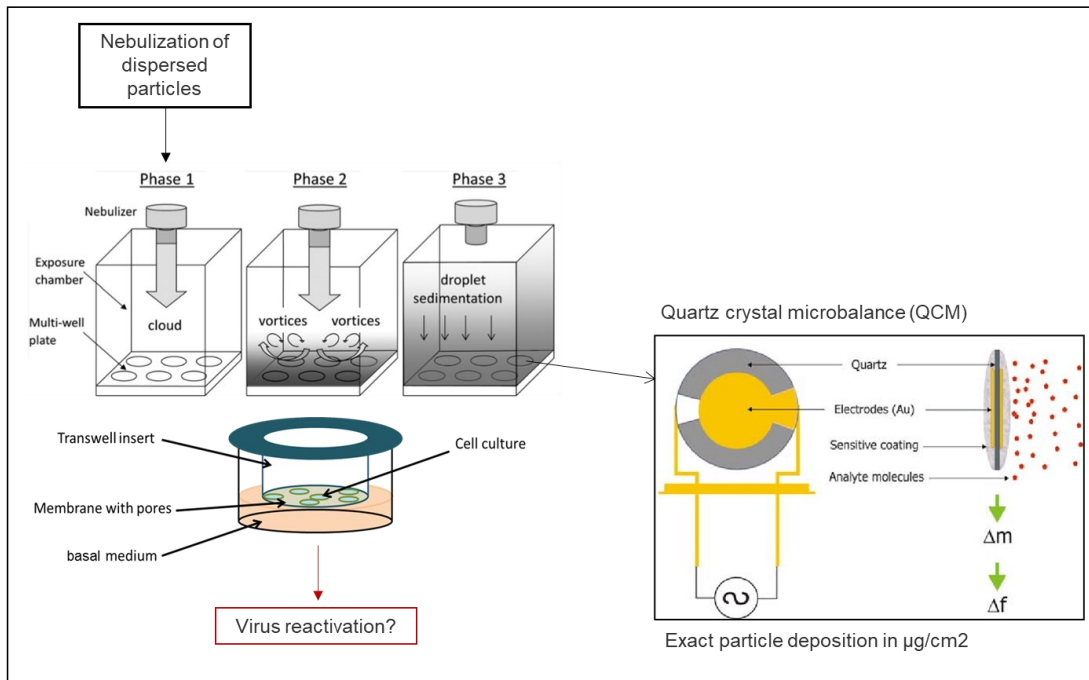
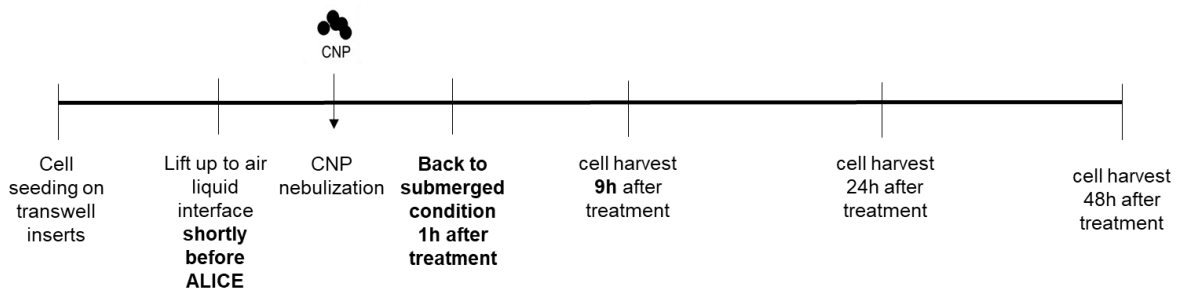


Figure 7.3. Schematic illustration of experimental setting of *in vitro* reactivation testing in ALICE-Cloud exposure.

Latently infected ANA-1/MHV-68 cells were seeded at day 0 in a transwell insert with medium on the basal and the apical site. 24h later, apical medium was removed, and cells were lifted up to the air liquid interface shortly before the ALICE-Cloud exposure with dispersed CNP nebulization. To avoid complete lysis of the latent infected cells, some apical medium was added 1h after CNP nebulization. 9h, 24h and 48h after treatment, cells and supernatant was collected to investigate CNP-triggered MHV-68 reactivation. Modified from Lenz et al., 2014 and Yuwono and Lammers, 2004.

Appendix B

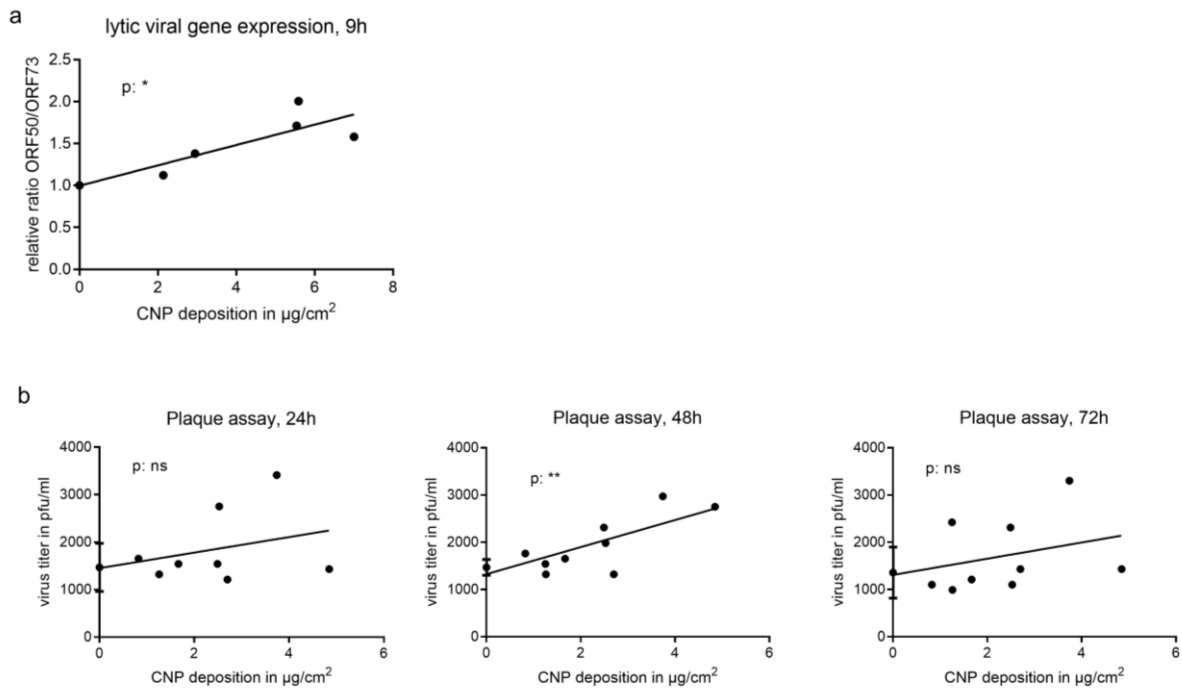


Figure 7.4. CNP-triggers MHV-68 reactivation in dose dependent manner.

Latently infected ANA-1 cells were treated with CNP on ALICE-Cloud system in different doses. (a) ANA-1/MHV-68 cells were lysed 9h after CNP exposure. MHV-68 reactivation was measured on genetic level by investigating gene expression of ORF50, a lytic virus gene in ratio to ORF73, a latently expressed MHV-68 gene. (b) Cell medium was collected at different time points after CNP exposure. Viral titers were measured with plaque assay. At 48h the graph shows a significant correlation between viral titers and CNP deposition. Data from 4 individual experiments. Correlation was measured with GraphPad Prism. “*” indicate significant correlation between (a) relative ratio ORF50/ORF73 vs. CNP deposition in $\mu\text{g}/\text{cm}^2$ and (b) virus titer in pfu/mL vs. CNP deposition in $\mu\text{g}/\text{cm}^2$. *: indicates P value < 0.05. **: indicates P value < 0.01.

7.2.3 CNP nebulization on epithelial-macrophage co-culture system in the ALICE-Cloud system doesn't influence MHV-68 reactivation from ANA-1 cells and cell viability

To mimic the *in vivo* nanoparticle exposure situation better in an *in vitro* setting with the ALICE-Cloud system, a co-culture model was established, illustrated in **Figure 7.38**. In this model, alveolar epithelial cells were cultured on air liquid interface on the apical site of the transwell insert, whereas the latently MHV-68 infected ANA-1 cells were cultured on the basal site of the insert with the stabilization in Matrigel. After nebulization and deposition of different CNP concentrations on the epithelial cells (LA4 and MLE-12). After experimental setting (**Fig. 7.39**) and measurement of CNP-triggered MHV-68 reactivation in the co-culture model, I could not see a correlation of particle deposition on top of the epithelial cells and an MHV-68 reactivation in the ANA-1 cells on the basal site. Either with the co-culture of ANA-1/MHV-68 with LA4, nor with MLE-12. Both virus reactivation on gene expression level and the formation of infectious virus particles were not affected by CNP deposition, tested with different timepoints (**Fig. 7.40**).

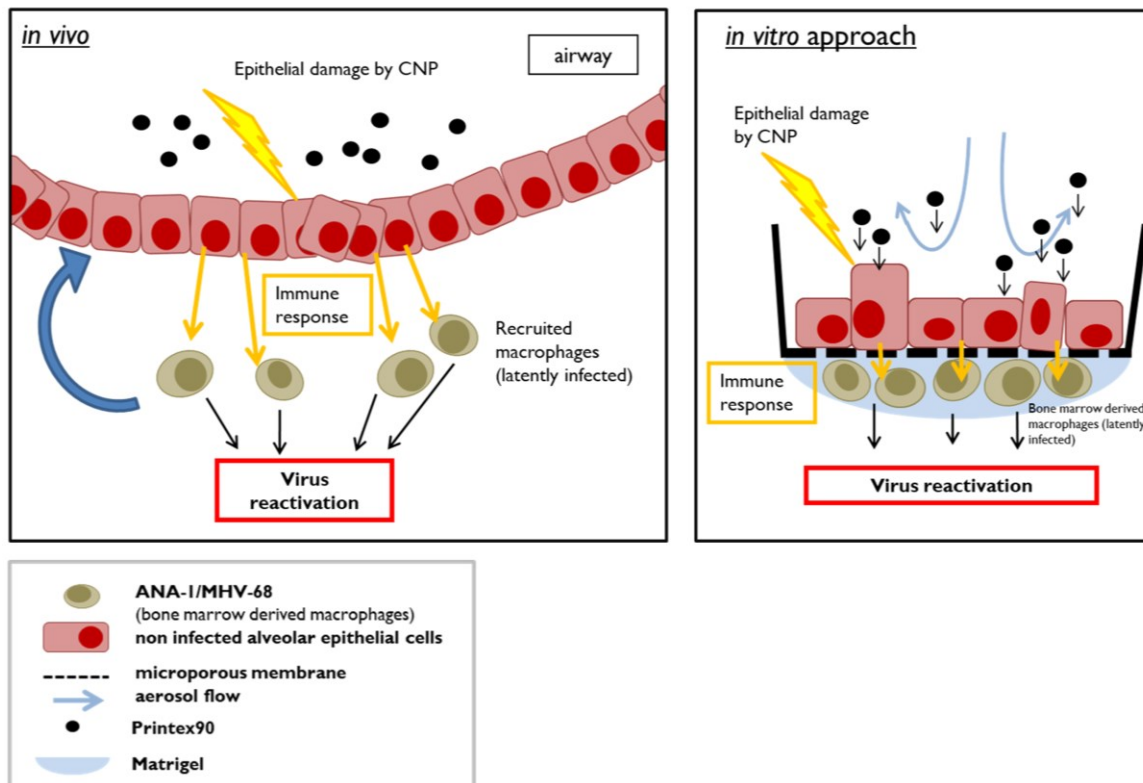


Figure 7.5. Schematic illustration of the similarities of the *in vitro* approach of co-culture reactivation model and *in vivo* situation.

The hypothesis beyond this *in vitro* model: under physiological conditions, nanoparticles get in direct contact with alveolar epithelial cells, which lead to epithelial damage. This leads to the recruitment of macrophages, carrying the latent MHV-68 infection. The epithelial cell damage send response after CNP exposure to the recruited macrophages, what might lead to the reactivation. Left picture shows hypothetical physiological condition. Right picture shows *in vitro* approach. Alveolar epithelial cells growing on the apical site of transwell insert and are on air-liquid interface during nanoparticle exposure. ANA-1/MHV-68 bone marrow derived macrophage cell line localized on the basal site of the transwell insert, directly under the semipermeable membrane. Attached in Matrigel.

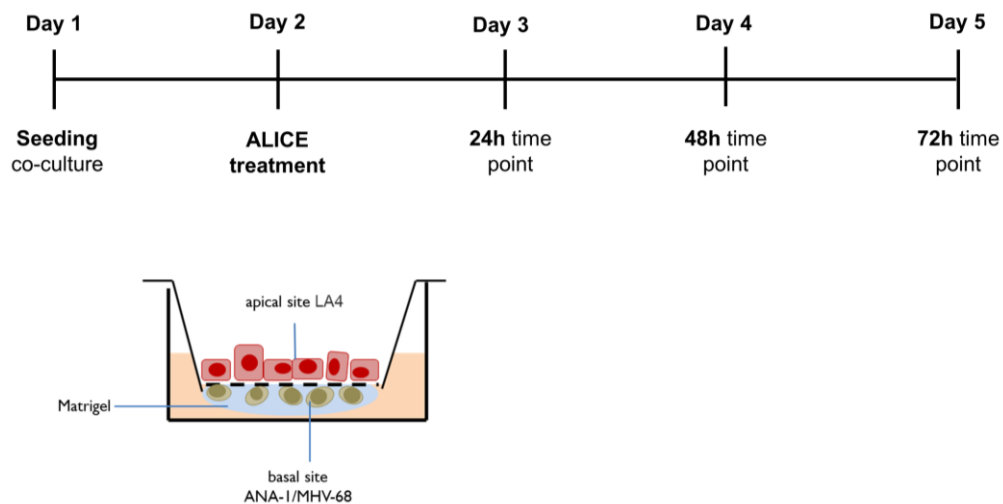


Figure 7.6. Schematic illustration of the ALICE-Cloud exposure of CNP to the co-culture system of LA4 or MLE-12 and ANA-1/MHV68.

At day 1 co culture was seeded with first attaching ANA-1/MHV-68 cells to the basal site of the transwell insert in Matrigel. After basal seeding, LA4 or MLE-12 cells were seeded to the apical site and basal insert was filled with cell growth medium. At Day2, epithelial cells were lifted up to the air-liquid interface and treated with ALICE-Cloud system with dispersed CNPs. After several timepoints, cells were lysed to observe MHV-68 reactivation on genetic level and medium was collected to investigate changes in virus titers.

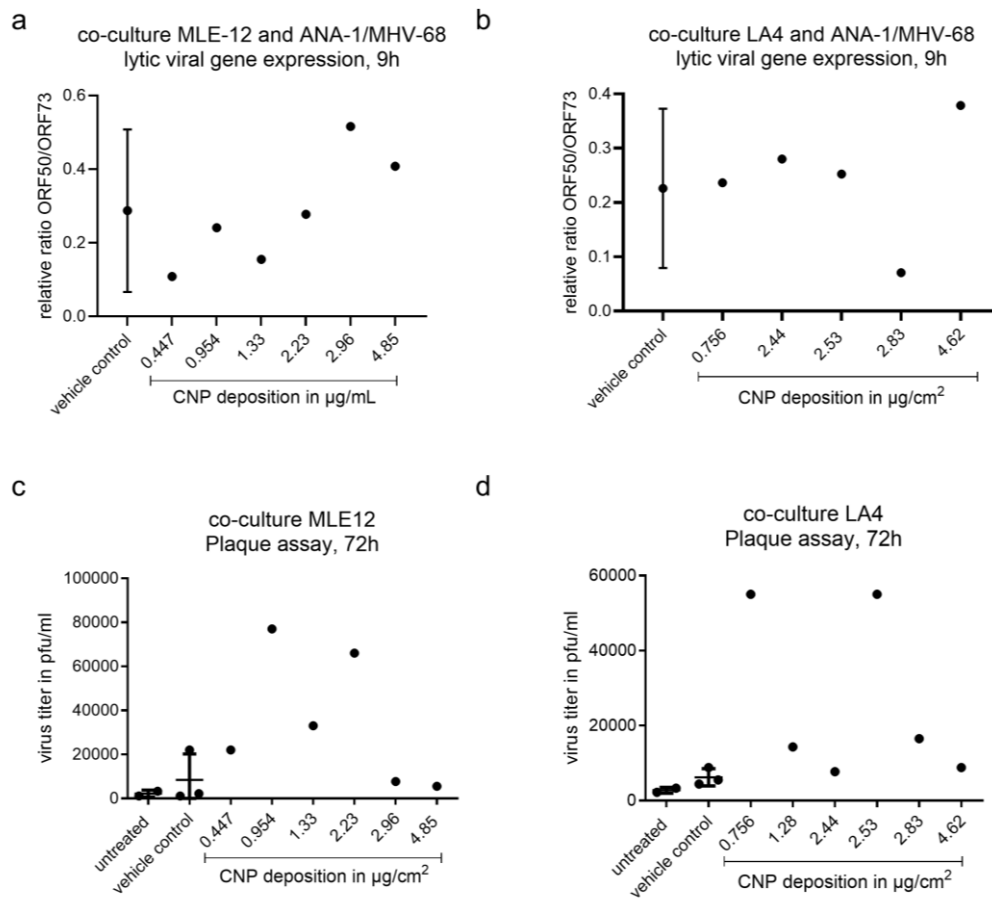


Figure 7.7. CNP does not trigger MHV-68 reactivation co-culture model.

The co-culture of alveolar epithelial cells and latently infected ANA-1 cells were treated with CNP on ALICE-Cloud system in different doses. (a and c) co-culture of MLE-12 and ANA-1/MHV-68 cells. (b and d) co-culture with LA4 and ANA-1/MHV-68 cells. ANA-1/MHV-68 cells were lysed 9h after CNP exposure to test the lytic virus gene expression (a and b). Lytic viral gene expression was tested with qPCR by investigating the ratio of lytic virus gene expression ORF50 and the viral housekeeper gene ORF73. Cell culture medium was collected 72h after CNP exposure to investigate the virus titers with the plaque assay (c and d). Data from 3 individual experiments. Correlation was measured with GraphPad Prism. No significant correlations between virus reactivation and CNP deposition was found.

7.3 Discussion – MHV-68 reactivation induced by CNP in ALICE-Cloud system

In previous work, nanoparticle-triggered MHV-68 reactivation was studied *in vitro* only under submerged conditions (Sattler et al., 2017). To investigate the potential toxicity of nanoparticles and for the investigation of the subsequent trigger for MHV-68 reactivation, relevant *in vitro* assays were established to mimic the *in vivo* situation and to approximate the cellular response to particle treatment *in vitro* to physiological *in vivo* conditions. Particle entry into the human lung is predominantly by inhalation. For a more realistic particle exposure strategy, *in vitro* exposure systems at the air-liquid interface (ALI) are gaining more interest than conventional submerged culture systems. To compare the *in vitro* results with the *in vivo* situation, Loret and colleagues (2018) found that the ALI method has the best predictive power in terms of absolute toxicity as well as *in vivo-in vitro* correlation in direct comparison with treatment under submerged conditions.

There are limitations for both exposure conditions that may reduce the validity of the results. For lung epithelial cells, submerged culture exposure is not representative of physiological conditions. In addition, ALI exposure requires the generation of an aerosol in which the particles are dispersed. This dispersion in liquid for aerosolization may alter particle properties and subsequently affect the analysis of potential toxicity and viral reactivity in the *in vitro* study. I used different cell lines in the ALI cell exposure system (ALICE-CLOUD) (Lenz et al., 2014) to test cell viability via mitochondrial activity and cytotoxicity via LDH release from different CNP depositions. ANA-1 cells, a murine BMDM cell line latently infected with MHV-68, were grown on ALI to mimic the situation in which BMDM are recruited to the alveolar region after the initial hit, MHV-68 infection. In the *in vivo* model, BMDM were shown to carry the latent MHV-68 infection and to be reactivated after CNP and DWCNT exposure. In the *in vitro* model, I could only use CNP exposure because DWCNTs form aggregations that are too large to penetrate through the pores of the nebulizer.

However, with CNP deposition by ALICE-CLOUD treatment, I can detect earlier reactivation in ALI treatment compared to previous studies conducted under submerged conditions. In previous studies, CNP-triggered viral reactivation at the gene expression level peaked at 24 hours, and 72 hours after treatment, infectious viral particle formation peaked. Under ALI conditions, lytic viral gene expression increased

significantly as early as 9 hours and correlated with CNP deposition; in addition, viral titer increased significantly at 48 hours. This earlier MHV-68 reactivation can be explained by faster CNP deposition and thus faster particle-cell interaction with cells growing on ALI.

In the environment, nanoparticles encounter the first barrier, alveolar epithelial cells, after inhalation. To study the biological effect of the particles, co-cultures with epithelial cells and recruited macrophages are used to mimic this first barrier. This first barrier, CNP-induced epithelial injury, may be the indirect trigger for reactivation of MHV-68 in BMDM. This co-culture of alveolar epithelial and latently infected recruited macrophage cell lines together with culturing under ALI conditions attempts to approximate the *in vivo* situation to reduce the extent of animal testing for initial screening of particles as potential triggers for MHV-68 reactivation. In ALI culture conditions, epithelial cells grow in contact with air on the apical side of a transwell membrane that contains pores. Through these pores, the cells are supplied with media from the basal side of the membrane. Aerosolized particles can come into direct contact with ALI cells growing on the membrane without initial contact with the cell culture medium, which can affect the mass deposition, dispersion, and properties of the particles under study. Latently infected ANA-1 cells were attached to the basal compartment of the transwell inserts with Matrigel. Possible elicitors or mediators released by CNP-injured epithelial cells should reactivate MHV-68.

Cell lines are most commonly used for *in vitro* particle toxicology assays. When using different cell lines from different origins, the physiological properties change, which may affect the comparison of the *in vitro* test situation with the *in vivo* relevance, so I tested LA-4 and MLE-12 cells. For epithelial cells, growth should be performed in a monolayer during cultivation to mimic the physiological situation.

Differences are also observed *in vitro* with respect to monocultures and advanced models with two or more cell lines or even with organoid models (Wang et al., 2020; Nabi et al., 2022; Müller et al., 2010; Cappellini et al., 2020).

Although the co-culture model should be close to the real situation, I did not detect significant MHV-68 reactivation. Neither at the level of gene expression nor viral titer. I tested different time points from 9 hours to 72 hours. But at no time point I was able to detect a correlation between CNP deposition on uninfected epithelial cells and MHV-68 reactivation from latency in ANA-1 cells. Neither cell co-culture model was suitable

Appendix B

for testing CNP-triggered viral reactivation *in vitro*. Neither the LA-4 co-culture with ANA-1/MHV-68 nor the MLE-12 co-culture with ANA-1/MHV-68.

Either the observed time points were not the correct ones to observe reactivation or the inflammatory cascade from epithelial cells to BMDM cells was not possible in this model with transwell membrane and Matrigel between these cell lines.

However, ALICE-CLOUD treatment with CNP in a single culture was a valid *in vitro* model for testing virus reactivation and may be used in the future to screen other environmental particles for the potential to reactivate gammaherpesviruses, such as biological particles (pollen), freshly generated diesel exhaust, or other airborne particles (Candeias et al., 2022; Oeder et al., 2015; Netkeuakul; Cervena et al., 2020).

Acknowledgements

In February 2018, I started my PhD program under the supervision of Prof. Dr. med. Erika von Mutius in Ludwig-Maximilians Universität München. For my PhD project I have been working for four years in Dr. Tobias Stögers Research Group in the Institute of Lung Health and Immunity, Comprehensive Pneumology Center (LHI/CPC) in the Helmholtz Zentrum München, Germany. At the same time, Prof. Dr. Heiko Adler as well as Dr. Ali Önder Yildirim additionally supervised my PhD project.

First, I want to thank to my supervisors, Prof. Dr. med. Erika von Mutius, Dr. Tobias Stöger, Prof. Dr. Heiko Adler and Dr. Ali Önder Yildirim for their professional supervisions in the past years. It was my great pleasure to work together with them. Every meeting and discussion make the project always ongoing and achieve a lot. As my university supervisor, Prof. Dr. med. Erika von Mutius gave great support in the thesis committee (TC) meeting discussion about clinical aspects as well as project maintenance. Besides, I feel so lucky to work together with Dr. Tobias Stöger. He is a talent scientist and a kind person; I learned a lot and improved a lot in research with his support. What I achieved in the last years with Dr. Tobias Stöger brings me confidence and enthusiasm. I also would like to thank to Prof. Dr. Heiko Adler, who is a professional virologist in my project, and provides me great support.

I want to thank to all the supports from our group Dynamics of Pulmonary Inflammation of the Institute of Lung Health and Immunity (LHI) for their support and help: Lianyong Han, Anna Fuchs, Beatrix Steer, David Kutschke, Dr. Carola Voss, Dr. Markus Rehberg, Chenxi Li, Mehwish Isaque, Hongyu Ren, Qiongliang Liu, Yasmin Shaalan, Eva Günther, Pheobe Cabanis, Camille Barro, Haiyun Zhang, Miriam Kastlmeier, Qiaoxia Zhou, Xiaoying Wang. Special thanks to Lianyong Han, he is a talented young scientist and great person, and it was always a pleasure for me to discuss and work with him in Neuherberg and Großhadern.

I also want to thank to all the supports from our Institute of Lung Health and Immunity (LHI) and the Translational Medicine (TIEM) for their support and help: Dr. Ali Önder Yildirim, Dr. Aicha Jeridi, Dr. Thomas Mark Conlon, Dr. Gizem Günsel Günes, Dr. Carmela Morrone, Christine Hollauer, Xiaomei Tan, Dr. Hengshuo Liu, Dr. Doreen

Acknowledgements

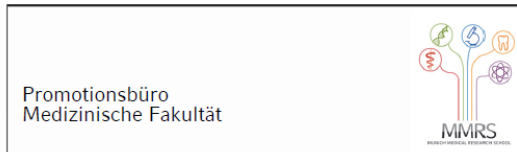
Franke, Dr. Melanie Penning, Dr. Beate Hagl, Dr. Ellen Renner. I am grateful to our secretary Kaori Sumikawa. They are always nice and helpful in the past years.

Many thanks to all my friends and my family, which provide me great support over the past years and always believed in me.

Im Besonderen möchte ich meinen Brüdern Christian und Andreas danken, in der Hoffnung unser Zusammenhalt wird niemals enden.

Zu guter Letzt danke ich von Herzen meinem Partner Maximilian Müller und seiner Familie, die mich über die vergangenen Jahre so warm unterstützt haben.

Affidavit



Affidavit

Häfner, Verena Carina

Surname, first name

Street

Zip code, town, country

I hereby declare, that the submitted thesis entitled:

Latent MHV-68 reactivation – The link between acute pulmonary inflammation and chronic lung diseases

.....

is my own work. I have only used the sources indicated and have not made unauthorized use of services of a third party. Where the work of others has been quoted or reproduced, the source is always given.

I further declare that the submitted thesis or parts thereof have not been presented as part of an examination degree to any other university.

Munich, 05.08.2023
Place, date

Verena Häfner
Signature doctoral candidate

Confirmation of congruency



LUDWIG-
MAXIMILIANS-
UNIVERSITÄT
MÜNCHEN

Promotionsbüro
Medizinische Fakultät



**Confirmation of congruency between printed and electronic version of
the doctoral thesis**

Häfner, Verena Carina

Surname, first name

Street

Zip code, town, country

I hereby declare, that the submitted thesis entitled:

Latent MHV-68 reactivation – The link between acute pulmonary inflammation and chronic lung diseases

.....

is congruent with the printed version both in content and format.

Munich, 05.08.2023

place, date

Verena Häfner

Signature doctoral candidate